CHAPTER

THIRTEEN

SOLAR ENERGY

13-1 INTRODUCTION

Of all the renewable energy sources, solar energy received the greatest attention in the decade of the 1970s and has been the hub of much emotion and pressure. Many regarded it as *the* solution for reducing the use of fossil and nuclear fuels and for a cleaner environment. Solar energy, as a result, has been the object of usually inflated, overly optimistic predictions ranging from largely supplementing to eventually replacing all the current means of production of both electric-power and thermal-energy requirements.

Solar energy, in sheer size, does have the potential to supply all energy needs: electric, thermal, process, and chemical, and even transportation fuels. It is, however, very diffuse, cyclic, and often undependable. It, therefore, needs systems and components that can gather and concentrate it efficiently for conversion to any of these uses and that can do the conversion as efficiently as possible. Much of the construction materials used for collecting and converting solar radiation, whether thermal or photovoltaic, are themselves very energy-intensive. For example, large quantities of aluminum, steel, copper, concrete, glass, and plastic are needed, all of which require large quantities of energy for conversion from ore to finished products. Direct conversion of solar radiation to electricity (photovoltaic) requires the extremely energy-intensive processing of sand to crystalline silicon. Both systems of converting the collected radiation to usable energy (solar thermal and photovoltaic) are rather inefficient, making them large per unit energy output and hence exacerbating the need for the materials mentioned above.

A rational assessment of the role of solar energy in the total energy picture would

have to take into account both the costs and the real, rather than the imaginary, environmental impact of that energy.

The costs are of two kinds: (1) the monetary cost of the finished products and of assembling them into workable systems and (2) the quantities of conventional energy sources such as coal, oil, natural gas, and nuclear fuel that have to be consumed in the processes of producing the above finished products and in constructing the systems. It is logical that one should expect the energy thus consumed to be a small fraction of the net energy generated during the life of the plant (a truism for any power system). It seems that this fraction is larger for solar systems than fossil or nuclear systems, often bordering on the unacceptable, except in special cases where solar energy is uniquely suited.

On the environmental question, solar-energy systems are not pollution-free as many of its proponents claim. (No power system, and for that matter, no human endeavor to improve the quality of life, is. The real criterion for success is whether the gains sufficiently outweigh the losses.) The mining of large quantities of mineral ores, the processing of these ores to the finished material, the manufacturing of the equipment, and the construction of the plants are processes that generate their own pollution and health and occupational safety risks. In addition, the low efficiency of electric-generating plants, whether thermal or photovoltaic, results in large heat-rejection rates in a concentrated manner (even though the energy input is diffuse) from the plants, hence thermal pollution.

Although solar energy may be used in many markets, such as in active and passive space heating and cooling, industrial process heating, desalination and water heating [116], and in electric generation, it is the latter we are concerned with in this book. After investments by federal and other agencies amounting to several hundred million dollars in the 1970s on all these technologies, only one is in commercial use today (1982), namely flat-plate collectors for space and water heating. All the others remain in various stages of research and development. It now appears that solar-electric systems are not expected to make engineering and economic sense as central electric-generating plants of hundreds of megawatts capacities (the economical sizes needed now by the world) in the foreseeable future. They do, however, make sense in cases where the power requirements are relatively small and in remote areas, both on earth and in outer space, that lack proximity to an efficient electricity-distribution network. On earth, they are most particularly suited to remote desert areas where the land is available, relatively inexpensive, and adequate for the very large collector surfaces required, and where the sunshine, although cyclic, is abundant and dependable.

13-2 HISTORY

Solar energy's place in the total needs of the human race is unquestionable. It grows all our crops and creates the fresh water for these crops and for our survival. It has, in addition, been used for millenia for passive heating of dwellings, as can be ascertained by examination of archaeological sites around the world. Serious experiments to use it to generate energy for specialized uses began, however, in the eighteenth

century. In 1774 Joseph Priestly concentrated it on mercuric oxide. The result was the generation of a gas that was found "to cause a candle to burn brightly and a mouse to live longer" which he called "air in a much greater perfection." This experiment, in reality, had led to the discovery of oxygen. It also led the French chemist, Lavoisier, to explain combustion as the chemical combination with oxygen.

A century later, a relatively large solar distilling plant was installed in a desert in northern Chile. It used 4800 m^2 of land and contained slanted roofs of glass plates that transmitted the sun's rays to troughs of water below them. The vaporized water condensed on the cooler underside of the glass, ran down, and was collected in channels. The plant produced some 25 m^3 of fresh water per day, which was used in a nitrate mine. It ran for 40 years until the mine was exhausted.

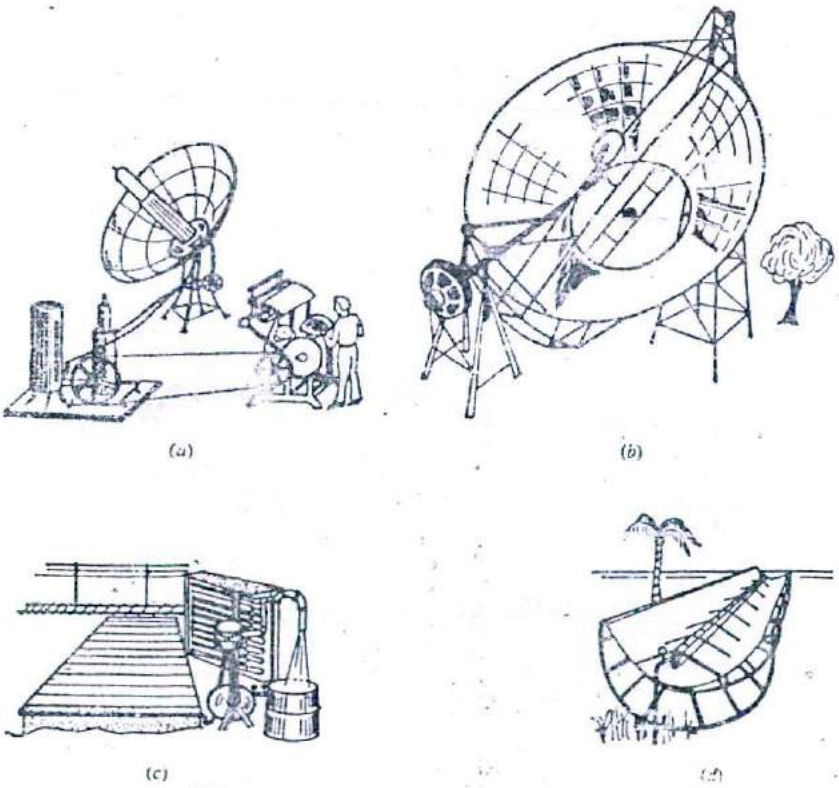


Figure 13-1 Some early examples of solar-power conversion to mechanical power. (*a*) Solar steam engine, Paris, 1878. (*b*) Solar steam engine, Pasadena, California, 1901. (*c*) Solar steam engine with flat-plate collector, Philadelphia, Pennsylvania, 1907, 1911. (*d*) Solar steam engine, Cairo, Egypt, 1913.

Solar-to-mechanical conversion was first demonstrated at an exhibition in Paris in 1878 when sunlight was concentrated by a focusing collector on a steam boiler that ran a small steam engine that in turn ran a small printing press. In 1901, a larger (6 m^2) focusing collector in the form of a truncated cone generated steam for a 4.5-hp engine. In 1907 and 1911, near Philadelphia, F. Shuman built solar steam engines of several horsepower that were used for pumping water. In 1913, in collaboration with C. V. Boys, Shuman built the then large 50-hp solar steam engine, which used a long parabolic collector that focused solar radiation onto a central pipe (with a concentration ratio of 4.5). The engine pumped irrigation water from the Nile, near Cairo. (The four systems mentioned above are shown in Fig. 13-1.)

An early attempt at solar-electric conversion, as well as energy storage, was made by J. A. Harrington in New Mexico around 1915. Sunlight was focused on a boiler that ran a steam engine that pumped water into a 19-m^3 tank 6 m above. The water thus stored was made to run down into a water turbine that powered an electric generator that lighted small electric bulbs inside a small mine.

These and other activities could not, however, survive the competition of cheap fossil fuels, and little activity in solar development took place for 30 years or so. Renewed interest began in the 1950s as a result of the efforts of a few such as Farrington Daniels of Wisconsin, an interest that was accelerated by the energy crisis of the 1970s.

13-3 EXTRATERRESTRIAL SOLAR RADIATION

The total quantity of solar energy incident upon the earth is immense, but the energy is very diffuse and, because of the earth's rotation and orbit around the sun, cyclic both daily and seasonally. It also suffers from atmospheric interference from clouds, particulate matter, gases, etc. In this section we will deal with the energy incident on the earth outside of its atmosphere. This is called *extraterrestrial radiation.*

The earth rotates around the sun on a slightly elliptical orbit with major and minor axes differing by 1.7 percent. The earth is closest to the sun on December 21 at a distance of about 1.45×10^{11} m, and farthest on June 22 at about 1.54×10^{11} m; the average distance is 1.49×10^{11} m (Fig. 13-2). The sun has a diameter of about 1.39×10^9 m and subtends an angle of only 32 minutes at the earth. For all practical purposes, therefore, the sun's rays may be considered parallel when they reach the earth. The sun has an effective black-body temperature, as seen from the earth, of 5762 K.* The spectral distribution of solar energy at the mean sun-earth distance outside the earth's atmosphere is shown in Fig. 13-3 by curve *A* as beam irradiance flux per unit wavelength width in $W/(s^2 \cdot \mu m)$ versus wavelength in μm (micrometers). As seen, it does not follow a smooth black-body spectral distribution curve. This spatial relationship between sun and earth and the sun's effective temperature result

* This is the temperature of a black body (a perfect radiator with both emissivity and absorptivity equal to 1.0) that radiates the same amount of energy as the sun. The sun's interior is much hotter and denser than its surface. At its center, the temperature is estimated at 8×10^6 to 40×10^6 K and the density at about 10^5 kg/m^3.

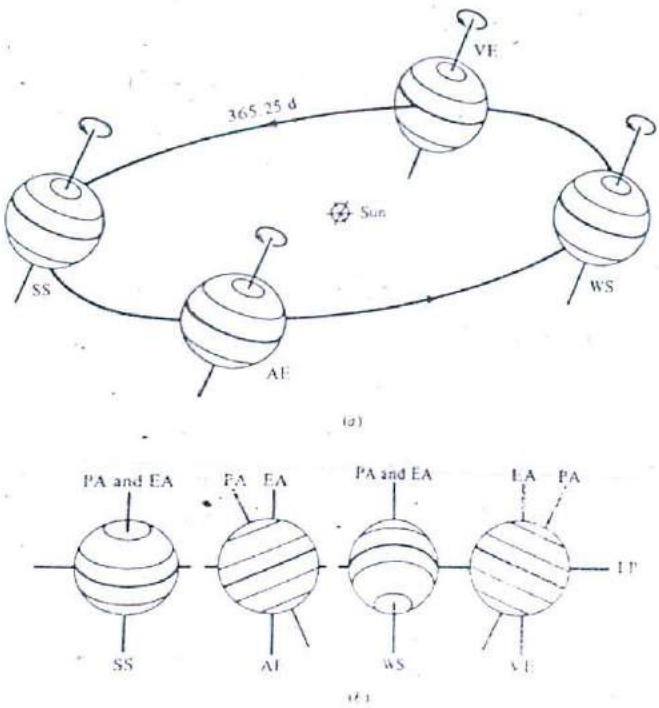


Figure 13-2 Orientation of earth and sun. (*a*) Earth's orbit around sun. SS = summer solstice, June 22; AE = autumnal equinox, September 23; WS = winter solstice, December 22; VE = Vernal (spring) equinox, March 21. (*b*) The earth as seen from the sun; PA = polar axis; EA = ecliptic axis; EP = ecliptic plane. Circles from north to south: Arctic circle (66.5° N. lat.), tropic of capricorn (23.5° N. lat.), equator, tropic of cancer (23.5° S. lat.), antarctic circle (66.5° S. lat.).

in extraterrestrial solar radiation intensity that is nearly constant and is called the *solar constant* S. It is equal to the area under curve A in Fig. 13-3 and has the values*

$$S = 1353 \text{ W/m}^2 = 1.353 \text{ kW/m}^2$$

$$S = 1.940 \text{ langley*/min}$$

$$S = 428 \text{ Btu/h} \cdot \text{ft}^2$$

$$S = 4871 \text{ kJ/(h} \cdot \text{m}^2\text{)}$$

The slightly elliptical orbit of the earth around the sun causes the actual extraterrestrial intensity to deviate only slightly from the solar constant with a range roughly ±3

* The *langley* is a unit frequently used in solar engineering. It is equal to 1.0 cal/cm².

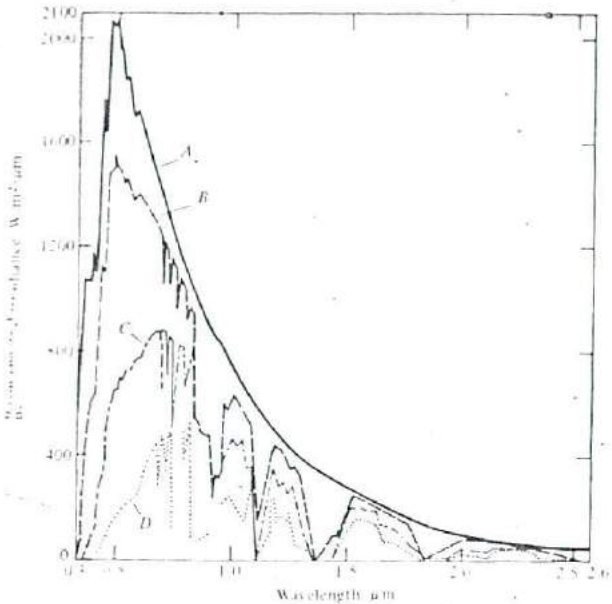


Figure 13-3 Solar-energy beam radiation as a function of wavelength (*A*) extraterrestrial with air mass $m_a = 0$ irradiance, $I = 1353$ W/m^2; (*B*) terrestrial, $m_a = 1.0$, $I = 924.9$ W/m^2; (*C*) terrestrial, $m_a = 4$, $I = 528.9$ W/m^2; (*D*) terrestrial, $m_a = 10$, $I = 234.5$ W/m^2. Curve *A* according to NASA/ASTM standards. Curves *B*, *C*, *D* and computed for 20-mm precipitate water vapor, 3.4 mm ozone, and clear atmosphere [117].

percent. Other small variations occur with different periodicities and as a result of sunspots.

Extraterrestrial solar radiation is all of the *beam-radiation* type, also called *direct radiation*. This is radiation received from the sun in essentially straight rays or beams that are unscattered by the atmosphere.

The earth's *polar axis* (the axis of rotation of the earth) is inclined a permanent 23.45° from a normal to the *ecliptic plane* (EP), the plane of the earth's orbit around the sun (Fig. 13-2*b*). The *ecliptic axis* (EA) of the earth is the one that goes through its center but which is always perpendicular to the ecliptic plane. The polar and ecliptic axes are in a plane normal to the sun's rays at the two equinoxes and in a plane parallel to them at the two solstices. Thus, although the earth's inclination is fixed in space, it appears to wobble around the sun with its northern hemisphere inclined toward it in the summer and away from it in the winter, with both hemispheres "seeing" it equally only at the equinoxes.

The angle between the sun's rays and the earth's equatorial plane (normal to the polar axis) is called the sun's *declination angle* θ_d. In the northern hemisphere θ_d is zero at both equinoxes and has a maximum value that corresponds to the tilt angle

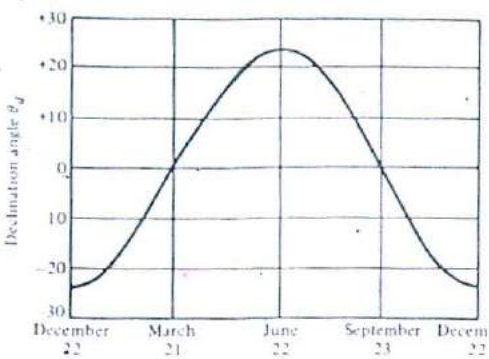


Figure 13-4 Seasonal variation in th sun's declination angle θ_d

$+23.45°$ at the summer solstice and $-23.45°$ at the winter solstice. The variation of θ_d during the year, for the northern hemisphere, is shown in Fig. 13-4. The seasonal variation of the terrestrial radiation on a horizontal surface at any one location on the earth's surface is accounted for by the variation in θ_d.

13-4 TERRESTRIAL SOLAR RADIATION

The solar energy falling on the earth's surface is called *terrestrial radiation*. The rate of terrestrial energy falling on a unit surface area in W/m^2, $J/(s \cdot m^2)$, or $Btu/(h \cdot ft^2)$ is variably referred to as radiation, irradiation, irradiance, insolation, or energy flux. Terrestrial radiation varies significantly, both daily because of the earth's rotation and seasonally because of the change in the sun's declination angle. During both the vernal and autumnal equinox, the sun's rays are perpendicular to the earth's surface at the equator and cause equal radiation intensities in the northern and southern hemispheres. At the summer solstice the earth's axis is tilted towards the sun so that its northern hemisphere receives more radiation than the southern hemisphere. At the winter solstice, the reverse is true, with local solar intensities strongly dependent upon latitude. Besides variations caused by the spatial changes between the sun and earth, terrestrial radiation is subject to reductions and changes due to the presence of various gases, vapors, and particulate matter in the earth's atmosphere. The extraterrestrial radiation is said to be *attenuated* by two mechanisms: scattering and absorption.

Scattering is a mechanism by which part of a radiation beam is scattered laterally and is, therefore, attenuated by the air molecules, water vapor, and the dust in the atmosphere. The mechanism is dependent upon the type of scattering medium and the wavelength of radiation and is a rather complex phenomenon. It is known, however, that scattered, or diffuse, radiation is mostly of shorter wavelengths, which is the reason the sky appears blue.

Absorption of solar radiation in the atmosphere is mainly by ozone O_3, water vapor H_2O, and carbon dioxide CO_2. X-ray and other very short wavelength radiations of the sun are absorbed high in the ionosphere by N_2, O_2, and other components. The

main effects are caused by: (1) Ozone in the ultraviolet (short wavelength) rays with absorption complete below 0.29 μm and decreasing between 0.29 and 0.35 μm, where it ceases except for a weak absorption band near 0.6 μm. (2) Water vapor with absorption strong in wavelength bands in the infrared (long wavelength) part of the spectrum, at 1.0, 1.4, and 1.8 μm. (3) Carbon dioxide with no absorption bands in the short or visible parts of the spectrum but several between 2.36 to 3.02 μm, 4.01 to 4.08 μm, and 12.5 to 16.5 μm. The extraterrestrial radiation is very low in that region (less than 5 percent of the total spectrum) so that absorption by both H_2O and CO_2 causes the energy received at wavelengths greater than 2.3 μm at the earth's surface to be insignificant.* For terrestrial applications, therefore, only the wavelength range 0.29 to 2.5 μm is significant.

The *terrestrial solar radiation*, that incident on the earth's surface, is composed of two parts: (1) *beam radiation*, defined above, and (2) *diffuse radiation*. The latter is radiation that had its direction changed by atmospheric scattering. It is sometimes called *sky radiation* because it is the radiation one feels if standing in the shade or under a small cloud on an otherwise sunny day. (It should not, however, be confused with radiation emitted by the atmosphere itself).

The incident radiation on the earth's surface is usually presented in terms of dimensionless *air mass* m_a, defined as

m_a = air mass = ratio of optical thickness of the atmosphere through which beam radiation passes to the surface to its optical thickness if the sun were at the zenith, i.e., directly above (dimensionless)

Thus, $m_a = 0$ means extraterrestrial, $m_a = 1$ indicates sea level on the earth when the sun is at the zenith, $m_a = 2$ when the sun is at a zenith angle θ_z equal to 60°. θ_z is the angle subtended by the solar beam and the zenith. The air mass m_a is related to zenith angles from $\theta_z = 0°$ to $\theta_z = 70°$, at sea level, by

$$m_a = (\cos \theta_z)^{-1} \tag{13-1}$$

For values of θ_z greater than 70°, the curvature of the earth becomes significant and m_a becomes progressively smaller than that given by Eq. (13-1).

Figure 13-3 shows the spectral distribution of extraterrestrial *beam radiation* ($m_a = 0$) as well as terrestrial beam radiations for air masses $m_a = 1$, 4, and 10. The spectral distribution of the *total radiation* is the sum of *both* the beam and diffuse components. Measurements show that the diffuse component distribution is similar to that of the total, though shifted somewhat toward the short wavelengths. (Recall that scattering occurs most at short wavelengths.) This suggests that the spectral-energy distribution from an overcast sky is similar to that from a clear sky.

Considering a horizontal surface on a clear day, both beam and diffuse radiation depend upon the hour of the day. Both are maximum around noon and both decrease

* The CO_2 infrared absorptions are, however, significant when one considers low-temperature radiation from the earth back to space, which typically covers a spectral range of 3 to 50 μm with a peak near 10 μm. An increase in CO_2 concentrations in the atmosphere are cause for concern because of the "greenhouse effect" (Sec. 17-6).

toward dusk, but beam radiation decreases at a faster rate. Thus the ratio of diffuse-to-beam radiation also depends upon the hour of the day, as it is very low around noon and increases slowly toward unity and slightly exceeds it at dusk. Table 13-1 shows calculated beam and diffuse radiations for a clear August day in the Midwest (Madison, Wisconsin), including beam radiation on a surface normal to the radiation, i.e., one that tracks the sun, $I_{b,n}$; beam radiation on a horizontal surface $I_{b,h}$; diffuse radiation I_d; and cumulative radiation on a horizontal surface $I_{c,h}$. All are in MJ/m^2 for 1-h periods as shown. The totals for the day would be twice the sums of the columns. Thus the day total beam radiation on a normal surface is $2 \times 15.38 = 30.76$ MJ/m^2 per day. Likewise the day total beam radiation, diffuse, and cumulative on a horizontal surface would be 18.82, 3.74, and 22.56 MJ/m^2 per day, respectively. The ratio of diffuse to beam radiation and their total are given only for a horizontal surface. The reason is that for a surface normal to the beam radiation, diffuse radiation is affected by the decrease of the "total" sky seen by the surface as well as reflectance effects from the ground.

The computations given in Table 13-1 dealt with a clear day. The available terrestrial solar energy at a given time and place is influenced not only by time of day or year, location, and scattering as mentioned above but also by cloudiness. All effects may be combined in one parameter called the *clearness index* C_i, defined as

C_i = clearness index = ratio of the average radiation on a horizontal surface for a given period to the average extraterrestrial radiation for the same period

The averaging could be monthly, daily, or hourly, in which case C_i would be a monthly, daily, or hourly clearness index. C_i varies widely from near 30 to as high as 70 percent in some localities on earth, with its value going down to zero in some locations because of bad weather even in the daytime.

Table 13-2 shows measured cumulative daily radiations on a horizontal surface in selected locations in the United States.

The total radiation received by a surface however is undoubtedly greater from a

Table 13-1 Beam and diffuse radiations for a clear August day in Madison, Wisconsin*

Hour, p.m.	$I_{b,n}$	$I_{b,h}$	I_d	$I_d/I_{b,h}$	$I_{c,h}$
12–1	2.96	2.50	0.36	0.14	2.86
1–2	2.90	2.31	0.35	0.05	2.66
2–3	2.77	1.95	0.34	0.17	2.29
3–4	2.53	1.44	0.31	0.22	1.75
4–5	2.12	0.87	0.27	0.31	1.14
5–6	1.58	0.31	0.20	0.65	0.51
6–7	0.72	0.03	0.04	1.33	0.07

*From Ref. 116.

Table 13-2 Average cumulative daily solar radiation on a horizontal surface*

Location	Latitude	Radiation, MJ/m^2 per day											
		Jan.	Feb.	Mar.	Apr.	May	June	July	Aug.	Sept.	Oct.	Nov.	Dec.
Albuquerque, N. Mex.	33.93	11.5	15.2	20.1	25.3	28.8	30.4	28.2	26.0	22.4	17.6	12.9	10.9
Chicago, Ill.	41.98	5.8	8.6	12.6	16.6	20.3	22.8	22.1	19.5	15.4	11.0	6.4	4.6
Fairbanks, Alaska	64.82	0.8	3.2	9.8	16.1	20.0	22.1	18.6	15.2	7.7	3.6	1.1	0.3
Los Angeles, Calif.	33.93	10.5	13.8	18.4	22.1	23.4	24.0	26.2	23.6	19.1	14.9	11.4	9.6
Phoenix, Ariz.	33.43	11.6	11.5	20.6	26.7	30.4	31.1	28.2	26.0	22.9	17.9	13.1	10.6
Madison, Wis.	43.13	5.8	5.7	12.9	15.9	19.8	22.1	22.0	19.4	14.7	10.3	5.7	4.4
San Francisco, Calif.	37.78	11.5	15.6	16.5	21.8	21.8		27.1	24.0	19.8	13.9	9.3	7.3
Seattle, Wash.	47.45	5.7	9.1	11.1	16.6	21.0	21.8	23.7	19.1	13.7	7.9	4.4	2.7

*From Ref. 116.

surface that is normal to beam radiations, as can be seen when comparing columns 2 and 6 of Table 13-1, even though diffuse radiation is not included in the former. This is the reason why a radiation "collecting" surface would be more effective if it were made to track the sun, i.e., to change angle, so that it would always remain perpendicular to the rays emanating from it. We will see later, however, that in a central-receiver system, the tracking is such that the collecting surface should alter its angle so that it reflects solar radiation to a fixed in-place central receiver.

The total amount of solar radiation received by the earth is, as indicated earlier, immense. Because the sun's rays are essentially parallel and hence perpendicular to the earth's projected area, the extraterrestrial power P_e received is given by the solar constant S times the projected area of the earth, or

$$P_e = S\pi R^2 \tag{13-2}$$

The radius of the earth R is 6.378×10^6 m and $S = 1.353$ kW/m^2, so that

$$P_e = 1.353 \times \pi(6.378 \times 10^6)^2 = 1.73 \times 10^{14} \text{ kW}$$

$$\text{Energy per year} = 1.73 \times 10^{14} \times 8766 \text{ h/year} = 1.516 \times 10^{18} \text{ kWh/year}$$

$$= 1.516 \times 10^{18} \times 3.6 = 5.457 \times 10^{18} \text{ MJ/year}$$

The continental United States land area is about 2.885×10^6 mi^2, about 7.5×10^{12} m^2. It thus receives extraterrestrial radiation at the rate of $7.5 \times 10^{12} \times 1.353 = 10^{13}$

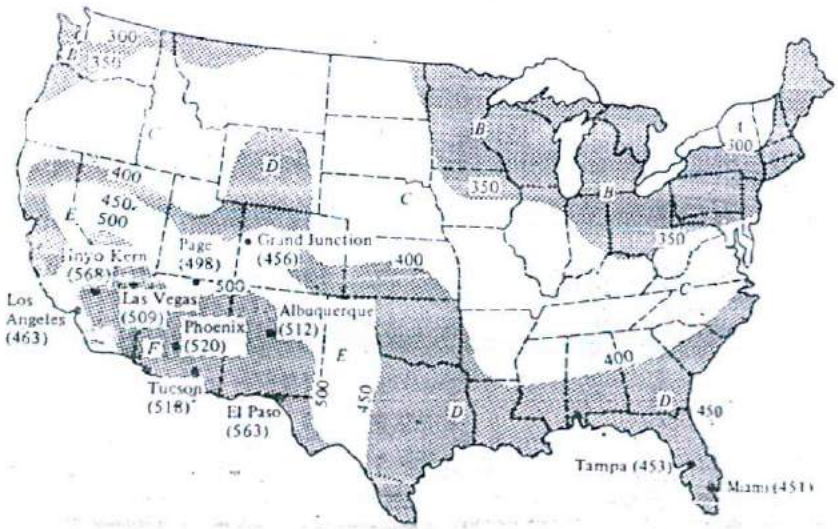


Figure 13-5 Annual mean daily solar radiation in the United States, areas $A < 300$, $B > 300$, $C > 350$, $D > 400$. $E > 450$, $F > 500$ langley/day. (1 langley = 1 cal/cm^2. 1 langley/day = 4.846×10^{-4} kW/m^2 = 0.01163 kWh/m^2 per day.)

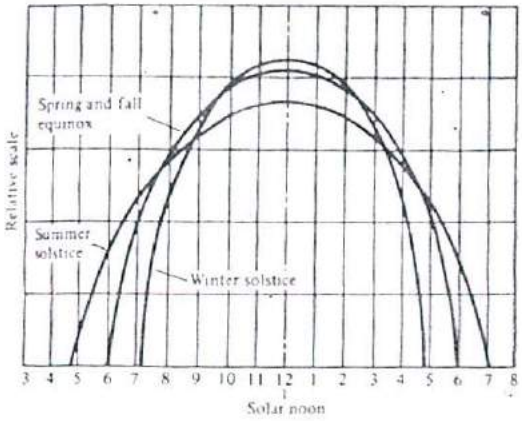


Figure 13-6 Daily variations of solar radiation falling on a surface perpendicular to beam radiation at both soltices and equinoxes in Albuquerque, New Mexico.

kW when the sun is shining. For a yearly average sunshine of 12 h/day, the total yearly extraterrestrial radiation would be $10^{13} \times 8766/2 = 4.43 \times 10^{16}$ kWh/year. Assuming an average clearness index C, of 50 percent, the terrestrial radiation received by the continental United States would be about 2.2×10^{16} kWh/year. Figure 13-5 shows the annual terrestrial mean daily solar radiation falling on the United States in langleys (1 langley = 1 cal/cm^2 = 41.87 kJ/m^2 = 0.0116 kWh/m^2 = 3.69 Btu/ft^2). Figure 13-6 shows an example of solar radiation falling on a surface normal to the sun's rays in Albuquerque, New Mexico, versus time of day based on the mean sun time* at the two solstices and either equinox. It is interesting to note that during the winter solstice, the maximum radiation is highest because the sky is clearest though it does not last as long during the day.

13-5 SOLAR-ELECTRIC CONVERSION SYSTEMS

The yearly consumption of all forms of energy in the continental United States in the early 1980s was 78×10^{15} Btu, or 2.286×10^{13} kWh, of which about 25 percent or 20×10^{15} Btu, or 5.86×10^{12} kWh, was used to generate electricity. At an average conversion efficiency of about 30 to 32 percent, the total electric-power consumption was about 1.8×10^{12} kWh/year.

* The *mean sun time* (MST) on earth is calculated from the *local standard time* (LST) for each longitude. The 360° of the earth are divided into twenty-four 15°-wide geographical time zones (artificially modified by political boundaries). An imaginary longitudinal line runs through the center of each time zone. It is called the *standard meridian* of that zone. (In the United States the standard meridians are located at longitudes 75° for eastern standard time, 90° for central standard time, 105° for mountain standard time, and 120° for Pacific standard time.) At each meridian the local standard time and the mean sun time are identical. At points within a zone east or west of its meridian, the mean sun time is later or earlier, respectively, than the local standard time. Because the earth rotates 360° in 24 h or 24 × 60 = 1440 min, each degree of rotation corresponds to 1440/360 = 4 min. Thus

It can be seen that the terrestrial solar incidence of 2.2×10^{16} kWh/year can supply some 1000 times all the energy consumption or some 12,000 the electric-energy consumption in the United States, if the entire surface area is available for collection and nothing is left for housing, industry, food growing, etc., and if the solar-to-electric conversion efficiency were 100 percent.

It is this abundance of "free" energy that has given solar proponents much ammunition, though their arguments ignore the fact that not all areas have dependable solar radiation (high average C_l), and even these suffer from daily and seasonal periodicity, and that solar-to-electric conversion is capital-intensive and inefficient. Still, such conversion is an engineering feasibility and, in locations remote from an electric grid, where the demands are low, may be an economic feasibility.

Solar energy may be converted to electricity by one of two means: *solar thermal conversion* or *photovoltaic conversion*.

Solar-Thermal Conversion

By this method solar radiation is converted to heat that in turn is added to a thermodynamic cycle to produce mechanical work and electricity. For this to be efficient, and hence economical, it is necessary to collect and concentrate the diffuse solar radiation in an efficient manner to arrive at a reasonably high-temperature heat source. The *collectors* gather the sun's energy and direct it onto *receivers* that contain the working fluid of the thermodynamic cycle. The receivers that are the subject of the most serious considerations are:

1. Central receivers.
2. Dispersed or distributed receivers. These could be of (a) the point-focus type or (b) the line-focus type.
3. Ponds.

$$\text{MST} = \text{LST} \begin{pmatrix} + \text{ degrees east} \\ \text{or} \\ - \text{ degrees west} \end{pmatrix} \text{of standard meridian} \times 4 \text{ min}$$

During periods of daylight saving time, LST is obtained by subtracting 1 h from the local daylight time (LDT).

The true or local sun time, called the *apparent solar time* (AST), and the mean sun time (MST) would be the same if the earth rotated around the sun in a circular orbit and thus at constant velocity. The somewhat elliptical orbit of the earth causes its velocity to vary and, therefore, the sun to appear on earth to be earlier or later than the mean sun time. The difference between AST and MST is called the *equation of time* (ET), which is not an equation at all but a variable correction factor that depends upon the time of the year as shown:

21st day of	Jan.	Feb.	Mar.	Apr.	May	June	July	Aug.	Sept.	Oct.	Nov.	Dec.
ET, min	−11.2	−15.9	−7.5	+1.1	+3.3	−1.4	−6.1	−2.4	+7.5	+15.4	+15.8	+1.6

Thus AST = MST ± equation of time.

The conversion systems used in solar-thermal-electric conversion are of many types. These include:

1. Rankine cycle, using steam or other working fluid
2. Brayton cycle, using helium or air as working fluid
3. Hybrid systems
4. Repowering systems

In addition, storage systems may be necessary. Systems producing process heat only are also receiving some attention.

Photovoltaic Conversion

Photovoltaic systems consist of direct-conversion devices in the form of cells that convert the solar radiant-energy photons to electricity without benefit of a thermodynamic cycle or working fluid. They can be their own collectors or can use concentrating collectors that focus the solar input on them.

The cells produce low currents and voltages and are therefore usually combined into modules that in turn are combined in panels and then arrays to meet specific power requirements. The cells are made of

1. Single-crystal silicon
2. Silicon with many crystals
3. Thin films with a wide range of single chemical compounds or combinations of them

These various devices will be covered in the next few sections in this chapter.

13-6 SOLAR-THERMAL CENTRAL-RECEIVER SYSTEMS

The central-receiver approach to solar-thermal-electric systems uses a large field of reflecting mirrors called *heliostats* that redirect the sun's energy and concentrate it on a central receiver mounted on top of a tower (Fig. 13-7). The heliostats are individually guided, since they cover a large field, so that each focuses the sun's energy it receives on the central receiver at all hours of sunlight. In the receiver the concentrated solar energy is absorbed by a circulating fluid. The fluid could be water, which vaporizes into steam that is used to drive a turbogenerator in a Rankine cycle, or an intermediate fluid that transports the heat to the steam cycle.

The system should incorporate storage for nighttime and cloudy periods, as shown in Fig. 13-7. The receiver output is made greater than that required by the steam cycle, and the excess output during periods of greatest solar incidence is bypassed to a thermal storage system. During periods of low or no solar incidence, the feedwater is shunted

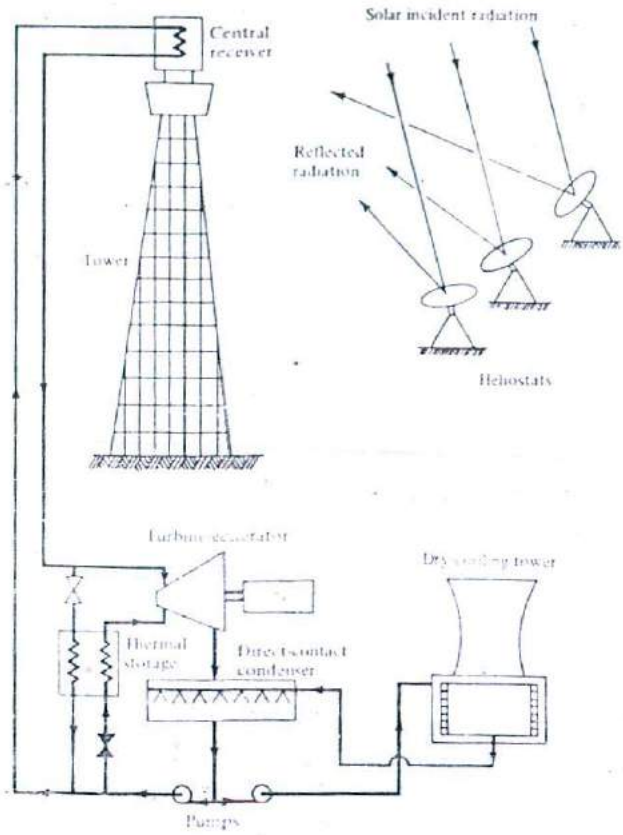


Figure 13-7 Schematic of a solar-thermal central-receiver system powerplant.

to the storage system, instead of to the receiver, where it vaporizes for use in the turbine. Proper valving in the system allows operation in either mode.

Because solar-thermal electric plants are most likely to be located in hot arid areas where land is plentiful (for the large heliostat field) and where the sun's energy is plentiful and dependable, but where cooling water is scarce, the condenser water is most probably cooled by a dry-cooling tower. Such towers are less effective and cause a reduction in Rankine cycle efficiency but require practically no makeup water (Sec. 7-7).

In the next five sections, the major subsystems of the central-receiver concept will be presented, with many of the design features and data obtained from the Solar One plant experience. Solar One is a 10-MW(e) (peak) pilot plant located in the Mojave Desert in California that went into operation and testing in mid-1982 (Sec. 13-11).

13-7 THE HELIOSTATS

The *heliostats** are reflecting mirrors that are steerable so that they can reflect the sun's rays on the central receiver at almost all times during the daylight hours. In essence, they keep the sun stationary as far as the receiver is concerned. They are made to track the sun, not by being perpendicular to its rays (as in distributed systems, Sec. 13-12) but by being at such an angle to these rays that they reflect them to the stationary receiver. This angle depends upon both the time of day and the position of the individual heliostat with respect to the receiver.

A heliostat is composed of a reflective surface or mirror, mirror support structure, pedestal, foundation, and control and drive mechanisms. Current designs have total reflective areas between 40 and 70 m^2. Ideally, the surface should be slightly parabolic with the focal length equal to the distance from the surface to the receiver but, because that distance is long, spherical or even flat surfaces offer good performance. There are two types of reflecting surfaces: *glass* and *plastic*.

A *glass heliostat* is typically divided into 10 to 14 panels rather than a single large surface for ease of manufacture and transportation (Fig. 13-8). A glass panel is typically a second-surface mirror (similar to household mirrors). The panels are usually rectangular, 1.2 × 3.6 m (4 × 12 ft) being typical. They are made of thin (1.5 to 3 mm) low-iron glass sheets to minimize absorption. The panels, when assembled, are canted slightly with respect to each other, with the canting varying throughout the field, to focus the sun's rays on the receiver.

Heliostats that use glass are much further developed at this time (1982) than plastic ones mainly because of their higher reflectance and strength. Current heliostats, therefore are constructed of glass and silver for the reflecting surface plus steel and aluminum or copper for the supporting structure. They must be constructed in a massive, sturdy manner to withstand strong wind loads and other severe weather conditions. They range widely in mass, from 5 to 60 kg/m^2 of mirror area, excluding foundation. The 10-MW(e) Solar One pilot plant uses 1818 glass heliostats of the type shown in Fig. 13-8, each containing 12 separate panels.

The heliostats currently account for about 45 percent of the total capital cost of a solar-thermal central-receiver powerplant (the tower and receiver account for about 11 percent each, the thermal storage system for about 17 percent, and the rest is divided among the land and the balance of the plant). A reduction in heliostat costs is therefore a major goal in reducing plant capital costs, which are currently estimated at 2 to 5 times the cost of conventional and nuclear powerplants, with a heliostat cost of about $\$250/m^2$. DOE second-generation heliostat studies indicate the cost would go down to $\$110/m^2$ to $\$150/m^2$ (in 1980 dollars) if ordered in quantity.

The *plastic heliostat*, although lower in reflectance and strength than the glass heliostat, promises lower costs, lower mass of the reflector surface, and hence lower mass and costs of the support structure and drive mechanism. A typical plastic heliostat design by Boeing (Fig. 13-9) has a reflecting, stretched plastic film disc of 16.7-m^2 area that is protected from wind loads by an air supported plastic bubble.

* From the Greek *helios*, "the sun." In Greek mythology: the sun god, son of Hyperion.

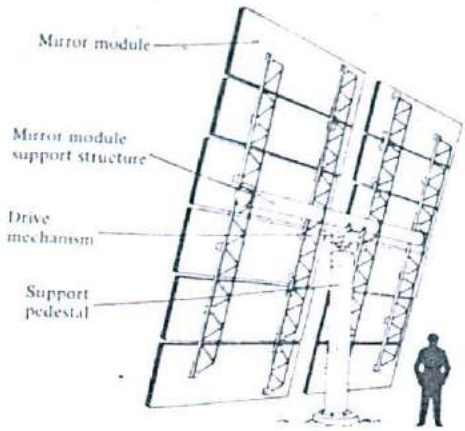


Figure 13-8 A typical glass-heliostat system, rear view *(McDonnell Douglas.)*

The Heliostat Field

The *heliostat field* supplying a central receiver, also called the *collector subsystem*, has a shape that must be optimized to suit the topography of the area and the power level of the plant. The field may be on a flat terrain, on the side of a hill, etc. In the northern hemisphere, the noontime sun is always south of the central-receiver tower, so a north field is usually most cost-effective because its cosine loss (below) is least.

For small plants, of less than 100 MW of thermal-energy input, a totally north field is optimum (Fig. 13-10*a*). As plant size increases, the field becomes larger and many heliostats are farther from the tower. The atmosphere around the plant attenuates the reflected radiation from the most distant north heliostats. The receiver input can then be improved by relocating the distant heliostats to the east and west of the tower and, as plant size increases further, to the south of it (Fig. 13-10*b*). In such cases, the additional cosine loss is less than the atmospheric attenuation loss from the distant north heliostats.

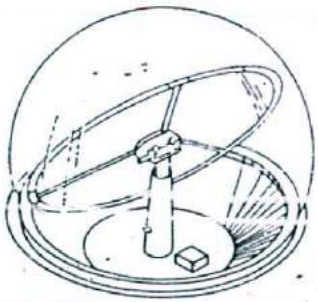


Figure 13-9 A typical plastic heliostat system *(Boeing.)*

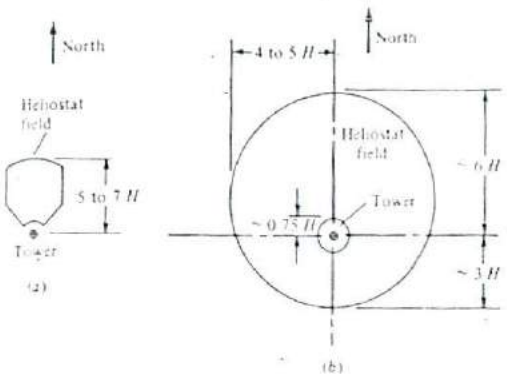


Figure 13-10 Optimum heliostat field shapes oriented for the northern hemisphere: (*a*) small plant < 100 MW(t) and (*b*) large plant > 5000 MW(t). Dimensions in multiples of receiver-tower height H [118]

The energy losses betwen the extraterrestrial (solar constant) and terrestrial insolations have already been discussed. There are, in addition, energy losses between the incident energy on the heliostat field and the receiver. These may be summarized by:

1. *Shadowing*. This is caused by one heliostat casting a shadow on the reflective surface of another at certain times of the day. (The tower shadow on the heliostats has a negligible effect.)
2. *Cosine loss*. Since the reflective surface of a heliostat is not perpendicular to the beam radiation from the sun, but assumes an angle that would reflect that beam to the central receiver, the area of solar flux intercepted by the heliostat is less than its reflective surface by the cosine of the angle between the surface and the perpendicular to the beam.
3. *Blocking*. This is the result when the reflected light from one heliostat is partially blocked by the back side of another.
4. *Reflective losses*. These result from absorption of the incident radiation by the glass and silvering and by scattering by dirt on the reflective surface. They prevent some of the light from being specularly reflected to the receiver.
5. *Attenuation*. This represents losses by absorption and scatter by water vapor, haze, fog, smoke, and particulates in the atmosphere between the heliostat and receiver.

The collector field, and the heliostat layout within that field, should therefore be optimized to transport the required thermal energy to the receiver at the lowest cost. As always, optimization implies trade-offs between usually conflicting requirements. For example, reducing shadowing and blocking by increasing spacing between heliostats results in greater attenuation, greater land use for a given energy input, and a larger image at the receiver, resulting in greater spillage (below).

Studies have shown that the most cost-effective layout of heliostats within their field is a radial stagger layout (Fig. 13-11). It minimizes losses by blocking and attenuation and results in minimum land use.

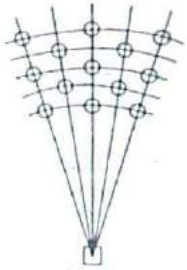


Figure 13-11 Radial stagger heliostat layout with respect to the receiver.

Heliostat Control

The insolation to the field varies from hour to hour, as well as seasonally (Fig. 13-6). At sunrise most of the heliostats are shadowed except in the extreme western sector. A similar situation occurs at sunset. A minimum practical amount of energy, usually considered at 10 percent of peak power, can only be collected when the sun is at an elevation of 15° or greater from horizontal. The reflected power and the receiver losses (below) are shown compared to the normal incident terrestrial insolation for the summer solstice, equinox, and winter solstice in Fig. 13-12, with a rapid rise and fall at 15° from sunrise and sunset. The receiver loss is nearly constant and independent of time of day as it operates at a fixed design temperature. Hence, that loss is a greater fraction of the input during off noon operation.

The daily operating cycle of solar-energy collection therefore includes morning start-up, operation during the power periods shown in Fig. 13-12, and evening shut-down. During nonoperation, the heliostats are placed in the *stow*, or storage, position. This is usually a horizontal face down or a vertical position. For morning start-up, they are maneuvered from the stow position to a standby position with the reflected sun rays aimed at a point adjacent to but not at the receiver itself. This maneuver may take as much as 15 min and may consume as much as 0.1 kWh per heliostat. The receiver is then started up (coolant pumped through), after which the heliostats are sequentially moved from the standby position to the operating position, i.e., with reflected sun rays aimed at the receiver surface. This prevents overheating of the receiver. Receiver flow controls also help prevent overheating.

During normal operation, the heliostats are in a *sun-tracking mode*, in which each is adjusted by a controller to keep the reflected sun rays at the aim point. Different heliostats can have slightly different aim points in order to spread the energy flux uniformly over the receiver surface. Sun tracking of the heliostats is accomplished by one of two methods. The first uses active reflected-beam sensors that control drive motors on the heliostat to orient the reflective surfaces so that the beam is continuously reflected to its aim point. The second method uses a preprogrammed computer control that orients the reflective surfaces according to their position with respect to the receiver.

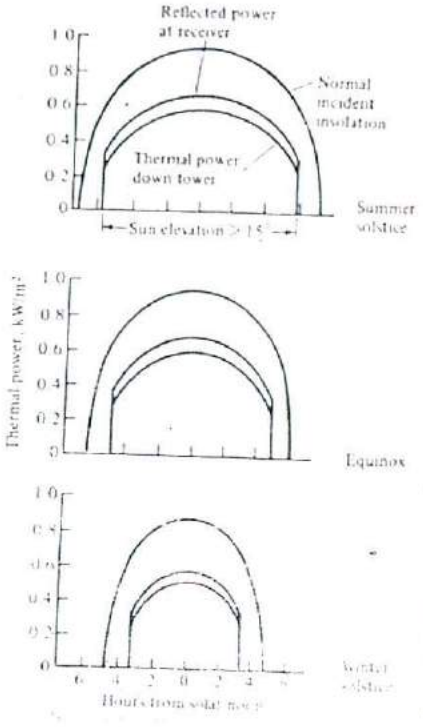


Figure 13-12 Incident normal insolation, reflected power reaching the receiver, and thermal power converted by the receiver at the two solstices and equinoxes, showing effects of start-up and shut down [118].

time of day, and day of year. Tracking in either method is done by adjusting two axes of rotation, azimuth and elevation, of the reflective surface.

The shutdown procedure is the reverse of the start-up procedure. The heliostats are moved from the sun-tracking mode positions to the standby position and then to the stow position. The stow position is used during the night but also during plant outages and periods of extreme weather (vertical stow in hail; horizontal for high winds; vertical slightly slanted upwards, for rain to take advantage of its cleaning action).

The control systems must be capable of extremely accurate reflective surface orientation (within a few milliradians) because even a tiny angle error would result in the reflected beam widely missing its aim point as a result of the long distance between heliostat and receiver. This accurate operation must also be maintained in strong winds by the rigidity of the heliostat support and structure.

Loss-of-coolant accidents (LOCA) require great attention to avoid damage to the receiver (a similar concern to that in nuclear reactors where a loss-of-coolant accident can result in overheating and damage to the reactor core and possible core fuel melt-

down). A LOCA must be met by shutting off the energy power input to the receiver by rapidly moving the heliostat aim points away from it, a process that might take 30 s. A back-up power-supply system is necessary in cases of concurrent loss of electric power. In that case, a passive-energy input reduction to the receiver, due to defocusing as the sun travels away from the set point, takes place, but the reduction is gradual and slow, taking 2 to 3 min for completion. As in nuclear reactors, consideration may have to be given to the installation of an emergency cooling system, especially for heavy receivers with a large thermal mass.

13-8 THE RECEIVER

Central receivers sit atop tall towers. [Solar One has a 94.5 m (310 ft) high tower.] They are subjected to peak radiation energy fluxes ranging roughly between 300 and 700 kW/m^2. The receiver is designed to intercept, absorb, and transport most of this energy to a heat-transfer fluid. Although radiation beams leaving the heliostats may be rectangular, the beam reaching the receiver is more circular because of the canting and focusing of the heliostat reflecting panels and because of the finite image of the sun. The flux distribution of the reflected beam reaching the receiver is approximately gaussian.

The heat-absorbing surface is usually similar to that in a water-wall, fossil-fueled boiler (Sec. 3-4): Panels of parallel tubes with headers at each end absorb the solar energy incident on their outside surface and conduct it to a heat-transfer or coolant fluid flowing inside. The panels are typically supported at the top to allow thermal expansion to occur downward.

There are two basic types of receivers under consideration: cavity and external (Fig. 13-13). A cavity receiver has coolant-tube panels lining the inner walls of the cavity. The tube-panel arrangement within the cavity is concave toward the heliostat field, and the panel area is 2 to 3 times the aperture area. The aperture area is sized about the same as the sun's image from the farthest heliostats. The aperture-to-panel area ratio is sized to minimize the sum of thermal losses and spillage (below). A cavity receiver may be designed with one or more cavities and apertures, each with a collecting sector with an angle between 60 and 120°. Figure 13-13*a* shows a four-aperture cavity receiver. The panels of adjacent cavities may form a common wall, heated from both sides, to reduce thermal stresses that result from one-sided heating (as in an external receiver).

The external receiver (Fig. 13-13*b*) has the coolant-tube panels lining the outside of the receiver. The panels may either be flat, for small plants, or slightly convex toward the heliostat field, for large plants. The external receiver shown is a multipanel polyhedron approximating a cylinder with a height-to-diameter ratio ranging between 1:1 to 2:1.

The coolant tubes range in diameter from 0.75 to 2.2 in (20 to 56 mm) and in thickness from 0.049 to 0.25 in (1.2 to 6.4 mm), depending upon pressure, material, and other engineering design considerations.

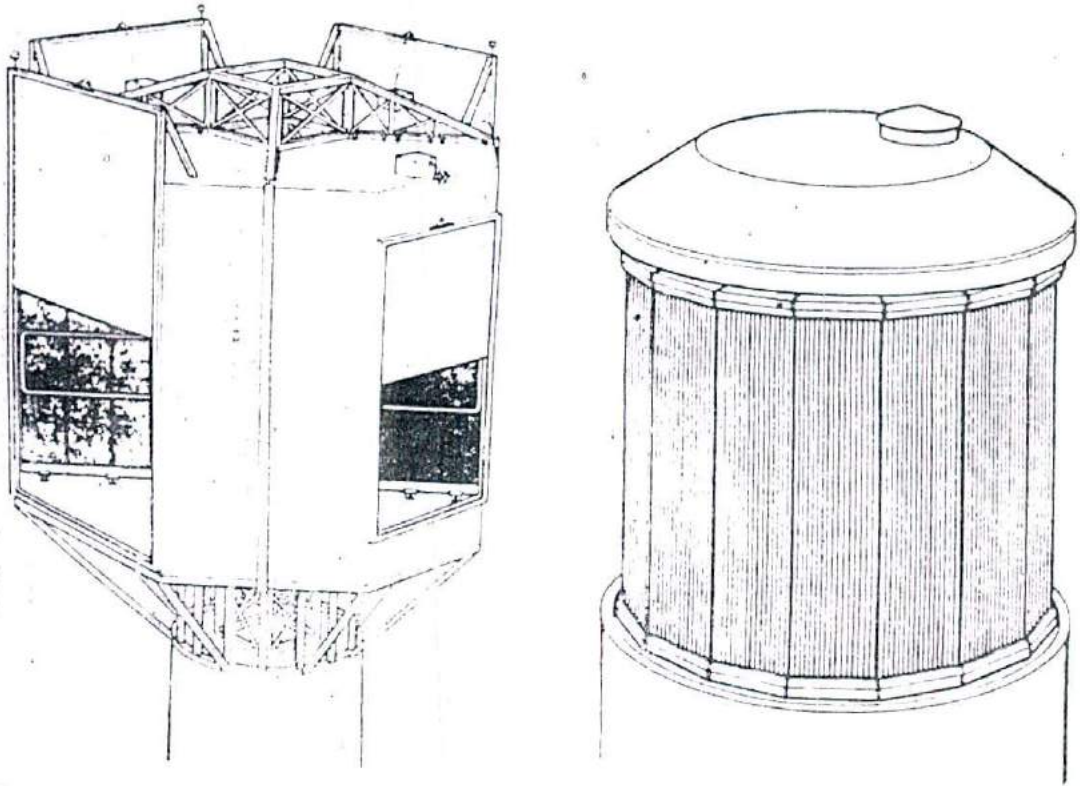


Figure 13-13 Typical central receivers: (*a*) four-aperture cavity type and (*b*) external type [118].

Receiver Efficiency

The efficiency of a receiver is defined as the ratio of the energy absorbed to that intercepted by it at the design point. The efficiency of a given receiver is the result of design compromises between several energy-loss mechanisms. These may be summarized as:

1. *Spillage.* This is energy reflected by the heliostats but not intercepted by the receiver heat-transport fluid. The reflected rays may miss the receiver altogether or fall outside an aperture (in a cavity receiver). Spillage may be caused by heliostat tracking errors caused by control system errors, wind effects, steering backlash, etc. Spillage is normally less than 5 percent in a well-designed system.
2. *Reflection.* This is energy scattered back from the receiver heat-transfer surface. It is minimized by painting these surfaces with high-absorptivity paint. It is typically less than 5 percent in a well-designed system.
3. *Convection.* This is energy lost by convection from the receiver body to the surrounding air. It is the sum of natural and forced (wind-driven) convection.
4. *Radiation.* This is energy lost by infrared radiation of the hot receiver surface back to the environment. Both convection and radiation losses are functions of the receiver temperature, its configuration, and type (cavity or external). The combined convection and radiation losses vary between 5 to 15 percent.
5. *Conduction.* This is energy lost internally through structural members, insulation, etc. It is the least of the losses, being typically much less than 1 percent.

Design optimization is important. For example, a large receiver enjoys low spillage but suffers from large convection and radiation losses. A cavity receiver has fewer reflection losses than an external receiver as well as less convection because the heat-transfer surfaces are protected (a cavity approximates a black body*). It does, however, have greater conduction losses because of its greater size and complexity.

Cavity receivers are therefore more efficient than external receivers. Cavity receivers designed by Honeywell and Martin Marietta companies showed efficiencies in excess of 90 percent. An external receiver designed by McDonnell Douglas Company showed an efficiency of approximately 80 percent. On the other hand, cavity receivers are much larger, heavier, and more costly than external receivers. In the designs proposed for Sōlar One, the cavity receivers had masses of more than 250 metric tons each, whereas the external receiver had a mass of approximately 136 metric tons.

* A black body can be closely approximated by a small aperture to a larger cavity. The radiation entering through the aperture is repeatedly reflected within the cavity with very little of it finding its way back out. The radiation is thus trapped inside, and the result is an absorbtivity nearly equal to unity.

13-9 THE HEAT-TRANSPORT SYSTEM

The heat-transport system is composed of the heat-transfer fluid (primary coolant), receiver piping, piping between receiver and power-generating equipment, and pumps. The primary coolant may or may not be the same as the powerplant working fluid. Five primary coolants have been extensively studied:

1. *Water-steam.* Water receives heat in the receiver, where it is converted to steam, which doubles as powerplant working fluid. The phase change in the receiver occurs as in conventional steam generators, either in a drum boiler with separate boiler and superheater sections, or in a once-through boiler without drum (Sec. 3-8). Steam may be generated at 1000 to 1100°F (540 to 600°C) and 1000 to 2000 psia (70 to 140 bar). The use of an all water-steam system has the advantages of least extension of technology and hence lower developmental costs. It is the one used in Solar One. Its performance, however, is considerd somewhat inferior to the other systems still under development.

2. *Liquid metals.* Liquid metals, particularly sodium Na, are under intensive development as heat-transport fluids for fast-breeder nuclear reactors (Secs. 11-3 to 11-5). Their main advantage is the high heat-transfer coefficients they are capable of, which result in a more-compact and lighter receiver. Sodium freezes at 208°F (98°C) and thus requires freeze protection during plant shutdown, either by heating the pipes or by draining them. Sodium is also chemically active, oxidizing rapidly in air or water. A cover gas such as argon, which is heavier than air, is used (as in sodium-cooled nuclear reactors) to protect the coolant and prevent oxidation and fires. Cold and hot traps need to be used to remove oxides and carbon respectively, from the sodium. Sodium may be operated up to 1000°F (540°C) as a single-phase liquid coolant [it has a normal boiling point of 1621°F, (883°C)] and must transport the solar heat to a steam generator at the plant site [119]. Liquid metals have low vapor pressures at the operating temperatures of interest and hence do not require high pressurization in the heat-transfer loop.

3. *Molten salts.* Molten salts are used as heat-transport agents in the chemical industry and have been used experimentally as nuclear-reactor fluid fuels. They, as liquid metals, do not require high pressurization at operating temperatures and, in addition, have high volumetric heat capacities. Nitrate salt mixtures have been proposed for solar central-receiver systems [120]. The salt can also operate at high temperature and transfer its heat to a steam generator at the plant site. It does, however, suffer from an even higher freezing point, about 290 to 430°F (140 to 220°C), which requires precautions against solidification during shutdown.

4. *Gases.* Gases can be operated at any temperatures desired that are compatible with component materials, often in excess of 1550°F (840°C). Pressurization is necessary only to overcome pressure losses in the coolant loop and to increase their mass-flow rates. The low heat capacities of gases require large volume flow rates and hence large flow velocities. Pressurization increases density and thus increases the volumetric heat capacity and decreases velocities, and hence pressure losses, for a given heat-transport rate. The gases considered are air and helium. They can be used as heat-

transport agents that generate steam in a steam generator in a Rankine-cycle powerplant, or they can be used directly in a Brayton-cycle powerplant gas-turbine of the open type (with air) [121], in a closed cycle (with helium) [122], or in a combined cycle [123] (Sec. 8-8).

5. *Heat-transfer oil.* Oils have the advantages of low-corrosion characteristics with most materials and can be selected for low vapor pressures. They are, however, flammable, can cause flow problems at low temperatures, and usually suffer pyrolitic damage, i.e., they decompose under high-temperature conditions, called *pyrolitic decomposition* (in a nuclear-radiation environment it is called radiolytic decomposition). The decomposition results in low boilers (gases and low-molecular-weight liquids) that cause an increase in system pressure and in high boilers (thick, gummy residue-type oils) that foul heat-transfer surfaces. They can only therefore be operated over a relatively narrow temperature range. Two suggested oils for solar central-receiver systems are Therminol 66 and Carolina HT-43 [124], which have an operating range of 20 to 600°F (−7 to 315°C). Oils are also used to transport receiver heat to a steam generator at the plant site.

The piping that takes the primary fluid from the receiver, down the tower, and across the heliostat field to the plant site is a major cost item of the total powerplant. Pipe sizes for a 400-MW(t) receiver range in ID from 1.0 to 1.5 ft (0.3 to 0.5 m) for molten salt to 8 ft (2.4 m) for air at 175 psia (12-bar) and in length up to 2000 ft (600 m) for both the hot and cold runs.

Because of the differences in their densities and heat-transport properties, the heat-transport fluids influence the mass of the receiver. For a 400-MW(t) receiver, the mass may range between 550,000 lb_m (2.5 metric tons) for a sodium-cooled external receiver to 5.5 million lb_m (2500 metric tons) for an air-cooled cavity receiver.

13-10 THE THERMAL-STORAGE SYSTEM

Although several energy-storage systems are possible, such as chemical, electrochemical (batteries), mechanical (compressed air, pumped hydro, flywheel), and single- or multiphase thermal energy (Chap. 16), the probable location of most solar powerplants precludes most such systems as being cost-ineffective. The one exception seems at present to be thermal single-phase energy storage. Such a system stores as sensible heat, i.e., without change in phase of the storage medium, some of the energy of the primary coolant after it has passed through the receiver. The energy thus stored is extracted when needed for use in the electric-generating station (or industrial process).

Energy storage is needed in solar-thermal-electric powerplants (and solar process-heat applications) because of normally variable solar insolation, nonsolar periods, and abrupt insolation changes in inclement weather. Conventional (fossil-fired) backup systems may, of course, be used during such periods, as in hybrid systems (Sec. 13-13), but thermal storage is another option that must be used in pure solar systems. There are two types of thermal storage that are considered with solar systems. These are (1) *single-tank*, or *thermocline*, and (2) *dual-tank*, or *hot-cold*, systems.

The *single-tank*, or *thermocline*, *storage system* is shown schematically in Fig. 13-7. Storage takes place by circulating some of the hot primary coolant through the storage medium and returning the cooled primary coolant from the bottom of the storage tank back to the receiver for reheating. Heat extraction during times of need is accomplished by reversing the process: cold primary coolant from the powerplant is heated by the storage medium, drawn from the top of the tank to the power system, and then returned to the bottom of the tank. The thermal gradient of hot at top, cold at bottom maintains stratification, allowing the hot fluid to remain afloat on the top, and gives the tank thermal stability. In addition, a solid storage medium of low thermal conductivity and high volumetric heat capacity, such as rock, is used to help impede mixing of hot and cold fluids. A solid storage medium is a necessity in case the primary coolant is a gas (such as air or helium) because of the low heat capacity of gases. A porous solid makes a good storage medium for gases.

Figure 13-14 shows temperature-time characteristics of a thermocline thermal-storage system. Note that the temperature gradient is never completely flat at any one time, a factor that affects the performance of such systems (below).

A variation of the thermocline system is one in which a separate storage fluid, other than the primary coolant, may be used. This would be a liquid of low thermal conductivity and high volumetric heat capacity, usually an oil. It may be used alone as a single medium or be assisted by a solid storage medium, such as rock in a dual-

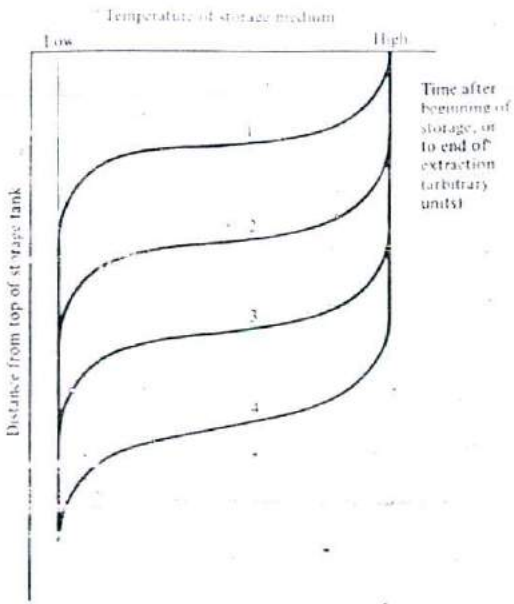


Figure 13-14 Temperature-time characteristics of a thermocline storage system.

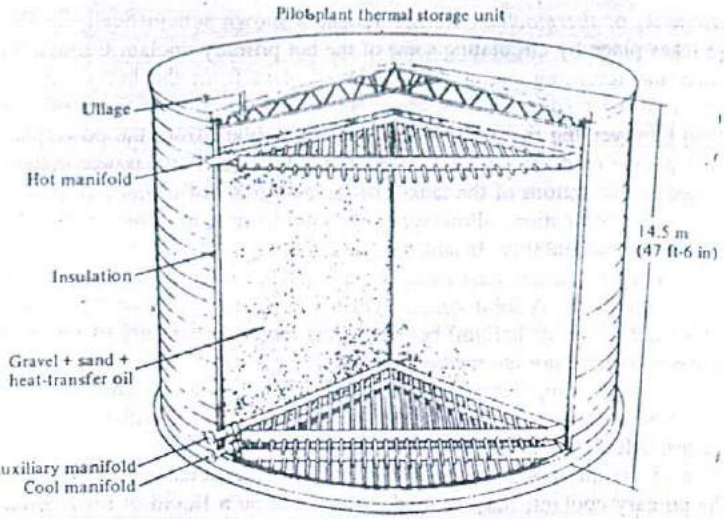


Figure 13-15 Thermocline storage system for the Solar One pilot powerplant.

medium system as above, to reduce the volume of costly storage liquid and impede its mixing. Heat would be added to and extracted from the primary coolant via intermediate heat exchangers.

The Solar One powerplant uses a dual-medium thermocline storage system, shown in Fig. 13-15. The liquid is oil. The solid is composed of 1-in diameter gravel plus sand. The oil is uniformly distributed over the rock bed and extracted uniformly from it by diffuser manifolds. The tank is large, being nearly 50 ft (14.5 m) high and more than that in diameter.

The *dual-tank*, or *hot-cold, system* uses two tanks. The fluid, a liquid, is, unlike the stratified thermocline system, at one temperature, hot in one tank, cold in the other. The amount of sensible energy stored varies by varying the level of the fluids in the well-insulated tanks (Fig. 13-16). Thus, during storage, cold liquid is drawn from the cold tank, heated, and added to the hot tank. During extraction the operation is reversed. This dual-tank technology is borrowed from refinery work. It is suitable only for liquid coolants such as sodium, molten salt, or oil. The hot tanks used with sodium and molten salt need be made of high-alloy material such as austenitic stainless steel.

Thermal-energy-storage densities vary widely among the different storage media. Some typical values for the temperature range 550 to 1050°F (290 to 565°C) are given in Table 13-3. The Solar One pilot plant has an oil-rock storage medium that operates at the much lower temperature range of 425 to 575°F (220 to 300°C) and has an energy storage density of 5300 Btu/ft^3 (0.05 MWh/m^3).

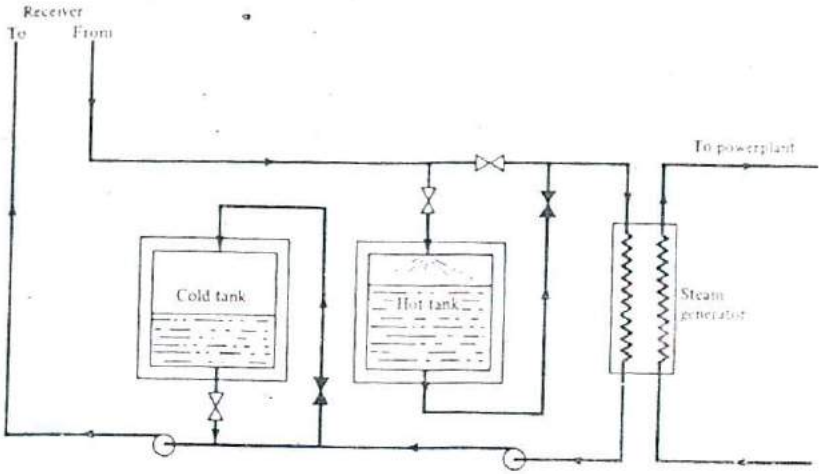


Figure 13-16 Schematic of a dual-tank, or hot-cold, thermal-storage system. Valves shown in normal plant operating and storing mode.

Insulation is an important consideration in storage tanks to minimize loss of energy during holding periods. Another important consideration is the fraction of stored energy that is usually extracted. This fraction is called the *storage utilization factor*. In dual-tank or hot-cold storage systems it is usually in excess of 0.98. In single-tank or thermocline systems the factor is lower because of the temperature gradient that exists at any one time during charging or discharging (Fig. 13-14). During discharge, there comes a time when the temperature drops below maximum, thus necessitating an operational limit on the total energy extracted. For thermocline systems the storage utilization factor is nearly 0.8 for liquid-solid systems but less than 0.5 for gas-solid systems. Note that a low utilization factor does not mean a loss of energy because in a well-insulated system energy losses are small. It simply means that a large and costly tank(s) is required.

Storage sizing can be made to supply enough thermal energy, together with direct

Table 13-3 Typical thermal-storage densities

Medium	Energy storage density	
	Btu ft^3	MWh/m^3
Sodium	8000	0.08
Rock, 25% void fraction	14,000	0.15
Molten salt (nitrate)	21,000	0.22

thermal power from the receiver, to operate the powerplant for 24 h/day. However, if the sizing is based on the long days of the year, it will not have sufficient capacity for the short days of the year. The opposite results in an excess storage capacity during part of the year. Sizing thus depends upon many factors, including variations in daily and seasonal load demands, cloud conditions, availability of backup power, and cost. The costs of storage capacity must include those of additional heliostats to fill it and a large receiver, as well as the storage system itself.

Figure 13-17*a* shows a cloudless daily operating cycle of a central-receiver system with thermal storage. The thermal-power down tower is less than direct solar insolation because of the various losses already explained. Morning start-up utilizes some of the stored energy, resulting in the dip in its curve shown between 4 and 6 h before solar noon. The plant operates on stored energy until the receiver input exceeds the end use (powerplant or process heat) demand. At that time, about 4 to 5 h before solar noon, the excess solar power is made to recharge the storage system and the receiver supplies both end use and storage. At 4 to 5 h after solar noon the declining solar input is supplemented from storage energy until the heliostats and receiver systems are shut-down. After that, all end use is supplied from storage. Figure 13-17*a* assumes, for

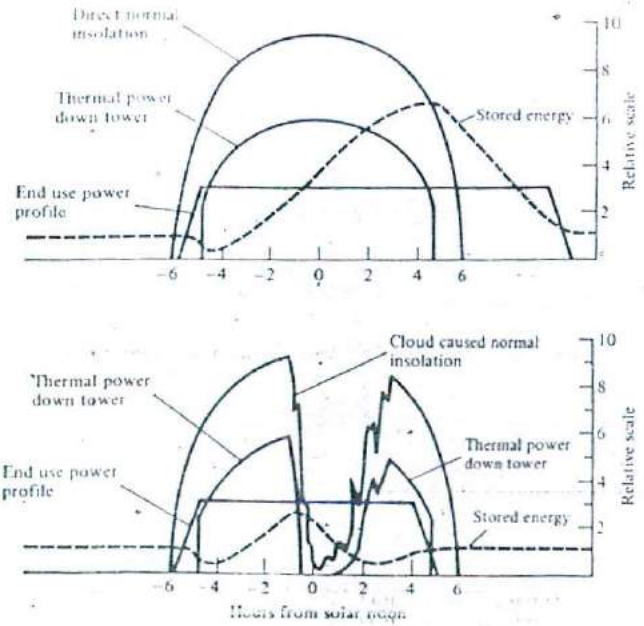


Figure 13-17 Typical daily operating cycle of a central-receiver system with thermal storage and constant power (end use): (*a*) cloudless day and (*b*) cloudy day [118].

simplicity, a constant end use, which is not usually the case. Figure 13-17*b* shows the effect of a cloudy period during the day. Note that the scales for all curves, except stored energy should be in power units, e.g., kilowatts. For the latter, the scale should be in energy units, e.g., kilowatt hours.

13-11 WORLD EXPERIENCE

Central-receiver systems are receiving attention in many parts of the world. In the United States, with 68 solar-thermal projects of various kinds taking place, the major activity in the late 1970s to early 1980s was the development, construction, and operation of Solar One, the 10-MW(e) (peak) pilot plant referred to earlier. The plant cost $140 million and is situated in the Mojave Desert at Dagget, about 12 mi southeast of Barstow, California. It is owned by Southern California Edison Company and is financed jointly by the Department of Energy (DOE) and a group of utilities. Figure 13-18 shows an overall view of Solar One.

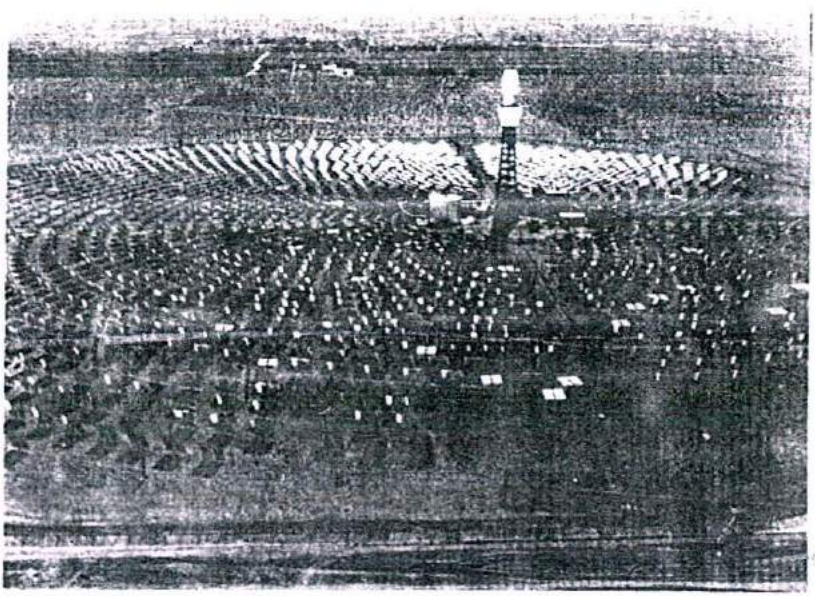


Figure 13-18 Overall view of Solar One, a 10-MW(e) (peak) central-receiver pilot powerplant near Barstow, California

McDonnell Douglas Corporation and Martin Marietta Corporation were the major contractors. The plant uses water-steam as the heat-transport and working fluid with thermal storage using oil as the storage heat-transport fluid. It started operation in the summer of 1982. It reached a 10.4-MW(e) net output on 10 October 1982. The storage system, rated at 7 MW(e) maximum, had not met that goal at that time. The first 2 years of operation are devoted to experimental testing of the major subsystems and evaluating requirements and costs of operation and maintenance. This period will then be followed by full power tests to obtain long-term operating, maintenance, and reliability data.

In Almeria, Spain, the International Energy Agency, several European countries and the United States have funded a 500-kW(e) plant that uses molten sodium as the heat-transport and thermal-storage fluid. The sodium-receiver exit temperature is 975°F (525°C). The plant has 93 heliostats of 430 ft^2 (40 m^2) each that are supplied by the Martin Marietta Corporation. It has a cavity receiver atop a 140-ft (43-m) tower. The plant started operation in September 1981. An interesting feature of this plant is the installation of a parallel distributed system of 500 kW(e) using line-focus receivers (Sec. 13-12) to compare its performance with that of the central-receiver system. Another plant in Almeria, Spain, scheduled for completion in late 1982, is a 1.2-MW(e) central-receiver system called CESA-1. It has 300 heliostats, 430 ft^2 (40 m^2) each, a cavity receiver, water-steam at 975°F (525°C) as the heat-transport and working fluid, and a 3-MWh(th) thermal storage using Hytec as the storage fluid. It is funded by Spain and the United States, with heliostats built in France and Germany.

In Adrano, Sicily, Italy, a 1-MW(e) central-receiver plant, called Eurelios, began operation in May 1981. It has a cavity receiver atop a 180-ft (55-m) tower that produces steam at 950°F (510°C), and a 30-min thermal-storage subsystem to even out cloud transients that uses Hytec as the storage fluid. The project was developed by a consortium from Italy, France, and Germany.

In France, a 2-MW(e) plant called Themis, has 200 heliostats, 560 ft^2 (52 m^2) each, a cavity receiver with molten salt heated to 975°F (525°C) as the heat-transport fluid, and a 4-MWh(th) thermal-storage system using Hytec as the storage fluid. Start-up was scheduled for early 1982.

Japan has its "Project Sunshine" in the form of a 1-MW(e) plant in Nio Town, Nagawa Prefecture. It has 807 small heliostats of 172 ft^2 (16 m^2) area each, a semicavity receiver atop a 197 ft^2 (60-m) tower producing steam at 480°F (250°C), and a 3-MWh(th) thermal storage system using pressurized water as the storage medium.

13-12 DISTRIBUTED SOLAR-THERMAL SYSTEMS

Another approach to solar-thermal energy conversion, besides the central-receiver-tower concept, is the *distributed* or *dispersed solar-thermal system*. Rather than hundreds of heliostats focusing solar energy on a single distant receiver atop a tall tower, this system is characterized by the use of a large number of collectors, called *concentrators*,

each focusing the solar energy it receives directly on its own receiver to heat locally a heat-transport fluid. The fluid is combined with those from other concentrators for thermal-electric conversion. Distributed systems are of two kinds: *point focus* and *line focus*.

The *point-focus system* generally uses concentrators each in the form of a mirrored parabolic dish that tracks the sun but focuses the captured energy on a receiver mounted at the focal point of the parabola, a few feet from it. Figure 13-19 shows two advanced concentrator concepts by Boeing, Inc., and E-Systems Corp., which are believed to offer the potential for low-cost production. The Boeing design uses a reflecting surface made of thin plastic films on sheet steel substrates. The E-Systems design uses a domed Fresnel-lens concept with the lenses focusing the solar energy at a common focal point.

The Jet Propulsion Laboratory (JPL) operates a facility for testing dish-concentrator systems and components at Edwards Air Force Base in California. The U.S. Department of Energy is in the process of building (1982) an array of parabolic dish concentrators to be used for electric production, heating and cooling, and low-temperature process steam for a knitwear plant nearby. Figure 13-20 shows a number of point-focus concentrators undergoing testing at the Sandia Laboratories, Albuquerque, New Mexico.

The *line-focus system*, also called the *trough system*, uses concentrators in the form of long troughs of cylindrical or parabolic cross sections, which are lined with mirrors to collect and concentrate the sun's radiation onto a focal linear conduit through which the primary coolant flows (Fig. 13-21). Because of their geometry such troughs are usually made to track the sun in only one plane, by being rotated about their focal line. Thus, other than solar noon, they receive sun's rays that get more inclined with respect to their projected surface as the sun deviates from solar noon. They, therefore, usually operate in the lower-temperature ranges of 200 to 600°F (about 90 to 315°C). Line-focus systems are thus believed suitable only for small-sized electric-generating systems for which thermal efficiency is not of prime importance and for other applications such as driving irrigation pumps (one of their earliest uses, Fig. 13-1*d*), providing industrial process heat, space heating and cooling, and other industrial applications, but not for large-scale electric production.

A variation of the line-focus system, called the *line-focus bowl*, which is being tested under DOE sponsorship, uses a stationary mirror-lined spherical collector that concentrates solar energy on a conduit receiver that moves during the day. Heat received from a number of such bowls can be used for small-scale electric production, space heating and cooling, the production of process steam, etc.

Of all the distributed concepts, the line-focus systems are the beneficiaries of the most experience in industrial and commercial process-heat installations where the temperature requirements are lower than necessary for efficient large-scale utility electric production. Point-focus systems, on the other hand, are least developed. It is believed, however, that they have the potential for achieving the temperatures necessary for utility electric production. Being modular, they have the additional advantages of meeting the demands of a wide range of load requirements and of adding to existing capacities by incremental installation.

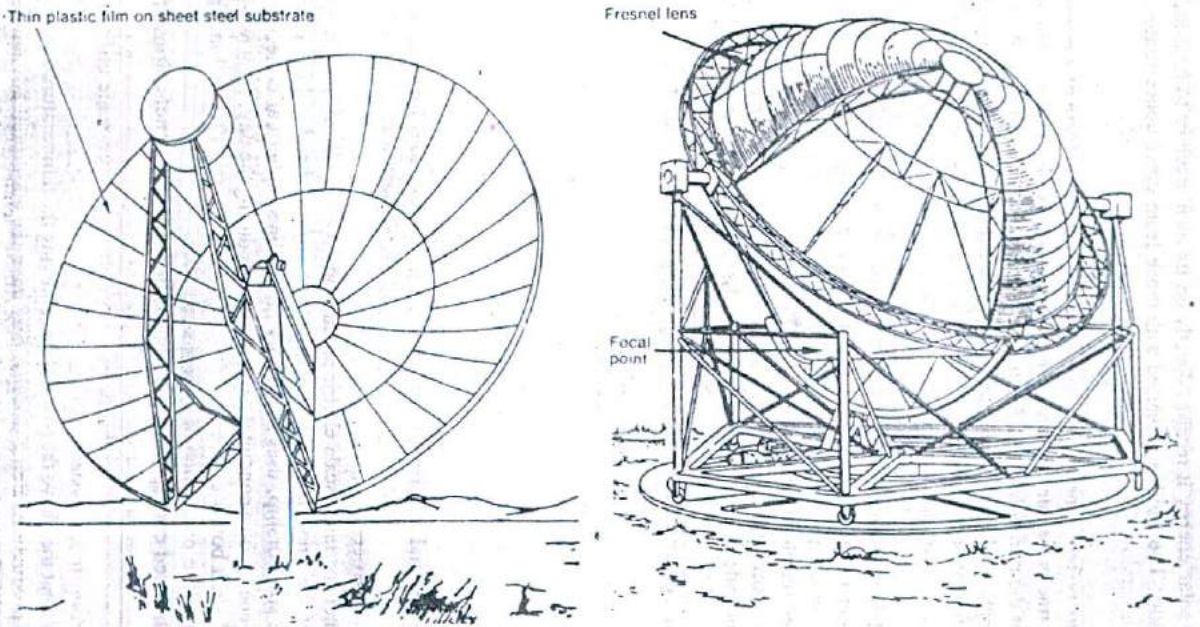


Figure 13-19 Point-focus distributed-type concentrators: (*a*) thin plastic film reflecting panels by Boeing, Inc. (*b*) Fresnel-lens concept by E-Systems Corporation [125].

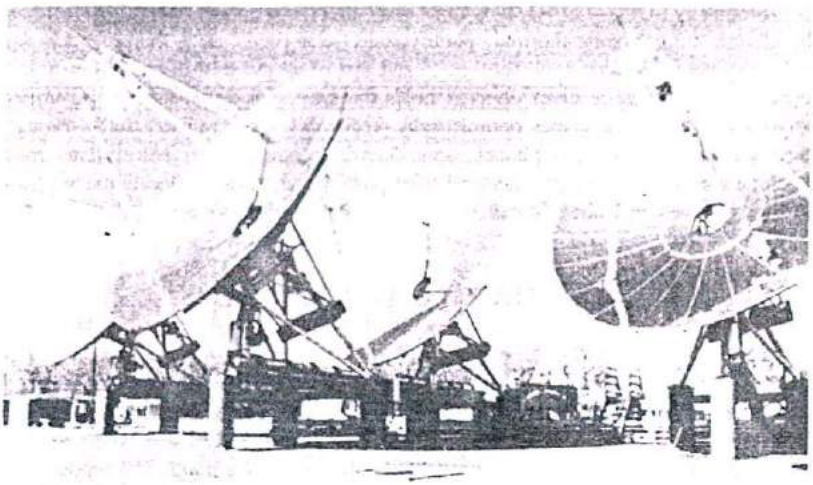


Figure 13-20 Point-focus dish concentrators. *(Courtesy Sandia Laboratories.)*

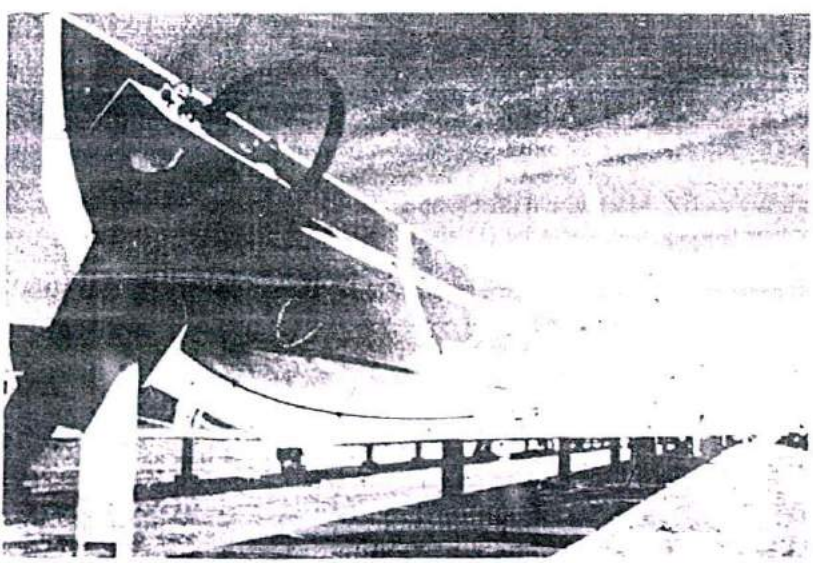


Figure 13-21 Line-focus trough concentrators. *(Courtesy Sandia Laboratories.)*

Studies by DOE and EPRI show that "of all direct solar options under consideration by electric utilities (solar-thermal, photovoltaic, solar ponds, etc.), the prospects for solar-thermal conversion look the best," and that of all the solar-thermal conversion concepts, the central-receiver concept holds the greatest potential for electric utility applications [126]. The studies optimistically predict that, if carried successfully through the test and demonstration phases, solar-thermal central-receiver powerplants may become competitive with gas- and oil-fired powerplants in certain locations, such as in the southwestern United States.

13-13 OTHER SOLAR-THERMAL POWER SYSTEMS

Repowering

It is believed by some that the next step that will pave the way toward commercialization of solar-thermal systems, after the pilot plants such as Solar One and others around the world are tested, would most probably be the *repowering plant*. The repowering concept implies the adding of a solar-thermal-conversion plant to an existing fossil-fueled plant in sunny locations to replace some of the fossil fuel used in the latter, perhaps 10 percent. It is believed that the concept of repowering might be economically attractive in case the fossil fuels being replaced are gas or oil, which are expensive, but it is doubtful that would be the case with coal or nuclear fuels.

Hybrid Plants

A *hybrid system* is conceived to compensate for the intermittency of solar energy, not by storage but by using the sun as the source of heat when available and sufficient and a fossil fuel, such as oil or gas, at other times. DOE and EPRI studies of the hybrid concept have concentrated on the Brayton cycle as the main prime mover. The primary coolant, which would double up as the receiver heat-transport fluid and gas-turbine working fluid, could be (1) air, (2) helium, or (3) other gas mixtures. (An interesting variation is the use of gases that undergo reversible chemical reaction with temperature, such as SO_3, to give proper specific heat and enthalpy properties.) Although a Brayton cycle is simpler in concept than a Rankine cycle, it requires much higher temperatures in order to attain comparable efficiencies. In general a Rankine-cycle powerplant, solar or fossil, uses steam at temperatures of 1000 to 1100°F (about 540 to 590°C) and pressures of 1000 psia (about 70 bar) and beyond. Solar Brayton-cycle plants operate with gases at much lower pressures but, to be competitive, at much higher temperatures. This poses severe design and materials problems on the receiver. DOE and EPRI have sponsored studies aimed at the design and operation of receivers containing high-temperature metallic alloy and ceramic components. Figure 13-22 shows a ceramic honeycomb receiver developed by Sanders Associates and tested at the JPL Parabolic Dish Test Site, Edwards, California. The receiver is mounted on an 11-m-diameter test concentrator so that concentrated solar energy passes through

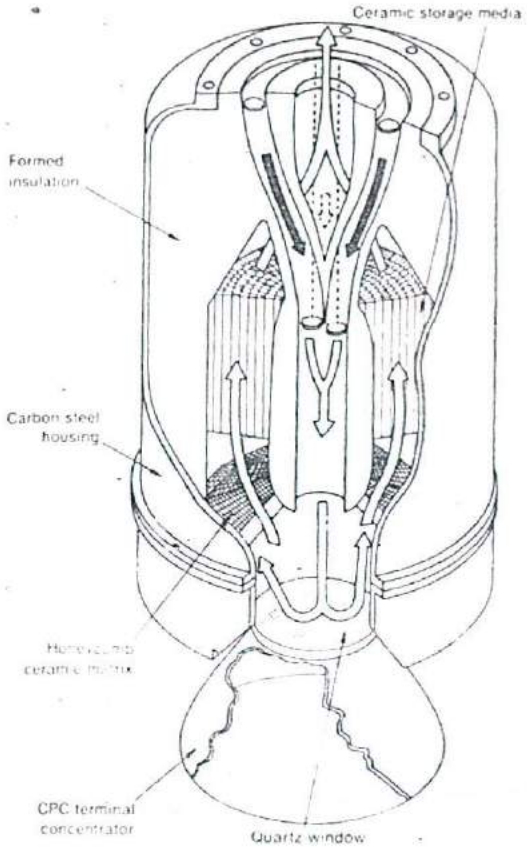


Figure 13-22 High-temperature honeycomb ceramic matrix receiver for Brayton-cycle applications [125].

the quartz window and is absorbed by the ceramic honeycomb. Air is pumped downward, reverses direction, and goes up the honeycomb, leaving at top center. Tests have shown air outlet temperatures ranging between 1470 and 2600°F (800 to 1430°C), which are useable in present-day gas turbines or those with cooled blades currently under development (Sec. 8-7).

Stirling-Cycle Conversion

Another hybrid concept uses the Stirling cycle. The ideal Stirling cycle is a regenerative cycle composed of four reversible processes: two constant volume and two constant temperature (Fig. 13-23). Heat is added and rejected during the constant temperature processes 2-3 and 4-1 respectively. Heat is exchanged internally between the constant-

volume processes 3-2 and 1-2. With all processes reversible and heat added and rejected only at constant temperatures, the ideal Stirling cycle has a thermal efficiency equal to that of Carnot. No actual engine can be built that simulates a Carnot cycle. However, actual Stirling engines have been built based on the ideal Stirling cycle (much as actual Diesel engines are based on the ideal Diesel cycle, etc.), and although they do not have efficiencies equal to the ideal cycle, they attain respectable efficiencies of 35 to 40 percent.

A Stirling engine driving an electric generator can be directly coupled to the receiver of a solar concentrator. A number of such engine-concentrator systems, hooked in parallel electrically, can then constitute a distributed point-focus-system powerplant. In addition the engines can have an integral fossil-fuel (oil or gas) burner, which results in a distributed hybrid powerplant.

An experiment at the JPL test site was conducted in the summer of 1981 using a model P-40 Stirling engine developed by United Stirling Company of Sweden. It was mounted on a parabolic dish that concentrated the solar energy on a receiver with a fused silica aperture. The engine was mounted directly on the receiver body (Fig. 13-24). The engine working fluid, air, operated in closed-cycle mode with a maximum temperature of 1500°F (816°C). Heat rejection was by a water coolant. The engine was equipped with fossil burners, and no storage was needed. The induction-type alternator produced 25 kW(e). The conversion efficiency was about 35 percent. The experiment was designed to pave the way for large generating plants based on dish Stirling modules with dish diameters 9 to 22 m and corresponding power outputs of 15 to 100 kW(e). A 10-MW(e) plant is envisaged to be composed of 150 modules of 65 to 75 kW(e) each and to occupy about 50 acres of land. Being modular, smaller systems can be erected to supply small remote communities, military installations, etc.

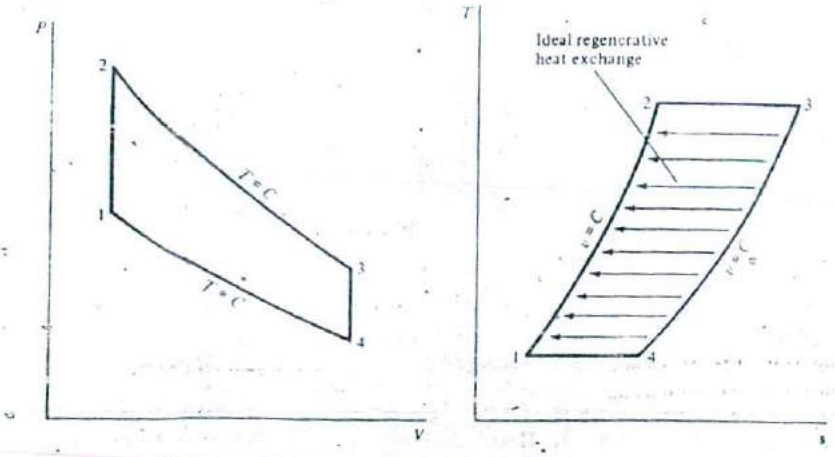


Figure 13-23 *P-V* and *T-s* diagrams of an ideal Stirling cycle.

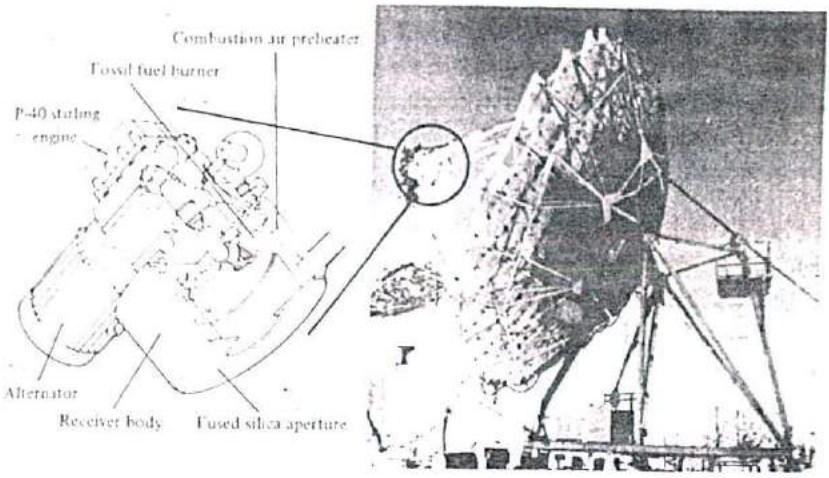


Figure 13-24 JPL test bed with parabolic bed concentrator and Stirling engine. *(Courtesy Jet Propulsion Laboratory.)*

Combined-Cycle Systems

Combined cycles are those using a combination of Brayton- and Rankine-cycle-type powerplants with the gas turbine of the Brayton cycle occupying the high-temperature end and exhausting to the steam generator of the Rankine cycle (Sec. 8-8).

Figure 13-25 shows a combined-cycle with a two-shaft gas turbine and a solar central-receiver system. Atmospheric air is compressed by the compressor into a high-temperature receiver where it is heated to perhaps 1500°F (815°C). It then expands through the compressor turbine and through the power turbine, which drives an electric generator. The exhaust air is then ducted to thermal storage and/or to the steam generator of the Rankine cycle, depending upon solar generation and load demand. During periods of no solar insolation the steam generator is heated by air driven through the thermal-storage system by a separate compressor. Supplemental auxiliary firing for the steam generator may be used.

An alternative scheme uses the gas-turbine exhaust air for industrial process heating.

13-14 SOLAR PONDS

Large bodies of water, such as lakes, receive vast quantities of solar radiation because of their large areas. Such bodies usually have water that contains solids in solution with concentrations that vary little with depth. When solar energy is received and absorbed below the surface (water at the surface is partially transparent to solar ra-

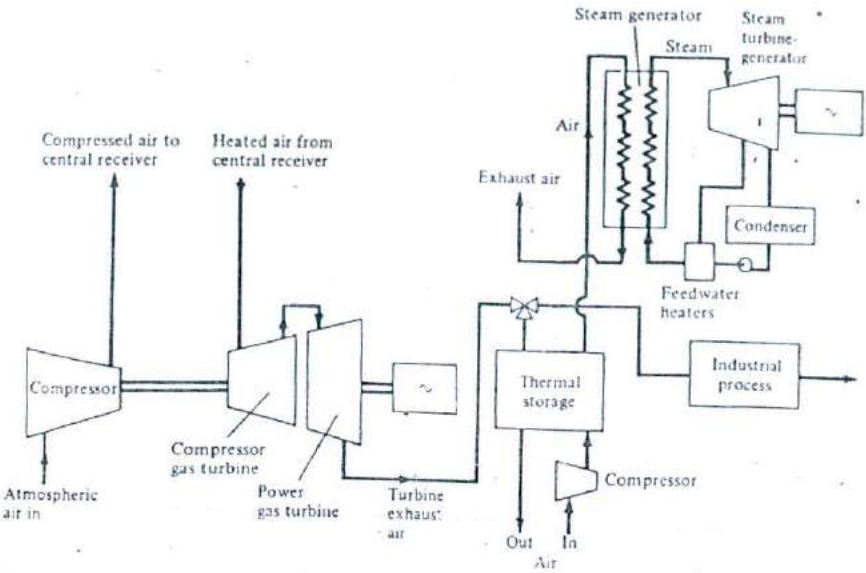


Figure 13-25 Schematic of a combined gas-steam cycle adapted to a solar central receiver.

diation), the warmer water becomes less dense and rises to the top. The result is a convective circulation that keeps cooler water at the bottom and retransports the solar energy back to the surface. There it is dissipated partly by conduction and convection to the atmosphere but mainly by evaporation since the vapor pressure at the surface is usually higher than the partial pressure of water vapor in the atmosphere. The latent heat of vaporization of the diffusing vapor is extracted from the water itself, and energy balances result in the water temperature remaining below ambient.

Some natural saltwater lakes, however, have exhibited the opposite behavior, namely, that the temperature gradient is reversed with warmer water at the bottom and cooler water at the top. That temperature gradient was found to exist because these lakes contained a nonuniform vertical concentration of salts with greater concentration at the bottom than at the top. This causes the bottom water to have a greater density and to remain at the bottom, even though it may be hotter. The solar energy absorbed in the deep layers is effectively trapped there because the effect of salt on density offsets the effect of thermal expansion. The temperature gradient is now reversed and temperature is higher at the bottom than at the top.

Solar ponds, also called *solar salt ponds*, take advantage of this phenomenon in two ways: (1) the conversion of solar energy to useful work as a result of the temperature difference between bottom and top and (2) the use of the pond as a thermal-storage medium so that the conversion can take place at a rate that is largely unaffected by

daily and weekly fluctuations in solar input. A solar pond is, therefore, in effect, a combined solar collector and storage medium.

Figure 13-26 shows a schematic of an artificial solar pond and conversion system. The bottom warm water is used as the heat source for the powerplant, the top cool water as the heat sink. Because these layers flow out and in to their respective heat exchangers, they are subjected to convection currents. The pond is therefore divided into three layers. The central layer is nonconvective and contains the required salinity (and density) gradient with salinity greatest at the bottom. This central layer isolates a low-salinity (and density) convective layer at top, which is the heat sink, and a high-salinity (and density) convective layer at the bottom, which is both heat source and storage medium and which is insulated from the atmosphere above.

In constructing solar ponds, about one-third of a ton of salt is added per square meter of pond area. Provisions must be made to prevent leakage of the solution into the ground and subsequent heat transfer to it. In a well-designed and constructed solar pond, the bottom layer can reach about 200°F (93°C).

The hot bottom water is pumped through an evaporator and back to the bottom. The working-fluid vapor drives a turbogenerator. The turbine exhaust is condensed in the condenser, and the condensate is fed back to the evaporator. The condenser cooling water is obtained from the top cool layer of the pond. Because the temperature difference between the heat source and heat sink is not great enough, a turbine cycle working fluid other than water-steam, such as an organic fluid, is used.

The salt in an artificial solar pond tends to spread throughout the height of the pond by diffusion, a process that is slow but one that if allowed to continue would result in uniform salinity, convection currents, and an ineffective pond. The required

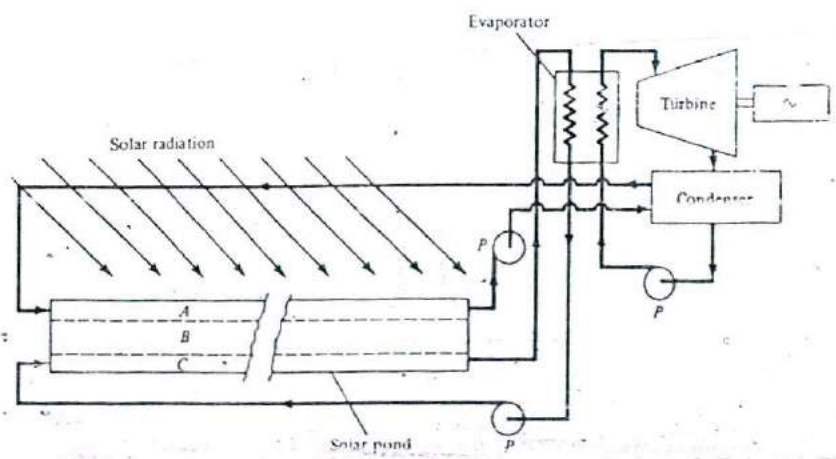


Figure 13-26 Schematic of a solar pond powerplant. A = low salinity-density convective layer; B = salinity-density gradient nonconvective layer; C = high salinity-density convective storage layer.

gradient is maintained by methods that include injecting salt to the bottom layer and flushing the top layer with fresh water.

Because of the relatively low temperature differences encountered in solar ponds, the thermal efficiency of the electric powerplants is nowhere near a fossil, nuclear, or even solar-thermal power system. They do, however, have the potential for trapping vast amounts of solar energy in regions where both solar energy and land are abundant. Besides electric generation, they may be more suitable for industrial uses such as space heating and cooling, crop drying, desalination, and other process heat. The necessity of having both large land mass and sunny climates, and also available water and salt, make solar ponds unlikely to be large contributors to the total energy picture, although they may have appeal in certain locations where there is land, sun, and salt or brakish water. Several test solar ponds have operated near the Dead Sea in Israel, for example. A 5-MW facility is under construction there (1982). In the United States studies are underway by the NUS Corporation to investigate the feasibility of a demonstration 300-kW solar pond facility in eastern California. Figure 13-27 shows an artist's conception of such a facility. The studies are aimed at determining the optimum pond areas, depths, salinity, and clarity and at evaluating the seasonal performance of ponds and conversion systems, the effects of atmospheric and ground and soil conditions, as well as costs of construction, operations, and maintenance.

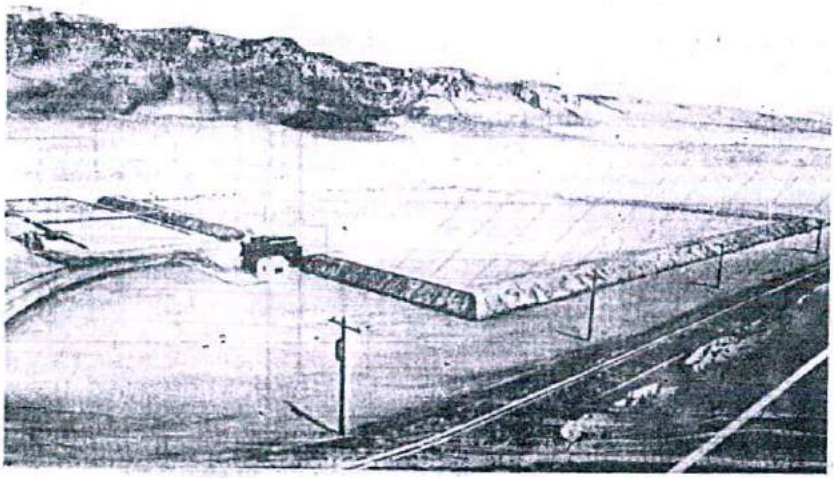


Figure 13-27 Artist's rendering of a solar pond powerplant for the Los Angeles Water and Power. *(Courtesy NUS Corporation.)*

13-15 PHOTOVOLTAIC-ENERGY CONVERSION

Photovoltaic energy conversion is a direct conversion technology that produces electricity directly from sunlight without the use of a working fluid such as steam or gas and a mechanical cycle such as Rankine or Brayton. Photovoltaic systems, therefore, appear simple, convenient and, lacking moving parts, dependable. In addition they are modular, so that arrays of identical modules can be assembled to meet various power needs ranging from small residential systems installed on rooftops to relatively large central systems.

The basic unit of a photovoltaic system is the *solar cell*. The most common solar cells are made of highly refined silicon that is solidified as a single crystal in ingots (by the slow withdrawal of a seed from molten silicon), from which thin wafers are cut and polished (with the loss of almost half the original material). A doping material is introduced into the wafers to convert them into semiconductors (below) that are used to make photovoltaic cells. When sunlight strikes the cells, an electric potential is produced and current flows when the cell is connected to an external load.

Silicon solar cells are typically circular wafers, about 3 in (7.6 cm) in diameter and 300 μm thick, although square or rectangular wafers are being developed to increase the useful fraction of the total area exposed to sunlight when the cells are assembled side by side. A single cell typically produces a power of 1 W at a voltage of 0.5 V. They are then connected electrically in series-parallel arrangement, called a *module*, to produce the required current and voltage. A module is typically 4 × 4 ft (1.2 × 1.2 m). Several modules make up a *panel*. A panel is the design unit for assembling large photovoltaic *arrays* to meet the required power generation. Figure 13-28 shows a photovoltaic array field covering three-fourths of an acre and consisting of 2366 modules. It supplies 60 kW to a U.S. Air Force base at Mt. Laguna, California.

Photovoltaic electricity was first generated for a meaningful purpose in 1958 to power a radio transmitter on the Vanguard space satellite. It has since been used successfully to generate electricity in remote areas, such as in space, for navigation aids, in telecommunications on offshore installations, for isolated microwave relay stations, and similar uses. Coupled with batteries for storage, solar cells generate electricity for such uses more economically than any other method.

The costs, however, are very high when compared with other means where fossil or nuclear fuels are available and where the demands for electricity are very large. The unit costs of photovoltaic electricity started around $200 per peak watt for electricity from satellite modules in 1959. The price came down to $22 by 1976. Currently (1982) with annual manufacture of cells nearly 4 MW of peak electric capacity for remote needs, the price came down further to around $10, still a very high cost that can be afforded only by the space and defense industries. Government planners optimistically estimated a goal of 500 MW of annual photovoltaic electricity by 1986, a volume production that would cut the cost to $0.70 per peak watt (in 1980 dollars). This market goal does not now look likely to be reached, and the price is expected to remain relatively high.

It is to be noted further that the cost of end-use electricity is not dependent only

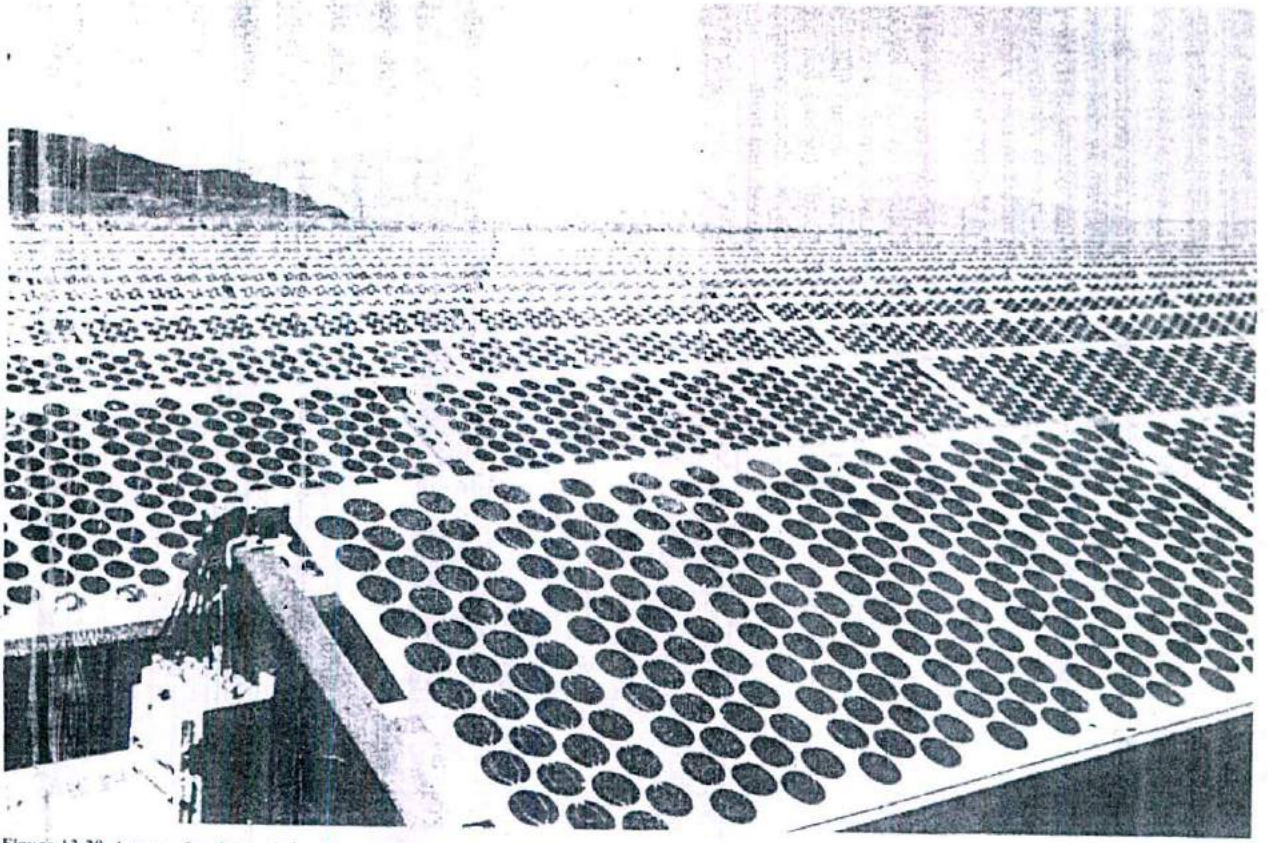


Figure 13-28 A view of a photovoltaic silicon-cell array field. *(Courtesy Solar Energy Research Institute, Golden, Colorado.)*

upon the cells alone but also upon the cost of the balance of the plant of which the cells are only a part. The nonphotovoltaic part of the plant, such as land, foundations, structures, wiring, dc-to-ac power conversion, connections to the utility grid, and cooling, currently represent two-thirds of the total capital cost. Thus, at $10 per peak watt the total plant capital cost would be about $30,000 per peak kW. This is some 15 to 20 times the cost of fossil or nuclear plants. Considering that a photovoltaic plant operates at peak only a small part of the time, the real ratio is much higher.

Efforts at reducing all costs include a search for lower-cost cell-manufacturing techniques [127] and for materials other than silicon. Besides single-crystal silicon, materials being investigated include multicrystal silicon, thin films of cadmium and copper sulfide, and amorphous (noncrystalline) silicon.

13-16 SOLID-STATE PRINCIPLES

In this and the next section we will cover some of the basic solid-state phenomena that are important in the study of the mechanism of direct conversion of solar radiation to electricity. These two sections may be bypassed without breaking the continuity of the chapter.

Solid Phenomena

A metallic crystalline solid contains atoms that have nuclei surrounded by electrons that are tightly bound to them (the shell model) and by outer electrons that are weakly bound to them. The latter are called *valence*, or *conduction*, electrons. They are free to migrate in the *interior* of the metal because there are no *net forces* on them because of the other free electrons or the ionized nuclei and their bound electrons. They thus move in an essentially equipotential field, each having a constant electrostatic *potential energy* E_i that is independent of its location inside the crystal, and they are considered to belong to the entire crystalline solid rather than to any one particular atom. These valence electrons constitute the primary mechanism of electric and heat conduction in a metal. At the surface, however, there are no positive ions on one side to give them equal attractive forces. Thus, while they are easily moved by electric fields within the metal, they encounter an *energy barrier* at the surface and require considerably more energy to get them out of the metal.

One therefore has an *electron gas* that is *confined* within the metal. It is not, however, equivalent to an ordinary gas whose energy distribution is given by the Maxwell-Böltzmann law. Electrons, instead, exist in states restricted by the so-called *Pauli exclusion principle* (which specifies that no two electrons in the same atom can exist in the same state at the same time), and their energy distribution is given by the *Fermi-Dirac distribution law*, given for temperatures that are not too high (not greater than 3000 K) by [128]

$$n(E)\,dE = \left[\frac{4\pi}{h^3}(2m_e)^{3/2}\right]\frac{E^{1/2}}{1 + e^{E - E_F/kT}}\,dE \tag{13-3}$$

where $n(E)\,dE$ is the number of electrons per unit volume in the energy range dE. The quantities between brackets are constants: h is Planck's constant (6.625×10^{-34} J · s), and m_e is the mass of the electron (9.13×10^{-28} g). The balance of the righthand side is energy dependent. k is the Boltzmann constant [1.38×10^{-23} J/(molecule · K)]. The quantity E_F is called the *Fermi energy*. It is a constant for many cases of interest, being nearly independent of temperature.

A plot of the energy distribution of an electron gas, Eq. (13-3), is shown in Fig. 13-29 at different temperatures. The quantity $E^{1/2}$ contributes the parabolic rise of the curves from $E = 0$. The quantity

$$P(E) = \frac{1}{1 + e^{(E - E_F)/kT}} \tag{13-4}$$

is called the *Fermi-Dirac probability distribution function*. Note that, unlike a classical gas, free electrons do *not* all have zero energy at absolute zero but rather finite energies *up to a maximum* given by E_F, the Fermi energy. At $T = 0$, the probability distribution function is 1 from $E = 0$ to $E = E_F$, meaning that the probability that any state between energies 0 and E_F is occupied by an electron is 1 and is zero for $E > E_F$.

At higher temperatures, the high-energy portion of the distribution is different from that at $T = 0$. The probability that states much less than E_F are occupied is still 1, the extent depending upon the value of T. For $E = E_F$ the probability is exactly 1/2 (independent of temperature). For energies much greater than E_F, the exponential term is much greater than the 1 in the denominator of Eq. (13-4), and the probability reduces to the Maxwell-Boltzmann distribution probability (given by $Ae^{-E/kT}$, where A is a constant).

The Fermi energy can be computed by evaluating the total number of free electrons per unit volume n as

$$n = \int_0^{E_F} n(E)\,dE = \frac{4\pi}{h^3}(2m_e)^{3/2} \int_0^{E_F} E^{1/2}\,dE$$

$$= \frac{8\pi}{3h^3}(2m_e)^{3/2}E_F^{3/2}$$

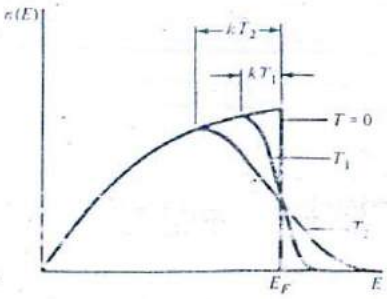


Figure 13-29 Energy distribution of an electron gas at different temperatures, $T_2 > T_1 > 0$.

from which

$$E_F = \frac{h^2}{2m_e}\left(\frac{3n}{8\pi}\right)^{2/3} \tag{13-5}$$

The values of E_f for metals are typically of the order of a few electron volts (eV),* about 7 eV for copper and 3.1 eV for sodium. It can also be easily shown that the *average energy* of a free electron at $T = 0$ is equal to 3/5 E_F, or a few electron volts, much higher than the average kinetic energy of a particle in a classical gas even at high temperatures, which is given by 3/2 kT, thus being zero at $T = 0$, about 0.025 eV at room temperature, and 0.1 eV at 1160 K.

The behavior of free electrons at temperatures higher than 0 is important. At moderate temperatures, the corners of the zero temperature distribution (Fig. 13-29) are only slightly rounded. The difference increases as the temperature increases and becomes significant only within the energy range

$$|E - E_F| \approx kT \tag{13-6}$$

and, as indicated previously, the probability that the state $E = E_F$ is occupied is 1/2. The free electrons whose energies are much less than the Fermi energy remain locked in the same energy states they occupied at $T = 0$ irrespective of temperature. A fraction of the most energetic electrons, those having energies within kT of the Fermi energy, occupy higher energy states than the Fermi energy. Such electrons can be elevated to these energies by collision with energetic particles such as high-energy photons or by thermal excitation (the basis for thermionics).

The Band Theory

Photovoltaic devices, like thermoelectric devices, require a knowledge of the distinction between conductors, insulators, and semiconductors. Electrical materials differ in their electrical conductivities by factors as high as 10^{30}. The *band theory* of solids helps us understand this distinction as well as the phenomena of electrical and thermal conduction. A quantitative treatment of the band theory involves detailed wave mechanics and is beyond the scope of this book. The following is an adequate (for our purposes) qualitative presentation of some aspects of that theory.

In a system of noninteractive (or isolated) atoms of the same species, as in a gas, the valence electrons occupy a set of single-energy levels, corresponding to permitted states of that species (Fig. 13-30*a*). When these atoms are brought together, such as in a crystalline solid, they interact strongly and thus cause the energy levels to spread throughout a set of *energy bands* (Fig. 13-30*b*). The regions between the energy bands of the interacting atoms, like those between the levels of noninteracting atoms, cannot be occupied by electrons and are called *forbidden bands*. The widths and spacings of

* An electron volt (eV) is a unit of energy equal to the energy acquired by a single electron charge when accelerated through a potential of 1.0 V. 1 eV = 1.6021×10^{-19} J = 4.44×10^{-26} kWh = 1.519×10^{-22} Btu. 1 million electron volts (MeV) = 1.6021×10^{-13} J.

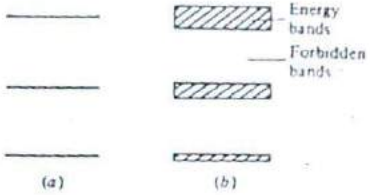


Figure 13-30 (*a*) Electron energy levels in a noninteractive atom. (*b*) Electron energy bands in an interactive atom.

the energy and forbidden bands depend upon the crystalline material in question. Energy bands may be occupied, only partially filled, or completely unoccupied. The shading in Figs. 13-30 to 13-32 indicates which bands are occupied.

High conductivity in a metallic crystal is caused by its uppermost band *not* being completely filled with electrons. An external electric field causes the electrons in this band to gain small amounts of energy that are sufficient to promote them to the continuum of available states immediately above this band. Distribution of electrons among the available states may be varied slightly by energizing them. The shift is controlled by the Fermi-Dirac statistics (above), and therefore significant shift occurs only for those electrons that are within a range $\pm kT$ of energy about the uppermost filled level at $T = 0°$.

Figure 13-31 shows energy bands of a conductor (sodium) and an insulator (diamond). For sodium, the 3*s* band is partially filled, the 3*p* band is unoccupied, and the two bands overlap. The number of unoccupied levels readily available for the 3*s* band electrons is therefore large, which results in high electrical conductivity. Diamond, on the other hand, has two 2*p* energy bands, one filled, one unfilled, separated by a forbidden band that is 6 eV wide. This *gap* is much larger than kT at room or high temperatures (above) so thermal excitation, or weak electrical or other fields, will not impart sufficient energy to promote the electrons to the unoccupied 2*p* band and create electron flow or an electric current. The same applies to photons of visible light that do not lose energy to the electrons, which is the reason why diamond is transparent to visible light.

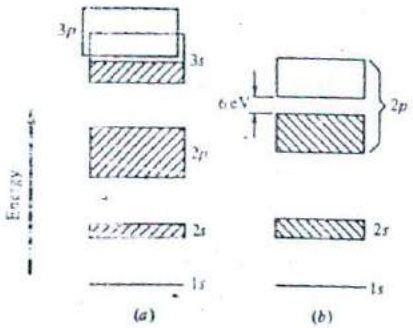


Figure 13-31 Electron bands for (*a*) a conductor, sodium, and (*b*) an insulator, diamond

The uppermost filled, or partially filled, energy band is called the *valence band*, and the next empty but available energy band is called the *conduction band*. A substance is a conductor if these two bands are separated by a very narrow forbidden gap or if they overlap. A substance is an insulator if they are separated by a large gap.

13-17 SEMICONDUCTORS

There is a class of crystalline solids where the forbidden band between the valence and conduction bands is relatively small, about 1 eV. Silicon and germanium are examples, with gaps of 1.1 and 0.7 eV, respectively. Such solids behave as insulators at low temperatures. At very high temperatures, an appreciable number of electrons receive sufficient thermal energy to be promoted into the conduction band, the number being a function of both the temperature and the gap width—and thus the material becomes a conductor. Such a material (a pure material) is called an *intrinsic semiconductor*.

Semiconductors are manufactured by adding controlled amounts of impurity to the pure material, 10^{17} atoms per cubic centimeter being typical. These are called *extrinsic*, or *doped, semiconductors*. The impurity adds an allowed energy level (not band) in the forbidden band between the valence and conduction bands. There are two types: *n-type* semiconductors and *p-type* semiconductors (Fig. 13-32).

In *n-type semiconductors* the allowed energy level is near the bottom of the conduction band; this is called the *donor level*. It has an abundance of electrons that, at room temperatures, are easily excited into the conduction band (since the gap is very narrow). By contrast only a few electrons (one shown) are intrinsically (due to the pure material) elevated from the valence to the conduction bands.

In *p-type semiconductors* the allowed energy level is near the top of the valence band; this is called the *acceptor level*. The impurity has an electron deficiency. At room temperatures, electrons are easily excited from the valence band to the acceptor level, thus leaving a deficiency of electrons in the valence band. The absence of an electron is called a *hole* and may be considered a positively charged particle. Again

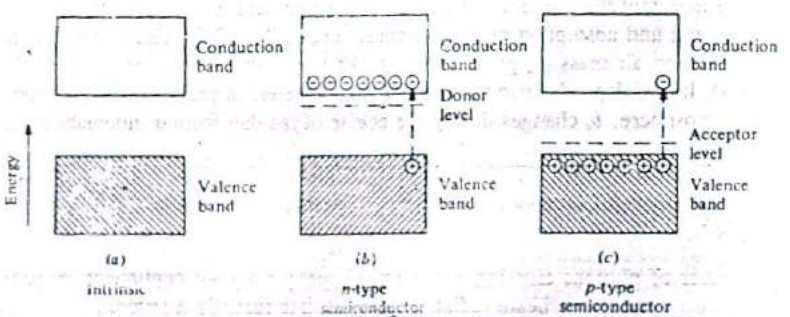


Figure 13-32 Electron energy bands for three types of semiconductors.

intrinsic motion of electrons is small by comparison and conduction in a p-type semiconductor, therefore, is largely the result of the movement of holes to the valence band. In both types of semiconductors, the conductivity is largely determined by the amount and form of the impurities.

Photons

Energy, on a microscopic scale, is transferred not continuously but in discrete pieces, the smallest of which is the *quantum*. Light is radiant energy, whose quantum is called a *photon*. Max Planck was the first to suggest that the energy of a photon is proportional to the frequency of radiation, or

$$E_p = h\nu = h\frac{c}{\lambda} \tag{13-7}$$

where E_p = photon energy

h = Planck's constant, 6.6256×10^{-34} J · s, 4.13576×10^{-15} eV · s

ν = frequency of radiation, hertz

c = speed of light, 2.997925×10^8 m/s

λ = wavelength of radiation, m

At any given frequency ν, light energy is thus a whole or multiple of $h\nu$, never a fraction of it. Light thus has a dual personality. It is characterized both as energy transferred in discrete amounts, the photons, and in waves having a frequency and, therefore, wavelength. Radiation from the sun, or any other radiant source, is therefore composed of energy chunks, the photons, each one carrying a quantity of energy exactly equal to its frequency times Planck's constant.

Thus a monoenergetic radiation beam having a wavelength of half a micrometer, 0.5 μm = 0.5×10^{-6} m, the energy of a single photon is

$$E_p = 4.13576 \times 10^{-15} \frac{3 \times 10^8}{0.5 \times 10^{-6}} = 2.48 \text{ eV}$$

Recall now that the spectral distribution of the terrestrial solar radiation depends upon scattering and absorption of several constituents (Fig. 13-3). Recall also that it depends upon an air mass m_a given by $m_a = 1/\cos \theta_z$, where θ_z is the zenith angle (Sec. 13-4). It also depends upon the number of centimeters of precipitate water vapor ω in the atmosphere. θ_z changes during the course of the day from a minimum $\theta_{z,\min}$ that occurs at noon and that varies with the seasons between $\theta_{z,\min}$ = latitude ± 23.45°, and 90°.

A quantity useful in photovoltaic-cell calculations is the photon flux ϕ_p. It is defined as

ϕ_p = number of photons crossing a unit area (usually a square centimeter) perpendicular to beam radiation per unit time (usually a second)

The solar energy flux E'' is related to the photon flux simply by

$$E'' = \Sigma_i \phi_{p,i}\, h\nu_i \tag{13-8a}$$

where the subscript i indicates a frequency or energy range. Equation (13-8*a*) may be simplified by assuming an average frequency ν_{av} and corresponding wavelength λ_{av} and obtaining a total photon flux ϕ_p. Thus

$$E'' = \phi_p h\nu_{av} = \phi_p h(c/\lambda_{av}) \tag{13-8b}$$

Outside the earth's atmosphere, the solar energy flux is equal to the solar constant $S = 1359$ W/m^2, or 0.1359 W/cm^2, $m = 0$, $\omega = 0$, and the average photon energy $h\nu_{av} = 1.48$ eV.

Thus
$$\phi_p \text{ (extraterrestrial)} = \frac{0.1359}{1.48} \times \frac{1}{1.6021 \times 10^{-19}}$$
$$= 5.8 \times 10^{17} \text{ photons/(s} \cdot \text{cm}^2\text{)}$$

Both terrestrial insolation and the average photon energy decrease as m increases and as ω increases. The photon flux thus decreases from $5.8 \times 10.^{17}$ above, to about half that amount at $m = 3$ and $\omega = 5$ [129].

When the sun's rays, i.e., the sun's photon flux, strike a *pn* semiconductor junction, they help generate electron-hole pairs; i.e., they cause electrons to be raised to the conduction band in the *n* material and holes to be moved to the valence band in the *p* material. When connected to a load, electrons will thus diffuse from *n* to *p* across the junction, thus creating an electric current through the load and hence electric power, which is a function of the photon flux.

13-18 THE SOLAR CELL

Figure 13-33 shows a schematic representation of a solar cell composed of *pn* semiconductor junctions. For single-crystal silicon, *p* is obtained by doping silicon with boron and is typically 1 μm thick; *n* is obtained by doping silicon with arsenic and is typically 800 μm thick. Thin film cells are composed of copper sulfide for *p*, typically 012 μm thick, and cadmium sulfide for *n*, typically 20 μm thick.

The sun's photons strike the cell on the microthin *p* side and penetrate to the junction. There they generate electron-hole pairs. When the cell is connected to a load as shown, the electrons will diffuse from *n* to *p*. The direction of current I is conventionally in the opposite direction of the electrons.

Typical voltage-current characteristics are shown in Fig. 13-34 at two different solar radiation levels. For each

V_o = open-circuit voltage

I_o = short-circuit current

P_m = point of maximum power $(VI)_{max}$

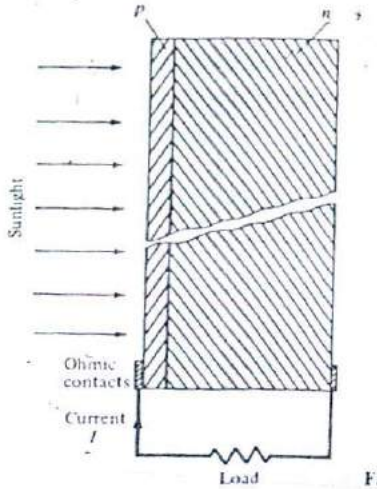


Figure 13-33 A schematic cross section of a solar cell.

Solar cells do not convert all solar radiation falling upon them to electricity. Weak, low-frequency (long-wavelength) photons do not possess sufficient energy to dislodge electrons. Strong, high-frequency (short-wavelength) photons are too energetic, and although they dislodge electrons, some of their energy is left over unused. Table 13-4 shows a breakdown of solar energy wavelength distribution, the fraction utilized by a typical cell and the percent solar energy converted, ideally, to electricity.

There, thus, is a maximum theoretical efficiency of solar cells, around 48 percent. *Efeciency* is defined as the ratio of electric power output of the cell, module, or array to the power content of sunlight over its total exposed area. Efficiencies of modules

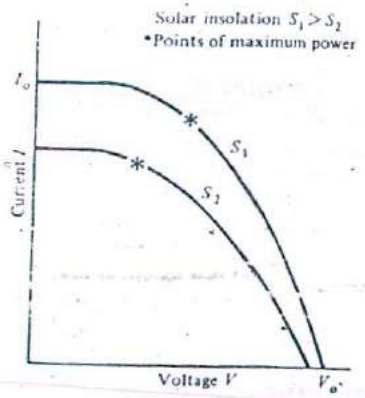


Figure 13-34 Typical performance characteristics of a silicon solar cell at two solar radiations.

Table 13-4 Ideal spectral solar energy utilized by silicon cells

Wavelength range, μm	Solar energy, %	Fraction converted, by cell	Solar energy converted, %
<0.3	0	0	0
0.3–0.5	17	0.36	5
0.5–0.7	28	0.55	15
0.7–0.9	20	0.73	15
0.9–1.1	13	0.91	12
>1.1	22	0	0
		Total	48

or arrays are therefore lower than those of the cells because of the areas between the individual cells. The fraction of cell to total areas is called the *packing factor*.

Actual efficiencies are much lower, however, because part of the solar energy is reflected back to the sky, absorbed by nonphotovoltaic surfaces, or converted to heat; and because of various electrical losses and the recombination of the electron-hole pairs, a process that is encouraged by increased temperatures. Cells are usually laboratory rated at 1000 W/m^2 and 28°C but normally operate at 50 to 60°C. This reduces the efficiency by 1 or 2 percent. With modules and arrays, there are additional losses that result from the mismatch between individual cells in a module and between modules in an array. Thus the best single-crystal cells yield efficiencies of about 16 to 17 percent. Mass-produced modules yield efficiencies seldom exceeding 10 percent. Table 13-5 gives a typical energy balance of a nonconcentrating-silicon photovoltaic array, showing an array efficiency of about 8 percent. Methods of increasing cell efficiency besides a search for other materials include *concentration*, *thermophotovoltaic*, and *cascade* systems.

Concentrators improve cell efficiency. They subject the cells to concentrated sunlight by putting them at the foci of parabolic or trough concentrators. EPRI-sponsored research indicates cell efficiencies of about 25 percent can be achieved with a concentration of about 500 suns.

Concentration has other advantages: With improvements in efficiency, fewer cells as well as fewer arrays, structures, and tracking equipment are needed per unit output, and the high cost becomes a bit more bearable. Concentrators, however, are more expensive than flat-plate photovoltaic arrays, are effective only with direct solar radiation, i.e., excluding most of the diffuse radiation, and lose about 15 percent of that radiation in various optical losses. In addition the high cell temperatures and high currents result in higher electrical losses. Concentrators, therefore, are cost-effective only if the improvement in cell efficiency results in performance far exceeding those obtained from flat-plate arrays.

Thermophotovoltaic systems, considered seriously at one time, involved the use of highly concentrated light that is absorbed by a refractory material that becomes hot and reradiates the solar energy to silicon cells at longer wavelengths. Such wavelengths are more efficiently converted to electricity by the silicon cells (column 3, Table 13-

Table 13-5 Typical energy balance of a nonconcentrating silicon photovoltaic conversion array, arbitrary units

Input on array	Energy distribution					
100	In nonphotovoltaic material	12	Reflection by and absorption in cover glass			
		13	Absorption by frames, structures, earth			
	In photovoltaic material		Nonelectric	64	Dissipation as heat in silicon	
		75	Electric	11	1.5	Losses due to cell temperature above 28°C
					0.5	Losses due to cell and module mismatch
					1.0	Losses in wiring and dc-to-ac conversion
					8.0	Delivered as ac power

4). The temperatures required, however, are in the neighborhood of 3400 to 3500°F (1870 to 1925°C), which results in severe materials problems. It is now believed that thermophotovoltaic systems do not attain efficiencies higher than concentrated systems to warrant these high temperatures.

Cascade systems are in essence multijunction systems in which different cells are subjected to different regions of the solar spectrum at which they operate most efficiently. Such systems are believed to yield conversion efficiencies even higher than 25 percent, but they are still in the developmental stage.

13-19 PHOTOVOLTAIC-ENERGY STORAGE

Solar-thermal systems, as has been noted, usually use thermal storage. Photovoltaic systems, on the other hand, must share conventional powerplant grids or must use electrical storage if their output is to last longer than sunlight. Several schemes are being considered. Some are:

1. *Electrochemical storage.* This is storage of electric energy by conversion to chemical energy in batteries. The most common and most highly developed is the lead-acid battery. Other battery systems, still in the developmental stages, have higher energy-to-mass ratios than the lead-acid battery. Large electric energy storage, on a utility scale, in lead-acid or other batteries, however, is not economically feasible.

2. *Pumped-hydro storage.* This method is more suitable to large powerplants. It involves the use of surplus electric energy to pump water into high reservoirs during sunny periods or periods of low demand and the extraction of power during evening or cloudy periods or periods of high demand by running the same down through waterturbines. The storage and regeneration are done via reversible pump-turbine motor-generator sets (Sec. 16-3). The energy extracted is less than that stored because of losses in both pumping and generation. Another problem is the necessity of finding sites with suitable topography near solar powerplants, which tend to be located in desertlike flat terrain. The system is in use with conventional plants as a load leveler but on a somewhat limited scale.

Variations of hydropump storage would be underground pumping and compressed-air storage (Sec. 16-4).

3. *Cryogenic storage.* This is a system in which electric energy is directly stored in large underground electrical coils at liquid-helium temperatures, about 4 K. At that temperature the electrical resistivity of the coils is nearly zero. The system is currently under development, and the costs are still an unknown factor (Sec. 16-7).

13-20 SATELLITE SOLAR-POWER SYSTEMS

The earth *satellite solar-power system* (SSPS) is based on technological advances stemming from the space program. First proposed by Glaser of Arthur D. Little, Inc., in the late 1960s [130], the concept has since received wide attention and serious consideration.

The concept involves the placement of earth satellites that would function as solar-energy collecting stations in geostationary or synchronous orbits around the earth. Such orbits would be at an altitude of about 22,300 mi (36,000 km) and would be equational, i.e., parallel to the earth's equational plane. A satellite traveling from east to west in that plane would have an angular velocity equal to that of the earth and would then appear stationary with respect to any point on earth. (Geostationary civilian and military communication satellites are in common use around the earth.)

Figure 13-35 shows a schematic of the concept. The satellites would have large collectors of photovoltaic arrays. They would also have conversion systems that would convert the electric power generated by the arrays into power at microwave frequencies. A large transmitting antenna on each satellite would beam the microwave energy from its fixed position relative to the earth to a receiving station on the surface of the earth. That station would have a large receiving antenna that would reconvert the microwave power into ac electric power and feed it into a conventional power transmission grid. The satellites, being so high above the earth, would be in sunlight *most* of the day, and no electric-energy storage would be needed.

The attitude controls of an SSPS, possibly through use of laser technology, must see to it that the collector areas are constantly facing the sun and that the transmitting antenna is constantly facing the receiving antenna on earth. Still, the SSPS would have to pass through the earth's shadow once a day (Fig. 13-36), so that a complex

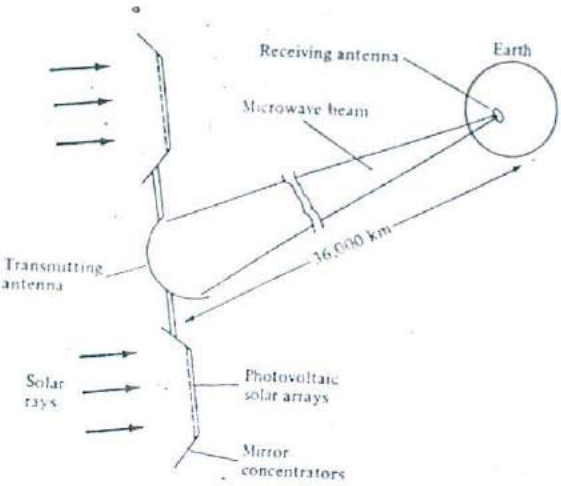


Figure 13-35 A schematic of an earth satellite solar-power system (SSPS).

cutoff of power from any one satellite is experienced about 5 percent of the time. A possible solution to this would be a system that would consist of two geostationary satellites separated by about 7900 mi (12,700 km) and thus about 20° out of phase, both having a direct line of sight to the same receiving antenna on earth. Such a system would ensure that one would be illuminated during the time the other is in the earth's shadow. This would mean a 50 percent power cutoff during roughly 10 percent of the time, instead of a 100 percent cutoff during 5 percent of the time, and a possibly

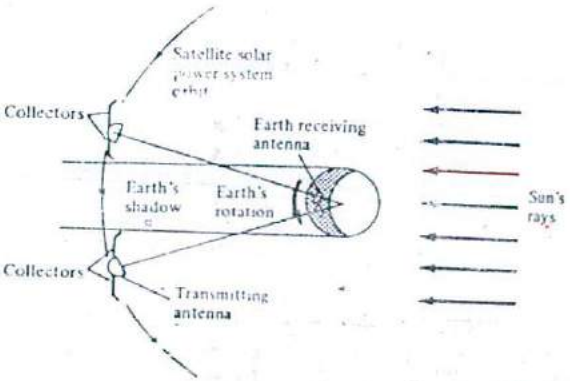


Figure 13-36 Effect of the earth's shadow on SSPS operation, showing satellite and receiving antenna at two different times (not to scale).

better match to load demands. Additional satellites would even the power output further.

Solar insolation in space is 40 percent larger than insolation on earth. It is available to the satellite for nearly 0.95 × 24 h/day, whereas on earth it is available for only 4 h/day figured at maximum intensity. Thus, the output of an SSPS would be about 8 times that of a photovoltaic plant located on the surface of the earth, with a comparable solar collector area.

Energy analyses on SSPS systems [130, 131] show them to be adaptable to various power ranges. A plant resulting in 10 GW on earth is believed to require two square photovoltaic arrays, each 4 km on the side, a 1-km-diameter transmitting antenna, and a 7-km-diameter receiving antenna on earth. A much higher density system envisages the transmission of 20 GW to an earth receiving antenna only 3 km in diameter. The microwave power density on that antenna would be less than 10 kW/m,^{2} about an order of magnitude greater than terrestrial solar radiation density. Highly efficient solid-state rectifiers would be required to absorb this power, and the converted power would be distributed through superconducting transmission lines operating at cryogenic temperatures.

It is estimated (Arthur D. Little, Inc.) that a number of SSPSs with a total solar-collector area of about 4900 km^2 of arrays of single-crystal silicon cells operating at their upper theoretical maximum efficiency of 24 percent would supply the total electric-energy demands of the United States in the year 2000. Such arrays would have a total mass of about 1460 million metric tons, excluding structures, etc. This is considered impractical, and other more efficient cell materials are being sought. Thin-film organic cells, still early in their development stage, are believed to attain efficiencies of 80 percent and require about 920 km^2 of collector area and a mass of about 5.9 million metric tons [130].

The launching, deployment, and assembly of the large structures of an SSPS, such as the collectors, transmitting antenna, attitude-control systems, and operator life-support systems in outer space, now seem like problems of gigantic proportions. However, it is not unreasonable to believe that if and when SSPSs are really ready to go into space, space technology will have also advanced to a point where such undertakings have become feasible. Space transportation is currently estimated to account for about 45 percent of the total capital cost of the system.

The transmitted energy should have frequencies in a spectral region having the least absorption and scattering in the earth's atmosphere. Most of the absorption occurs at the 22 GHz line of the water vapor molecule and the 60 GHz line of the oxygen molecule [131]. Below 10 GHz the attenuation caused by molecular absorption is approximately 10 dB or less. Attenuation by rain, cloud droplets, snow, and hail depends upon their size distribution and composition. The most serious is the result of rain clouds and may reach 4 percent at 3 GHz, and a 1-km path through wet hail may cause 13 percent attenuation at the same frequency.

Scattering, which causes a broadening of the main microwave beam, is not expected to be a significant problem. A 5-GW beam operating at 3 GHz is believed to scatter only 3 mW isotropically in a 1-km-high storm; the result is a scattered beam density of only about 2 × 10^{-4} mW/cm^2 at a 10-km range.

Environmental Effects

Studies have been made to ascertain expected various environmental and biological effects of SSPS microwave beams [132]. Some of these are:

1. *Stratospheric pollution.* This is caused by the space vehicles that deploy the satellites and transport personnel and equipment. This is already a problem of concern due to present military and civilian supersonic aircraft and space shuttle exhaust. Although not fully evaluated, the injection of water vapor and NO_x is believed to lower the ozone concentrations and requires further investigation.
2. *Thermal pollution.* This is a result of waste heat at the receiving antenna. It is believed to be in the neighborhood of 15 percent, which is about a fourth of the waste heat generated by the most efficient conventional powerplants and hence of little concern.
3. *Land exclusion.* A 5-GW plant is believed to require a land area of about 105 mi^2 (270 km^2) from which the public would be excluded (of which one-third would be covered by the receiving antenna.) This compares favorably to the land required by conventional plants of the same output. Offshore locations may also be an attractive alternative.
4. *Radio-frequency interference.* The most desirable SSPS frequencies are in heavy use for worldwide communications and are based on internationally assigned frequencies. Thus, there is a high probability of interference with existing communications systems. Such radio-frequency interference can be controlled by careful selection of frequencies, narrow-band operation, and the use of filters. Detailed and specific effects will have to be carefully studied, however.
5. *Biological effects.* Standards for microwave exposure are already in effect. In the United States, the maximum, based on microwave heating of body tissue, is 10 mW/cm^2. In the USSR, the maximum is based on possible effects on the central nervous system and is a much more conservative 0.01 mW/cm^2. The induced biological effects of the SSPS thus need careful study. It is important that adequate, fail-safe controls of the microwave-beam pointing apparatus be incorporated in the development program.

Microwave effects on birds in flight through the microwave beam need evaluation. Preliminary evidence suggests that birds are affected at 25 mW/cm^2 exposures in the X-band. Effects on aircraft flying through the beam are also of concern, although the shielding effect of the metal fuselage and the short exposure time at aircraft speeds make it unlikely to result in significant human exposure. A more worrisome effect, perhaps, is that of microwaves on aircraft operations, such as fuel tank susceptibility to electrical discharges (now a standard protective feature of aircraft design) and interference with aircraft communications and radar equipment.

PROBLEMS

13-1 From the solar constant and the average distance between the sun and the earth, estimate (*a*) the total power emitted by the sun, in megawatts, and (*b*) the mass loss of the sun, in tons per day (Sec. 9-4).

13-2 For the city of Albuquerque, New Mexico, estimate the average yearly and maximum and minimum monthly clearing indices on a horizontal surface, and the corresponding possible power generation, in kilowatthours per square meter per day, if the average solar-electric conversion efficiency is 0.08.

13-3 A central-receiver solar thermal powerplant uses 1000 heliostats that have 50 m^2 of reflecting surface each. The steam plant has an overall efficiency of 27 percent and generates 3.0-MW peak power. Using a reasonable solar energy insolation on the heliostats on a clear sunny day, estimate (*a*) the overall efficiency of the solar powerplant and (*b*) the efficiency of energy transmission to the steam in the central receiver, both at peak conditions.

13-4 A central receiver solar thermal powerplant uses 1000 heliostats that have 60 m^2 of reflective surface each. The overall efficiency of the plant is 5 percent. The efficiency of the steam powerplant is 30 percent. A constant 20 percent of the incident energy on the receiver is assumed to go to storage during operation. Estimate the powerplant output, in megawatts, at peak conditions and at shutdown. Assume all efficiencies are constant during the day.

13-5 A 300-ft-long 6-ft-wide parabolic trough concentrator receives normal solar radiation at 905 W/m^2. A pipe at the focal line receives 450 lb_m/h of water at 200 psia and at 100°F and exits at 180 psia. Calculate the pipe exit conditions. Assume concentrator reflective losses of 5 percent.

13-6 A central receiver thermal solar powerplant has 2670 heliostats, each composed of 12 1.2 × 3.6 m reflecting glass panels. The average solar insolation during 10 h of operation is 635 W/m^2. The steam cycle has a 10-MW average output and an overall efficiency of 30 percent, assumed constant. The average power lost in radiation transmission from solar insolation on the heliostats to that received by the steam generator is 35 percent. Calculate (*a*) the sizes, in cubic meters, of storage with 25 percent void rock and with sodium, and (*b*) the number of hours the storage system can run the plant at average output.

13-7 A central receiver solar thermal powerplant with storage has 1000 heliostats that have 60 m^2 reflective surface each. The transmission efficiency between incidence and the receiver is 25 percent. The steam plant efficiency is 30 percent, both considered constant during the day. Assume that the solar incidence in June follows a sine curve beginning with zero at −6 h before solar noon, and ending with zero at +6 h after solar noon, with a peak of 1 kW/m^2. The plant operates between −5.5 h and +5.5 h around solar noon. During that period the end use power profile is constant at 2.5 MW. Calculate (*a*) the peak powerplant output, in megawatts, (*b*) the powerplant output at startup, in megawatts, (*c*) the total energy output during operation, in megawatt hours, (*d*) the total equivalent electric energy going into storage, in megawatt hours, and (*e*) the time end use stops withdrawing from storage and energy input to storage begins, hours before solar noon.

13-8 A parabolic dish solar concentrator has 60 m^2 of reflective surface. A Stirling engine is mounted at the focal point. It is assumed to have a constant efficiency of 38 percent and is connected to an electric generator that has an efficiency of 95 percent. The concentrator reflective losses are 4 percent. The peak solar insolation is 1 kW/m^2. Assuming for simplicity that the concentrator shape can be approximated by a spherical surface subtended by a 60° solid angle from its center, determine (*a*) the peak power of the generator, in kilowatts, (*b*) the estimated power when the sun's elevation is 15° (summer solstice), and (*c*) the fuel oil, in grams per second, necessary to produce peak power at night. Assume fuel oil with a heating value of 42,000 kJ/kg is used.

13-9 A solar thermal central receiver system uses 2000 heliostats each 40 m^2 in reflective surface area. The receiver converts feedwater from the condenser at 1 psia to steam at 500 psia and 600°F. No feedwater heaters are used. Assuming absorption by the steam in the receiver to be 60 percent of all radiation incident on the heliostats, that 20 percent of all receiver energy goes to storage at peak radiation, and that the combined turbine-generator polytropic-mechanical-electrical efficiency to be 80 percent, find for the conditions at peak radiation (*a*) the heat added to the cycle, in Btus per hour, (*b*) the turbine steam flow rate, in pounds mass per hour, and (*c*) the generator output, in megawatts.

13-10 A combined thermal-solar powerplant operates on a flow diagram similar to that identical with that of Fig. 13-25. At peak solar insolation, 10^7 lb_m/h of atmospheric air at 520 R is compressed to 9.6 atm, after which it is heated in the central receiver, entering the high-pressure gas turbine at 9.6 atm at 1960°R. It leaves the low-pressure turbine at 20 psia to the steam generator, leaving it at 600°R. Superheated steam is generated at 1000 psia and 780°F and expands in the steam turbine to 1 psia. The compressor and both gas turbines have polytropic efficiencies of 0.82 and 0.88, respectively. The steam turbine has a

polytropic efficiency of 0.90. The compressor and all turbines have mechanical efficiencies of 0.95. The electric generator has a combined mechanical-electrical efficiency of 0.96. For simplicity ignore storage, feedwater heating and condensate pump work. Calculate (*a*) the steam mass flow rate, in pounds mass per hour, (*b*) the net power output of the plant, in megawatts, if 20 percent of the gross power is used internally, (*c*) the combined plant net efficiency, and (*d*) the number of heliostats needed if their reflective areas are 100 m^2 each and the radiation transmission losses to the air in the tower are 40 percent of solar insolation.

13-11 A 7.5-cm-diameter circular photovoltaic solar cell is subjected to a solar energy flux of 2.5×10^{17} photons/s · cm^2 at an average photon wavelength of 0.838 μm. Calculate (*a*) the solar insolation on the cell, in watts per square meter, and (*b*) the maximum theoretical power that can be produced by the cell, in watts.

13-12 A 0.08-m-diameter circular photovoltaic cell receives the following solar fluxes, in photons per second per square centimeter, in the wavelength ranges between the parentheses: 0.5×10^{17} (0.3–0.5 μm), 0.85×10^{17} (0.5–0.7 μm), 0.5×10^{17} (0.7–0.9 μm), 0.45×10^{17} (0.9–1.1 μm), and zero below 0.3 and above 1.1 μm. Estimate (*a*) the number of such cells necessary to produce 10 kW of ac power, and (*b*) the array area on which they are mounted.

13-13 Calculate the overall efficiency of a satellite solar-power system that produces 10 GW on earth from two square photovoltaic arrays, each 5 km on the side. Assume a 0.95 packing fraction of the cells.

CHAPTER

FOURTEEN

WIND ENERGY

14-1 INTRODUCTION

Wind energy is rightfully an indirect form of solar energy since wind is induced chiefly by the uneven heating of the earth's crust by the sun. The topic would have fit in Chap. 13 except that that chapter was already quite lengthy and a separate chapter devoted to wind energy seemed appropriate.

Winds can be broadly classified as *planetary* and *local*. *Planetary winds* are caused by greater solar heating of the earth's surface near the equator than near the northern or southern poles. This causes warm tropical air to rise and flow through the upper atmosphere toward the poles and cold air from the poles to flow back to the equator nearer to the earth's surface. The direction of motion of planetary winds with respect to the earth is affected by the rotation of the earth. The warm air moving toward the poles in the upper atmosphere assumes an easterly direction (in both the northern and southern hemispheres) that results in the *prevailing westerlies* (Fig. 14-1). (Winds are named according to the direction they come *from*.) At the same time, the inertia of the cool air moving toward the equator nearer the earth's surface causes it to turn west, resulting in the *northeast trade winds* in the northern hemisphere and the *southeast trade winds* in the southern hemisphere.

The western motion toward the equator and the eastern motion toward the poles result in large counterclockwise circulation of air around low-pressure areas in the northern hemisphere and clockwise circulation in the southern hemisphere. The westerlies control events between the 30° and 60° latitudes (where a majority of the earth's population lives). Because the earth's axis is inclined to its orbital plane around the sun (Fig. 13-2), seasonal variations in the heat received from the sun result in seasonal

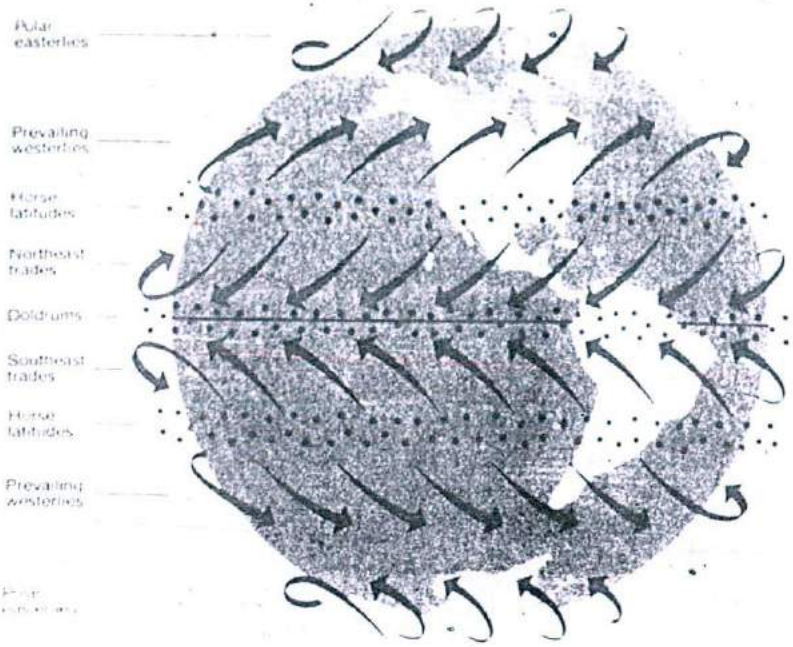


Figure 14-1 Planetary winds in the earth's atmosphere *(EPRI.)*

variations in the velocity and direction of the wind from the general flow pattern described above.

Local winds are caused by two mechanisms. The first is *differential heating* of land and water. Solar insolation during the day is readily converted to sensible energy of the land surface but is partly absorbed in layers below the water surface and partly consumed in evaporating some of that water. The land mass becomes hotter than the water, which causes the air above land to heat up and become warmer than the air above water. The warmer lighter air above the land rises, and the cooler heavier air above the water moves in to replace it. This is the mechanism of shore breezes. At night, the direction of the breezes is reversed because the land mass cools to the sky more rapidly than the water, assuming a clear sky. The second mechanism of local winds is caused by *hills and mountain sides*. The air above the slopes heats up during the day and cools down at night, more rapidly than the air above the low lands. This causes heated air during the day to rise along the slopes and relatively cool heavy air to flow down at night.

It has been estimated [133,134] that about 2 percent of all solar radiation falling on the face of the earth is converted to kinetic energy in the atmosphere and that 30 percent of this kinetic energy occurs in the lowest 1000 m (3280 ft) of elevation. It is thus said that the total kinetic energy of the wind in this lowest kilometer, if harnessed,

can satisfy more than 3 times the energy demands of the United States at the early 1980s' rates. It is also claimed that wind power is pollution free and that its source of energy is free. Such are the seemingly compelling arguments for wind-power, not unlike those for solar-power. Although solar energy is cyclic and predictable, and even dependable in some parts of the globe, wind energy, however, is erratic, unsteady, and often treacherous except in very few areas. It does, however, have a place in the total energy picture, particularly for those areas with more or less steady winds, especially those that are far removed from central power grids, and for small, remote domestic and farm needs.

14-2 HISTORY OF WIND POWER

Human beings have always dreamt of converting wind power to mechanical and, more recently, electric power. Wind, more than any other renewable energy source, has intrigued serious and amateur inventors over the ages. It is said that more patents for wind systems have been applied for than almost any other device to date.

In ancient times the kinetic energy of the wind was used to propel ships by sails. Windmills, however, are more recent, having been used for a little over a thousand years. The earliest reference to windmills appeared in Arab writings from the ninth century A.D. that described mills that operated on the borders of Persia and Afganistan some two centuries earlier.

Vertical-Axis Windmills

These early machines, sometimes referred to as the *Persian windmills*, were vertical-axis machines. They evolved from ships. Sails, first made of canvas and then of wood, were attached to a large horizontal wheel. The wind pressure against the sails caused the wheel to turn. A vertical axle attached to the wheel usually turned a grindstone to grind grain into flour, hence the name windmill. Similar mills were known to have been used in the thirteenth century A.D. in China to evaporate seawater for the production of salt, and later in the Crimea, Europe, and the United States, though few of them remain today.

One of the most successful early forms of the vertical-axis mill is the one named after Savonius of Finland. The *Savonius windmill* had single or multiple S-shaped sails and a vertical axis (Fig. 14-2). Vertical-axis machines that are still being investigated are the Madaras (Magnus effect) and Darrieus machines (Secs. 14-9 and 14-10).

One advantage of vertical-axis machines is that they operate in all wind directions and thus need no yaw adjustments.

Horizontal-Axis Windmills

The vertical-axis windmill was changed, after the idea of a windmill reached Europe, into a vertical-wheel horizontal-axis configuration. The first designs had sails built on a post that could be made to face into any wind direction. The vertical wheel drove

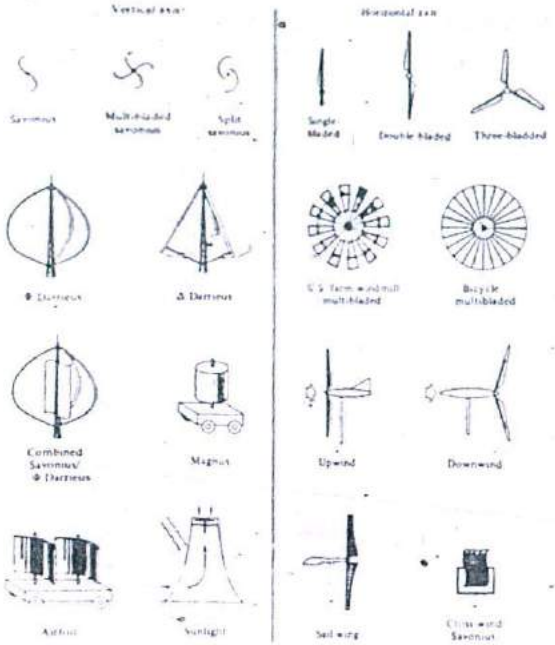


Figure 14-2 Some of the more workable (though not necessarily economical) windmills of the vertical- and horizontal-axis types [135].

a vertical axle through gears. Such machines first appeared in France and England in the late twelfth century and were called *post mills*. Various modifications of these mills evolved in Europe and America throughout the middle ages and were used for grinding grain, drainage, pumping, sawmilling, and other purposes. In the Netherlands, where very large land areas are below sea level and constantly threatened with flooding, windmills were widely used to pump water out of the fields and into canals which took it back to the sea. Nowadays, only a few romantic mills remain and pumping relies mostly on electric drives.

Electrical Generation

The first windmill to drive an electrical generator was built by P. La Cour of Denmark late in the nineteenth century. After World War I, sails with airfoil cross sections (like the blades of an airplane propeller) were developed for use in windmills; the result was what is now called the *propeller-type windmill*, or *wind turbine*. In 1931, such a windmill was built in the Crimea and produced low-voltage electricity that was fed directly into the local grid.

Experiments on twin-bladed mills were conducted in the United States, resulting, notably in 1940, in a large mill called the Smith-Putnam machine, which was designed by Palmer Putnam with the assistance of Theodore von Karman, the famed aerodynam-

icist, and others. The plant, rated at 1.25 MW of ac power [135], was constructed by the S. Morgan Smith Company of York, Pennsylvania, atop a 2000-ft (610-m) high mountain called Grandpa's Knob, near Rutland, Vermont. The mill had a twin-bladed, 175-ft (55-m) diameter propeller-type rotor that weighed 16 tons, was mounted on top of a 110-ft (34-m) tower, and rotated at 28 r/min. After intermittent operations for a number of years, one of the blades broke off in March 1945, near the hub where a previously discovered weakness was not corrected because of wartime shortages. The project was abandoned when it was decided that, even if repaired, the plant could not compete economically with fossil or hydro powerplants.

The tranditional nonelectrical windmill still survives around the world, however (1000 mills were still operating in Portugal in 1965), mainly in areas not easily accessible to central power grids and in areas of mainly peasant economy.

14-3 PRINCIPLES OF WIND POWER

Total Power

The total power of a wind stream is equal to the rate of the incoming kinetic energy of that stream KE_i, or

$$P_{tot} = \dot{m}KE_i = \dot{m}\frac{V_i^2}{2g_c} \tag{14-1}$$

where P_{tot} = total power, W or ft · lb_f

$\dot{m}$ = mass-flow rate, kg/s or lb_m/h

V_i = incoming velocity, m/s or ft/h

g_c = conversion factor = 1.0 kg/(N · s^2) or

4.17×10^8 lb_m · ft/(lb_f · h^2)

The mass-flow rate is given by the continuity equation

$$\dot{m} = \rho A V_i \tag{14-2}$$

where ρ = incoming wind density, kg/m^3 or lb_m/ft^3

A = cross-sectional area of stream, m^2 or ft^2

Thus

$$P_{tot} \cong \frac{1}{2g_c}\rho A V_i^3 \tag{14-3}$$

Thus the total power of a wind stream is directly proportional to its density, area, and the cube of its velocity. Figure 14-3 is a plot of P_{tot} as a function of A and V_i for wind at 1 standard atmosphere pressure and 15°C (59°F).

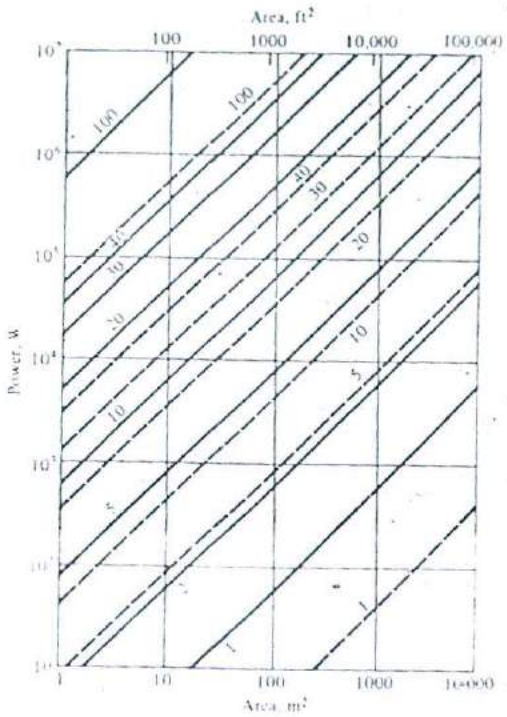


Figure 14-3 Total power available in wind streams of incoming velocities V_i and cross-sectional areas A. P = 1 atm, T = 15°C = 59°F. Solid lines, V_i in m/s. Dashed lines, V_i in mi/h.

Maximum Power

It will shortly be apparent that the total power discussed above cannot all be converted to mechanical power. Consider a horizontal-axis, propeller-type windmill, henceforth to be called a wind turbine, which is the most common type used today. Assume that the wheel of such a turbine has thickness a-b (Fig. 14-4); that the incoming wind pressure and velocity, far upstream of the turbine, are P_i and V_i, and that the exit wind pressure and velocity, far downstream of the turbine, are P_e and V_e, respectively. V_e is less than V_i because kinetic energy is extracted by the turbine.

Considering the incoming air between i and a as a thermodynamic system, and assuming that the air density remains constant (a good assumption since the pressure and temperature changes are very small compared to ambient), that the change in potential energy is zero, and no heat or work are added or removed between i and a, the general energy equation (Eq. 1-1c) reduces to the kinetic and flow energy terms only.

Thus

$$P_i v + \frac{V_i^2}{2g_c} = P_a v + \frac{V_a^2}{2g_c} \qquad (14\text{-}4a)$$

or
$$P_i + \rho\frac{V_i^2}{2g_c} = P_a + \rho\frac{V_a^2}{2g_c} \tag{14-4b}$$

where v and ρ are the specific volume and its reciprocal, the density, respectively, both considered constant. Equation (14-4*b*) is the familiar Bernouilli equation.

Similarly, for the exit region b-e

$$P_e + \rho\frac{V_e^2}{2g_c} = P_b + \rho\frac{V_b^2}{2g_c} \tag{14-5}$$

The wind velocity across the turbine decreases from a to b since kinetic energy is converted to mechanical work there. The incoming velocity V_i does not decrease abruptly but gradually as it approaches the turbine to V_a and as it leaves it to V_e. Thus $V_i > V_a$ and $V_b > V_e$, and therefore, from Eqs. (14-4) and (14-5), $P_a > P_i$ and $P_b < P_e$; that is, the wind pressure rises as it approaches, then as it leaves the wheel.

Combining Eqs. (14-4) and (14-5) gives

$$P_a - P_b = \left(P_i + \rho\frac{V_i^2 - V_a^2}{2g_c}\right) - \left(P_e + \rho\frac{V_e^2 - V_b^2}{2g_c}\right) \tag{14-6}$$

It is reasonable to assume that, far from the turbine at e, the wind pressure returns to ambient, or

$$P_e = P_i \tag{14-7}$$

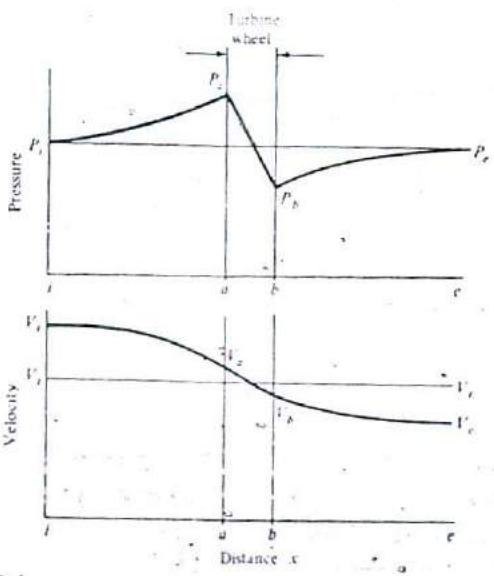


Figure 14-4 Pressure and velocity profiles of a wind moving through a horizontal-axis propeller-type wind turbine.

and that the velocity within the turbine, V_t, does not change because the blade width a-b is thin compared with the total distance considered, so that

$$V_t \approx V_a \approx V_b \tag{14-8}$$

Combining Eqs. (14-6) to (14-8) gives

$$P_a - P_b = \rho\left(\frac{V_i^2 - V_e^2}{2g_c}\right) \tag{14-9}$$

The axial force F_x, in the direction of the wind stream, on a turbine wheel with projected area, perpendicular to the stream A, is given by

$$F_x = (P_a - P_b)A = \rho A\left(\frac{V_i^2 - V_e^2}{2g_c}\right) \tag{14-10}$$

This force is also equal to the change in momentum of the wind $\Delta(\dot{m}V)/g_c$ where $\dot{m}$ is the mass-flow rate given by

$$\dot{m} = \rho A V_t \tag{14-11}$$

Thus

$$F_x = \frac{1}{g_c}\rho A V_t(V_i - V_e) \tag{14-12}$$

Equating Eqs. (14-10) and (14-12) gives

$$V_t = \frac{1}{2}(V_i + V_e) \tag{14-13}$$

We shall now consider the total thermodynamic system bounded by i and e. The changes in potential energy are, as above, zero, but so are the changes in internal energy ($T_i = T_e$) and flow energy ($P_i v = P_e v$), and no heat is added or rejected. The general energy equation now reduces to the steady-flow work W and kinetic energy terms

$$W = \mathrm{KE}_i - \mathrm{KE}_e = \frac{V_i^2 - V_e^2}{2g_c} \tag{14-14}$$

The power P is the rate of work. Using Eq. (14-11)

$$P = \dot{m}\frac{V_i^2 - V_e^2}{2g_c} = \frac{1}{2g_c}\rho A V_t(V_i^2 - V_e^2) \tag{14-15}$$

Combining with Eq. (14-13)

$$P = \frac{1}{4g_c}\rho A(V_i + V_e)(V_i^2 - V_e^2) \tag{14-16}$$

Equation (14-15) reverts to Eq. (14-3) for P_{tot} when $V_t = V_i$ and $V_e = 0$; that is, the wind comes to a complete rest after leaving the turbine (Fig. 14-5). This, obviously, is an impossible situation because the wind cannot accumulate at turbine exit. It can

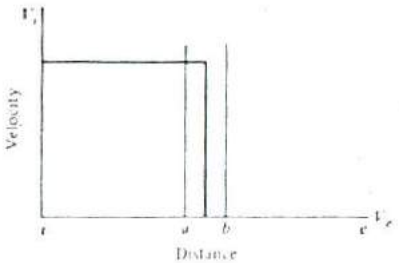


Figure 14-5 Total conversion of incoming wind kinetic energy to work.

be seen from Eq. (14-16), where V_e is positive in one term and negative in the other, that too low or too high a value for V_e results in reduced power. There thus is an *optimum exit velocity* $V_{e,\text{opt}}$ that results in maximum power $P_{\max}$, which is obtained by differentiating P in Eq. (14-16) with respect to V_e for a given V_i and equating the derivative to zero, i.e., $dP/dV_e = 0$, which gives

$$3V_e^2 + 2V_iV_e - V_i^2 = 0$$

This is solved for a positive V_e to give $V_{e,\text{opt}}$

$$V_{e,\text{opt}} = \frac{1}{3}V_i \tag{14-17}$$

Combining with Eq. (14-16) gives $P_{\max}$

$$P_{\max} = \frac{8}{27g_c}\rho A V_i^3 \tag{14-18}$$

The *ideal*, or *maximum, theoretical efficiency* $\eta_{\max}$ (also called the *power coefficient*) of a wind turbine is the ratio of the maximum power obtained from the wind, Eq. (14-18), to the total power of the wind, Eq. (14-3), or

$$\eta_{\max} = \frac{P_{\max}}{P_{\text{tot}}} = \frac{8}{27g_c} \times 2g_c = \frac{16}{27} = 0.5926 \tag{14-19}$$

In other words, a wind turbine is capable of converting no more than 60 percent of the total power of a wind to useful power.

Actual Power

Like steam- and gas-turbine blades (Sec. 5-5), wind-turbine blades experience changes in velocity dependent upon the blade inlet angle and the blade velocity. Because the blades are long, the blade velocity varies with the radius to a greater degree than steam- or gas-turbine blades and the blades are therefore twisted. The maximum efficiency (or power coefficient) given by Eq. (14-19) assumes ideal conditions along the entire blade. A rigorous treatment of the power extracted from the wind by a propeller-type wind turbine shows that the power coefficient is strongly dependent on

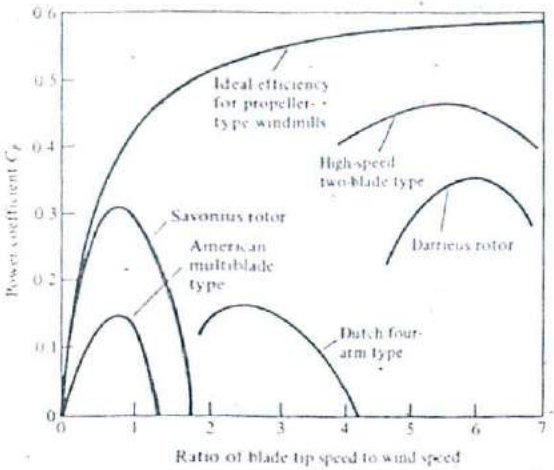


Figure 14-6 Power coefficient of various windmills vs. ratio of blade tip to wind speeds [135].

blade-to-wind speed ratio, that it reaches its maximum value of about 0.6 only when the maximum blade speed, i.e., the blade speed at the tip, is some 6 or 7 times the wind speed, and that it drops rapidly at blade tip-to-wind speed ratios below about 2.0. Figure 14-6 shows the power coefficient for an ideal propeller-type wind turbine and various other wind turbines.

Because a wind-turbine wheel cannot be completely closed, and because of spillage and other effects, practical turbines achieve some 50 to 70 percent of the ideal efficiency. The *real efficiency* η is the product of this and η_{max} and is the ratio of actual to total power

$$P = \eta P_{tot} = \eta \frac{1}{2g_c} A V_i^3 \tag{14-20}$$

where η varies between 30 and 40 percent for real turbines.

Forces on the Blades

There are two types of forces operating on the blades of a propeller-type wind turbine. They are the *circumferential forces* in the direction of wheel rotation that provide the torque and the *axial forces* in the direction of the wind stream that provide an *axial thrust* that must be counteracted by proper mechanical design.

The *circumferential force*, or *torque*, T is obtained from

$$T = \frac{P}{\omega} = \frac{P}{\pi DN} \tag{14-21}$$

where T = torque, N or lb_f

ω = angular velocity of turbine wheel, m/s or ft/s

D = diameter of turbine wheel = $\sqrt{4A/\pi}$, m or ft

N = wheel revolutions per unit time, s^{-1}

For a turbine operating at power P, Eq. (14-20), the torque is given by

$$T = \eta \frac{1}{8g_c} \frac{\rho D V_i^3}{N} \tag{14-22}$$

For a turbine operating at maximum efficiency $\eta_{max} = 16/27$, the torque is given by T_{max}

$$T_{max} = \frac{2}{27g_c} \frac{\rho D V_i^3}{N} \tag{14-23}$$

The *axial force*, or axial thrust, given by Eq. (14-10), here repeated, is

$$F_x = \frac{1}{2g_c} \rho A (V_i^2 - V_e^2) = \frac{\pi}{8g_c} \rho D^2 (V_i^2 - V_e^2) \tag{14-10}$$

The axial force on a turbine wheel operating at maximum efficiency where $V_e = 1/3\ V_i$ is given by

$$F_{x,max} = \frac{4}{9g_c} \rho A V_i^2 = \frac{\pi}{9g_c} \rho D^2 V_i^2 \tag{14-24}$$

The axial forces are proportional to the square of the diameter of the turbine wheel, which makes them difficult to cope with in extremely large-diameter machines. There is thus an upper limit of diameter that must be determined by design and economical considerations.

Example 14-1 A 10-m/s wind is at 1 standard atm pressure and 15°C temperature. Calculate (1) the total power density in the wind stream, (2) the maximum obtainable power density, (3) a reasonably obtainable power density, all in W/m^2, (4) the total power (in kW) produced if the turbine diameter is 120 m, and (5) the torque and axial thrust N if the turbine were operating at 40 r/min and maximum efficiency.

SOLUTION For air, the gas constant $R = 287\ J/(kg \cdot K)$. 1 atm = 1.01325×10^5 Pa.

$$\text{Air density } \rho = \frac{P}{RT} = \frac{1.01325 \times 10^5}{287(15 + 273.15)} = 1.226\ kg/m^3$$

(1) Eq. (14-3):

$$\frac{P_{tot}}{A} = \frac{1}{2g_c}\rho V_i^3 = \frac{1}{2 \times 1} 1.226 \times 10^3 = 613 \text{ W/m}^2$$

(2) Eq. (14-18):

$$\frac{P_{max}}{A} = \frac{8}{27g_c}\rho V_i^3 = \frac{8}{27 \times 1} 1.226 \times 10^3 = 363 \text{ W/m}^2$$

(3) Assuming $\eta = 40\%$:

$$\frac{P}{A} = 0.4\left(\frac{P_{tot}}{A}\right) = 0.4 \times 613 = 245 \text{ W/m}^2$$

(In English units this corresponds to 22.76 W/ft² at 22.37 mi/h.)

(4) $$P = 0.245 \times \frac{\pi D^2}{4} = 0.245 \times \frac{\pi 120^2}{4} = 2770 \text{ kW}$$

(5) Eq. (14-23):

$$T_{max} = \frac{2}{27g_c}\frac{\rho A V_i^3}{N} = \frac{2}{27 \times 1} \times \frac{1.20 \times 1.226 \times 10^3}{40/60}$$

$$= 16{,}347 \text{ N } (= 3675 \text{ lb}_f)$$

Eq. (14-24):

$$F_{x,max} = \frac{\pi}{9g_c}\rho D^2 V_i^2 = \frac{\pi}{9 \times 1}(1.226 \times 120^2 \times 10^2)$$

$$= 616{,}255 \text{ N } (= 138{,}540 \text{ lb}_f)$$

14-4 WIND TURBINE OPERATION

Equations (14-18) and (14-20) demonstrate an inherent weakness of all wind machines, namely, the strong dependence of the power produced on wheel diameter and wind speed, being proportional to turbine wheel area, i.e., to the square of its diameter, and to the cube of the wind velocity. The latter dependence means that even small fluctuations in wind velocity, which almost always occur, would mean large fluctuations in power. For example, a drop in wind velocity by only 20 percent would result in the loss of a little less than half the power, whereas a drop in velocity to approximately one-half (0.464) would result in a drop in power to one-tenth, assuming constant efficiency (Fig. 14-7). Actually, a greater loss in power occurs because many of the machine losses are independent of wind velocity; the results are an increase in machine fractional losses and a decrease in efficiency as wind velocity and power decrease. The maximum machine efficiency occurs over a relatively narrow power range.

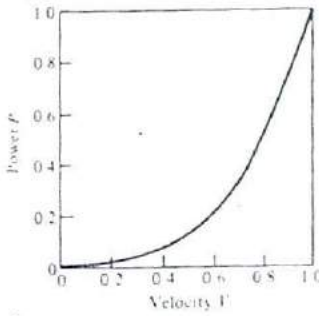


Figure 14-7 Power-velocity characteristics of a wind turbine with constant efficiency, arbitrary units.

Flat Rating

Severe fluctuations in power are, of course, undesirable. They pose power-oscillation problems on the grid and severe strains on the windmill hardware. From an economic point of view, a windmill designed to produce a rated power output corresponding to the maximum, or near maximum, prevailing wind velocity at a given site would generate low powers, with the full capacity of the turbine and electric generator unused much of the time.

It is, therefore, more cost-effective to design a windmill to produce rated power at less than the maximum prevailing wind velocity, using a smaller turbine and generator, and to maintain a constant output at all wind speeds above rating. This is called *flat rating* (Fig. 14-8).

Because of the severe loss in efficiency and power at low wind velocities, a wind turbine is also designed to come into operation at a minimum wind speed, called the *cut-in velocity*. To protect the turbine wheel against damage at very high wind velocities, it is designed to stop operation (such as by feathering the blades) at a *cut-out velocity*. Thus the wind turbine operates with variable load over a narrow range between the cut-in and the rated velocities and a constant power between the rated and the cut-out velocities and ceases operation above the cut-out velocity.

An example of flat rating is that of the MOD-2, a second-generation class of wind turbines, each of which produces 2.5 MW (peak) (Sec. 14-8). The cut-in, rated, and cut-out wind velocities are 9.0, 20.0, and 30.0 m/h, respectively.

Wind-turbine ratings are usually given for a wind velocity occuring at a reference height, usually 30 ft (9.1 m) above grade, and with an availability factor, usually 90 percent. The *availability factor* is defined as the fraction of time, during a given period, that the turbine is actually on line (Fig. 14-9). The actual wind velocity at the propeller hub, that determines the turbine power is usually higher [Eq. (14-28), Sec. 14-5].

Because they do not always operate at rated power because of changing wind velocities, the overall load factor is much lower than the availability factor. The *overall load factor*, also called the *plant operating factor* and the *plant capacity factor*, is the ratio of the total energy generated during a given period of time to the total rated

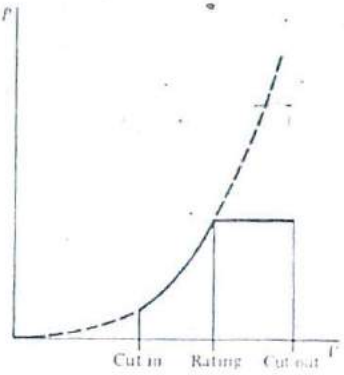


Figure 14-8 Power-velocity characteristics of a flat-rated wind turbine.

generation capacity during the same period (Fig. 14-9). This factor thus takes into account operations at less than rated wind velocity, nonoperation below cut-in and above cut-out velocities, and power outages caused by various situations, such as repairs, maintenance, etc.

The overall load factor is typically 30 to 40 percent (the MOD-0A 200-kW machine in Oahu, Hawaii, accumulated an impressive 45 percent factor in 1981 because of favorable wind patterns there). Considering an average load factor of 1/3, a wind powerplant of a particular rating would have to be nearly 2.5 times as large as a conventional powerplant of the same rating operating at a load factor of about 80 percent. The unit capital cost, $/kW rating, for a wind powerplant would have to be multiplied by about 2.5 to yield a more realistic cost to a utility. This is one of the economic burdens of wind power.

14-5 SITE CHARACTERISTICS

Small Machines

Wind turbines are broadly classified as small or large. *Small wind turbines* are those of less than 100 kW rated capacity. They are usually used for generating power for

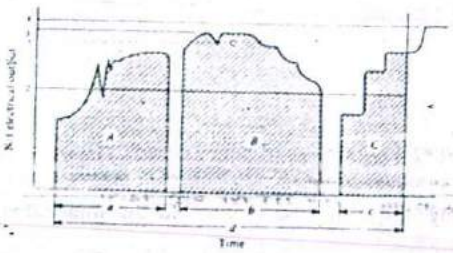


Figure 14-9 Hypothetical diagram of operation of a powerplant: x = rated net capacity of plant, y = peak load during period d, z = average load during period d. *Plant overall load factor*, or *plant operating factor*, = $(A + B + C)/xd$. *Plant load factor* = z/y. *Plant availability factor* = $(a + b + c)/d$. d is usually taken as 1 year.

local use in a particular location. Siting procedures for small machines involve accurately evaluating the wind characteristics and finding the best acceptable site within that location. Guidelines for siting small machines may be found in the *Handbook for Siting Small Wind Energy Conversion Systems* [136].

Large Machines

Large wind turbines are those of 100 kW rated capacity or greater. They are used to generate power for distribution in central power grids. Siting procedures for such machines are approached differently. The geographic area in which they may be located may be very large, and there usually is a great deal of freedom in site selection. The main objective is to minimize the cost of power production for the entire grid, and this requires rather extensive analysis. A handbook for siting large machines was in preparation at the time of this writing, but various techniques have already been developed as tools in the different stages of siting. These include flow modeling, measurements, and biological, geological, topographical, social, and cultural indicators of wind. Some are included in the proceedings of a 1979 Conference and Workshop on Wind Energy Characteristics and Siting [137].

Suitable sites for large windmills around the world depend upon favorable wind activity and, in the United States, have been consolidated under a program area called Wind Energy Prospecting. They result in maps showing annual average wind-power density, W/m^2, such as that shown in Fig. 14-10. The map is general in the sense that good sites may occasionally be found in low power density areas and vice versa.



Figure 14-10 Annual distribution of average wind power in the United States *(EPRI)*.

Mean Wind and Energy Velocities

Wind-power potential can be estimated from the *mean wind velocity* $\overline{V}$, which is based on measurements over a period of time. It is given by

$$\overline{V} = \frac{\sum_{i}^{n} V_i}{n} \tag{14-25}$$

where $\sum_{i}^{n} V_i$ is the sum of all velocity observations and n is the number of these observations.

Powerplant sizing would, however, be grossly underestimated if it were rated at the mean wind velocity. A more representative figure would be based on the *mean energy velocity* $\overline{V}_E$, which because of the power dependence on the cube of the wind velocity, is given by

$$\overline{V}_E = \left(\frac{\sum_{i}^{n} V_i^3}{n} \right)^{1/3} \tag{14-26}$$

The ratio of $\overline{V}_E$ to $\overline{V}$ depends upon the distributions of velocity in the observations. Taking a hypothetical case in which 10 observations yielded velocities of 0 to 9 (in any units) with increments of of 1, $\overline{V}$ would be 4.5 while $\overline{V}_E$ would be 5.872, greater by a little over 30 percent. Another in which nine observations are zero and one was 9 would yield $\overline{V} = 0.9$ and $\overline{V}_E = 4.177$, which is 364 percent greater. A third in which one observation was zero and nine were 9 would yield $\overline{V} = 8.1$ and $\overline{V}_E = 8.69$, an increase of about 7 percent.

Long-term observations taken by the U.S. National Storms Laboratory at a number of sites in Oklahoma showed $\overline{V}_E$ to be greater than $\overline{V}$ by about 25 percent. The use of $\overline{V}$ to estimate energy potential in that case would underestimate it by a factor of 1.25^3, or almost 2.

The total energy production of a wind turbine of a given rating during a given period is, as by now known, not equal to its rating times the number of hours during that period because (1) the availability factor of less than 100 percent and (2) the variations of wind velocity during that period. The effect of this variation on energy production can be obtained only if it is precisely known.

For estimation purposes a distribution, called the *Weibull distribution model*, discussed in Ref. 138, has been found useful and appropriate for wind-turbine performance analysis by many investigators. That model gives the probability that the wind velocity is greater than a selected value V for a locality where the mean wind velocity $\overline{V}$ is known. It is given at reference height $H_r = 9.1$ m (30 ft), where V_r and V are in m/s, by

$$P(V_r > V) = e^{-(V/C_r)^{K_r}} \tag{14-27}$$

where $P(V_r > V)$ = probability that incoming wind velocity exceeds a value V at reference height H_r

$$K_r = 1.09 + 0.20V$$

$$C_r = \frac{\overline{V}}{\Gamma[1 + (1/K_r)]} \text{ m/s}$$

Γ = gamma function

Figure 14-11 shows *wind-distribution curves* (also called *exceedance* and *endurance curves*) for three values of $\overline{V}$ [139]. The abscissa shows the number of hours per year during which the wind velocity exceeds that given by the ordinate. For example, for $\overline{V}$ = 15 mi/h, the wind velocity exceeds 20 mi/h about 2000 h/year, or about 22 percent of the time. [Some sites in Oklahoma, one of the high power density states, have reported winds at 8 knots (about 9.2 mi/h) or greater about 70 percent of the time.]

A height above ground of 30 ft (9.1 m) is usually used as a reference elevation for which wind velocities are tabulated or listed (as in Fig. 14-11). The velocity to be used in determining the power of a wind turbine, however, is that at the hub of the turbine wheel, which is 100 to 260 ft (~30 to 80 m) for current large wind turbines. The ratio of wind velocity V at a height H to the reference velocity V_r at reference height H_r is given by a wind-shear model [137] as

$$\frac{V}{V_r} = \left(\frac{H}{H_r}\right)^{\alpha} \tag{14-28}$$

where $$\alpha = \alpha_O\left(1 - \frac{\log V_r}{\log V_O}\right)$$

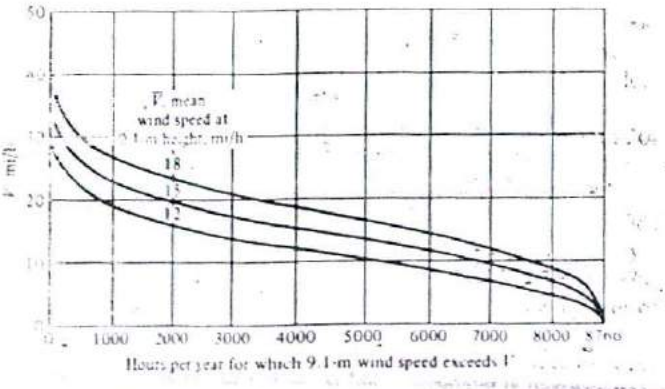


Figure 14-11 Wind speed distribution (exceedance) curves for three values of the mean wind speed $\overline{V}$ at a height of 30 ft (9.1 m) [139].

$$\alpha_O = \left(\frac{Z_O}{H_r}\right)^{0.2}$$

Z_O = surface roughness length, varying widely but taken as 0.4 m for evaluation purposes to conform with the empirical values used in the model

V_O = a fixed velocity = 67.1 m/s

At elevations H, other than the reference H_r (30 ft, 9.1 m), the Weibull distribution model is used, but the parameters K_r and C_r are modified to K_H and C_H, given by

$$K_H = \frac{K_r}{1 - \alpha_O\left[\left(\log \frac{H}{H_r}\right) \Big/ \log V_O\right]} \tag{14-29}$$

and

$$C_H = C_r\left(\frac{H}{H_r}\right)^{\alpha_H} \tag{14-30}$$

where

$$\alpha_H = \alpha_O\left(1 - \frac{\log C_r}{\log V_O}\right) \tag{14-31}$$

The annual energy output for any horizontal-axis wind turbine can now be estimated for a given mean wind velocity $\bar{V}$ using the wind-distribution curves by calculating the power output at each wind velocity and integrating it over the time duration for that wind velocity.

Specifications for wind turbines usually include estimated annual power output,

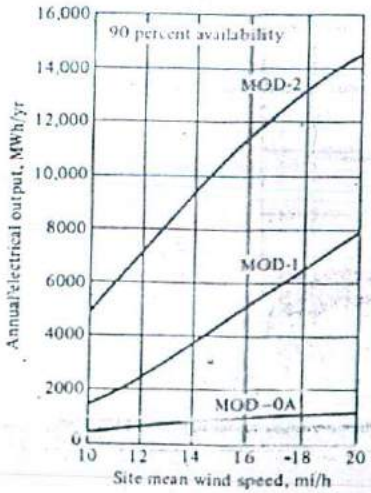


Figure 14-12 Computed annual power generation of three large horizontal-axis wind turbines, assuming 90 percent availability factor. Weibull wind-speed distribution at 30-ft elevation, and various aerodynamic, mechanical, and electrical losses [139].

in MWh/year, computed for the reference elevation of 9.1 m (30 ft), for a machine availability factor of 90 percent, for a Weibull wind-velocity distribution, and including the effects of aerodynamic, mechanical, and electrical losses, up to the busbar (beyond the step-up transformer). Such calculations have been made for three large machines, the MOD-0A, MOD-1, and MOD-2 (Sec. 14-6) at various values of the mean wind speed $\bar{V}$ (Fig. 14-12).

14-6 NEW DEVELOPMENT: SMALL MACHINES

As indicated earlier, small machines are classified as those less than 100 kW rated capacity. They are designed primarily for local use at or near their intended load for farm, home, or rural use. In the United States, the Department of Energy has a "Small Wind Energy Conversion Systems (SWECS)" test program that is managed and operated by Rockwell International at a test center at Rocky Flats, Colorado (Fig. 14-13). The program is designed to develop small advanced machines with the goal of their earliest possible commercialization by attempting to make their costs competitive with the costs of power obtained from conventional systems and by dealing with the problems of small consumer and institutional acceptance. The program is producing

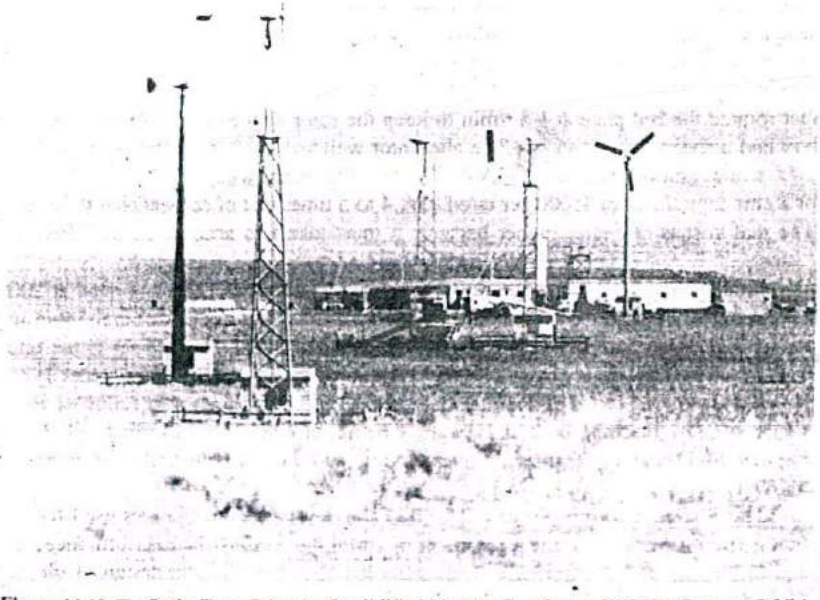


Figure 14-13 The Rocky Flats, Colorado, Small Wind Machine Test Center, SWECS. *(Courtesy DOE.)*

technical data on machine costs, construction, output, durability, and behavior under varying as well as extreme weather conditions.

The first cycle of the SWECS program included nine contracts to build machines in the 1-, 8-, and 40-kW ranges. In the 40-kW range, McDonnell Aircraft Company is building a three-bladed, 65-ft-diameter rotor geared to a vertical axis, while Kaman Aerospace Corporation is building two prototypes—each a twin-bladed, 64-ft-diameter rotor, horizontal-axis machine—one to generate electricity and the other to drive equipment, such as irrigation pumps, mechanically.

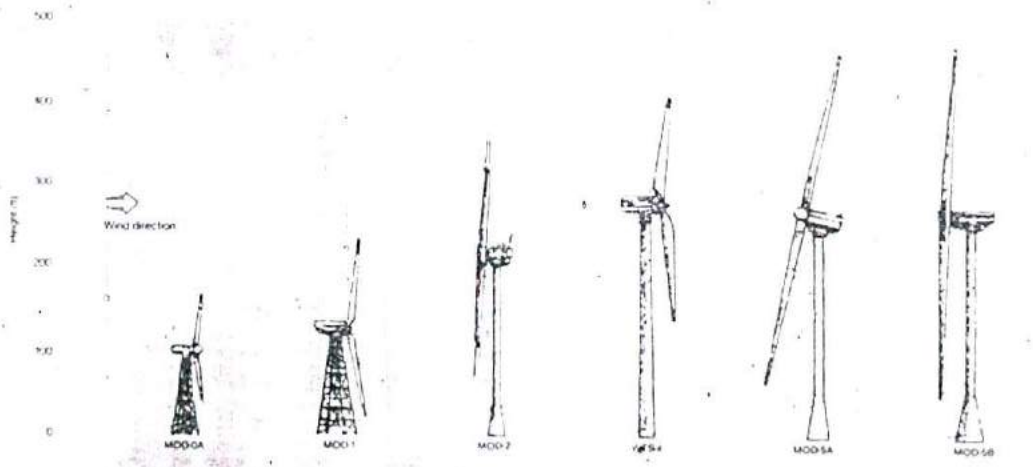
14-7 NEW DEVELOPMENTS: LARGE MACHINES

The large horizontal-axis wind turbine is currently receiving the lion's share of research and development funds and is the beneficiary of the most advanced technology for harnessing wind power. In the United States the development effort is managed by the National Aeronautics and Space Administration (NASA) for the Department of Energy and by the U.S. Bureau of Reclamation. The program has gone through three generations of machines (Fig. 14-14).

The *first generation* started with the MOD-0 machine, which was rated at 100 kW in 18-mi/h wind (at the reference height of 30 ft) and first tested in September 1975 at a NASA experimental station near Sandusky, Ohio. MOD-0, not shown in Fig. 14-14, has a power coefficient of 0.375, a power train efficiency of 0.75, a cut-in wind velocity of 8 mi/h (13 km/h), and a rotor speed of 40 r/min in winds over 6 mi/h (10 km/h). The blades are fully feathered in 60-mi/h winds, and the system was designed to withstand 150-mi/h (240-km/h) winds. The rotor, transmission train, generator, and controls are mounted on a bed plate atop a 100-ft (30-m) tower of pinned-truss design. The controls included a blade pitch change mechanism and a yaw control that rotated the bed plate at 1/6 r/min to keep the rotor aligned to the wind. The gear box had a speed ratio of 45 : 1. The alternator weighed 1425 lb_m (645 kg), rotated at 1800 r/min, and was rated at 125 kVA. The installation had a capital cost of $500,000, or a unit capital cost of $5000 per rated kW, 4 to 5 times that of conventional systems. The real cost is of course higher because it must take into account the overall load factor.

Four upgraded versions of the MOD-0 machine, called MOD-0A and rated at 200 kW, were subsequently built between 1977 and 1980. Their design data are shown in Fig. 14-14. The most improved and successful of the MOD-0A machines is the one built in Oahu, Hawaii. It generated 1.14 GWh between July 1980 and November 1981 for an overall load factor of about 0.45. The MOD-0A machines were followed by a single MOD-1 machine built at Howard's Knob, Boone, North Carolina, in 1979. Figures 14-15 and 14-16 show an overall view and a cross section of the nacelle of MOD-1.

The first-generation machines described above were research prototypes used for field experimentation, for the assessment of structural and aerodynamic performance, and to gain operating experience. Data gathered have been used in the design of the second-generation machines.



	First Generation		Second Generation		Final Generation	
Height of blade axis (ft)	100	140	200		250	362
Rotor diameter (ft)	125	200			400	450
Rated power (kW)	200	2000			6200	
Rated wind speed at 30 ft (mph)	18.3	25.5			20.4	
Cut-in/cut-out speed at 30 ft (mph)	6.9/14.2	11.0/25.0			7.8/49.3	
Weight on tower (short tons)	45	125			600	
Weight/Rated power (lbs/kW)	447	325	247		193	
Annual electric output at 12 mph (GWh)	0.64	2.4			16.7	
Annual electric output at 16 mph (GWh)	0.98	5.1			27.1	
Prime contractor	Westinghouse Electric Corp	General Electric Co	Boeing Engineering & Construction	Hamilton Standard Div. United Technologies Corp	General Electric Co	Boeing Engineering & Construction
Location (year of first installation)	Clayton, New Mexico (1977); Culebra Island, Puerto Rico (1978); Block Island, Rhode Island (1979); Oahu, Hawaii (1980)	Boone, North Carolina (1979)	Goldendale, Washington (Launch, 1980; Hatfield, Medicine Bow, Wyoming (1981); Solano County, California (1982)		Medicine Bow, Wyoming (1982)	To be determined	To be determined

Figure 14-14 Stages in the development of large horizontal-axis wind turbines in the United States. *(Courtesy Electric Power Research Institute.)*

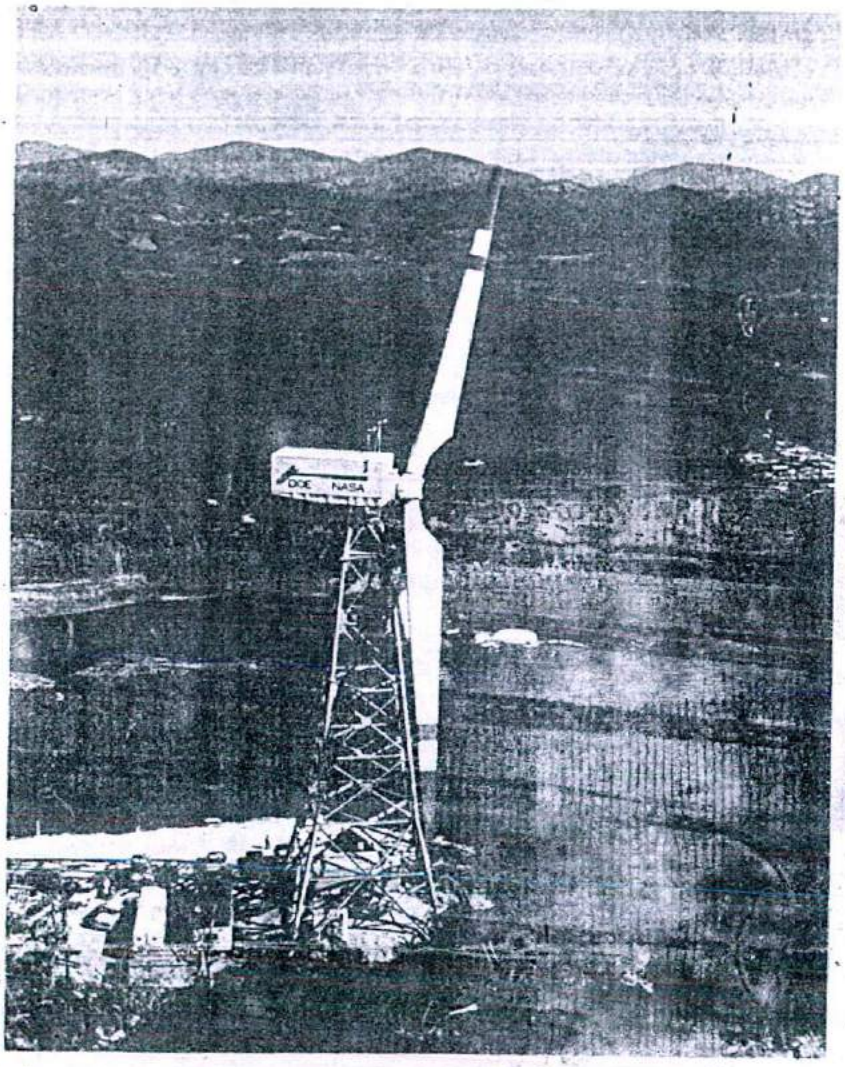


Figure 14-15 The MOD-1 wind turbine at Howard's Knob, Boone, North Carolina. (*Courtesy DOE.*)

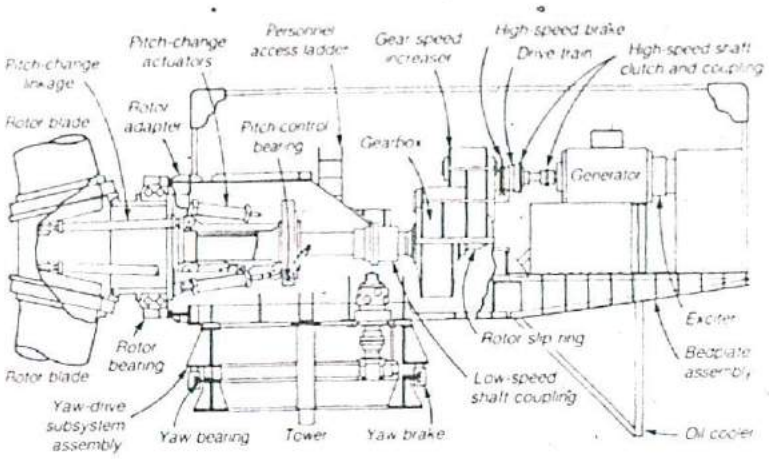


Figure 14-16 The MOD-1 nacelle showing rotor and blades (in part) on the left, electrical generator on the right, and yaw drive on the bottom.

The *second-generation machines*, called MOD-2 (Fig. 14-14), have two-bladed upwind turbines and are rated at 2.5 MW and situated atop 200-ft (61-m) cylindrical towers. The rotor is 300 ft (91 m) in diameter (which is the length of a football field) and is constructed as a continuous blade without a protruding hub. Speed control is accomplished by pitching the tips of the rotor. The cut-in, rated, and cut-out wind velocities (at tower top) are 14, 27.5, and 45 mi/h (6.3, 12.3 and 20.1 m/s), respectively. Five such machines have been built, three in Goodnoe Hills, Goldendale, Washington (in 1980, 1981, and 1981), and one each in Medicine Bow, Wyoming (in 1981), and Solano County, California (in 1982). Figure 14-17 is an artist's rendering of one of the Goodnoe Hills MOD-2 machines, and Fig. 14-18 is a cross section of the MOD-2 nacelle. Some design parameters of the MOD-2 machines are given in Table 14-1.

The *third-generation machines*, called MOD-5, are currently (1982) in the design stage. They are designed as advanced multimegawatt systems with the goal of reducing unit capital costs approximately 30 percent below the second-generation machines. There are two MOD-5 designs (Fig. 14-14), both upwind and twin-bladed. MOD-5A is rated at 6.2 MW with a rotor diameter of 400 ft (122 m). MOD-5B is rated at 7.2 MW with a rotor diameter of 420 ft (128 m). They are being designed with new features, such as two-speed and variable-speed operation, induction generators, and blades made of laminated wood.

Much of the early work on blades and their controls benefited from the experience of the helicopter rotor industry. The advanced wind turbines, however, have rotor diameters much greater than those common in helicopters, though their control systems are somewhat less complicated.

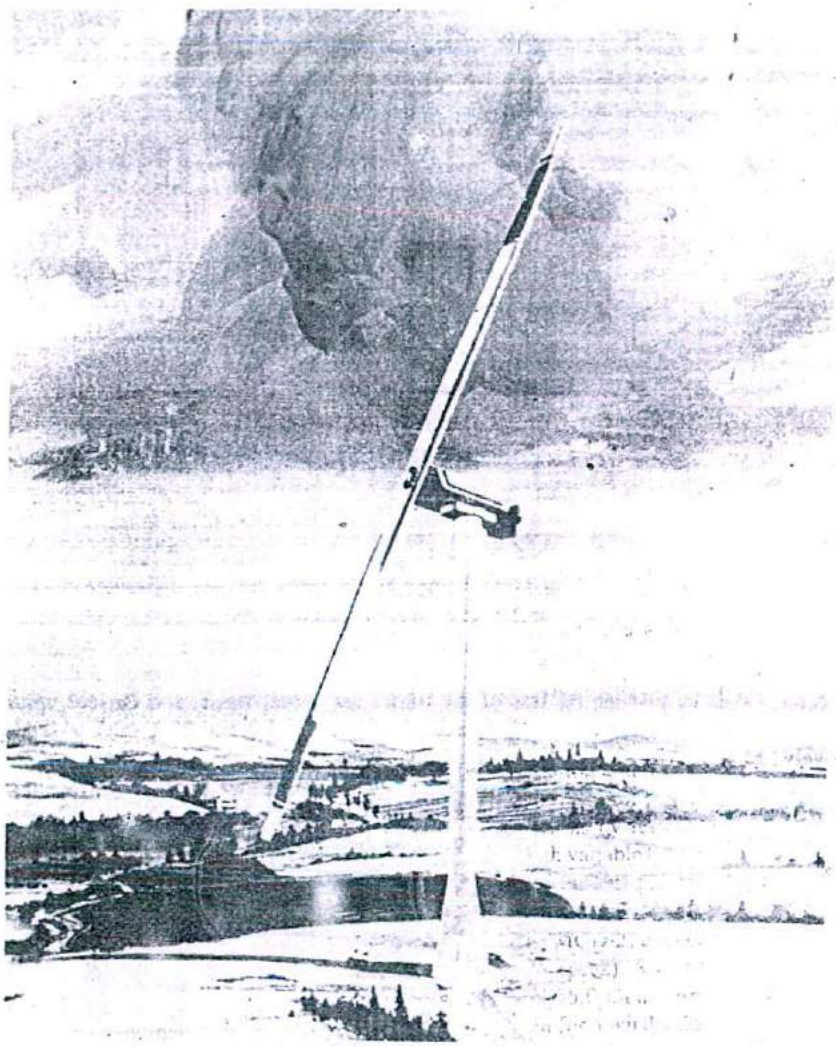


Figure 14-17 Artist's conception of the MOD 2 wind turbine at Goodnoe Hills [illegible] (*Courtesy DOE.*)

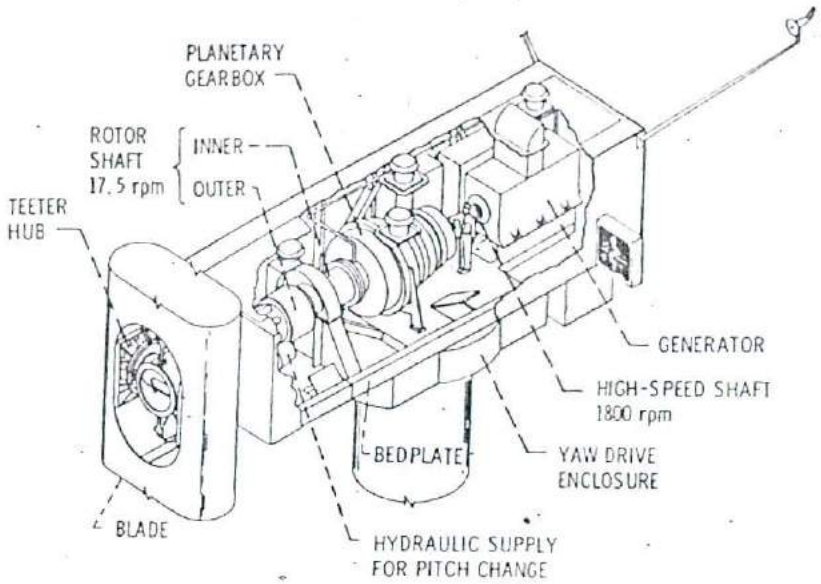


Figure 14-18 The MOD-2 nacelle [139].

Materials for the blades have varied over the years, including steel, aluminum, fiberglass, laminated wood, and combinations such as steel spar with foam trailing edge (MOD-1).

Novel Wind Turbines

Although research and development funds have gone largely to propeller-type wind turbines, some have been expended to investigate other designs that may offer future technical and economic advantages. Two of these will be covered in the next sections, the *Madaras concept* and the *Darrieus rotor*. While they are referred to here as "novel," the principles behind them are not new.

14-8 THE MAGNUS EFFECT

The Madaras concept is based on the *Magnus effect*, which was first demonstrated experimentally by Magnus in 1852. The effect showed that if a horizontal cylinder is rotated about its axis and moved through a still wind, a lift force is produced. Similarly, if a stationary horizontal cylinder is rotated about its axis in a cross wind, it will experience a lift force. The effect is equally applicable to a vertical cylinder being

Table 14-1 Some design parameters of the MOD-2 wind-turbine plant

Performance	Rated power	2.5 MW	
	Wind velocity, mi/h	At 30-ft height	At hub
	Cut-in	9.0	14.0
	Rated	20.0	27.5
	Cut-out	36.0	45.0
	Max. design	120.0	125.0
Rotor	Diameter	300 ft, 91 m	
	Number of blades	Two	
	Location, rotation	Upwind, counterclockwise	
	Revolutions per minute	17.5	
	Cone, tilt, twist angles	0°, 2°, 8°	
	Tip length, each	45 ft, 13.7 m	
	Material	Steel	
Tower	Height	192 ft, 58.5 m	
	Hub height	200 ft, 61 m	
	Type	Flared shell	
	Access	Power manlift	
Controls	Power regulation	Rotor-tip pitch control, hydraulic	
	Yaw	Internal toothing gear	
	Yaw motor, rate	Hydraulic, 0.25 deg/s	
	Supervisory	Microprocessor	
Generator	Rating, power factor	3125 kVA, 0.8	
	Voltage, frequency	4160 (three-phase), 60 Hz	
	Revolutions per minute	1800	
	Gearbox	Three-stage planetary	
	Gear step-up ratio	103	
Mass	Rotor	180,000 lb_m, 81,670 kg	
	Rotor and nacelle	364,000 lb_m, 165,150 kg	
	Tower	255,000 lb_m, 115,700 kg	

rotated about its axis in a cross wind. It will experience a force perpendicular to its axis, which will cause it to move in a direction essentially perpendicular to that of the wind.

The magnus effect can be explained by first considering a cylinder in nonviscous flow (Fig. 14-19). The cylinder has a length much greater than its diameter, so end effects are unimportant and flows around it can be considered two dimensional.

In Fig. 14-19*a* the cylinder is not rotating and a uniform stream is flowing past it, which gives rise to streamlines as shown. The velocity at any point on the surface of the cylinder is given [140] by

$$V_\theta = 2V_i \sin \theta \tag{14-32}$$

where V_θ = air velocity on the cylinder surface at angle θ

V_i = incoming uniform air velocity, far from the cylinder

θ = polar angle, measured from the stagnation point

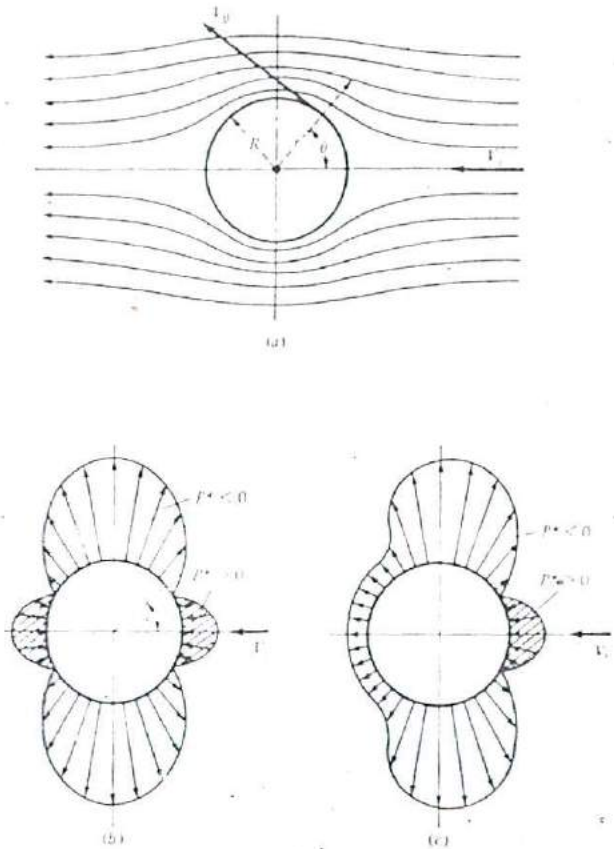


Figure 14-19 Streamlines and pressure distributions for two-dimensional flow past a nonrotating cylinder. $P^* = (P_\theta - P_s)/(\rho V_i^2/2g_c)$. *a* and *b*, nonviscous flow; *c*, viscous flow.

Applying Bernoulli's equation to any position θ on the surface of the cylinder gives

$$\frac{P_s}{\rho} + \frac{V_s^2}{2g_c} = \frac{P_\theta}{\rho} + \frac{V_\theta^2}{2g_c} \tag{14-33}$$

Combining with Eq. (14-32) gives

$$P_\theta = P_s + \frac{1}{2g_c}\rho V_i^2(1 - 4\sin^2\theta) \tag{14-34}$$

or

$$P_\theta^* = \frac{P_\theta - P_s}{\rho V_i^2/2g_c} = 1 - 4\sin^2\theta \tag{14-35}$$

where P_i = pressure of incoming stream

P_θ = pressure on the cylinder surface at θ

ρ = air density, considered constant

P^*_θ = nondimensional pressure on cylinder surface at θ

Thus P_θ is greater than P_i at the stagnation point ($\theta = 0$) by the quantity $\rho V_i^2/2g_c$, which is the *dynamic pressure* of the undisturbed stream. P_θ is equal to P_i at $\theta = \pm 30°$ and $\pm 150°$ and less than P_i at $\theta = \pm 90°$ by the quantity $3\rho V_i^2/2g_c$. The variation with θ is shown by the P^*_θ plot in Fig. 14-19*b*, which shows a symmetrical distribution about the cylinder. Thus no resultant forces occur either parallel or perpendicular to the undisturbed stream; i.e., there is neither lift nor drag on the cylinder for the case of ideal nonviscous flow.

Now we will consider that the cylinder is rotated about its axis but that the air far from the cylinder is at rest this time. The cylinder rotation produces a circulatory flow around it (Fig. 14-20) where the velocity is inversely proportional to the distance from the cylinder axis. Thus

$$2\pi r V_r = 2\pi R V_p = \Gamma$$

or
$$V_r = \frac{\Gamma}{2\pi r} \tag{14-36}$$

and
$$V_p = \frac{\Gamma}{2\pi R} \tag{14-37}$$

where V_r = velocity at distance r from the cylinder axis

V_p = cylinder peripheral velocity = $2\pi RN$

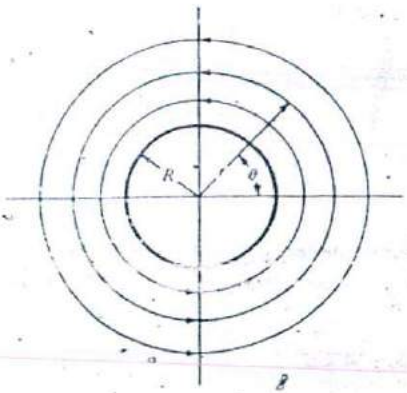


Figure 14-20 Circulatory flow around a rotating cylinder in an otherwise still air.

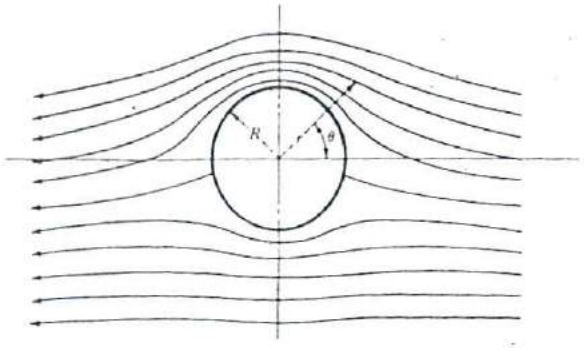


Figure 14-21 Velocity streamlines around a rotating cylinder in a stream of air.

r = radial distance from cylinder axis

R = cylinder radius

Γ = a constant = $2\pi RV_p = (2\pi R)^2 N$ having the dimension length^2/time and called the *circulation constant*

N = number of revolutions per unit time

Now we will combine the two cases from above, i.e., a rotating cylinder in a stream of air. When Figs. 14-19*a* and 14-20 are superimposed, it is obvious that the two velocity patterns will reinforce each other when in the same direction, i.e., at the cylinder top, and oppose each other at the bottom. Thus there will be a velocity increase at the top and a velocity decrease at the bottom (Fig. 14-21). The velocity V on the cylinder surface is given by the sum of V_θ and V_p from Eqs. (14-32) and (14-37), or

$$V = 2V_t \sin\theta + \frac{\Gamma}{2\pi R} \tag{14-38}$$

where $\sin\theta$ is positive between $\theta = 0$ and 180° and negative between 0 and −180°. The pressures on the cylinder will therefore be higher at the bottom (where the velocities are lower) and lower at the top (where the velocities are higher) than in the case of no cylinder rotation. Note the stagnation points where $V = 0$ are no longer at $\theta = 0$ and 180° but are slightly on the lower side of the cylinder.*

* The two stagnation points approach each other as V_p increases until only one stagnation point occurs at $\theta = -90°$ when $V_p = 2V_t$ and $\Gamma = 4\pi RV_t$.

The Lift Force

There will, therefore, be a *lift force* acting perpendicular to the direction of the stream. The lift force is obtained by integrating the component of the pressure on the cylinder that is perpendicular to the free stream. The pressure is obtained by using Bernoulli's equation, as was done for Eq. (14-33), except that the velocity from Eq. (14-38) is used in place of P_a. Thus

$$P = P_i + \frac{1}{2g_c}\rho\left[V_i^2 - \left(2V_i \sin\theta + \frac{\Gamma}{2\pi R}\right)^2\right] \tag{14-39}$$

where P = pressure on cylinder surface at θ (Fig. 14-21*b*). The lift force is obtained from

$$F_L = \int_{-\pi}^{+\pi} -P \sin\theta \, R \, d\theta \, H \tag{14-40}$$

Combining with Eq. (14-39) and integrating results in

$$F_L = \frac{2\pi}{g_c}\rho R H V_p V_i = \frac{4\pi^2}{g_c}\rho R^2 H N V_i \tag{14-41}$$

where F_L = lift force on cylinder

H = length (or height) of cylinder

It is convenient to give the lift force in terms of a dimensionless *lift coefficient* C_L, the dynamic pressure of the free stream $\rho V_i^2/2g_c$, and the projected area of the cylinder $A = 2RH$, or

$$F_L = C_L A \rho \frac{V_i^2}{2g_c} \tag{14-42}$$

Comparing this with Eq. (14-41) gives, for nonviscous flow

$$C_L = 2\pi\frac{V_p}{V_i} \tag{14-43}$$

or the value of the lift coefficient in nonviscous flow is directly proportional to the ratio of the cylinder peripheral to the free stream velocities.

As indicated, the above development of the Magnus effect was based on ideal nonviscous flow. For a real fluid, the effects of viscosity and boundary layer separation result in a pressure distribution for nonrotating cylinders as shown in Fig. 14-19*c*. Experimental measurement on rotating cylinders in real fluids show values of C_L that are much lower than those given by Eq. (14-43), reaching a maximum between 9 and 10 beyond a speed ratio V_p/V_i of 4 or 5 (Fig. 14-22). Equation 14-42 should be used with a value of C_L obtained from Fig. 14-22.

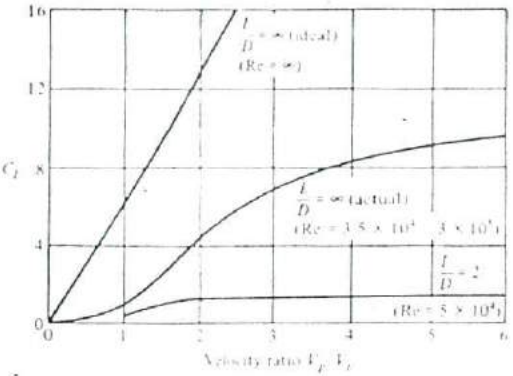


Figure 14-22 Lift coefficient of a rotating cylinder in an air stream as a function of the ratio of the cylinder peripheral and free stream velocities.

The Drag Force

The *drag force* for an ideal fluid was found above to be zero. For a real fluid the imbalance in pressures (Fig. 14-19c), results in a drag force in the direction of the free stream, given, similarly to Eq. (14-42), by

$$F_D = C_D A \rho \frac{V_t^2}{2g_c} \tag{14-44}$$

where C_D = drag coefficient, dimensionless. It is a function of the Reynolds number

$$\text{Re} = \frac{DV_t\rho}{\mu} \tag{14-45}$$

where D = diameter of cylinder = $2R$

μ = viscosity of fluid

The relationship between C_D and Re for long smooth cylinders is shown in Fig. 14-23.

The force acting on the cylinder is the resultant force between the lift and drag forces.

Example 14-2 Calculate the lift, drag, and resultant forces on a 6-ft-diameter, 90-ft-long smooth cylinder rotating at 140 r/min in a 30 mi/h wind. The wind is at 1 standard atm pressure and 60°F.

SOLUTION For air at 1 atm and 60°F

$$\rho = \frac{P}{RT} = \frac{14.69 \times 144}{53.34 \times (60 + 460)} = 0.0763 \text{ lb}_m/\text{ft}^3$$

$$\mu = 0.046 \text{ lb}_m/(\text{h} \cdot \text{ft})$$

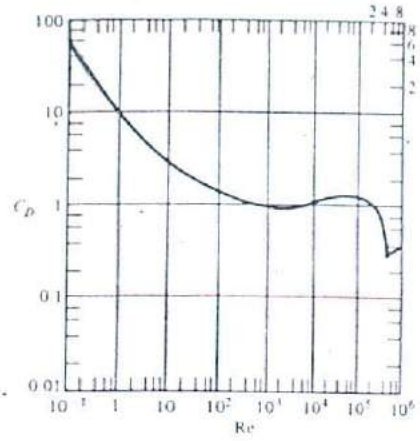


Figure 14-23 Drag coefficient as a function of Reynolds number for long smooth cylinders [140].

$$V_r = \pi DN = \pi \times 6 \times \frac{140}{60} = 44 \text{ ft/s}$$

$$V_t = 30 \text{ mi/h} = \frac{30 \times 5280}{3600} = 44 \text{ ft/s}$$

$$V_r/V_t = 1.0$$

$$\text{Re} = \frac{DV\rho}{\mu} = \frac{6 \times 44 \times 0.0763}{0.046/3600} = 1{,}576{,}400$$

Therefore

$$C_L = 1.0 \quad \text{(Fig. 14-22)}$$

and

$$C_D = 0.4 \quad \text{(by extrapolation from Fig. 14-23)}$$

Dynamic pressure $\rho V_t^2/2g_c = 0.0763 \times 44^2/(2 \times 32.2) = 2.294 \text{ lb}_f/\text{ft}^2$

Lift force = $1.0 \times 6 \times 90 \times 2.294 = 1239 \text{ lb}_f$

Drag force = $0.4 \times 6 \times 90 \times 2.294 = 495 \text{ lb}_f$

Resultant force = $\sqrt{1239^2 + 495^2} = 1334 \text{ lb}_f$

Ideal lift coefficient = $2\pi \times 1 = 2\pi$

Ideal lift force = $2\pi \times 60 \times 90 \times 2.294 = 7785 \text{ lb}_f$

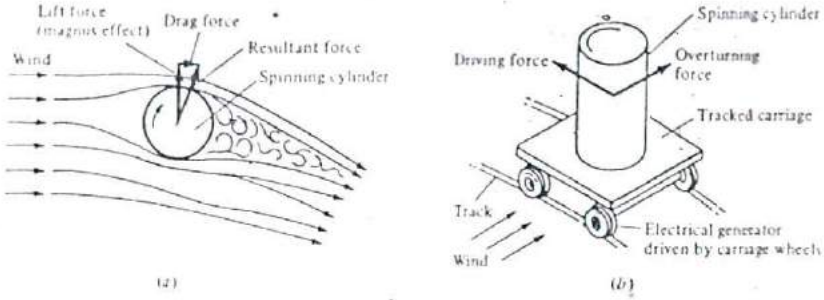


Figure 14-24 Resultant force of lift and drag propelling a spinning vertical cylinder along a track [135].

14-9 THE MADARAS ROTOR WIND MACHINE

Based on the Magnus effect, the Madaras rotor powerplant was invented by Julius D. Madaras in 1912 and was soon sponsored by the Detroit Edison Company, which actually built a pilot model of it at Burlington, New Jersey, in 1933. It generated much interest because of the novel idea behind it and because it was sponsored by an important utility.

The concept consists of several tall vertical cylinders that are rotated about their axes in the presence of a wind. The resultant of the lift and drag forces, more in the direction of lift because of its larger value (Fig. 14-24*a*), propels the cylinders horizontally* along a track (Fig. 14-24*b*).

The powerplant concept as proposed by Madaras consists of a circular train track with a continuous train of four-wheel flat cars on it (Fig. 14-25). Each flat car has a 90-ft-high cylinder that is rotated about its vertical axis at 120 r/min by a small electric motor. The resultant force along each cylinder moves flat cars around the circular track. To keep the force in the same circumferential direction along the track, the direction of rotation of the cylinders is reversed twice each complete turn around the track. The carriage wheels drive electrical generators, and the electricity generated is transmitted to the mains by a trolley.

The Madaras project generated a lot of excitement and attracted a number of highly qualified engineers who agreed that it was a sound, economical, and safe means of electric-power generation. It was relatively insensitive to wind velocity changes, above about 6 mi/h, and was believed able to withstand winds of 100 to 120 mi/h. Its capital cost was estimated in 1928 at $40/kW for a 10-MW plant. The pilot plant erected at Burlington, New Jersey, in 1933, unfortunately, blew down in a high wind before it was even tested with the loss of several million dollars and much time and effort.

It was the failure of both the Madaras and Smith Putnam (Sec. 14-2) machines that caused commercial utilities in the United States to quietly abandon efforts at

* The Magnus effect was used to propel a ship across the Atlantic Ocean in the early 1930s.

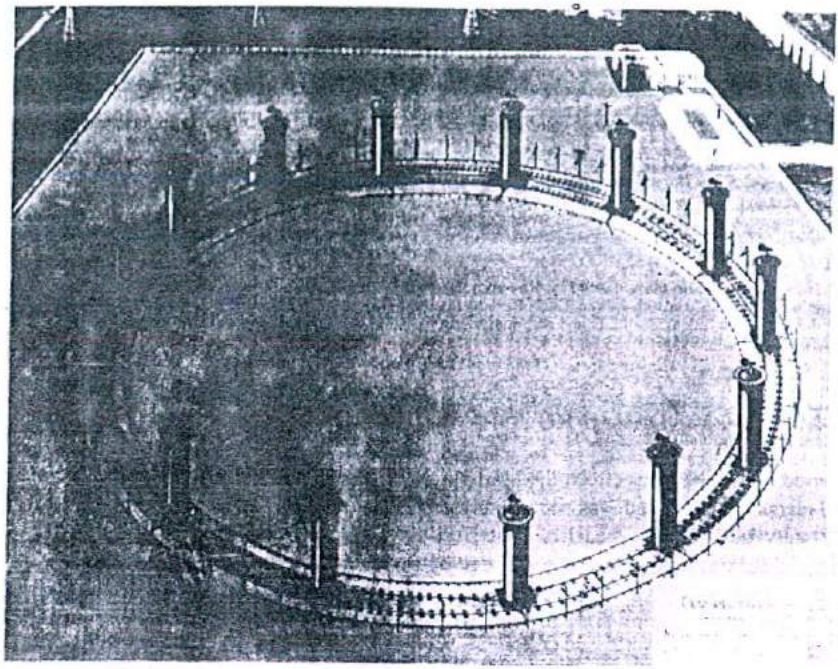


Figure 14-25 The Madaras concept in perspective [135]

generating power from the wind back in the 1930s and 1940s. It was thus up to the federal government to sponsor wind-power research and development when interest was rekindled with the energy crisis of the 1970s.

14-10 THE DARRIEUS MACHINE

The *Darrieus* wind turbine, shown in two forms, the ϕ and the Δ in Fig. 14-2 is an invention of Georges Darrieus of France, who patented it in 1920. The ϕ-Darrieus has received renewed interest as a machine that may efficiently fill the gap between the small domestic and large utility wind turbines. Unlike the large modern machines, but like the ancient Persian ones, it is a vertical-axis machine, but here the similarity with the ancient machines ends. A Darrieus wind turbine is invariably described as looking like an egg beater, with either two or three slender wires or blades that loop over the top and that are joined at top and bottom to the vertical axis (Fig. 14-26).

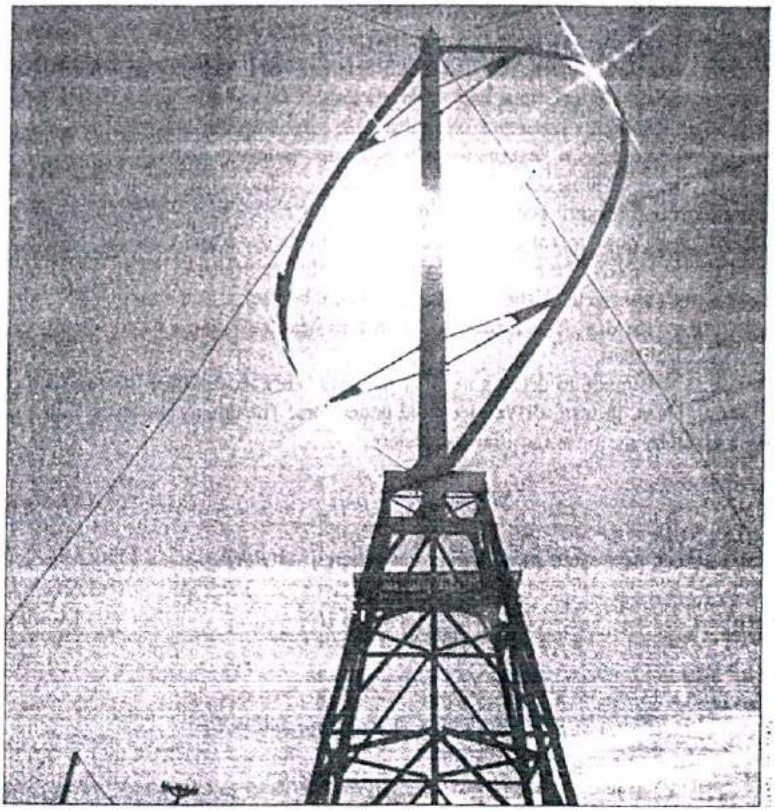


Figure 14-26 A Darrieus windmill under testing at West Texas State University (*Courtesy DOE.*)

The Darrieus machine has the advantages of spinning in any wind direction, thus requiring no yaw control, and a vertical axis that allows the power-conversion equipment, such as an electrical generator or pump, to be located in a stationary ground installation.

The Darrieus concept is under investigation by Sandia Laboratories for the DOE. Several machines have been constructed and were undergoing tests in the early 1980s, the largest being used for a deep-well irrigation system in Bushland, Texas. It has two blades 37 ft in diameter and 55 ft high, produces 56 hp (42 kW) in 30-mi/h (13.4-m/s) wind, and is used to pump 300 gal/min of water from a 280-ft-deep well. Pump speed is maintained in this experimental unit by connecting the pump in parallel to an electrical motor or a governed Diesel engine.

14-11 OTHER WIND TURBINE DESIGNS

Besides the propeller, Madaras, and Darrieus, there has been a plethora of designs for wind machines. Wind, more than any other renewable energy source, has intrigued professional and amateur inventors over the ages. In recent years DOE has been evaluating literally dozens of designs for wind systems, some have already been shown in Fig. 14-2. The governing consideration, as always, is the economic one: what size and cost are needed per unit power output.

One intriguing powerplant design, called an *aeroelectric plant*, uses the flow up a tower that looks much like a cooling tower. Its walls are heated by solar radiation. Because the walls are circular, the sun's rays need not be tracked as it changes position in the sky during the day. The heated walls in turn heat the inside air and a flow up the tower is established.

This air flow is made to drive a number of air turbines located near the top of the tower. The turbines, in turn, drive electrical generators. The driving pressure causing airflow is given by the now familiar expression

$$\Delta P_d = (\rho_o - \rho_i)H\frac{g}{g_c} \tag{14-46a}$$

and, since air can be treated as a perfect gas where $\rho = P/RT$

$$\Delta P_d = \frac{1}{R}\left(\frac{P_o}{T_o} - \frac{P_i}{T_i}\right)H\frac{g}{g_c} \tag{14-46b}$$

where ΔP_d = driving pressure needed to overcome the pressure losses in the tower and to drive the air turbines

P_o = outside air pressure

P_i = average inside air pressure

R = air gas constant

T_o = outside air absolute temperature

T_i = average inside air absolute temperature

H = height of tower

g = acceleration of gravity

g_c = conversion factor

A variation of the above system is one proposed by P. Carlson of California. The interior air in a very tall tower would be cooled by pumping water to the top. The water evaporates in the low-pressure air there, causing a downward flow of the cooled air. The driving pressure is obtained from Eq. (14-46*a*) but with P_i/T_i and P_o/T_o in reversed positions. They are to be calculated in a manner similar to that for wet cooling

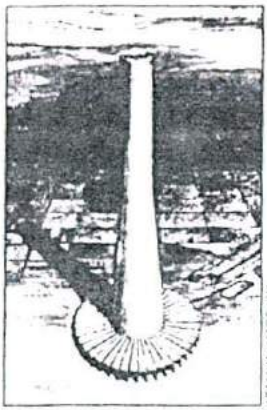


Figure 14-27 The Carlson aeroelectric tower (*ASME*.)

towers (Sec. 7-5). A conceptual design of such a plant called for a 1.5-mi-high, 900-ft-diameter tower located in a hot desert and 10 wind turbines surrounding the tower periphery at the bottom producing 2500 MW (Fig. 14-27).

PROBLEMS

14-1 A 27 mi/h wind at 14.65 psia and 70°F enters a turbine wheel that has a 1000-ft^2 cross-sectional area. Calculate (*a*) the power of the incoming wind, (*b*) the theoretical maximum attainable turbine power, (*c*) a reasonably attainable turbine power, all in horsepower and kilowatts, (*d*) the torque, and (*e*) the axial thrust, in pound force, if the turbine wheel rotates at 30 r/min.

14-2 Consider two cases: (*i*) a constant wind velocity twice the mean velocity and operating half the time, and (*ii*) a constant wind velocity three times the same mean velocity operating one third of the time. At all other times the wind velocity is zero. Determine for each case (*a*) the ratio of total energy in the wind to that if it operated continuously at the mean velocity, and (*b*) the mean energy velocity as a function of the mean velocity.

14-3 A 15-ft-diameter wind turbine operates in 25 ft/s wind at 1 atm and 60°F. The turbine is used to pump 60°F water from a 30-ft-deep well. How much water is pumped, in cubic feet per day, if the overall efficiency of the wind-turbine-pump system is 0.25?

14-4 A wind turbine with a diameter of 100 ft operates during a 24-h period in which the wind velocity may be approximated by half a sine wave as $V(\theta) = V_m \sin(\pi\theta/24)$, where θ is time in hours and $V_m = 10^5$ ft/h. The wind density is 0.076 lb$_m$/ft^3. Calculate (*a*) the theoretical maximum turbine energy during that 24-h period, in foot-pound force and kilowatt hours, and (*b*) the wind mean energy velocity, in feet per hour.

14-5 Consider a wind velocity pattern during a 24-h period in which the wind velocity increased steadily and linearly from zero to 48 ft/s. The wind density is 0.0768 lb$_m$/ft^3. A 200-ft-diameter wind turbine operates in that wind with cut-in, rating, and cut-out wind velocities of 12, 24, and 42 ft/s, respectively. The turbine-generator overall efficiency is assumed, for simplicity, constant at 0.25. Calculate (*a*) the power generated during the day, in kilowatt hours, and (*b*) the wind mean energy velocity, in feet per second.

14-6 A wind at 1 atm and 62.4°F had a velocity pattern during one day that could be approximated by half a sine wave with an amplitude of 1.1×10^5 ft/h. A 100-ft-diameter wind turbine with a cut-in, rated, and cut-out velocities of 4.0×10^4, 8.0×10^4, and 1.2×10^5-ft/h, respectively, operated in that wind.

Calculate (*a*) the energy generated, in kilowatt hours during that day, if the overall efficiency of the turbine-generator is 0.34, and (*b*) the wind mean energy velocity, in feet per hour.

14-7 A wind at 14.5 psia and 55°F had a velocity pattern during one day that followed a full sinusoidal wave with a mean velocity of 20 mi/h and an amplitude of 10 mi/h. A wind turbine with a 30,000-ft² area operated in that wind. Calculate for that day (*a*) the total energy of the wind, (*b*) the theoretical maximum energy developed by the turbine, (*c*) the theoretical maximum energy developed by the turbine if the wind had a constant velocity at the mean value, (*d*) a reasonably attainable turbine energy in the actual wind, all in foot-pound force and kilowatt hours, and (*e*) the wind mean energy velocity, in miles per hour.

14-8 Repeat Prob. 14-7, but assume that the wind turbine had cut-in and cut-out velocities of 8 and 20 mi/h, respectively, and was not flat-rated.

14-9 Two wind patterns follow the Weibull distribution model. One has a mean wind velocity of 12 m/s, the other 8 m/s. Calculate the percent of time that each exceeds a velocity of 10 m/s.

14-10 A wind pattern that follows the Weibull distribution model has a reference mean velocity 10 m/s. Consider a wind turbine that has cut-in, rated, and cut-out velocities of 4.97, 8.84, and 16.29 m/s, respectively, all at the reference height above ground of 9.1 m. Calculate for the reference height (*a*) the turbine availability factor, (*b*) the percent time it operates below rated capacity, and (*c*) the percent time it operates at rated capacity.

14-11 Repeat Prob. 14-10 but for a wind turbine with a hub 50 m above ground.

14-12 Wind at 1 bar and 20°C has a velocity of 15 m/s, measured at the reference height above ground of 9.1 m (30 ft). Calculate (*a*) the power density in the wind at the reference height. Estimate (*b*) the power density at the hub of a large 60-m-diameter wind turbine, 60 m above ground, (*c*) the maximum theoretical power delivered by the turbine, and (*d*) a reasonably attainable power by the turbine generator if the latter has an efficiency of 94.2 percent, all in watts per square meter.

14-13 A 30-m-long 2 m-diameter cylinder rotates at 120 r/min in a 10 m/s wind that is at 1 atm and 15°C. Calculate (*a*) the ideal and actual lift forces, in newtons, (*b*) the ideal and actual drag forces, in newtons, and (*c*) the positions of the stagnation points.

14-14 A Madaras rotor wind machine consists of 14 vertical cylinders such as the one described in Prob. 14-13. Assume for simplicity that the wind at 1 atm and 15°C is at standstill and that the cylinders move around a 220-m-diameter track at 10 m/s circumferential velocity. Calculate (*a*) the magnitude, in newtons, and direction of the resultant force on each cylinder with respect to the direction of motion, (*b*) the maximum power generated by one cylinder, in kilowatts, (*c*) the power of the entire machine if it takes each cylinder 5 percent of the travel distance to change its direction of rotation (ignore the power produced during that change), and (*d*) the energy produced by the machine during one complete circle, in kilowatt hours.

14-15 An aeroelectric wind powerplant with turbines on top has a 1.5-mi-high tower. The outside air is at 1 atm and 60°F. The inside air is at an average temperature of 160°F. The tower diameter is very large so that only 2.5 percent of the driving pressure goes to overcome frictional and other losses in it. The balance drives the turbines. Calculate (*a*) the total pressure drop in the tower, in pounds per square inch, and (*b*) the power produced by the turbines, in watts, per unit air volume flow rate, in cubic feet per hour, if they have an overall efficiency of 0.75.

14-16 A Carlson aeroelectric wind powerplant has a 1.5-mi-high tower. The outside air is at 1 atm, 60°F, and 20 percent relative humidity. Water is injected at top so that the air becomes saturated. The process is one of evaporative cooling which is a constant wet-bulb temperature process. Calculate (*a*) the driving pressure on the turbines, in pounds per square inch, and (*b*) the power produced by the turbines, in watts, per unit air volume flow rate, in cubic feet per hour, if they have an overall efficiency of 0.75. Ignore pressure losses in tower.

CHAPTER

FIFTEEN

ENERGY FROM THE OCEANS

15-1 INTRODUCTION

Solar energy, which may be used directly (Chap. 13), creates other forms of energy that can also be harnessed to generate power. One, the wind, is caused by the uneven solar heating and cooling of the earth's crust combined with the rotation of the earth (Chap. 14). Another is the result of the absorption by the seas and oceans of solar radiation, which causes, like the wind, ocean currents and moderate temperature gradients from the water surface downward, especially in tropical waters. The oceans and seas constitute some 70 percent of the earth's surface area, so they represent a rather large storage reservoir of the solar input.

The temperature gradient can be utilized in a heat engine to generate power. This is called *ocean temperature energy conversion* (OTEC). OTEC power is collected solar energy once removed. Because the temperature difference is small, even in the tropics, OTEC systems have very low efficiencies and consequently have very high capital costs.

The wind, whose energy is also solar energy once removed, generates large *ocean waves* with energies that can be used to generate power. Ocean-wave energy thus is said to be solar energy twice removed. Ocean waves, unfortunately, vary widely with time and place in amplitude and frequency, and hence in their energies, much like the wind that causes them. There are, however, areas in the world where energetic waves persist a good deal of the time. Such waves have been considered for [illegible] by a wide variety of ingenious means.

A third form of energy that emanates from the sun-ocean system stems from the mechanism of surface water evaporation by solar heating. This forms clouds that

condense into rains. Part of that rain falls over land, which causes river flows, which may be trapped behind dams to even out the variations in these river flows and thus become the source of either low-head (river) or high-head (dam) *hydroelectric energy*. Hydroelectricity accounts for some 25 percent of the world's total electricity capacity. Some countries, such as Norway, Switzerland, and Canada, because of favorable topographies and rainfall, far exceed this average. In the United States, the percentage was 15 percent in the 1970s, going down to some 10 percent in the 1980s. Hydroelectricity used to account for much more than these percentages in the nineteenth century, but the advent of cheap coal and steam powerplants, and the lack of additional favorable hydro sites, caused a decline in its use. Many small river hydroelectric plants were abandoned. With the coming of the energy crisis of the 1970s, interest was renewed in these small plants to supplement input to power grids.

A fourth major, though different, source of energy in the oceans that can be exploited for power generation is the *tides*. Tides are primarily caused by lunar, and only secondarily by solar, gravitational forces acting together with those of the earth on the ocean waters to create tidal flows. These manifest themselves in the rise and fall of waters with ranges (height differences) that vary daily and seasonally and come at different times from day to day. They also vary widely from place to place, being as low as a few centimeters but may exceed 8 to 10 m (25 to 30 ft) in some parts of the world. The potential energy of the tides can be trapped to generate power, but at extremely high capital costs.

In this chapter, power production from the energies associated with the ocean temperature difference (OTEC), the waves, and the tides will be discussed. Hydroelectric power is a major topic in its own right and deserves a separate course of study. The interested reader is advised to consult the many books that are devoted to it. See, for example, the *Handbook of Applied Hydraulics* [141].

15-2 OCEAN TEMPERATURE DIFFERENCES

As the seas and oceans of the earth constitute about 70 percent of its surface area, the total terrestrial solar-energy incidence on them is immense, being equal to the total extraterrestrial solar energy received by the earth, which is about 1.516×10^{18} kWh/year, or about 5.457×10^{18} MJ/year, times an average clearness index of 0.5 (Sec. 13-14), times the fraction of the area 0.7 or about 0.53×10^{18} kWh/year, or 1.9×10^{18} MJ/year. This corresponds to an average terrestrial incidence on the waters of the solar constant $S = 1353\ \text{W/m}^2 \times 0.5 = 676\ \text{W/m}^2$. This energy is not totally absorbed by the water because some of it is reflected back to the sky. A good estimate of the amount absorbed is obtained from the annual evaporation, which averages 120 cm (or 120 cm^3/cm^2, or 1.20 m^3/m^2).* At an average water surface temperature of 20°C (68°F), the latent heat of vaporization is 2454 kJ/kg and the sea water density is a little over 1000 kg/m^3. The annual energy absorbed would therefore be $1.20 \times 1000 \times 2454$, or about $3 \times 10^6\ \text{kJ/m}^2$ per year, which is equivalent to about

* This amount is, of course, replenished by rainfall back on the water and by runoff from land.

95 W/m² or about 14 percent of the incidence. This figure varies, being a little higher than 100 W/m² in the tropics to much less in arctic waters.

Solar-energy absorption by the water takes place according to *Lambert's law of absorption*, which states that each layer of equal thickness absorbs the same fraction of light that goes through it. In other words

$$-\frac{dI(y)}{dy} = \mu I$$

or

$$I(y) = I_o e^{-\mu y} \tag{15-1}$$

where I_o and $I(y)$ are the intensities of radiation at the surface ($y = 0$) and at a distance y below the surface. μ is an *extinction coefficient* (also called *absorption coefficient*) that has the unit length^{-1}. μ has values of 0.05 m^{-1} for very clear fresh water, 0.27 m^{-1} for turbid fresh water, and 0.50 m^{-1} for very salty water. Thus the intensity falls exponentially with depth and, depending upon μ, almost all of the absorption occurs very close to the surface of deep waters. Because of heat and mass transfer at the surface itself, the maximum temperatures occur just below the surface.

Considering deep waters in general, the high temperatures are at the surface, whereas deep water remains cool. In the tropics, the ocean surface temperature often exceeds 25°C (77°F), while 1 km below the temperature is usually no higher than 10°C (50°F). Water density decreases with an increase in temperature (above 3.98°C, where pure water's density is maximum, decreasing again below this temperature, the reason ice floats). Thus there will be no thermal convection currents between the warmer, lighter water at the top and the deep cooler, heavier water. Thermal conduction heat transfer between them, across the large depths, is too low to alter this picture and thus mixing is retarded, so the warm water stays at the top and the cool water stays at the bottom.

It is said, therefore, that in tropical waters there are two essentially infinite heat reservoirs, a heat source at the surface at about 27°C (81°F) and a heat sink, some 1 km directly below, at about 4°C (39°F); both reservoirs are maintained annually by solar incidence.

The concept of ocean temperature energy conversion (OTEC) is based on the utilization of this temperature difference in a heat engine to generate power, a concept first recognized by the Frenchman d'Arsonval in 1881. The maximum temperature difference on earth is in the tropics and is about 15°C (59°F). Ocean currents carry the 27 to 28°C warm tropical surface waters on a journey to the arctic circles during which they are gradually cooled to 4°C and maximum density (Fig. 15-1). In the arctic circle they then settle below the surface, and a surface–deep water siphon is created that keeps cold water below the surface.

The surface temperatures (and temperature differences) vary both with latitude and season (Fig. 15-2), both being maximum in tropical, subtropical, and equatorial waters, i.e., between the two tropics, making these waters the most suitable for OTEC systems [143].

The claims for OTEC systems are just as grandiose as those for most other renewable energy systems. For example, it is said that the Gulf stream is known to

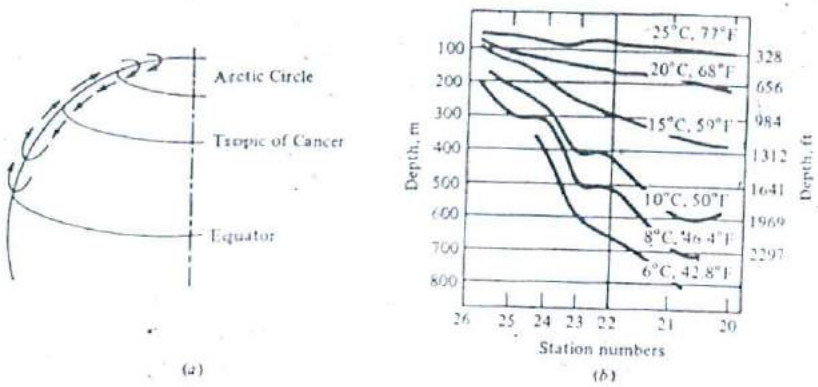


Figure 15-1 (*a*) Ocean-water movement in the northern hemisphere. (*b*) Measured water temperatures at various stations and depths in the Straits of Florida [142].

carry some 30 to 40 million m^3/s of near tropical sea water through the Gulf of Florida, flowing in a path about 32-km (20-mi) wide. Within 800 km (500 mi) of that path, the temperature differences between surface and deep waters varies between 22°C (40°F) and 15°C (27°F). Assuming a practical conversion efficiency of 2 percent (below), the Gulf stream represents an annual power potential of 700×10^{12} kWh. An array of conversion plants moored on 1-mi (1.6-km) spacings along the length and breadth of that path would be capable of an annual 26×10^{12} kWh. Such are the claims for OTEC, but as we will soon learn, practical and financial problems effectively preclude such dreams.

The maximum possible efficiency of a heat engine operating between two temperature limits cannot exceed that of a Carnot cycle operating between the same temperature limits. For heat source and sink temperatures, T_1 and T_2, the Carnot efficiency η_C is

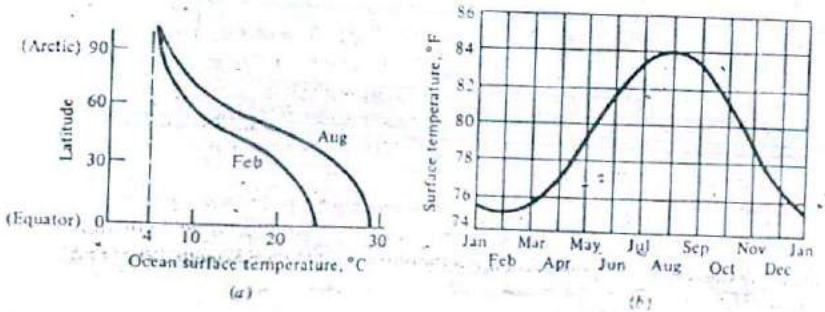


Figure 15-2 Ocean surface temperature as a function of (*a*) latitude and (*b*) the seasons, in tropical waters.

$$\eta_C = \frac{T_1 - T_2}{T_1} \tag{15-2}$$

It is thus important to have a large temperature difference $T_1 - T_2$. In OTEC systems this may average 20°C (68°F) compared with about 500°C (932°F) for modern fossil powerplants. Taking the temperature difference of 20°C and a surface temperature of 27°C, the Carnot efficiency would be

$$\eta_C = \frac{20}{27 + 273} = 0.0667 = 6.67\%$$

Thus for 27°C (300 K) surface temperature an OTEC system can have no efficiency greater than $\Delta T/300$ or 1/3 ΔT percent, where ΔT is the difference between surface and deep waters. Because of temperature drops in steam or other vapor generator and condenser in an actual system (external irreversibilities, Chap. 1), inefficiencies in turbine and pumps, pressure drops of the large volumes of water and working fluid flows (internal irreversibilities), and inefficiencies of other components, the efficiency of a real OTEC powerplant seldom exceeds 2 percent.

The extremely low efficiency of an OTEC system implies extremely large powerplant heat exchangers and components. At 2 percent efficiency the heat exchangers must handle 50 times the net output of the plant. Although there are no fuel costs, the capital costs are extremely high and so are the unit capital costs, $/kW. In addition to the large size per unit power generation, the developmental problems and the uncertainties of market penetration make the financial risks associated with the development of large OTEC technologies so high as to effectively preclude most utilities. (The same can be said for other ocean energy systems, as well as most solar-electric systems, especially the solar satellite system, Sec. 13-20).

There are two basic designs for OTEC systems: the *open cycle*, also known as the *Claude cycle* and the *closed cycle*, also known as the *Anderson cycle*. These are covered in the next two sections.

15-3 THE OPEN, OR CLAUDE, CYCLE

The first OTEC plant to be constructed was built by the Frenchman Georges Claude in 1929 on the Matanzas Bay in Cuba [144]. It used the warm waters of the Gulf Stream as a heat source and a submarine cliff adjacent to the bay that descends nearly vertically to depths of 105 to 260 m as the heat sink. The warm surface water was at 25°C (77°F). The cold water, at 14°C (51.8°F), was tapped by a 2-km-long, 2-m-diameter pipe that weighed 400 tons. The laying of the cold-water pipe was the most difficult part of the construction: two such pipes were lost before a third was successfully installed.

The Claude plant used an *open cycle* (also called the Claude cycle) in which seawater itself plays the multiple role of heat source, working fluid, coolant, and heat sink. Schematic flow and corresponding T-s diagrams are shown in Figs. 15-3 and 15-4, respectively.

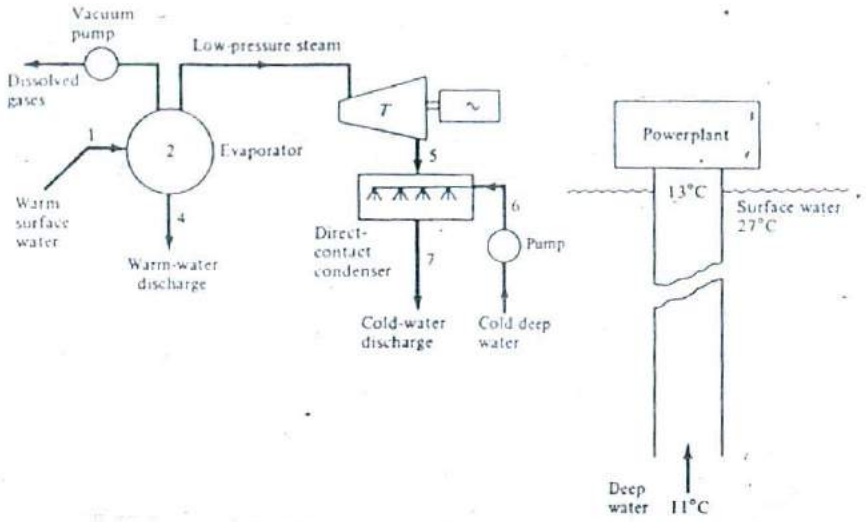


Figure 15-3 Flow diagram and schematic of a Claude (open-cycle) OTEC powerplant

In the cycle shown warm surface water at 27°C (80.6°F) is admitted into an evaporator in which the pressure is maintained at a value slightly below the saturation pressure corresponding to that water temperature. Water entering the evaporator, therefore, finds itself "superheated" at the new pressure. For example, in Fig. 15-4, the warm water at 27°C has a saturation pressure of 0.0356 bar (0.517 psia), point 1. The

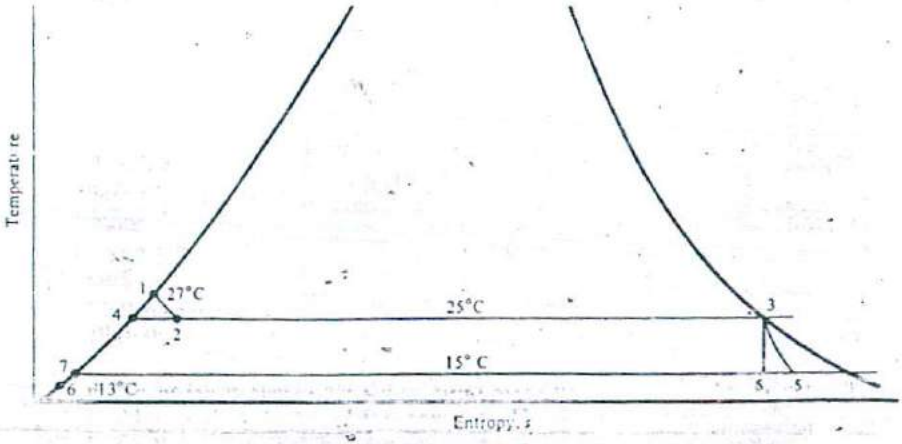


Figure 15-4 T-s diagram corresponding to Fig. 15-3.

evaporator pressure is 0.0317 bar (0.459 psia), which corresponds to 25°C (77°F) saturation temperature. This temporarily superheated water undergoes *volume boiling* (as opposed to *pool boiling*, which takes place in conventional boilers due to an immersed heating surface), causing that water to partially flash to steam to an equilibrium two-phase condition at the new pressure and temperature of 0.0317 bar and 25°C, point 2. Process 1-2 is a throttling and hence constant enthalpy process. The low pressure in the evaporator is maintained by a vacuum pump that also removes the dissolved noncondensable gases from the evaporator.

The evaporator now contains a mixture of water and steam of very low quality at 2. The steam is separated from the water as saturated vapor at 3. The remaining water is saturated at 4 and is discharged as brine back to the ocean. The steam at 3 is, by conventional powerplant standards, a very low-pressure, very high specific-volume working fluid (0.0317 bar, 43.40 m^3/kg, compared to about 160 bar, 0.021 m^3/kg for modern fossil powerplants). It expands in a specially designed turbine that can handle such conditions to 5. In Fig. 15-4, the condenser pressure and temperature at 5 are 0.017 bar (0.247 psia) and 15°C (59°F). Since the turbine exhaust system will be discharged back to the ocean in the open cycle, a direct-contact condenser (Sec. 6-2) is used, in which the exhaust at 5 is mixed with cold water from the deep cold-water pipe at 6, which results in a near-saturated water at 7. That water is now discharged to the ocean.

The cooling water reaching the condenser at 13°C is obtained from deep water at 11°C (51.8°F). This rise in temperature is caused by heat transfer between the progressively warmer outside water and the cooling water inside the pipe as it ascends the cold-water pipe. In Claude's first plant, that pipe was oversized to minimize this heat transfer and carried some 4000 m^3/h of water of which only 10 percent was needed for actual cooling.

There are thus three temperature differences, all about 2°C: one between warm surface water and working steam, one between exhaust steam and cooling water, and one between cooling water reaching the condenser and deep water. These represent external irreversibilities that reduce the overall temperature difference between heat source and sink from 27 − 11 = 16°C (28.8°F) to 25 − 15 = 10°C (18°F) as the temperature difference available for cycle work. It is obvious that because of the very low temperature differences available to produce work, the external differences must be kept to absolute minimum to realize as high an efficiency as possible. Such a necessary approach, unfortunately, also results in very large warm and cold water flows and hence pumping power, as well as large heavy cold water pipes.

Example 15-1 A Claude cycle producing 100 kW (gross) operates on the conditions of Fig. 14-4. The turbine has a polytropic efficiency of 0.80 and the turbine-generator has a combined mechanical-electrical efficiency of 0.90. Calculate the surface and deep-water flow rates in kg/s and m^3/s, and the gross cycle and plant efficiencies.

SOLUTION Use the low-temperature steam data (in SI units) shown in Table 15-1 (from App. A).

Table 15-1 Saturated steam data at low temperatures (SI units)

Temp., °C	Pressure, bar	Pressure, psia	Specific volume, m^3/kg, v_f	Specific volume, m^3/kg, v_g	Enthalpy, kJ/kg, h_f	Enthalpy, kJ/kg, h_{fg}	Enthalpy, kJ/kg, h_g	Entropy, kJ/(kg · K), s_f	Entropy, kJ/(kg · K), s_{fg}	Entropy, kJ/(kg · K), s_g
13	0.01497	0.2171	0.0010007	88.18	54.60	2470	2525	0.1952	8.6324	8.8276
15	0.01704	0.2471	0.0010010	77.97	62.97	2465	2528	0.2244	8.5562	8.7806
25	0.03166	0.4592	0.0010030	43.40	104.8	2442	2547	0.3672	8.1898	8.5570
27	0.03564	0.5169	0.0010036	38.82	113.2	2437	2550	0.3951	8.1196	8.5147

The evaporator

$$h_1 = h_f \text{ at } 27°C = 113.2 \text{ kJ/kg} \qquad v_1 = 0.0010036 \text{ m}^3/\text{kg}$$

$$h_2 = h_1 = 113.2 = (h_f + x_2 h_{fg}) \text{ at } 25°C$$

$$= 104.8 + x_2 \times 2442$$

Therefore

$$x_2 = 0.00344, \text{ or } 0.344\%$$

Warm water mass-flow rate per unit turbine mass-flow rate

$$\dot{m}_w = \frac{m_1}{m_3} = \frac{m_2}{m_3} = \frac{1}{x_2} = \frac{1}{0.00344} = 290.7$$

The turbine

$$h_3 = h_g \text{ at } 25°C = 2550 \text{ kJ/kg}, \; s_3 = 8.5570 \text{ kJ/(kg·K)}$$

For an adiabatic reversible turbine, the expansion is to 5,

$$s_{5,s} = s_3 = 8.5570 = (s_f + x_{5,s} s_{fg}) \text{ at } 15°C$$

$$= 0.2244 + x_{5,s} \times 8.5562$$

Therefore

$$x_{5,s} = 0.9739, \text{ or } 97.39\%$$

$$h_{5,s} = (h_f + x_{5,s} h_{fg}) \text{ at } 15°C = 62.97 + 0.9739 \times 2465 = 2463.6 \text{ kJ/kg}$$

$$\text{Adiabatic reversible turbine work} = h_3 - h_{5,s} = 2550 - 2463.6$$

$$= 86.4 \text{ kJ/kg}$$

$$\text{Actual turbine work } w_T = 86.4 \times \text{polytropic efficiency}$$

$$= 86.4 \times 0.8$$

$$= 69.1 \text{ kJ/kg}$$

$$h_5 = h_3 - \text{actual work} = 2550 - 69.1 = 2480.9 \text{ kJ/kg}$$

at which $x_5 = 0.9809$ or 98.09% and $v_5 = 76.48 \text{ m}^3/\text{kg}$

$$\text{Turbogenerator output} = 69.1 \times 0.88 = 60.8 \text{ kJ/kg}$$

The condenser

$$h_6 \approx h_f \text{ at } 13^\circ\text{C} = 54.60 \text{ kJ/kg} \qquad v_6 = 0.0010007 \text{ m}^3/\text{kg}$$

$$h_7 = h_f \text{ at } 15^\circ\text{C} = 62.97 \text{ kJ/kg}$$

Cold water mass-flow rate per unit turbine mass-flow rate

$$\dot{m}_c = \frac{h_5 - h_7}{h_7 - h_6} = \frac{2480.9 - 62.97}{62.97 - 54.60} = 288.9$$

The cycle

$$\text{Turbine mass-flow rate } \dot{M}_T = \frac{\text{turbine work}}{w_T} = \frac{100}{69.1}$$

$$= 1.447 \text{ kg/s}$$

$$\text{Turbine volume flow rate at throttle} = \dot{M}_T v_3 = 1.447 \times 43.40$$

$$= 62.8 \text{ m}^3/\text{s}$$

$$\text{Turbine volume flow rate at exhaust} = \dot{M}_T v_5 = 1.447 \times 76.48$$

$$= 110.7 \text{ m}^3/\text{s}$$

$$\text{Warm-water mass-flow rate } \dot{M}_w = \dot{M}_T \dot{m}_w = 1.447 \times 290.7$$

$$= 420.6 \text{ kg/s}$$

$$\text{Warm-water volume flow rate } \dot{V}_w = \dot{M}_w v_1 = 420.6 \times 0.0010026$$

$$= 0.422 \text{ m}^3/\text{s}$$

$$\text{Cold-water mass-flow rate } \dot{M}_c = \dot{M}_T \dot{m}_c = 1.447 \times 288.9$$

$$= 418.0 \text{ kg/s}$$

$$\text{Cold-water volume flow rate } \dot{V}_c = \dot{M}_c v_6 = 418.0 \times 0.0010007$$

$$= 0.418 \text{ m}^3/\text{s}$$

$$\text{Gross cycle efficiency} = \frac{w_T}{q_A} = \frac{h_3 - h_5}{h_3 - h_7} = \frac{69.1}{2487}$$

$$= 0.0278 = 2.78\%$$

$$\text{Gross plant efficiency} = 0.0278 \times 0.9 = 0.0250$$
$$= 2.5\%$$

Note: The gross plant power, 100 kW, and the gross plant efficiency, 2.5 percent, do not take into account pumping and other auxiliary power inputs to the plant.

It can be seen that very large ocean-water mass and volume flow rates are used in open OTEC systems and that the turbine is a very low-pressure unit that receives steam with specific volumes more than 2000 times that in a modern fossil powerplant. Thus the turbine resembles the few last exhaust stages of a conventional turbine and is thus physically large.

Another attempt at building a Claude-type powerplant was undertaken by the French corporation Energie Electrique de la Cote d'Ivoire at Abidjan in the Ivory Coast, Africa, in the 1950s. The plans were for a 7000-kW plant operating on a temperature difference of 20°C (36°F). The cold-water pipe was 2.4 m in diameter and extended to a depth of about 4.8 km at about 5 km from the shore. In actual operation about a quarter of the plant's gross output was used to drive the various accessories. Full output was never realized because of maintenance difficulties on the cold-water pipeline.

15-4 MODIFICATIONS OF THE OPEN OTEC CYCLE

Improvements and modifications of the Claude cycle have been proposed in an attempt to change it into an economically viable system. The attempts focused mainly on two areas: a different, more efficient type of evaporator, called the *controlled flash evaporator*, and the use of the plant for the *cogeneration* of electricity and fresh water.

The Controlled Flash Evaporator

The principle of controlled flash evaporator (CFE) [145] has been successfully used for the production of pure boiler feedwater from heated condenser cooling seawater in a conventional powerplant, as well as for the production of fresh water from hot tropical seawater.

In the volume-boiling flash evaporator used in the early cycle, the water violently flashes upon depressurization. Bubbles of vapor emanate from the turbulent surface carrying with them some entrained saltwater, which increases the corrosion problem. This may be alleviated by adding demisters (which entrap the brine droplets) but at the expense of further pressure and temperature drop.

A controlled flash evaporator, by contrast, has the warm seawater (called brine) descend by gravity in thin films, about 1 mm thick, in a quiescent manner down chutes. A typical CFE chamber is a vertical structure, 2.5 m (~8 ft) or more in height, that

contains a large number of such vertical parallel chutes. The water film, on both sides of the chutes, vaporizes without the violent processes of bubble formation and bursting that occur in a conventional evaporator. Pure vapor, devoid of entrained solids, emanates from the films and increases in mass and volume flows as it progresses downward. Because of energy transfer caused by the evaporative process, both brine and vapor progressively cool down as they descend down the chutes. The pure low-pressure steam is then admitted to the turbine, where it expands to the condenser (Fig 15-5).

A minimum of deaeration is required in a CFE because no violent release of noncondensable gases takes place. Deaeration is accomplished by an "ingestor" that operates on a principle similar to that of a steam-jet air ejector SJAE (Sec. 6-3) except that low pressure is obtained by a liquid jet aspirator that uses cooled brine from the chute exit for its liquid. The noncondensables and the liquid leave the ingestor via a barometric leg (diffuser), and the gases come out of solution upon discharge to atmospheric pressure.

The high quality of the vapor going through the turbine from the CFE is well suited to electrical and fresh-water cogeneration (described below).

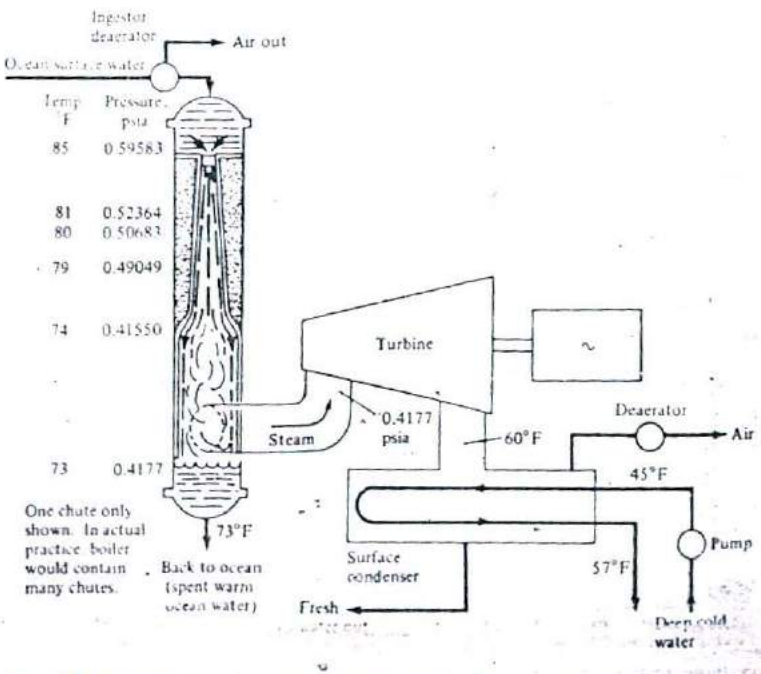


Figure 15-5 Schematic of an open cycle with both controlled-flash evaporator and a surface condenser for the cogeneration of electricity and fresh water.

Electrical and Fresh-Water Cogeneration

Here a shell-and-tube or plate-type surface condenser is used in the plant instead of the direct-contact condenser used in the Claude cycle. The deep cold water is pumped through the tubes or on one side of the plates of the surface condenser and is discharged back to the ocean without mixing with the turbine exhaust steam (Fig. 15-5). The turbine exhaust becomes a fresh-water condensate. It can be pumped to atmospheric pressure and used as fresh water for various uses. When combined with a controlled flash evaporator, the quality of the condensate is so high as to meet standards for potable water with a salt content between 1 and 5 ppm.

A disadvantage of the surface condenser, however, is that it is less effective than a direct-contact condenser and thus operates at a slightly higher turbine exhaust temperature (and therefore pressure), which results in a slight reduction in net cycle work and efficiency.

The plant shown in Fig. 15-5 shows turbine inlet at 0.4177 psia (0.0288 bar) and 73°F (22.8°C) and exhaust at 0.25611 psia (0.0177 bar) and 60°F (15.6°C). If fresh water were not desired, a direct-contact condenser could have been used with turbine exhaust at perhaps 0.2330 psia (0.0161 bar) and 57°F (13.9°C), and a higher plant efficiency and output.

Other ideas for use with the open cycle involve using the deep water after it has been brought up to the surface and passed through the condenser. Such water, rich in nutrients because it contains the remains of the organisms that primarily live in the sunny water layers near the surface, can then be used after being warmed up in the condenser as a food source for marine life in surface sea farms (mariculture).

15-5 THE CLOSED, OR ANDERSON, OTEC CYCLE

Although the first attempt at producing power from ocean temperature differences was the open cycle of Georges Claude in 1929, d'Arsonval's original concept in 1881 was that of a closed cycle that also utilizes the ocean's warm surface and cool deep waters as heat source and sink, respectively, but requires a separate working fluid that receives and rejects heat to the source and sink via heat exchangers (boiler and surface condenser) (Fig. 15-6).

The working fluid may be ammonia, propane, or a Freon. The operating (saturation) pressures of such fluids at the boiler and condenser temperatures are much higher than those of water, being roughly 10 bar at the boiler, and their specific volumes are much lower, being comparable to those of steam in conventional powerplants (Table 15-2). (See also the Appendix.)

Such pressures and specific volumes result in turbines that are much smaller and hence less costly than those that use the low-pressure steam of the open cycle. The closed cycle also avoids the problems of the evaporator. It, however, requires the use of very large heat exchangers (boiler and condenser) because, for an efficiency of about 2 percent, the amounts of heat added and rejected are 50 times the output of the plant. In addition, the temperature differences in the boiler and condenser must

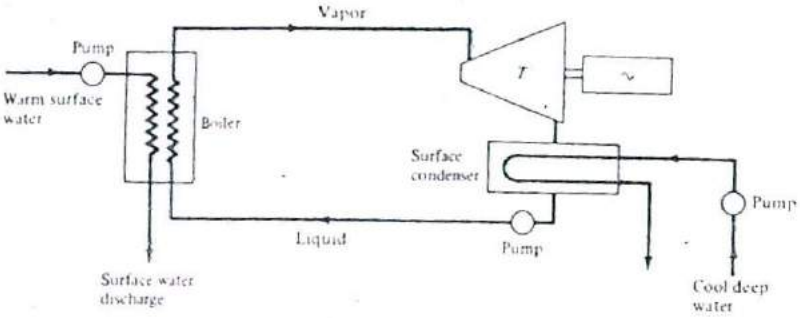


Figure 15-6 Schematic of a closed-cycle OTEC powerplant.

be kept as low as possible to allow for the maximum possible temperature difference across the turbine, which also contributes to the large surfaces of these units.

The closed-cycle approach was first proposed by Barjot in 1926, but the most recent design was by Anderson and Anderson in the 1960s [146]. The closed cycle is sometimes referred to as the *Anderson cycle*. The Andersons chose propane as the working fluid with a 20°C (36°F) temperature difference between warm surface and cool water, the latter some 600 m (~2000 ft) deep. Propane is vaporized in the boiler at 10 bar (145 psia) or more and exhausted in the condenser at about 5 bar.

In order to minimize the mass and the amount of material (and hence cost) used to manufacture the immensely large heat exchangers, the Anderson OTEC system employs thin plate-type heat exchangers instead of the usual heavier and more expensive shell-and-tube heat exchangers. To help reduce the thickness of the plates, the heat exchangers are placed at depths where the static pressure of the water in either exchanger roughly equals the pressure of the working fluid. Thus if propane is the working fluid in the boiler at 80°F (26.7°C) and 143.6 psia (9.9 bar) (Table 15-2), the boiler

Table 15-2 Comparison of saturation pressures and specific volumes of four fluids at low temperatures

	Saturation pressure, psia		Specific volume, ft^3/lb_m			
			v_f		v_g	
Fluid	40°F	80°F	40°F	80°F	40°F	80°F
Steam	0.1216	0.5068	0.01602	0.01607	2.4458	633.3
Ammonia	73.32	153.0	0.025 33	.0267	3.571	1.955
Propane	77.80	143.6	0.03055	0.0327	1.330	0.745
Freon-12	51.68	98.76	0.0116	0.0123	0.792	0.425
Steam	Superheated at 2400 psia and 1000°F, $v = 0.321$					

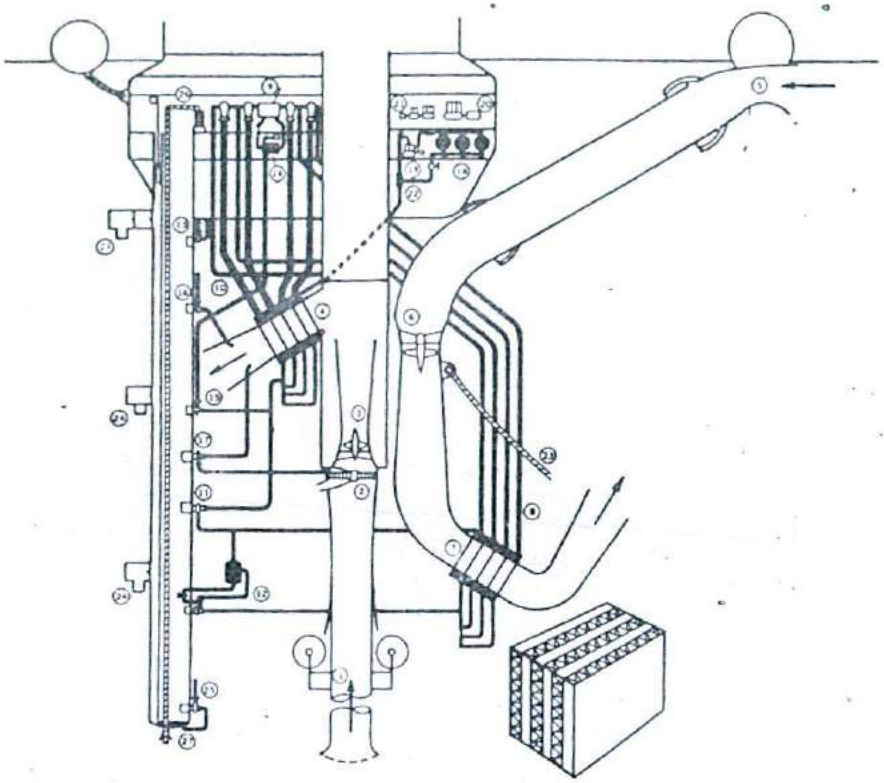


Figure 15-7 Closed-cycle floating powerplant [142].

would be placed at a depth of (g/g_c) 143.6 × 144/64 ≈ 325 ft (~100 m),* where 64 is the average density of seawater in $lb_m/ft.^3$ The condenser, on the other hand, if operating at 40°F (14.4°C) and 77.8 psia (5.36 bar), would be placed at (g/g_c) 77.8 × 144/64 ≈ 175 ft (≈53 m). In other words the powerplant would be designed so that it would be mostly submerged and anchored so that the condenser would actually be higher than the boiler. The turbine, pumps, storage tanks, compressors, and other plant equipment would be placed at intermediate decks. Figure 15-7 shows such a floating plant. Note the arrangement by which the condenser (4) receives cool water from the cold-water pipe (1). That pipe extends 2000 ft (~610 m) below the surface. The condenser is placed above the boiler (7), which receives warm surface water from a buoyantly supported surface inlet pipe (5). Note also the decompression chambers

* 1 bar is roughly equivalent to 10 m of seawater head.

required for operating and maintenance personnel. The inset in the figure shows the proposed design of the plate-type heat exchangers. The plant design was based on a 20°C (36°F) warm-cold-water temperature difference and propane as the working fluid. Roughly 14 percent of the gross power is expected to be consumed internally. The size of the plant is gigantic indeed.

15-6 RECENT OTEC DEVELOPMENTS

Problems facing commercial development of OTEC systems are legion. Some, like the low temperature differences and evaporator problems, have already been discussed. In addition, for open systems, turbines capable of generating 10 MW or more using low-pressure steam are yet to be developed. For closed systems, heat exchangers much larger than any that have been built must be designed and built. For all systems, pumps capable of handling larger amounts of water than any developed so far have to be developed. It is said that a relatively small-output (by modern powerplant standards) OTEC plant producing 100 MW would have a water flow comparable to that going through Boulder Dam. Long (~1 km), large-diameter (up to 30 m) cold-water pipes, larger than ever made, have to be designed, fabricated, and installed. The whole plant has to be stationed and moored at depths at which no vessel has ever been before. The deployment of the electrical cable required to carry the power to shore must be carefully done because it would be subjected to severe stresses from its own weight as well as from ocean currents and eddies.

In addition, an OTEC powerplant will have to be capable of withstanding severe ocean storms over its lifetime, corrosion by seawater salts, erosion due to large volume flows, biofouling due to algae growth, and encrustation by various marine life such as barnacles.

Because commercial-size OTEC systems are very large and suffer from various problems when placed in a stationary position, recent OTEC demonstration plants have instead concentrated on small-scale plants and used an *OTEC plant ship* concept. In this concept, the plant is built on or as part of a specially designed ship. A so-called *grazing plant ship* would move at low speed (about 0.5 knots) in search of the warmest surface water. The electricity generated must then be used on board to power manufacturing of energy-intensive products like aluminum, magnesium, nickel, various alloys, semiconductors, etc., for deep sea bed mining of such minerals as manganese, cobalt, and nickel, or for chemical processing of products such as ammonia.

The continental United States has a relatively small ratio of coastal to inland areas and relatively limited warm-water resources. Few commercial electric utilities have therefore shown interest in OTEC, and it fell to the federal government to undertake research and development in this field. The case for OTEC is more promising for islands that have low population densities, that are dependent upon imported fossil fuels for generating electricity, and that have relatively large warm-water resources in relation to their energy needs. The U.S. Department of Energy (DOE) has therefore aimed its first efforts at such islands as Hawaii, Puerto Rico, the Virgin Islands, Guam,

American Samoa, and others. The federal OTEC program started in the early 1970s as one of six options selected for investigation in an effort to reduce the United States' dependence on imported oil.

The first result of the program was a test facility called OTEC-1, which was installed on a 26,000-ton converted tanker and operated in July 1980. The effort was funded by DOE and built by TRW, Inc., and Global Marine Development Company. The ship was first moored 29 km (18 mi) off Kawaihae Harbor, Hawaii in 1220-m (4000-ft) deep waters. OTEC-1 was a closed-cycle "heat exchanger" facility without turbine or electrical generator. Its aims were to test heat-exchanger design and performance and evaluate the extents of corrosion and biofouling. It contained a 1-MW titanium shell-and-tube heat exchanger designed to simulate a larger 10-MW unit. It had three cold-water pipes 853 m (2800 ft) long and 1.2 m (4 ft) diameter each. OTEC-1, now retired, was to have been succeeded by a complete electric-generating system for operation in the mid-1980s. Federal funding, however, was withheld.

The second U.S. demonstration, called Mini-OTEC, was a small $3 million electric-generating plant funded cooperatively by the State of Hawaii, Lockheed Missile and Space Company, Inc., Alfa-Laval Thermal, Inc., and the Dillington Corporation. This plant was also housed in a ship, a converted U.S. Navy scow, and was operated between August and November 1979 off Keahole Point, Hawaii. It included a titanium plate-type heat exchanger and one cold-water pipe 660 m (2170 ft) long and 0.6 m (2 ft) in diameter. It produced 50 kW of gross electric power but only between 12 and 15 kW net. This performance was found to be close to design predictions.

For the contiguous United States, only the Gulf of Mexico and the lower eastern coast of Florida are near waters that have sufficient temperature differences and that are close enough to land for ease of power transmission. Because of these limitations, the future of OTEC in the United States is uncertain at best.

In the international arena, a number of countries have recently been active in OTEC research and development. These include Japan, France (which, of course, had been an early pioneer in the field via the Claude system), Sweden, West Germany, and the Netherlands. An interesting effort that may prove to be successful is a 100-kW land-based plant that the Pacific Ocean equatorial island nation of Nauru has contracted for with the Japanese. The hope is that with this and future larger units, Nauru might develop into a center for energy-intensive industries.

15-7 OCEAN WAVES

Like the wind (Chap. 14) and OTEC, ocean and sea waves are caused indirectly by solar energy. Waves are caused by the wind, which in turn is caused by the uneven solar heating and subsequent cooling of the earth's crust and the rotation of the earth. Wave energy at its most active, however, can (like wind energy) be much more concentrated than incident solar energy even at the latter's peak. Devices that convert energy from waves can therefore produce much higher power densities than solar devices.

This "harvesting" of energy from waves has been the subject of some of human-

kind's wildest dreams for ages. However, it was the recent energy crisis that prompted serious attempts at harnessing the waves for the production of electricity. During the decade of the 1970s dozens of patents were filed to do this, though most are complicated and rather fragile in the face of the gigantic power of ocean storms.

The main advantage of power from waves, like most of the so-called alternative energy sources, is a free and renewable energy source. In addition, wave-power devices, unlike solar or wind devices, do not use up large land masses, are relatively pollution free and, because they remove energy from the waves, leave the water in a relatively placid state in their wakes. Thus a string of devices situated, as they must, where there is a large amount of wave activity, can in addition to producing electricity protect coastlines from the destructive action of such waves, minimize erosion, and even help create artificial harbors. A concept of staggered array of devices has been proposed to do this.

There are several disadvantages. Like most of the so-called alternative energy sources, waves lack dependability, and there is relative scarcity of accessible sites of large wave activity. In addition most devices that have been proposed are relatively complicated and lack the necessary mechanical strength to withstand the enormous power of stormy seas. Economic factors such as the capital investment, costs of maintenance, repair and replacement, as well as problems of biological growth of marine organisms, are all relatively unknown and seem to be on the large side.

World sites that may be suitable include the Molakai and Alenuihaha channels in the Hawaiian islands, where 6 to 10-ft-high (crest to trough) waves are typical during normal trade wind periods, the Pacific coast of North America, the Arabian Sea off Pakistan and India, the North Atlantic coast of Scotland, the coast of New England, and others [147]. Figure 15-8 is a spectrum of wave heights and periods for the New England coast. It shows that waves 6 ft high or more with periods 6 s long or less occur about half the time.

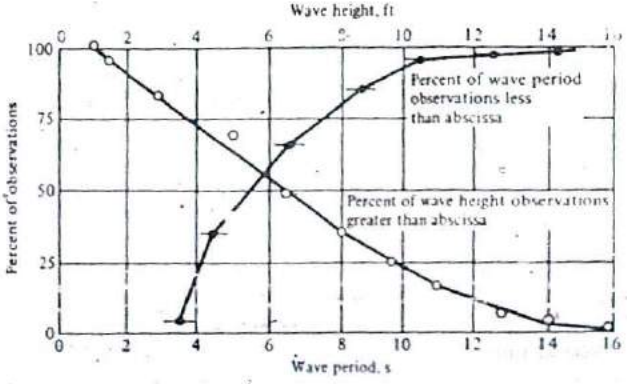


Figure 15-8 Spectrum of wave heights and periods for the New England coast [147].

The basic mechanism of wave motion will be presented in the next section. The theory of energy conversion from waves will be presented in the following section. These will be followed by sections describing a few selected wave-power devices.

15-8 WAVE MOTION

A two-dimensional progressive wave that has a free surface and is acted upon by gravity (Fig. 15-9) is characterized by the following parameters:

λ = wavelength = $c\tau$, m or ft

a = amplitude, m or ft

$2a$ = height (from crest to trough), m or ft

τ = period, s

f = frequency = $1/\tau$, s^{-1}

c = wave propagation velocity λ/τ, m/s or ft/s

n = phase rate = $2\pi/\tau$, s^{-1}

The period τ and wave velocity c depend upon the wavelength and the depth of water (Table 15-3 and Fig. 15-10). The range below the dashed line in the table represents the most common waves.

The relationship between wavelength and period can therefore be well approximated by

$$\lambda = 1.56\tau^2 \qquad (\lambda \text{ in m}, \tau \text{ in s}) \tag{15-3a}$$

or

$$\lambda = 5.12\tau^2 \qquad (\lambda \text{ in ft}, \tau \text{ in s}) \tag{15-3b}$$

Figure 15-9 shows an isometric of a two-dimensional progressive wave, represented by the sinusoidal simple harmonic wave shown at time 0. Cross sections of the wave are also shown at time 0 and at time θ. That wave is expressed by

$$y = a \sin\left(\frac{2\pi}{\lambda}x - \frac{2\pi}{\tau}\theta\right) \tag{15-4a}$$

or

$$y = a \sin(mx - n\theta) \tag{15-4b}$$

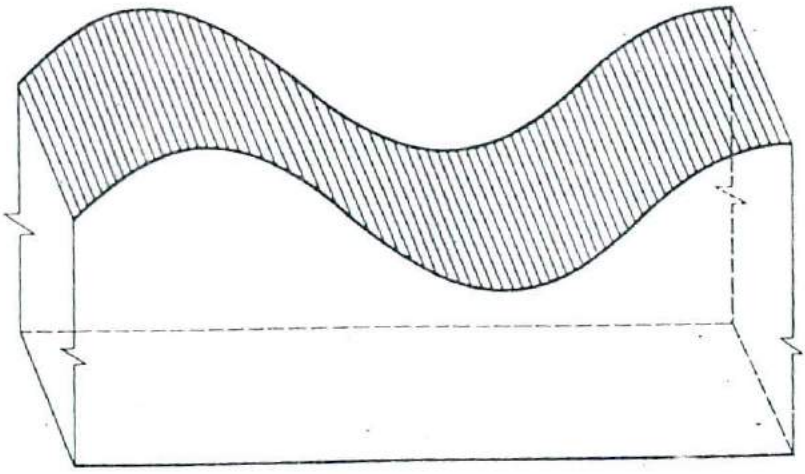
where y = height above its mean level, m or ft

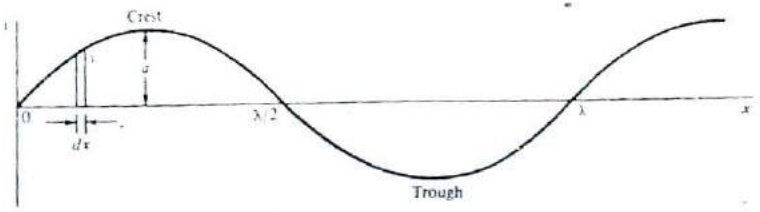
θ = time, s

$m = 2\pi/\lambda$, m^{-1} or ft^{-1}

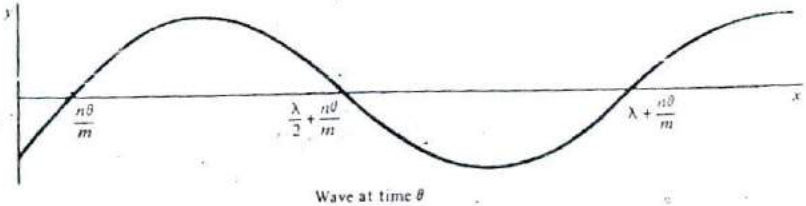
$(mx - n\theta) = 2\pi(x/\lambda - \theta/\tau)$ = phase angle, dimensionless

Note that the wave profile at time θ has the same shape as that at time 0, except that it is displaced from it by a distance $x = \theta/\tau = \theta\,(n/m)$. When $\theta = \tau$, $x = \lambda$ and the wave profile assumes its original position.





Wave at time 0



Wave at time θ

Figure 15-9 A typical progressive wave, a = amplitude, λ = wavelength, showing two-dimensional wave and amplitudes at time 0 and at time θ.

Table 15-3 Wave periods, s*

Water depth h, ft	Wavelength, ft				
	1	10	100	1000	10,000
1	0.442	1.873	17.645	176.33	1763.30
10	0.442	1.398	5.923	55.80	557.62
100	0.442	1.398	4.420	18.73	176.45
1000	0.442	1.398	4.420	13.98	59.23
10000	0.442	1.398	4.420	13.98	44.20

* From Ref. 148.

Although the wave motion is continually lateral, i.e., in the x direction with a speed of propagation $c = \lambda/\tau$, the motion of water itself is not, although it deceptively appears to be so. In reality a given particle of water rotates in place in an elliptical path in the plane of wave propagation, with specified horizontal and vertical semiaxes, as can be witnessed when placing a cork on water. The paths of water particles at different depths but with the same mean position are shown in Fig. 15-11. The horizontal and vertical semiaxes of the ellipses are given, respectively, by [148, 149].

$$\alpha = a \frac{\cosh m\eta}{\sinh mh} \tag{15-5a}$$

$$\text{and } \beta = a \frac{\sinh m\eta}{\sinh mh} \tag{15-5b}$$

where α = horizontal semiaxis

β = vertical semiaxis

h = depth of water

η = distance from the bottom

Equations (15-5) show that in general $\alpha > \beta$, that β varies from 0 at the bottom where $\eta = 0$ to a, at the surface where $\eta = h$, and that for large depths $\alpha \approx \beta \approx a$ and the motion is essentially circular at the surface.

A wave therefore possesses both potential and kinetic energies. These are evaluated in the next section.

15-9 ENERGY AND POWER FROM WAVES

The total energy of a wave is the sum of its potential and kinetic energies.

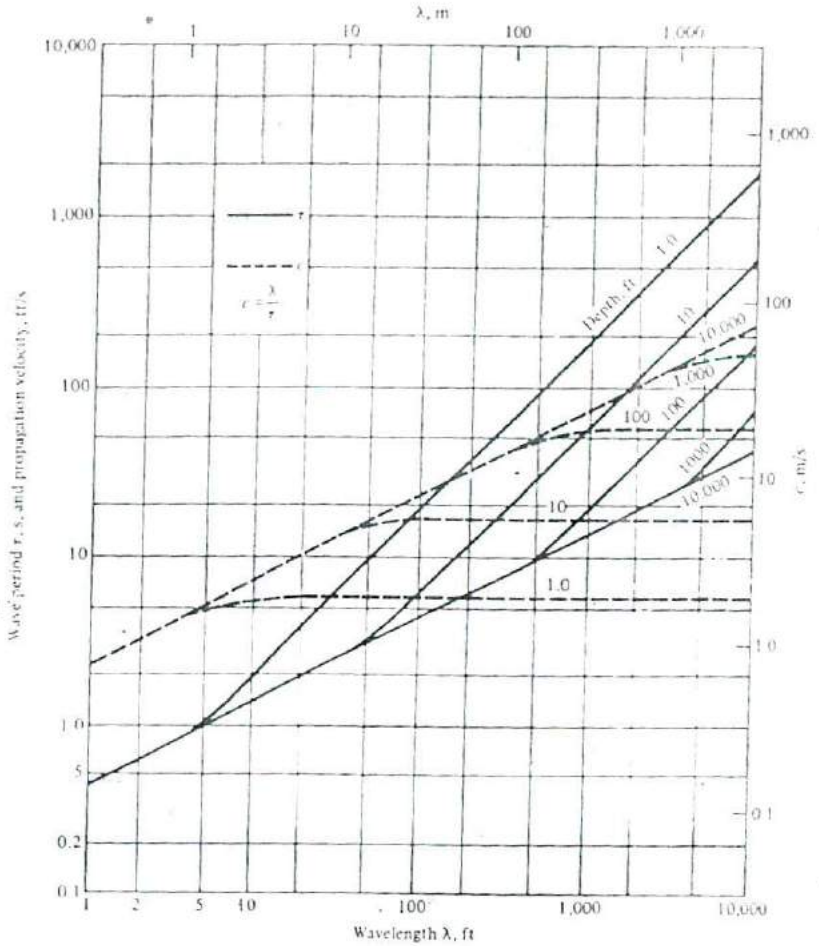


Figure 15-10 Variation of wave period τ and velocity c with wavelength λ and depth.

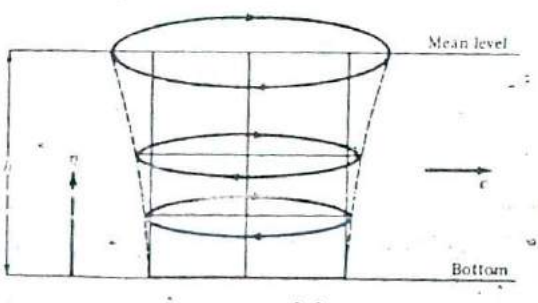


Figure 15-11 Elliptical paths of water particles at different heights. c = wave propagation velocity, h = water depth, η = distance from bottom.

Potential Energy

The *potential energy* arises from the elevation of the water above the mean level ($y = 0$). Considering a differential volume $y\,dx$ (Fig. 15-9), it will have a mean height $y/2$. Thus its potential energy is

$$d\text{PE} = m\frac{yg}{2g_c} = (\rho y\,dx\,L)\frac{yg}{2g_c}$$

$$= \frac{\rho L}{2}y^2\,dx\,\frac{g}{g_c} \tag{15-6}$$

where m = mass of liquid in $y\,dx$, kg or lb_m

g = gravitational acceleration, m/s^2 or ft/s^2

g_c = conversion factor 1.0 kg · m/(N·s²) or 32.174 lb_m · ft/(lb_f · s²)

ρ = water density, kg/m^3 or lb_m/ft^3

L = arbitrary width of the two-dimensional wave, perpendicular to the direction or wave propagation x, m or ft

Combining Eqs. (15-6) and (15-4*b*) and integrating gives the potential energy PE in J or ft · lb_f

$$\text{PE} = \frac{\rho L a^2}{2}\frac{g}{g_c}\int_0^{\lambda}\sin^2(mx - n\theta)\,dx$$

$$= \frac{\rho L a^2}{2m}\frac{g}{g_c}\left(\frac{1}{2}mx - \frac{1}{4}\sin 2mx\right)_0^{\lambda}$$

$$= \frac{\rho L a^2}{2m}\frac{g}{g_c}\left[\frac{m\lambda}{2}\right] = \frac{1}{4}\rho a^2\lambda L\frac{g}{g_c} \tag{15-7}$$

The *potential energy density* per unit area is PE/A, where $A = \lambda L$, in J/m^2 or ft · lb_f/ ft^2, is then given by

$$\frac{\text{PE}}{A} = \frac{1}{4}\rho a^2\frac{g}{g_c} \tag{15-8}$$

Kinetic Energy

The *kinetic energy* of the wave is that of the liquid between two vertical planes perpendicular to the direction of wave propagation x and placed one wavelength apart. The derivation of kinetic energy is rather complex and beyond the scope of this book. However, from hydrodynamic theory, it is given by [148]

$$\text{KE} = \frac{1}{4}i\rho L\frac{g}{g_c}\int\omega\,d\bar{\omega} \tag{15-9}$$

where ω is a complex potential given by

$$\omega = \frac{ac}{\sinh(mh)} \cos(mz - n\theta)$$

and z is distance measured from an arbitrary reference point. The integral in Eq. (15-9) is performed over the cross-sectional area bounded between two vertical planes. The result is

$$\text{KE} = \frac{1}{4}\rho a^2 \lambda L \frac{g}{g_c} \tag{15-10}$$

and the *kinetic energy density* is

$$\frac{\text{KE}}{A} = \frac{1}{4}\rho a^2 \frac{g}{g_c} \tag{15-11}$$

Total Energy and Power

It can be seen that the potential and kinetic energies of a progressive sine wave are identical, so that the total energy E is half potential and half kinetic. The *total energy density* is thus given by

$$\frac{E}{A} = \frac{1}{2}\rho a^2 \frac{g}{g_c} \tag{15-12}$$

The power P energy per unit time is given for a wave by energy times frequency. Thus the *power density*, W/m^2 or ft · lb$_f$/(s · ft^2), is given by

$$\frac{P}{A} = \frac{1}{2}\rho a^2 f \frac{g}{g_c} \tag{15-13}$$

Example 15-2 A 2-m wave has a 6-s period and occurs at the surface of water 100 m deep. Find the wavelength, the wave velocity, the horizontal and vertical semiaxes for water motion at the surface, and the energy and power densities of the wave. Water density = 1025 kg/m^3.

SOLUTION

Wavelength $\lambda = 1.56 \times 6^2 = 56.16$ m $= 184.25$ ft (Eq. 15-3*a*)

Wave velocity $c = \lambda/\tau = 9.36$ m/s $= 30.71$ ft/s

Wave height $2a = 2$ m Amplitude $a = 1$ m $= 3.28$ ft

$m = 2\pi/\lambda = 2\pi/56.16 = 0.1119$ m^{-1}

At the surface $\eta = h = 100$ m

$$\text{Horizontal semiaxis } \alpha = 1 \times \frac{\cosh 11.19}{\sinh 11.19} = 1 \text{ m} \qquad \text{(Eq. 15-5}a\text{)}$$

$$\text{Vertical semiaxis } \beta = 1 \times \frac{\sinh 11.19}{\sinh 11.19} = 1 \text{ m} \qquad \text{(Eq. 15-5}b\text{)}$$

$$\text{Wave frequency } f = 1/\tau = 1/6 \text{ s}$$

$$\text{Energy density } \frac{E}{A} = \frac{1}{2} \times 1025 \times 1^2 \times \frac{9.81}{1} = 5027.6 \text{ J/m}^2$$

$$= 344.5 \text{ ft} \cdot \text{lb}_f/\text{ft}^2 \qquad \text{(Eq. 15-12)}$$

$$\text{Power density } \frac{P}{A} = \frac{E}{A} f = 5027.6 \times \frac{1}{6} = 837.9 \text{ W/m}^2$$

$$= 0.0778 \text{ kW/ft}^2 \qquad \text{(Eq. 15-13)}$$

Note that, because of the large depth, the semiaxes are equal, so the motion is circular. Note also that they are small compared with the wavelength, so the water motion is primarily vertical.

Two-meter waves, of course, do not occur all the time. However, in regions of high wave activity, 2 m is a median with heavier and calmer seas occurring about 50 percent of the time (Fig. 15-8). The total energy and power densities over a period of time should take this spectrum into account. With these densities proportional to a^2, the average densities would be greater than the values obtained in Example 15-2.

It is instructive to compare these values with the *average daily solar incidence* where, in the southwestern United States, a value of 240 W/m^2, or 0.0223 kW/ft^2, is often used. Thus, wave power density is much higher. A complete comparison should take into account the efficiency of conversion to electric energy as well as other factors, like capital costs for land and equipment, operational costs, costs of energy storage, and other factors. In the next sections some selected devices that convert wave energy to mechanical energy, and hence to electric energy, will be described.

15-10 WAVE-ENERGY CONVERSION BY FLOATS

As seen above, wave motion is primarily horizontal, but the motion of water is primarily vertical. This latter motion is made use of by floats to obtain mechanical power. The concept envisages a large float that is driven up and down by the water within relatively stationary guides. This reciprocating motion is converted to mechanical and then electric power.

A system proposed by Martin [150] is shown in Fig. 15-12. A square float moves up and down with the water, guided by four vertical manifolds that are part of a platform. The platform is stabilized within the water by four large underwater floatation tanks so that it is supported by buoyancy forces and no significant vertical or horizontal

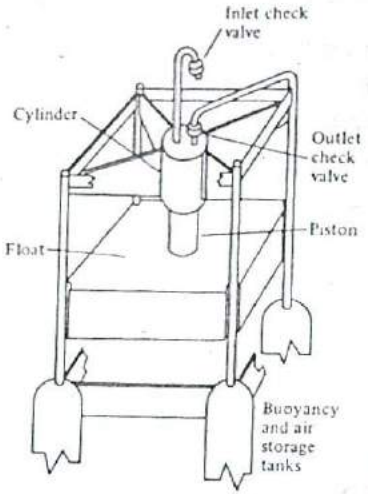


Figure 15-12 Schematic of a float wave-power machine [150].

displacement of the platform due to wave action occurs. Damping fins may be used to further reduce motion if necessary. The platform is therefore expected to be relatively stationary in space, even in heavy seas. An alternative design uses piles to support the platform, if water depth permits. It is proposed that the platform be made of molded plastic with a foamed plastic core to arrive at the required density and strength.

Attached to the float is a piston that moves up and down inside a cylinder that is attached to the platform and is therefore relatively stationary. This piston-cylinder arrangement is used as a reciprocating air compressor. The downward motion of the piston draws air into the cylinder via an inlet check valve. The upward motion compresses the air and sends it through an outlet check valve to the four underwater floatation tanks via the four manifolds. The four floatation tanks thus serve the dual purpose of bouyancy and air storage, and the four vertical manifolds serve the dual purpose of manifolds and float guides.

The compressed air in the buoyancy-storage tanks is in turn used to drive an air turbine that drives an electrical generator. The electric current is transmitted to the shore via an underwater cable.

Assuming an idealized reciprocating compressor cycle, (Fig. 15-13), the work, mass-flow rates, and other relationships may be obtained by common thermodynamic analysis as a function of stroke volume and clearance, wave-height, and inlet conditions. The float height is usually subtracted from the wave height $2a$ to obtain the piston stroke.

The air enters the compressor at atmospheric pressure, volume, and temperature P_0, V_0, and T_0. It leaves it as P_1, V_1, and T_1. It, however, cools in the storage tanks back to T_0 (as if it were isothermally compressed along the dotted line). The new volume $V_2 = V_0 P_0/P_1$, and pressure $P_2 \approx P_1$.

This air now expands in the turbine. Assuming ideal (adiabatic reversible) ex-

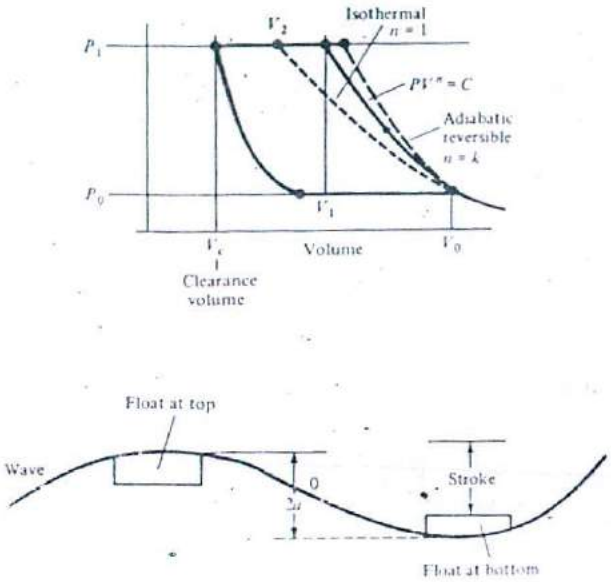


Figure 15-13 Idealized reciprocating compressor cycle and piston stroke

pansion, the work, in J/kg or Btu/lb$_m$, obtained from that turbine per unit mass of air would be given by

$$\frac{W_{\text{turbine}}}{m} = c_p T_0 \left[1 - \left(\frac{r_c}{r_e} \right)^{(k-1)/k} \cdot r_c^{(1-k)/k} \right] \qquad (15\text{-}14)$$

where m = mass of air, kg or lb$_m$

c_p = specific heat of air, J/(kg · K) or Btu/(lb$_m$ · °R)

r_c = Pressure ratio in compressor = P_1/P_0

r_e = expansion ratio in turbine = $P_2/P_3 = P_1/P_3$

P_3 = exhaust pressure in turbine, Pa or lb$_f$/ft^2

k = ratio of specific heats for air

r_c/r_e may be taken as 1.1, when allowing for reasonable mechanical clearances.

Optimization of a system as above [150] has shown that the power density is roughly given by

0.05 kW/ft^2

This compares with 0.0223 kW/ft^2 incident solar energy in hot regions, which is yet to be multiplied by the efficiency of solar conversion, usually less than 10 percent.

A linear array of such modules perpendicular to wave motion is recommended because the modules attenuate the wave amplitude in the direction of wave motion and would affect other modules in that direction. It would thus take miles of linear arrays to produce 100 MW or more. Other problems of such a scheme, some of them shared by other schemes, are:

1. Waves not perfectly sinusoidal
2. Aspiration of water into intake and even submersion by large waves
3. Water entering turbine
4. Materials problems, such as cost and corrosion (which may be partly overcome by the use of molded plastic)
5. Design to withstand storms
6. Marine growth
7. Power transmission to shore

15-11 HIGH-PRESSURE ACCUMULATOR WAVE MACHINES

In these machines, instead of compressing air the water itself is pressurized and stored in a high-pressure accumulator or pumped to a high-level reservoir, from which it flows through a water-turbine-electrical generator. This is done by transforming large volumes of low-pressure water at wave crest into small volumes of high-pressure water by the use of a composite piston. This piston is composed of a large-diameter main piston and a small-diameter piston at its center.

In one design, that of the *hydraulic accumulator* (Fig. 15-14), the main large piston moves inside a submerged cylindrical generator while the small piston moves inside a power cylinder. Wave water enters and leaves through openings at the bottom, thus causing the main piston to move up and down. A closed water loop exists above the small piston. On the upstroke, the pressure on the main piston is magnified on the small piston by the inverse ratio of the square of their diameters. Thus if the piston diameters are 100 and 20 cm, respectively, a wave head of 2 m would be magnified 25 times to a head H of 50 m. With seawater density averaging 1025 kg/m^3 (64 lb$_m$/ft^3), this head corresponds to a pressure of $\rho H_g' g_c$, which is about 5 bar (~ 72.5 psi).

The high-pressure water is conducted through a one-way up valve to a hydraulic accumulator at the top of the generator. Two air (or other gas) volumes counterbalance and act as cushions in a chamber above the main piston and in a sealed compartment in the hydraulic accumulator. The latter also maintains the high water pressure. Part of the high-pressure water flows through a Pelton wheel or Francis hydraulic turbine that drives an electrical generator and is then discharged to a storage chamber below the turbine.

On the trough of the wave, the composite piston is pushed downward by the gas pressure above the main piston, which thus acts also as a spring. The turbine exhaust

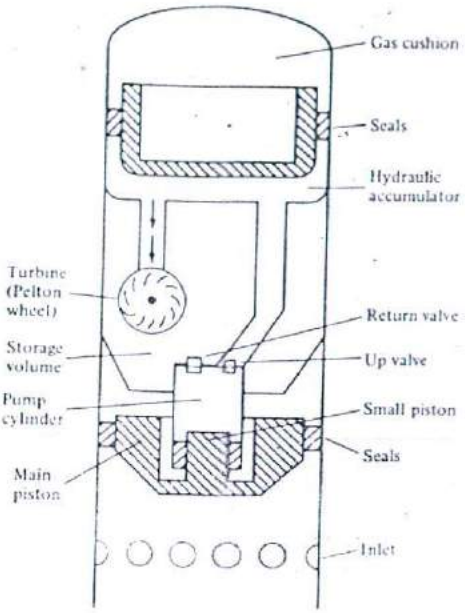


Figure 15-14 Schematic of a hydraulic-accumulator wave machine [151].

water in the storage volume is now sucked into the pump cylinder via a one-way return valve while the up valve is closed, and the cycle is repeated. The hydraulic accumulator is large enough to permit continuous turbine operation even though the waves are cyclic.

A 500-W prototype hydraulic-accumulator generator was constructed in Germany by Harold Kayser in 1975 for the purpose of powering a navigation buoy [151]. A design for a 1-kW generator has piston diameters of 100 and 25 cm and a 12-cm-diameter Pelton-wheel turbine that has 7-mm nozzles and that runs at 2300 r/min. The design calculations for that unit, based on 70 percent system efficiency and 2.5-m waves of 7-s period, show a piston stroke of 0.64 m, a high-pressure water flow rate per pump cycle of 20 dm^3/s, and a continuous Pelton-turbine flow rate of 3 dm^3/s under a head of 50 m.

A liquid, other than water, may be chosen for the closed loop to eliminate corrosion and freezing. Alcohol is one candidate for such a liquid. Particular attention must be paid to the seals between pistons and cylinders that must be gas tight and have low friction. A rolling diaphram seal has been selected. The piston and cylinders are to be constructed of glass fiber–reinforced plastic, ferro-concrete, aluminum, or steel.

An alternative to the high-pressure accumulator concept is the *high-level reservoir concept* (Fig. 15-15). A similar pressure magnification piston is used, but the pressurized water is elevated to a natural reservoir above the wave generator, which would have to be near a shoreline, or to an artificial water reservoir. The water in the reservoir

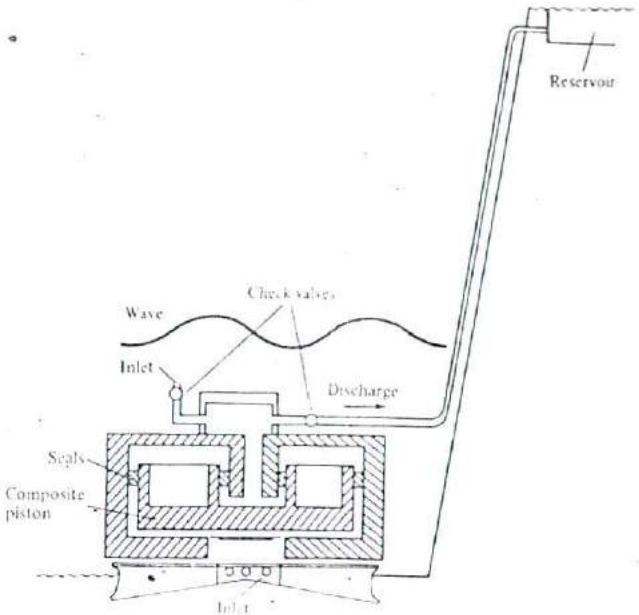


Figure 15-15 Schematic of a high-level reservoir wave machine.

is made to flow through a turbine back to sea level. Calculations show that a 20-m-diameter generator of this type can produce 1 MW.

Although the hydraulic accumulator is a free-floating device, the high-level reservoir machine is stationary. Problems needing solutions are motion and vibration damping in the former and tide compensation in the latter.

15-12 OTHER WAVE MACHINES

The Dolphin-Type Wave-Power Machine

The basic design of a dolphin-type wave-power generator has been worked out by Tsu Research Laboratories in Japan. The major components of the system (Fig. 15-16) are a dolphin, a float, a connecting rod, and two electrical generators.

The float has two motions. The first is a rolling motion about its own fulcrum with the connecting rod. It causes relative revolving movements between the float and the connecting rod. The other is a nearly vertical or heaving motion about the connecting rod fulcrum. It causes relative revolving movements between the connecting rod and the stationary dolphin. In both cases, the movements are amplified and converted by gears into continuous rotary motions that drive the two electrical generators.

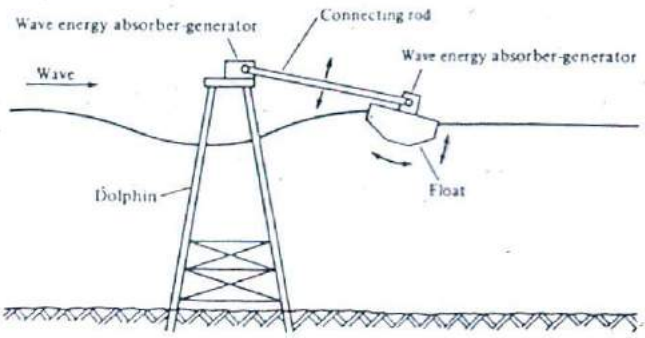


Figure 15-16 Schematic of the dolphin-type water generator (*Tsu Research Laboratories.*)

A scale-model was tested in 1980 in an inland basin. The results were the absorption of the applied wave power of 90 W and the complete elimination of waves downstream. 20 W were used up in mechanical and electrical losses resulting in a net 70 W of electric output. The experiments on a 3 × 1 × 0.5 m float showed the linear power output to be given by

$$\frac{P}{L} = 1.74a^2\tau \tag{15-15}$$

where P/L = power per unit length perpendicular to the wave, kW/m

a = wave amplitude (half the height), m

τ = wave period, s

Thus if the wave height is 2 m and the period is 6 s, the linear-power output is about 10 kW/m. A linear array of units totaling 1 km would thus generate some 10 MW.

Offshore experiments are planned for the future. The system is envisaged to be used for electric-power generation, pumping for desalination equipment, or for uranium extraction from the sea. Because it completely eliminates waves, it can provide suitable sites for fish farming, port facilities, etc.

The Dam-Atoll Concept

The *dam-atoll* is a wave-power conversion device (Fig. 15-17) designed by Wirt and Morrow of the Lockheed Corporation, Burbank, California. It is a massive and robust device that appears to overcome some of the disadvantages of many other devices, namely, complexity and fragility in heavy seas. It is said to be strong enough to survive any ocean storm.

The dam-atoll derives its name from the fact that it incorporates some of the characteristics of both dams and atolls. The principle of operation is based on the

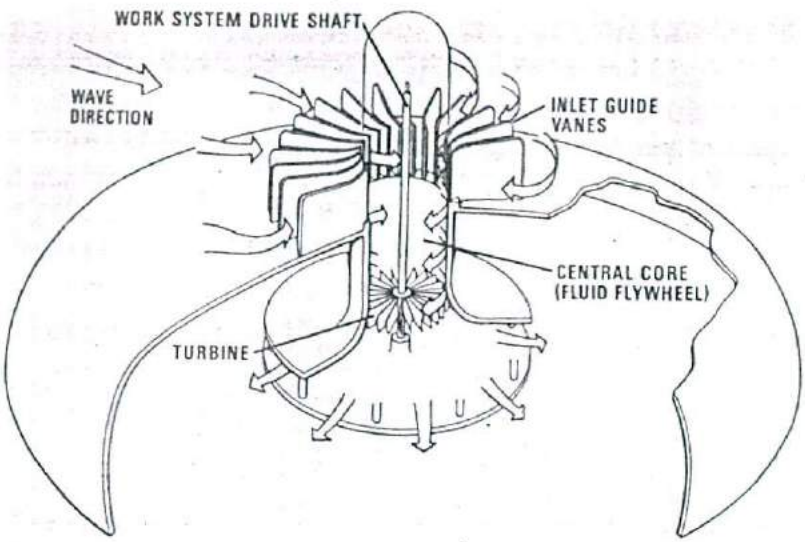


Figure 15-17 Cross section of a dam-atoll wave machine showing water flow (*Lockheed.*)

observed action of waves as they approach atolls (small volcanic islands) in an ocean. The waves wrap themselves around the atolls from all sides, ending in a spiral in the center, driving a turbine before discharging laterally outward. A module, 80 m in maximum diameter and 20 m high, is said to be capable of generating 1 to 1.5 MW in 7- to 10-s period waves. Figure 15-18 shows an artist's conception of a dam-atoll wave energy "farm."

The Multiple-Pontoon Raft

This is a system developed with British government support by Wavepower, Ltd., of Southampton. The concept was designed by Sir Christofer Cockerell, inventor of the hovercraft. A 1-kW scale model underwent sea trials in the solent of the Isle of Wight in 1978.

Taking advantage of favorable wave activity around the British Isles, future full-scale versions may be located off the west coast of Scotland or the western approaches to the English Channel. They would generate 2 MW per raft. A series of rafts 8 to 16 km (5 to 10 mi) offshore and stretching some 24 km (15 mi) parallel to the coast could generate 500 MW. It is believed that for the United Kingdom wave power offers greater potential than any other renewable energy source and that a 1000-km (630-mi) line of wave-power machines might generate half of the United Kingdom's electrical demand.

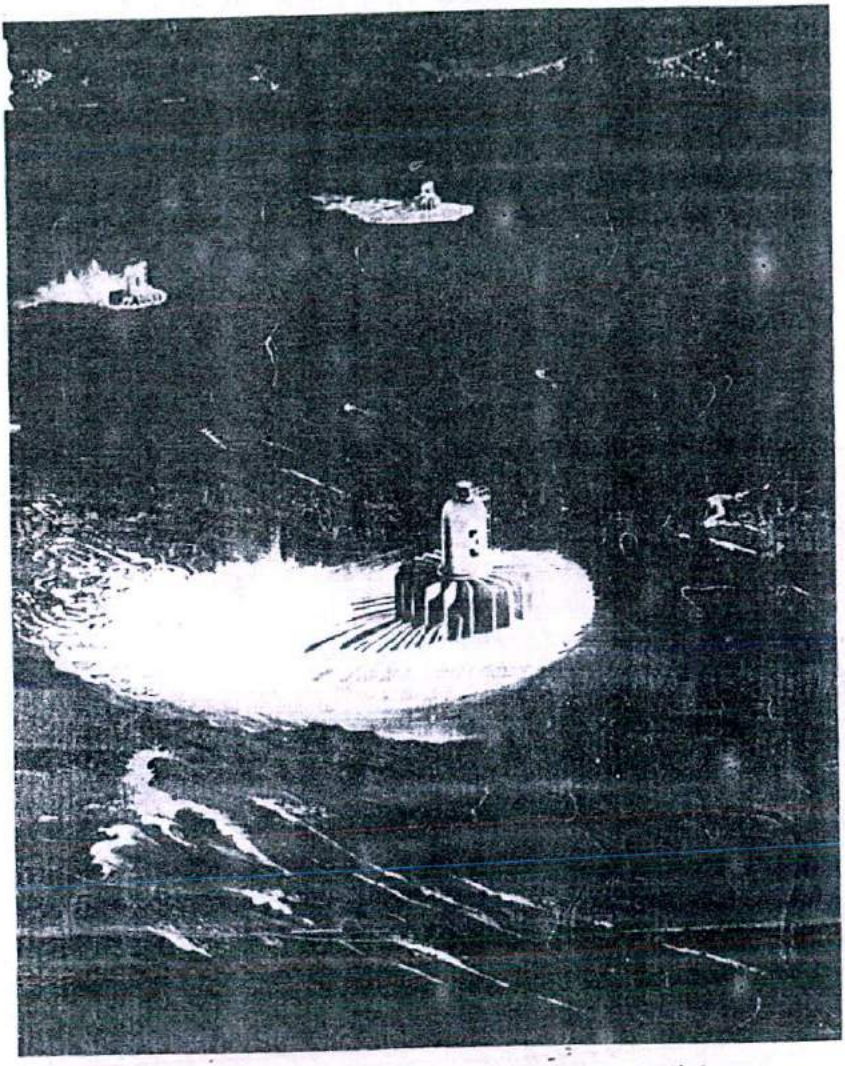


Figure 15-18 An artist's conception of a dam-atoll wave machine farm. *(Courtesy the Lockheed Corporation, Burbank, Calif.)*

15-13 THE TIDES

The tides are yet another source of energy from the oceans. This energy can be tapped from coastal waters by building dams that entrap the water at high tide and release it at low tide back to the sea. Power can then be obtained by turbines from both in-out flows of the water. The amount of energy available is very large but only in a few parts of the world.

Tidal energy is somewhat similar to hydro energy in that it uses the potential energy of water.* Both have been in use for centuries. Tidal "mills" were used in England and Europe. An early example is that of a miller in Woodbridge, Suffolk, who used the tide to mill grain in 1170. Another is a tidal waterwheel that was constructed in the sixteenth century under the London Bridge and that supplied water to London up to the nineteenth century. Other tidal mills were common for hundreds of years. They were used, particularly in the seventeenth and eighteenth centuries, for grinding grain, sawing wood, pumping water, etc. Mills were to be found in Britain, New England, Russia, and other places. One of the earliest scientific works on the tides was written by George Darwin, son of the great biologist Charles Darwin, and published in 1898 [152].

The tides, as we will see, although free, were inconvenient because they come at varying times from day to day, have varying ranges (heads) and, for large outputs, required large capital expenditures. Their early use declined and eventually came to a halt with the coming of the age of steam and cheap coal. With the beginning of the energy crisis in the 1970s, tidal energy, like other renewable energy sources, received renewed attention.

The tides are rhythmic but not constant, nor do they occur on a regular daily schedule. Their occurrence is due to a balance of forces, mainly the gravitational force of the moon but also that of the sun, both acting together with that of the earth to balance the centrifugal force on the water due to the earth's rotation. The result is the rhythmic rise and fall of water. The tides are characterized by their *schedule* and *range* R.

The *tidal schedules* vary from day to day because the orbit of the moon does not occur on a regular, 24-h, daily schedule. Instead, the moon rotates around the earth every 24 h, 50 min. During this time the tide rises and falls twice, resulting in a *tidal cycle* that lasts 12 h 25 min.

The *tidal range* R is defined as

$$R = \text{water elevation at high tide} - \text{water elevation at low tide} \quad (15\text{-}16)$$

* Hydro energy, not covered in this text, converts the potential energy of water (trapped at relatively high elevation or behind an artificial dam) to mechanical work by a water turbine. Before the introduction of electricity in the nineteenth century, hydro energy was used to power industrial machinery directly. In the mid-nineteenth century, wind and hydro power accounted for some two-thirds of all mechanical power used in the United States. This percentage rapidly dropped, however, with the introduction of steam in the latter part of the nineteenth century. Hydro energy is now used almost exclusively to generate electricity.

The range is not constant. It varies during the 29.5-day lunar month (Fig. 15-19), being maximum at the time of new and full moons, called the *spring tides*, and minimum at the time of the first and third quarter moons, called the *neap tides*. The spring-neap tidal cycle lasts one-half of a lunar month. A typical *mean* range is roughly one-third of the spring range. The actual variations in range are somewhat complicated by seasonal variations caused by the ellipticity of the earth's orbit around the sun.

The variations in daily periodicity and monthly and seasonal ranges must, of course, be taken into account in the design and operation of tidal powerplants. The tides, however, are usually predictable, and fairly accurate tide tables are usually available.

Tidal ranges vary from one earth location to another. They are influenced by such conditions as the profile of the local shoreline and water depth. When these are favorable, a resonancelike effect causes very large tidal ranges. Ranges have to be very large to justify the huge costs of building dams and associated hydroelectric powerplants. Such tides occur only in a few locations in the world. One of the most suitable is the Bay of Fundy between Maine, USA, and New Brunswick, Canada, where the range can be as high as 20 m (~66 ft). Other potential sites are the estuary of the River Severn in Britain, the English Channel, the Patagonian coast of Argentina, the Kislaya inlet on the Barents Sea in the USSR near the Norwegian border, the Rance estuary on the Brittany coast of France, the coast along the Sea of Okhotsk in Japan, and several others with ranges equal to or exceeding 10 m (~33 ft).

The total tidal power that is dissipated throughout the world is estimated at 2.4×10^6 MW, which is about one-third of world consumption in the early 1970s. Of these, some 10^6 MW are dissipated in shallow seas and coastal areas and are not recoverable. Because of the very high capital costs of dams and other structures associated with tide energy-conversion systems, only a small fraction of the rest, and a smaller fraction of increasing world energy needs, is expected to be satisfied by tidal energy.

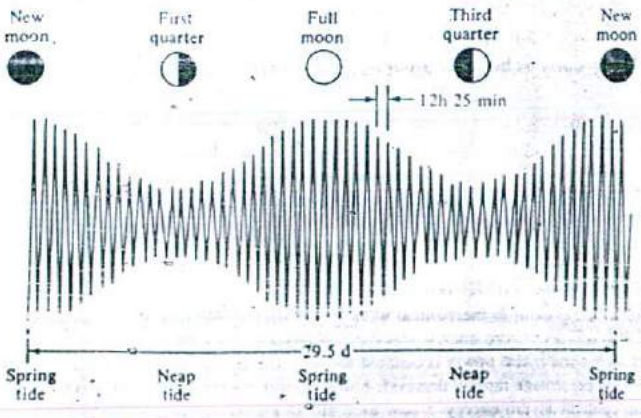


Figure 15-19 Relative high and low tides showing variation in range during lunar month.

We will next discuss three schemes of tidal-energy conversion for the production of electric energy: two depend upon a single-pool or basin, the third on a two-pool design. A discussion of recent developments in tidal electric powerplants may be found in the proceedings of a conference held in Nova Scotia in 1970 [153].

15-14 THE SIMPLE SINGLE-POOL TIDAL SYSTEM

The *simple single-pool tidal system* has one pool or basin behind a dam that is filled from the ocean at high tide and emptied to it at low tide. Both filling and emptying processes take place during short periods of time: the filling when the ocean is at high tide while the water in the pool is at low-tide level, the emptying when the ocean is at low tide and the pool at high-tide level (Fig. 15-20). The flow of water in both directions is used to drive a number of reversible water turbines, each driving an electrical generator. Electric power would thus be generated during two short periods during each tidal period of 12 h, 25 min, or once every 6 h, 12.5 min.

The maximum *energy* that can be generated during one generation period can be evaluated with the help of Fig. 15-21, which shows the case of the pool beginning at high-tide level, emptying through the turbine to the ocean, which is at low tide. (The reverse process results in identical energy).

For a tidal range R, and an intermediate head h at a given time during the emptying process, the differential work done by the water is equal to its potential energy at the time, or

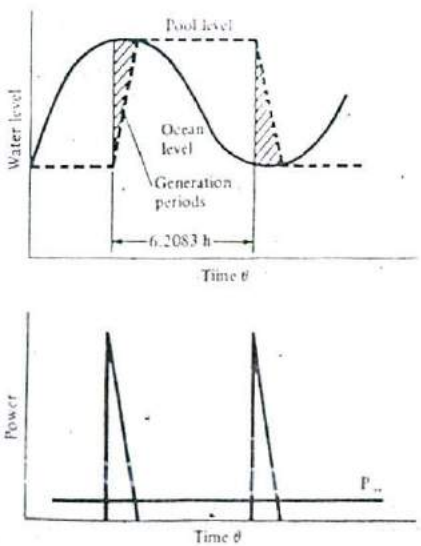


Figure 15-20 Ocean and pool levels and power generated in a simple single-pool tidal system.

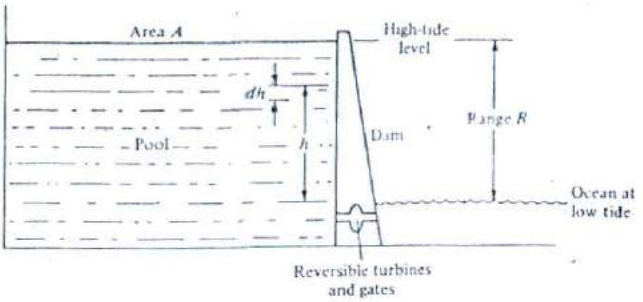


Figure 15-21 Level changes during power production in a single-pool tidal system.

$$dW = \frac{g}{g_c}\, dm\, h \tag{15-17}$$

but

$$dm = -\rho A\, dh \tag{15-18}$$

so that

$$dW = -\frac{g}{g_c}\rho A h\, dh \tag{15-19}$$

where W = work done by the water, ft · lb_f or J

g = gravitational acceleration, 32.2 ft/s² or 9.81 m/s²

g_c = conversion factor, 32.2 lb_m · ft/(lb_f·s²) or 1.0 kg/(N · s²)

m = mass flowing through turbine, lb_m or kg

h = head, ft or m

ρ = water density, lb_m/ft^3 or kg/m^3

A = surface area of pool, considered constant, ft^2 or m^2

The total theoretical work during a full emptying (or filling) period is obtained by integrating Eq. (15-19) as

$$W = \int_R^0 dW = -\frac{g}{g_c}\rho A \int_R^0 h\, dh$$

or

$$W = \frac{1}{2}\frac{g}{g_c}\rho A R^2 \tag{15-20}$$

Thus the work is proportional to the range to the power 2. The power generated during each of the periods is equal to W divided by the time duration of that period.

Zero power is generatgd during the rest of the time (Fig. 15-20). The *average theoretical power* delivered by the water is W divided by the total time it takes each period to repeat itself, or 6 h, 12.5 m, or 22,350 s. Thus

$$P_{av} = \frac{1}{44{,}700} \frac{g}{g_c} \rho A R^2 \tag{15-21}$$

where P_{av} = average theoretical power, ft · lb_f/s or W

Assuming an average seawater density of 64 lb_m/ft^3, or 1025 kg/m^3, the average theoretical power per unit pool area would be given by

$$\frac{P_{av}}{A} = 1.43 \times 10^{-3} R^2 \quad \text{ft} \cdot lb_f/(s \cdot ft^2) \tag{15-22a}$$

$$= 0.225 R^2 \quad W/m^2 \text{ or } MW/km^2 \tag{15-22b}$$

The actual power generated by a real tidal system would be less than the above because of frictional losses and inefficiencies in the turbines and electric generators and might only be 25 to 30 percent of the above.

The power generated, however, could be immense. The Bay of Fundy, for example, has an area of 13,000 km^2 and an average range of 8 m. If we assume an efficiency of 27.5 percent, it has a potential of generating more than 50,000 MW, or 50 GW, which is about twice the electric-power consumption of Canada in 1980.

15-15 THE MODULATED SINGLE-POOL TIDAL SYSTEM

In the simple single-pool system (above), two high-peak, short-duration power outputs occur every tidal period. Such peaks necessitate large turbine-generators that remain idle much of the time. The power peaks also occur at different times every day (50 min later each successive day), at times of high and low tides that almost surely will not always correspond to times of peak power demand, and pose a burden on the electric-power grid they are connected to.

The *modulated single-pool tidal system* partially corrects for these deficiencies by generating power more uniformly at a lower average head, though still with some periods of no generation. Because the average head h is lower and work and power are proportional to h^2, the turbine-generators are much smaller and operate over much longer periods. The resulting total work is reduced, however.

In the system, shown by the ocean and pool level and power diagrams of Fig. 15-22, the reversible turbines are allowed to operate *during* periods of pool filling and emptying instead of at high and low levels only. They cease to operate when the head is too low for efficient operation. Period G_1 begins with both pool and ocean at low-tide level (1), the ocean at the beginning of tide rise, and all gates closed. When the head is sufficient (2), gates to the turbines are opened and water from the ocean is allowed through. Power is generated during period G_1 as both ocean and pool levels rise. The ocean level reaches its peak and begins to decrease but the pool level is still

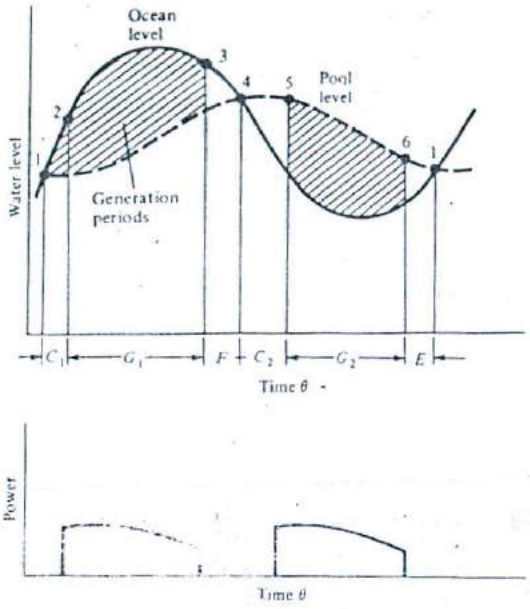


Figure 15-22 Ocean and pool levels in a modulated single-pool tidal system. C = gates closed, G = generation, F = pool filling, E = pool emptying.

increasing until, at 3, the head is too low for efficient generation. The gates to the turbines are closed and bypass gates are opened so that the pool is allowed to fill up during period F to 4. At 4 all gates are once again closed and the pool level remains constant while the ocean level decreases during period C_2. At 5 the head is once again sufficient to allow for turbine water flow in the opposite direction and a second generation period G_2 begins. At 6 generation ceases but the pool is allowed to empty during period E and the system goes back to point 1, repeating the cycle. The power generation shown is certainly not uniform but much more so than in the case of the simple system.

The evaluation of the total work is obtained by assessing the characteristics of the system, i.e., the variation of water mass flow and head with time θ, and integrating their products over the time span during which generation is taking place. When we consider the first generation period (Fig. 15-23), the general relationships take the form

$$H = f_1(\theta) \tag{15-23}$$

$$y = f_2(\theta) \tag{15-24}$$

$$dW = \frac{g}{g_c}\, dm\, h = \frac{g}{g_c}\, dm\, (H - y) \tag{15-25}$$

but

$$dm = \rho A\, dy \tag{15-26}$$

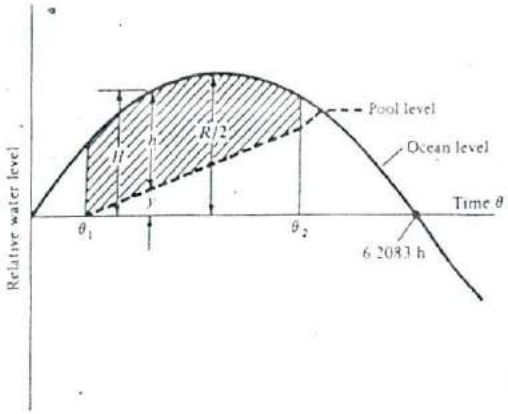


Figure 15-23 Relative ocean and pool levels in the first-generation period of a modulated single-pool tidal system.

Thus

$$dW = \frac{g}{g_c}\rho A\left[f_1(\theta) - f_2(\theta)\right] df_2(\theta) \tag{15-27}$$

and

$$W = \frac{g}{g_c}\rho A\int_{\theta_1}^{\theta_2}\left[f_1(\theta) - f_2(\theta)\right] df_2(\theta) \tag{15-28}$$

where H = ocean level above mean or other appropriate datum

y = pool level above mean or datum

θ = time

and the other symbols have already been defined. H may be closely approximated by a sinusoidal function of θ such as

$$H = f_1(\theta) = \frac{R}{2}\sin\frac{\pi\theta}{6.2083} \tag{15-29}$$

where θ is in hours and 6.2083 in hours is one-half of a tidal period. y may be approximated by a linear function of θ, starting at 0 at θ_1 for a constant mass-flow rate such as

$$y = f_2(\theta) = aR(\theta - \theta_1) \tag{15-30}$$

where a is a constant having the dimension time^{-1}, e.g., h^{-1}, or y could be a function of $h = H - y$ for a constant flow resistance or some other function determined from operational data. Using the relationships for H and y of Eqs. (15-29) and (15-30), the work during period G_1 (or G_2) would be evaluated from

$$dW = \frac{g}{g_c}\rho A\left[\frac{R}{2}\sin\frac{\pi\theta}{6.2083} - aR(\theta - \theta_1)\right] d\left[aR(\theta - \theta_1)\right] \tag{15-31}$$

and

$$W = \frac{g}{g_c}\rho A \int_{\theta_1}^{\theta_2}\left[\frac{R}{2}\sin\frac{\pi\theta}{6.2083} - aR(\theta - \theta_1)\right]aR\,d\theta$$

$$= \frac{g}{g_c}\rho AR^2 \int_{\theta_1}^{\theta_2}\left[\frac{a}{2}\sin\frac{\pi\theta}{6.2083} - a^2(\theta - \theta_1)\right]d\theta$$

$$= \frac{g}{g_c}\rho AR^2\left[a\frac{6.2083}{2\times\pi}\left(-\cos\frac{\pi\theta}{6.2083}\right) - \frac{a^2}{2}\theta^2\right]_{\theta_1}^{\theta_2}$$

Thus

$$W = \frac{g}{g_c}\rho AR^2\left[0.988a\left(-\cos\frac{\pi\theta_2}{6.2083} + \cos\frac{\pi\theta_1}{6.2083}\right) - \frac{a^2}{2}\left(\theta_2^2 - \theta_1^2\right)\right]_{\theta_1}^{\theta_2} \quad (15\text{-}32)$$

This shows that the work, like in the simple single-pool system, is also a function of L^2.

Example 15-3 Calculate the total energy and average power of a modulated single-pool tidal system using Eqs. (15-29) and (15-30) for H and y and the values $R = 12$ m, $a = 0.0625\ \text{h}^{-1}$, $\theta_1 = 1$ h, $\theta_2 = 4$ h, $A = 10{,}000\ \text{km}^2$, and $\rho = 1025\ \text{kg/m}^3$. Compare the results with those for a simple single-pool system.

Solution Using Eq. (15-32):

$$W = \frac{9.81}{1} \times 1025 \times 10^{10} \times 12^2\left[0.988 \times 0.0625(0.43795 + 0.87468) - \frac{(0.0625)^2}{2}(16 - 1)\right]$$

$$= 1.448 \times 10^{16}(0.08105 - 0.02930)$$

$$= 7.493 \times 10^{14}\ \text{J}$$

The average power during the generation period of 4 h is

$$P_{av,gen} = \frac{7.493 \times 10^{14}}{4 \times 3600} = 5.2 \times 10^{10}\ \text{W} = 5200\ \text{MW}$$

The average power during the total period of 6.2083 h is

$$P_{av} = \frac{7.493 \times 10^{14}}{6.2083 \times 3600} = 3.35 \times 10^{10}\ \text{W} = 33{,}500\ \text{MW}$$

In the simple single-pool system, the corresponding values from Eqs. (15-20) and (15-21) are

$$W = \frac{1}{2}\frac{g}{g_c}\rho A R^2 = \frac{1}{2} \times \frac{9.81}{1} \times 1025 \times 10^{10} \times 12^2 = 7.24 \times 10^{15}\ \text{J}$$

and $$P_{av} = 3.24 \times 10^{11}\ \text{W or } 324{,}000\ \text{MW}$$

Thus the simple single-pool system produces some 10 times the work and average power of the modulated single-pool system. However, the former does so almost in a "spike," which is very hard on the power grid and requires very large turbines that remain idle most of the time. The latter produces its work over several hours and hence avoids these problems.

The actual work and power above must be multiplied by the efficiency of the system, which is probably in the 25 to 30 percent range.

Only two tidal powerplants have been built in the world to date, one in France, the other in the USSR. The French plant (Fig. 15-24) was built in the Bay of Rance, across the River Rance, near St. Malo in Brittany, France, in 1966. The Bay of Rance has a basin of 22×10^6 m^2 area and a maximum tidal range in excess of 13 m. The plant consists of twenty-four 10-MW reversible turbine generators that operate on the modulated single-basin system described above for a peak power of 240 MW. The average power, however, is 160 MW. An added feature of the Rance plant is that the tidal basin behind the dam is also used for pumped storage from the main power grid. At periods of low power demand and high tide, excess energy from the power grid is used to pump water into that basin raising its level almost 0.5 m above high tide level. This pumping energy is more than recovered during the normal tidal-basin discharge to the ocean when at low tide because the head at discharge is greater than at pumping. Since the energy is proportional to h^2, the energy gain in this operation is estimated at 12:1 maximum. Operating and maintenance difficulties have resulted in a low plant availability factor (fraction of total time plant is on line) of about 25 percent, with the plant operating only about 2000 h/year for a yearly average of about 62 MW. The unit plant capital cost, based on 1962 economics, was $300/kW.

The USSR plant, a small 2-MW demonstration unit, also of the modulated single-basin type, started producing power in 1970 at Kislaya Guba on the Kislaya inlet on the Barents Sea, about 1000 km north of Murmansk, near the Norwegian border. It is believed that the USSR has been studying proposals for larger systems.

15-16 THE TWO-POOL TIDAL SYSTEM

The *two-pool tidal system* is one that is much less dependent on tidal fluctuation but at the expense of more complex and hence more costly dam construction. An inland basin (Fig. 15-25) is enclosed by dam *A* and divided into a high pool and a low pool by dam *B*. By proper gating in dam *A*, the high pool gets periodically filled at high tide from the ocean and the low pool gets periodically emptied at low tide. Water flows from the high to the low pool through the turbines that are situated in dam *B*. The capacities of these two pools are large enough in relation to the water flow between

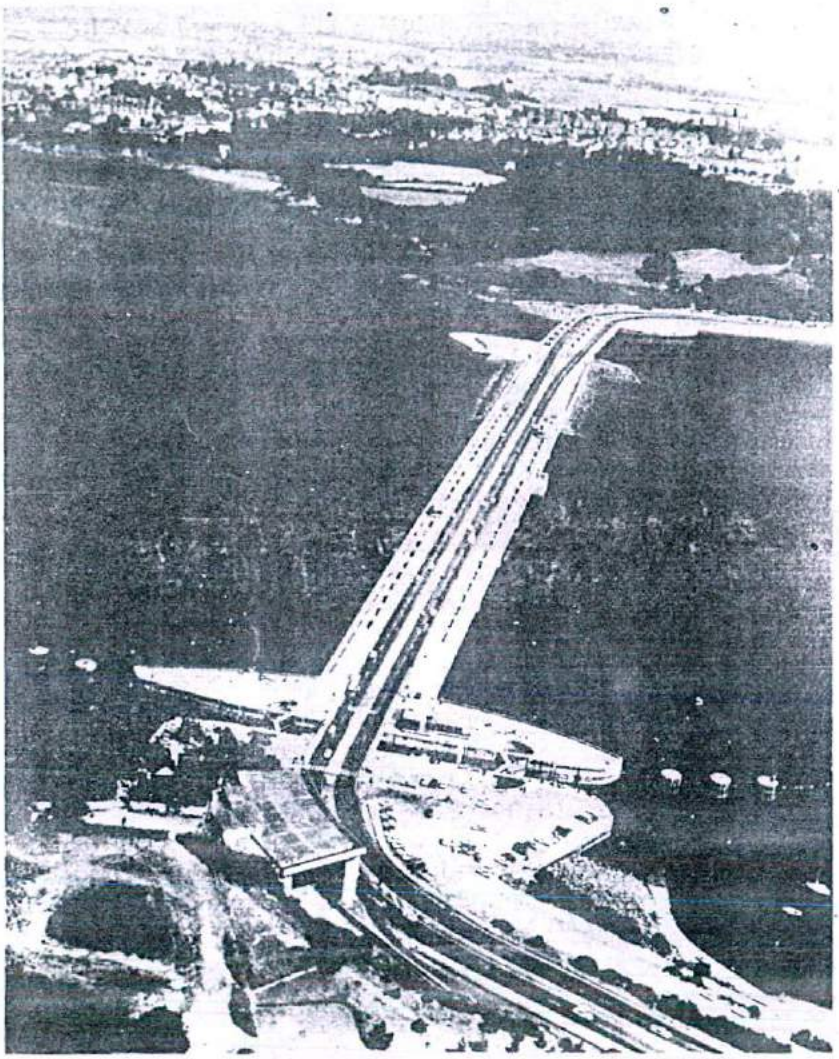


Figure 15-24 A view of the 240-MW (peak) tidal powerplant built on the River Rance, Brittany, France. *(Courtesy Phototeque, Electricité de France, Paris.)*

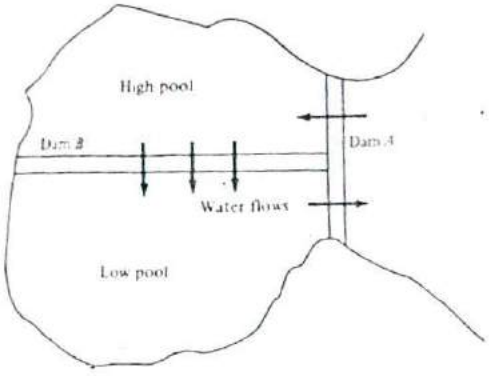


Figure 15-25 Schematic of a two-pool tidal system.

them that the fluctuations in the head are minimized, which results in continuous and much more uniform power generation.

The two-pool system has been considered for the Passamaquoddy Bay tidal project. Passamaquoddy Bay is an arm of the Bay of Fundy. (Enclosing the whole Bay of Fundy is economically prohibitive and not technically feasible, and it is more feasible to enclose its basins and estuaries.) Passamaquoddy Bay itself would constitute the high pool. The adjacent Cobscook Bay would be the low pool. A modest 300-MW plant was under consideration as a joint venture of the U.S. and Canadian governments, but the project was abandoned in 1961 because it was considered uneconomical. Another larger plant of 1-GW capacity was again considered from 1963 to 1974, but no agreement was reached because of similar economic considerations.

PROBLEMS

15-1 Ocean water, just below the topmost layer (where reflection back to the sky and a complex mechanism of heat transfer and evaporative mass transfer occurs) receives 65 W/m^2 of solar energy in one locality. The extinction coefficient is 0.4 m^{-1}. Calculate (*a*) the volumetric heat-generation rate q''', in watts per cubic meter, near the surface and 1 m below the surface, and (*b*) the distance below the surface, in meters, where 99.99 percent of solar energy has been absorbed.

15-2 An OTEC powerplant of the Claude type has an ideal turbine operating between 25 and 15°C. For a turbine output of 1 MW, calculate (*a*) the mass flow rate of steam, in kilograms per second, (*b*) the mass flow rate of warm water, in kilograms per second, if the evaporator temperature drop is 2°C, (*c*) the mass flow rate of cold water, in kilograms per second, if the condenser temperature drop is 2°C, and (*d*) the cold water pipe diameter, in meters, if the water velocity in it is not to exceed 1 m/s.

15-3 An OTEC powerplant of the Claude type uses 10^7 lb$_m$/h of warm surface water at 70°F. The evaporator temperature is 66°F. The condensor pressure is 0.25 psia. The turbine polytropic efficiency is 0.84. The combined turbine-generator mechanical and electrical effeciency is 0.87. Calculate (*a*) the steam mass flow rate into the turbine, in pounds mass per hour, (*b*) the gross generator output, in kilowatts, (*c*) the gross cycle efficiency, and (*d*) the cold-water pipe diameter if the cold-water temperature and velocity in the pipe are 56°F and 1.0 ft/s, respectively.

15-4 Consider the powerplant in Fig. 15-5. Assume an ocean surface water flow of 10^7 lb_m/h, a turbine polytropic efficiency of 0.85, and turbine-generator combined mechanical-electrical efficiency of 0.80. Calculate (*a*) the gross power generated by the turbine generator, in kilowatts, (*b*) the cold-water volumetric flow rate, in cubic feet per minute, and (*c*) the quantity of fresh water produced, in cubic feet per minute.

15-5 Compare the mass flow rates, in pounds mass per hour, and volume flow rates, in cubic feet per minute, at turbine inlet of all four fluids in Table 15-2, for a 1-MW turbine operating with saturated vapor at 70°F and exhausting at 50°F. The turbine polytropic efficiency is 0.88, assumed the same in all cases.

15-6 An Anderson OTEC cycle generates 150 MW of net power. It uses ammonia as the working fluid. Ammonia vapor is generated at 70°F saturated and condenses at 50°F. The turbine has an adiabatic efficiency of 0.80 and the turbine-generator has a combined mechanical-electrical efficiency of 0.88. The temperature drop of the ocean warm water in the evaporator and rise of the cold water in the condenser are both 8°F. 14 percent of the gross output of the generator is used for plant pumps and other auxiliaries. Calculate (*a*) the ammonia mass and volume flow rates, in pounds mass per hour and cubic feet per minute at turbine inlet, (*b*) the warm and cold water mass and volume flow rates, in pounds mass per hour and cubic feet per minute, and (*c*) the plant net thermal efficiency.

15-7 An Anderson OTEC powerplant uses propane as the working fluid. Saturated propane vapor enters the turbine at 70°F and the condenser at 50°F. The turbine polytropic efficiency is 0.88 and the turbine-generator combined mechanical-electrical efficiency is 0.80. 10^9 lb_m/h of hot water enters the evaporator at 82°F and leaves at 74°F. Pumps and other auxiliaries consume 14 percent of the generator gross output. Calculate (*a*) the ammonia mass and volume flow rates, in pounds mass per hour and cubic feet per minute, at the turbine inlet, (*b*) the plant net output, in megawatts, (*c*) the cold-water flow, in pounds mass per hour, if its temperature increases 8°F in the condenser, and (*d*) the plant net efficiency.

15-8 A 2.5-m ocean wave has a 60-m wavelength in 10-m deep water. Calculate (*a*) the probable period, in seconds, (*b*) the major and minor axes, in meters, of the water motion at the surface and at middepth, and (*c*) the wave power kilowatts per meter width of the wave front. Take water density as 1025 kg/m^3.

15-9 A wave-energy generator system is to produce 1 MW in the ocean where the waves have a steady 4-ft amplitude and 227.1-ft wavelength. The floats measure 12 × 12 × 1 ft. Calculate the number of floats necessary if the overall efficiency of the system is 9.6 percent. Sea water density is 64 lb_m/ft^3.

15-10 A wave-energy generator float measures 40 × 40 ft. For simplicity, assume that it experiences waves on a given day that are 7 ft high half the time and 4 ft high the other half. All waves have a wavelength of 184 ft. The overall conversion efficiency of the plant is 5 percent. The water density is 64 lb_m/ft^3. Calculate (*a*) the total energy output during the day in foot pounds force and kilowatt hours and (*b*) the mean energy wave height, and (*c*) the percent error obtained if the "arithmetic mean" wave height were used for the whole day.

15-11 A single square float measuring 10 × 10 × 1 ft is placed in the ocean where the waves have a steady 3.5-ft amplitude and 200-ft wavelength. The float is connected to a piston of 1-ft diameter that operates within a cylinder. The compressed air is expanded in a turbine. Both compression and expansion ratios are 6. The air temperature is 40°F and the water density is 64 lb_m/ft^3. Calculate (*a*) the power, in foot pounds force per second and kilowatts, imparted to the float by the waves, (*b*) the air flow to the turbine, in pounds mass per second, and (*c*) the ideal turbine work, in kilowatts.

15-12 An ocean wave power system of the float type uses a 25-cm-thick float in 2-m waves that have a 60-m wavelength. The cylinder has a diameter of 1 m. The compressor pressure ratio is 10. The air is at 1 atm and 10°C. Calculate the power produced by the turbine if the compressor-turbine system has an efficiency of 76 percent of ideal.

15-13 An ocean wave power device of the high-pressure accumulator type operates in 2.5-m waves that have a wavelength of 60 m. The composite piston has diameters of 20 and 3 m. The water has a density of 1025 kg/m^3. Calculate (*a*) the height of the reservoir above the accumulator if frictional losses in the discharge pipe average 1 bar, (*b*) the average water volumetric flow rate to the reservoir, in cubic meters per second, (*c*) the power generated, in kilowatts, by a turbine-generator of 70 percent efficiency that is situated 2 m above average ocean water level, assuming water level in the reservoir is constant, and (*d*) the length, in meters, of dolphin arrays (Fig. 15-16) that would produce the same power.

15-14 A tidal powerplant of the simple single pool type, has a pool area of 300×10^6 ft^2. The tide has a range of 36 ft. The turbine, however, stops operating when the head on it falls below 9 ft. Calculate the energy generated in one filling (or emptying) process, in foot pounds force and kilowatt hours if the turbine-generator efficiency is 0.73.

15-15 A 300×10^6 ft^2 tidal pool level follows a sinusoidal curve during the tidal cycle of 6.2083 h. Assume for simplicity that it discharges into a reservoir with constant level. The maximum head is 36 ft. Calculate the power generated during the cycle in foot pounds force and kilowatt hours. Assume for simplicity that the water mass flow rate is constant. Take density of water to be 64 lb$_m$/ft^3.

15-16 Calculate the total energy and average power of a modulated single-pool tidal plant operating with a range of 12 m. The tidal pattern is assumed to be sinusoidal. The water level in the pool may be approximated by the relation $0.0625R(\theta_2 - \theta_1)$ where θ is time, in hours. Power generation occurs between $\theta_1 = 1$ and $\theta_2 = 4$ h. The pool has a constant area of 10,000 km^2. The water density is 1025 kg/m^3.

15-17 A tidal powerplant of the two-pool type has upper pool area A_1 and lower pool area A_2. (*a*) Derive expressions for (*a*) the energy that can be detained if the upper pool is emptied into the lower pool when the initial head difference between them is R and when all gates to the ocean are closed, and (*b*) the ratio of this energy to that obtained from a single pool of area A. Determine the numerical value of this ratio if $A_1 = A_2 = 0.5A$.

15-18 Consider for simplicity that the two-pool tidal powerplant proposed for the Bay of Fundy operates with a constant head of 26 ft. Calculate the necessary ocean flow rate into the system, in cubic feet per day, if the powerplant is to produce 200 GW with a 60 percent efficiency. Take water density as 64 lb$_m$/ft^3.

CHAPTER

SIXTEEN

ENERGY STORAGE

16-1 INTRODUCTION

The need for energy storage arises because the demand for electric energy in a utility system is characterized by hourly, daily, and seasonal variations, whereas the supply from that system, in the majority of cases, has a fixed capacity. That capacity must be selected to correspond to the maximum demand plus a reasonable excess to take care of scheduled plant shutdowns for maintenance and unscheduled shutdowns due to abnormal occurrences. The result of this is large, expensive plants that operate much of the time below capacity, thus causing high operating and capital costs.

An example of electric-energy fluctuations in consumption during a typical week in the life of a largely university town is shown in Figs. 16-1 and 16-2 [154]. They demonstrate the differences between daytime and nighttime consumption, between weekdays and weekends, and between summer and winter. More severe fluctuations occur in an industrial or commercial region, where demands drop on weekends. Seasonal fluctuations in all regions also occur. The picture is more clouded, and the need for energy storage is greater, if plants using renewable forms of energy such as solar and wind are used to generate electricity. It is the output of these plants that fluctuates severely because of their input energy intermittency. Their conversion systems are also much more expensive than those of conventional plants.

The objective of energy storage, therefore, is to counteract the disadvantages that result from the fluctuations in demand for electric energy by assuring a steady high output from existing powerplants. When the demand is lower than capacity, energy is stored. When the demand is higher than that capacity, the stored energy is released. The result then is to be able to supply electricity reliably, efficiently and economically,

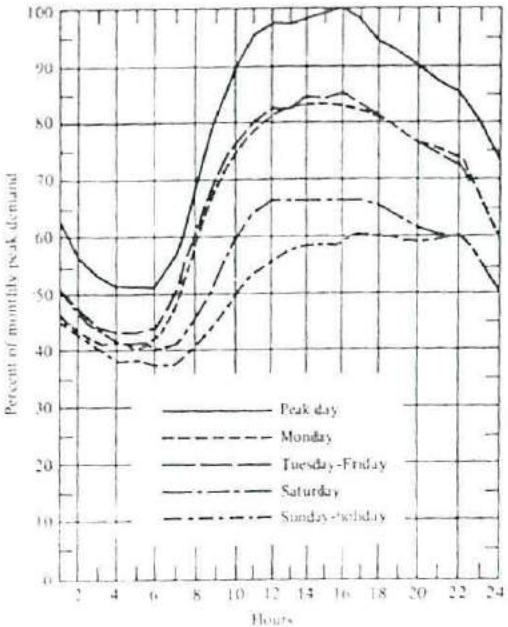


Figure 16-1 Hourly and daily electric-power consumption during summer (average July 1976–1980) in Madison, Wis. [154].

while being able to provide peak electrical demands on short notice during certain times of the day or week.

The need for energy storage was not acute when the generating plants were cheap and the fuel supply plentiful. Indeed, energy storage has, in a sense, been historically done in the form of the latent energy stored by nature in the fuels themselves. The energy density in this "natural" storage is large. Fossil fuels, coal, oil, and gas (at 1000 psia), all contain about a million Btu/ft^3 ($\sim 37 \times 10^6$ kJ/m^3). Natural uranium metal (0.071 percent U^{235}) contains about 3×10^{12} Btu/ft^3 ($\sim 10^{14}$ kJ/m^3). With increasing supply problems of all fuels, the need to conserve resources, and the increasing unit capital costs ($/KW) and production costs (mills*/kWh) of electric-generating plants, suitable methods of *energy management* become necessary. Examples of these are:

1. Supply power peaks by interconnecting power networks that might have different power demands on them.
2. Use newer and more efficient powerplants for base-load generation and use older less efficient plants for peak-power generation.

* 1 mill = one thousands of a dollar = 0.1¢.

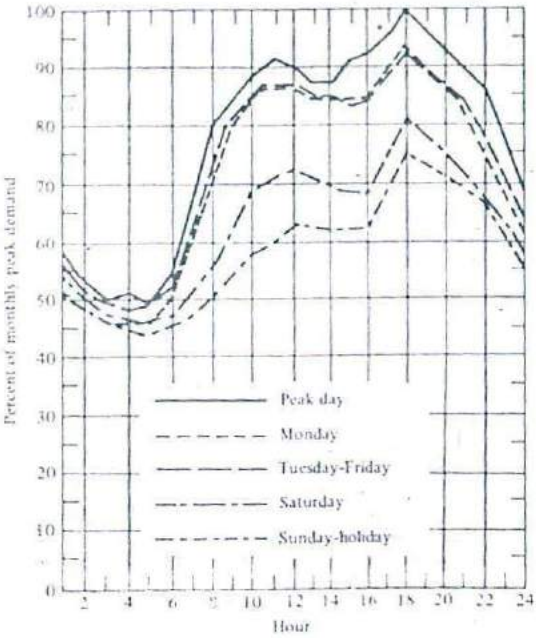


Figure 16-2 Hourly and daily electric-power consumption during winter (average December 1976–1980) in Madison, Wis. [154].

3. Construct smaller, low capital cost, though not so efficient powerplants, as power-peaking units. Examples are special steam plants, small hydroelectric plants, or gas-turbine peaking plants (Chap. 8).
4. Add energy-storage systems.

In general, reliability and economy of electrical supply can best be achieved by having a mix of three types of powerplants: a base-load plant, a cycling plant, and a peaking plant.

Base-load plants are used to provide a base electrical load to the grid. Such plants are usually large, efficient, steam-generating, Rankine-cycle type stations powered by fossil or nuclear fuels. They operate continuously except for scheduled maintenance or forced outages. They have a power operating factor (POF) (Fig. 14-9) between 60 and 70 percent. This relatively high POF results in a comparatively low unit cost of power (mills/kWh).

Cycling plants, also called *intermediate plants*, usually are older, less efficient steam plants, or new ones specifically designed for cyclic operation, such as combined cycles (Sec. 8-8). They operate primarily during hours of high load demand and have an annual POF between 25 and 50 percent. This rather wide range is primarily the result of seasonal variations, such as those due to periods of high industrial output, air-conditioning loads in the summertime, etc.

Peaking plants are specifically designed to provide relatively inexpensive power

during peak-demand periods, such as due to abnormal air-conditioning loads and peak-hour domestic demands in the evenings. They operate at a low annual POF of 5 to 15 percent. They also operate at a low availability factor (Fig. 14-9) i.e., intermittently according to system requirements. Their operation may be for as little as 2 or as much as 12 h/day, for as many as 5 days/week.

The last of the courses of action, energy storage, is the one discussed in this chapter. We are here concerned with large-scale storage suitable for incorporation with utility electrical powerplants. Energy storage would allow the plants to be designed for nearly constant load operation below peak demand, a process called *peak shaving*, which would thus reduce the high capital cost of the initial plants. Energy storage, of course, becomes attractive only when the capital and operating costs of the storage system are more than offset by the reduction in the corresponding costs of the original system.

One drawback to all energy-storage systems is that their energy densities are much lower than those mentioned above for fossil and nuclear fuels.

16-2 ENERGY-STORAGE SYSTEMS

There are basically two generic approaches to energy storage in utility systems (Fig. 16-3). These are (1) electrical storage and (2) thermal storage.

Electrical Storage

The primary electric-generating plant is continuously operated in a base-load mode, which results in excess electricity production during the off-peak periods $ab + cd$ (Fig. 16-4). Electrical storage is then used to hold this excess electricity for use during peak demand, period bc. Note that the total energy stored is greater than the total energy supplied because of conversion losses to and from storage. Storage schemes in this category that are in use or under investigation are:

1. Electrical mechanical energy storage
   a. Potential, pumped hydro
   b. Potential, compressed air
   c. Potential, springs, torsion bars, mass elevation
   d. Kinetic, flywheels
2. Direct electrical energy storage
   a. Batteries
   b. Superconducting coils

Thermal Storage

In thermal storage, all schemes deal with storing energy in a thermal form in a material during periods of low power demand and releasing it back during periods of high demand. The primary electric-generating plant is operated to meet the real-time elec-

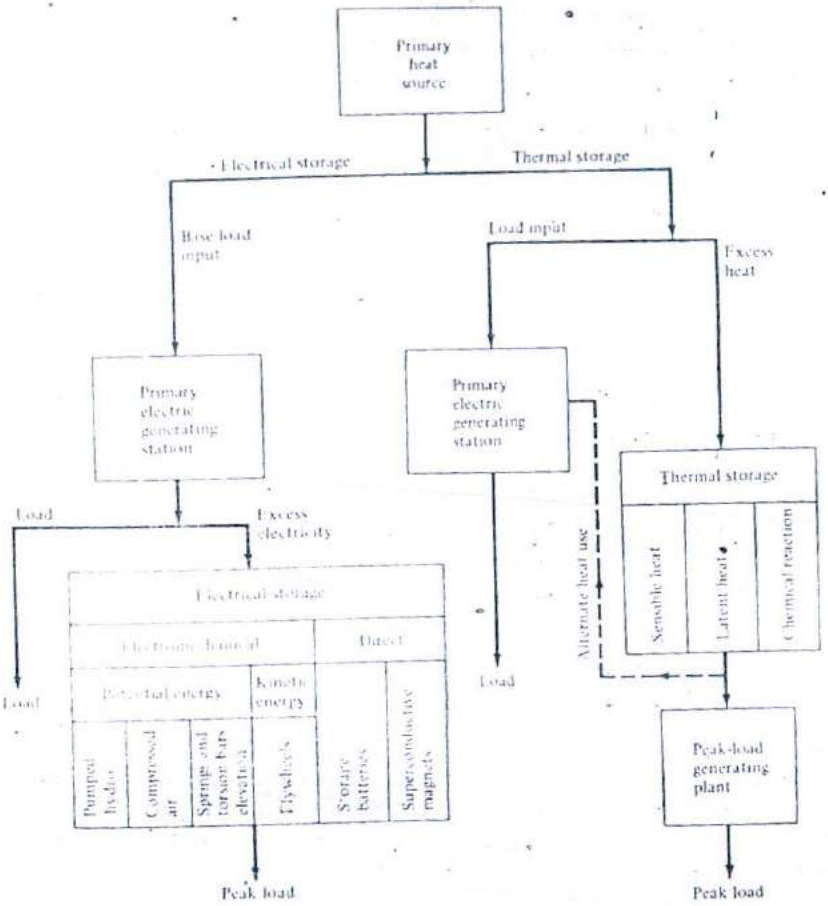


Figure 16-3 Energy storage systems.

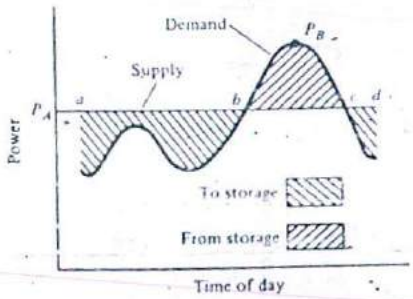


Figure 16-4 Thermal-energy storage with constant thermal input as from fossil or nuclear fuel.

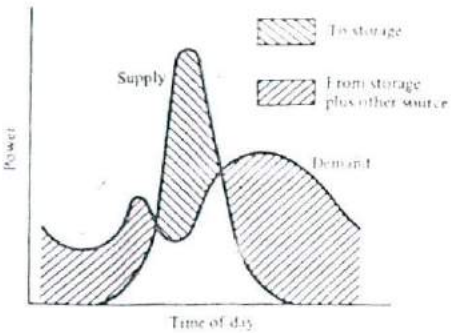


Figure 16-5 Thermal energy storage with hypothetical varying thermal input as from solar incidence

trical demands during off-peak hours. The available thermal energy input to the plant may be essentially constant, as is that from fossil or nuclear fuel (Fig. 16-4), or varying, as from solar incidence (Fig. 16-5). The excess thermal energy is stored as such and withdrawn to be converted to meet peak electrical demands. Conversion could occur in the primary plant itself or in a separate peaking plant (Fig. 16-4). Again, note that because of storage losses and conversion inefficiencies the total stored energy is greater than that supplied.

Thermal storage schemes include:

1. Sensible heat
2. Latent heat
3. Chemical reaction

Not all the various electrical and thermal energy-storage schemes are suitable for large utility energy storage. Some, like springs, torsion bars, and mass elevation, are very low-capacity systems that are used to power such small devices as watches, clocks, toys, and instruments. They will not be covered in this book. Others, like flywheels and batteries, are in the developmental stages and will probably be suitable for intermediate storage. A few, like pumped hydro, compressed air, and superconductivity are, or will be, suitable for large utility energy storage. These and the various other schemes are covered in the following sections.

16-3 PUMPED HYDRO

Pumped hydro, like compressed air (Sec. 16-4), is a potential-energy storage system suitable for large utility energy storage. It is the most developed and used of all storage systems. The principle behind pumped hydro is simple and follows the law of potential energy PE that is, the raising of mass to an elevation, height, or head H. It is given by

$$\text{PE} = \frac{g}{g_c} mH \qquad (16\text{-}1)$$

where PE = potential energy, ft · lb_f or J

g = gravitational acceleration = 32.2 ft/s² or 9.81 m/s²

g_c = conversion factor = 32.2 lb_m · ft/(lb_f · s²) or 1.0 kg/(N · s²)

m = mass, lb_m or kg

H = head, ft or m

The operating heads on the pump turbine in the pumping mode H_p and in the turbine-generating mode H_T are different and are made up of two components each

$$H_p = H + H_\ell \tag{16-2}$$

and

$$H_T = H - H_\ell \tag{16-3}$$

where H is the static head or height and H_ℓ represents the losses during flow conditions (which are different because of the different flow rates).

The pumping and generation powers are given by replacing the mass in Eq. (16-1) with the mass-flow rate $\dot{m}$ lb_m/s or kg/s and using the proper head, or with

$$P_p = \frac{g}{g_c}\rho \dot{Q}_p H_p \tag{16-4}$$

and

$$P_T = \frac{g}{g_c}\rho Q_T H_T \tag{16-5}$$

where P_p and P_t = pumping and turbine powers, respectively, ft · lb_f/s or W

ρ = density of water, lb_m/ft³ or kg/m³

$\dot{Q}_p$ and $\dot{Q}_T$ = volumetric flow rates in pumping and generation, respectively, ft³/s or m³/s

Equation (16-1) shows that 1000 kg raised 100 m will store 9.81×10^5 J or 0.2725 kWh. Thus large masses must be elevated to sufficiently large heights to store large quantities of energy. Fortunately large masses are available in pumped-hydro systems by the elevation of large quantities of water from a lower to an upper reservoir. One or both of these reservoirs may be artificially excavated or may be a natural river or lake.

Pumped-hydro systems, unfortunately, require a suitable topography that will allow the design and construction or selection of two reservoirs with sufficient capacities, maximum available elevation difference H, and minimum horizontal distance L between them to reduce flow losses. Values of $L/H < 2$ are considered very favorable, although most existing plants average L/H between 4 and 6 with some nearly as high as 10. Good topographies are obviously not available everywhere.

Although high heads are desirable, some topographies do not allow them, and thus pumped-hydro systems are often classified as *above-ground*, which includes the preferred *high head* and *medium head*, and *underground*.

Above-Ground Pumped Hydro

In *high-head* installations, the upper reservoir may have originally been a stream descending a steep slope which has been dammed to form the reservoir. From that reservoir, water is diverted into a horizontal pressure tunnel driven through the rock to the valve house from which the main steel pipeline slopes down to the powerhouse. At the head of the steel pipeline there usually is a surge tank and a valve house. It contains the main sluice valves, which are automatic isolating valves that come into operation in the case of pipeline burst. Automatic air valves, also, may be used. These contain buoyancy floats that fall when sufficient air separates from the water. These floats are attached to a spindle which then opens the valve to vent the air to the atmosphere. Other automatic air valves allow air to enter the pipeline in case the pipeline is drained. They safeguard the pipeline against internal collapse when thus emptied. A surge tank or surge chamber is built near the mouth of the pressure tunnel to relieve the pipes of undue inertia pressure set up in the tunnel when the flow is checked following a reduction of load. Should this pressure exceed a predetermined amount, water merely spills over the lip of the surge tank. The surge tank also provides a reservoir of water that can be drawn upon when the load on the turbine suddenly increases. At every point of deviation of the pipelines, either in the horizontal or the vertical plane, anchorages are constructed with expansion joints provided immediately below. The powerhouse itself is located as close as possible to the lower reservoir into which the tail race discharges.

In *medium-head* installations, a nearly horizontal open canal or conduit may be carried along the side of the valley as far as the powerhouse site. A relatively short pressure pipe, often called a *penstock*, leads to the turbine.

A typical pumped-hydro system of a conventional design is shown in Fig. 16-6.

Underground Pumped Hydro

To overcome the requirement of a suitable topography, *underground pumped hydro* is being considered in this system. The upper reservoir may be at or near ground level. The lower reservoir is placed underground in natural caverns, old mines, or other underground cavities. Such a system is shown in Fig. 16-7.

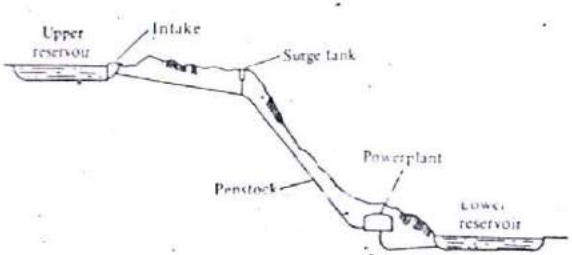


Figure 16-6 Schematic of a conventional above-ground pumped-hydro storage system.

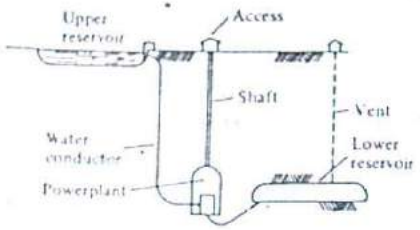


Figure 16-7 Schematic of an underground pumped-hydro storage system.

In all systems, a principal piece of equipment is a reversible pump-turbine or motor-generator set or sets. The excess electric energy supplied by the primary power station during off-peak hours is used to drive it in the motor-pump mode to pump water from the lower to the upper reservoir. During periods of peak demand, the system reverses to the turbine-generator mode to generate the excess electricity needed. (Some old installations use separate conventional pumps and turbines rather than reversible machines.)

The losses in pumped-hydro systems include motor and pump losses and flow losses during upflow; seepage into ground, leakage from pipes and equipment, and evaporation during storage; and turbine and generator losses and flow losses during downflow. The combined efficiency of a pumped-hydro system, called the *turnaround efficiency*, is defined as the total energy output divided by the total energy input during a charge-discharge cycle. In most plants, the turnaround efficiency is in the neighborhood of 65 percent. Pumped-hydro systems are rated according to their power output, usually in megawatts (MW). The maximum power output in the turbine-generator mode is usually greater than the maximum power input in the motor-pump mode, but operation in the latter lasts longer than the former, so the input energy is greater. (Recall that energy = power × time.)

16-4 COMPRESSED-AIR STORAGE

Compressed-air energy storage is analogous to pumped-hydro energy storage. Whereas in the latter excess energy generated by a base-loaded plant during periods of low demand is used to increase the potential energy or hydrostatic pressure of water, compressed-air energy storage compresses and stores air in reservoirs, aquifers, or caverns. The stored energy is then released during periods of peak demand by expansion of the air through an air turbine. In general, the turnaround efficiency of compressed-air storage is comparable to that of pumped-hydro storage.

Reservoirs

The underground compressed-air reservoirs are subjected to repeated fluctuations in pressure, humidity, and temperature. The long-range effects of such fluctuations remain to be determined. Usually multiple reservoirs, operating in parallel, serve one storage

system. Three types of reservoirs show the most promise [155]: (1) salt caverns, (2) aquifiers, and (3) hard-rock caverns.

Salt caverns These have been used in the past to store petroleum products. Research so far indicates that they are stable under compressed-air storage loadings for the duration-of plant life. The major concerns are cavern geometry, size and spacings, long-term creep and creep-rupture of rock salt, and air leakage.

Aquifers These are naturally occurring porous-rock formations. They have been used for natural gas storage for over 50 years but with annual rather than daily cycling. The effects of the different physical properties of air and its oxygen and the high temperatures of storing remains to be evaluated. Among other concerns are cyclic fatigue of the porous rock, air-water interface movement (water is usually present in aquifers), and the generation and transport of fine particulate matter.

Hard-rock caverns Because of their size these require water-compensating surface reservoirs to maintain air pressure and therefore are more costly than the two reservoir types above. However, they are believed to be most stable in the absence of severe temperature fluctuations (50°C). The major concerns here include the effervescence of air in the water shaft (called the champagne effect), hard-rock properties under cyclic conditions, and the residual strength of hard rock after an initial failure.

Adiabatic and Hybrid Systems

When air is compressed for storage, its temperature will rise (since it is a compressible gas) according to the relationship

$$T_2 = T_1 \left(\frac{P_2}{P_1}\right)^{(n-1)/n} \tag{16-6}$$

where T and P are the absolute temperature and pressure and the subscripts 1 and 2 refer to before and after compression, respectively. n is the polytropic exponent for the nonreversible compression process.

The heat of compression may be retained in the compressed air or in another heat-storage medium and then restored to the air before expanding through the turbine. This is called *adiabatic storage* and results in high storage efficiency. Recall that at a given pressure ratio, turbine work is directly proportional to the inlet absolute temperature (Chap. 8). Recall also that constant-pressure lines on a temperature-entropy diagram for gases diverge at high temperatures so that isentropic work, equal to the vertical distance between any two constant-pressure lines, increases with temperature. Restoring the heat to the air also prevents the turbine parts from freezing if low-temperature air is allowed to expand through it. If the heat of compression is allowed to dissipate, additional heat could be added by fuel combustion to retain the high storage efficiency, but the results would be extra expense and maintenance problems. This is called a *hybrid system*.

Figure 16-8 shows a simple adiabatic compressed-air energy-storage system. The

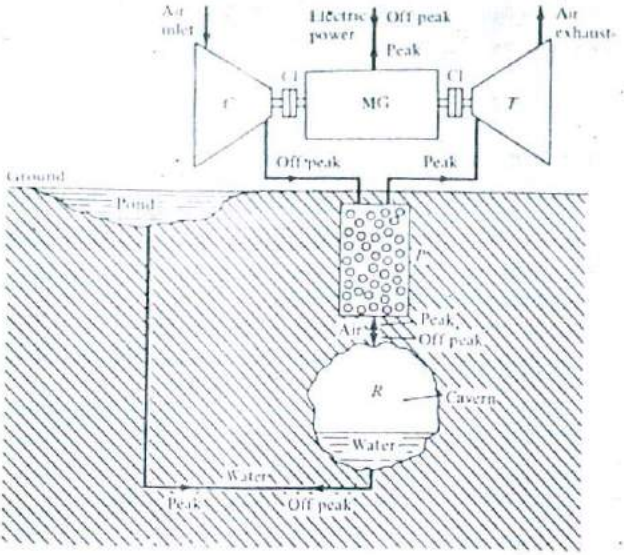


Figure 16-8 Schematic of a simple single-stage adiabatic compressed-air energy storage system with pressure-compensation pond. C = compressor, T = turbine, MG = motor-generator set, P = packed-bed thermal-energy storage, R = air-storage reservoir.

main plant is not shown. During off-peak hours, electric energy from the main plant generator is used by the motor-generator set (MG) operating in the motor mode to drive the compressor (C). The compressed air passes first through a packed bed (P) for sensible thermal-energy storage (Sec. 16-7), then to a constant-pressure underground reservoir (R). The constant pressure is obtained by displacing water to a pressure-compensation pond that has a nearly constant head above the reservoir. During peak hours, air from the reservoir flows through the packed bed picking back sensible heat, then through the air turbine that now drives the motor-generator set in the generator mode. Clutches (Cl) separate the compressor during peak (generation) periods and the turbine during off-peak (storage) periods.

As expected, the air-reservoir (cavern) volume is a strong function of the storage pressure. For a peak unit capacity of 1500 MWh that volume is estimated at nearly 2,000,000 m^3 for 10 bar, or 64,000 m^3 for 100 bar storage pressures. The packed bed thermal-energy storage volume is about a tenth of that of the storage reservoir in most cases. Thus to reduce storage volume and hence cost, operation at high pressure is necessary.

Example 16-1 Calculate the airflow, compressed-air temperature, and storage volume for a 1500-MWh peaking unit charging for 7.5 h. Assume compressor inlet is at 1 bar and 20°C, compressor exit at 100 bar, a compressor polytropic

efficiency of 70 percent, a peaking turbine efficiency of 60 percent, and a constant specific heat for air $c_p = 1.05$ kJ/(kg · °C). The air-gas constant $R = 284.75$ kJ/(kg · K).

SOLUTION For a compressor polytropic efficiency of 70 percent and constant specific heat

$$0.7 = \frac{h_{2s} - h_1}{h_2 - h_1} = \frac{T_{2s} - T_1}{T_2 - T_1}$$

where the subscripts 1, 2, and 2s are for compressor inlet, exit, and isentropic exit conditions, respectively.

$$T_{2s} = T_1\left(\frac{P_2}{P_1}\right)^{(k-1)/k} = (20 + 273)\left(\frac{100}{1}\right)^{(1.4-1)/1.4} = 1092 \text{ K} = 819°\text{C}$$

$$T_2 = \frac{819 - 20}{0.7} + 20 = 1162°\text{C}$$

(This corresponds to a polytropic exponent $n = 1.5266$.)

For a turbine output of 1500 MWh

$$\text{Storage capacity} = \frac{1500}{0.60} = 2500 \text{ MWh}$$

$$\text{Mass of air required} = \frac{2500 \times 3.6 \times 10^6}{1.05(1162 - 20)} = 7.5 \times 10^6 \text{ kg}$$

Assuming air is stored in the cavern at 100 bar (10^7 Pa) and 20°C

$$\text{Total volume needed} = \frac{7.5 \times 10^6 \times 284.75(20 + 273)}{10^7} = 62{,}575 \text{ m}^3$$

Average air flow to cavern during 7.5 h of charging = 8343 m³/h

It can be seen that a system such as that described above requires a very large compressor with an inlet airflow at 1 bar of about 834,000 m³/h (~490,000 ft³/m), capable of an exit pressure of about 100 bar (1450 psia), and an exit temperature of more than 1100°C (~2000°F). Such compressors or combination of compressors need to be developed before a large utility compressed-air energy-storage system can be a reality.

A method of reducing the above temperature is the so-called two-stage compressed-air energy-storage system. It employs two compressor-motor-generator-turbine sets.

The Huntorf Compressed-Air Storage System

The first compressed-air storage system to be built is a 290-MW plant designed by Brown Boveri and built at Huntorf, West Germany [156]. It provides storage for the Nordwestdeutsche Kraftwerke (NWK) utility of Hamburg. The plant (Fig. 16-9) has

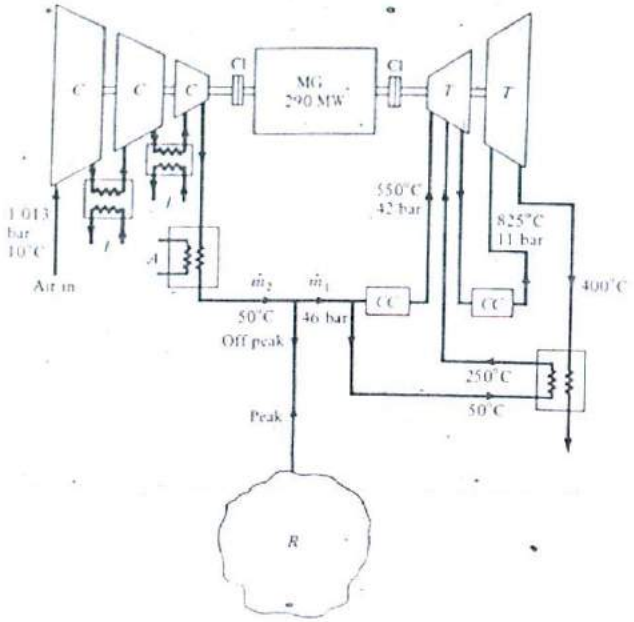


Figure 16-9 The Huntorf hybrid air-storage gas-turbine powerplant. I = intercooler, A = aftercooler, CC = combustion chamber, mass-flow rates: $\dot{m}_2 = 0.9$ to $0.25\dot{m}_1$ [155].

been in operation since 1978. It uses two 150-m-high salt caverns with a total volume of 300,000 m^3 created by leaching a salt dome at a depth between 650 and 800 m below ground. The system is composed of a motor-generator set connected by clutches to a three-stage compressor with intercoolers and a two-stage gas turbine with reheat. It is of the hybrid variety that requires heat addition prior to the gas turbine.

In the storing mode, the compressor pumps atmospheric air into the caverns, where it is stored at 50 to 70 bar (725 to 1015 psia). In the generation mode, the stored air, reduced in pressure to 46 bar (667 psia), enters a natural gas–fueled combustion chamber before the high-pressure section of the gas turbine. Reheat is accomplished by a low-pressure natural-gas burner. Storage occurs daily for about 8 h, generation for about 2 h. The compressor and turbine are each sized independently to suit the power requirements during these periods, an advantage over the usual gas-turbine cycle in which the compressor absorbs more than two-thirds of the turbine output.

Huntorf has shown good availability exceeding 98 percent at times and good reliability. The caverns have shown no detectable creep or stability problems.

In the United States, a 220-MW compressed-air energy-storage system is in the planning stages by Soyland Power Cooperative of Decatur, Illinois. It will have hard-

rock reservoirs, with water-compensating surface reservoirs. Siting studies have been conducted by Batelle Pacific Northwest Laboratories. Brown Boveri has been awarded the contract for the electrical and mechanical equipment. Soyland hopes to have the plant in operation by 1985, and they estimate a savings due to energy storage of $34 million (in 1981 dollars) over the first 16 years of operation.

16-5 ENERGY STORAGE BY FLYWHEELS

Flywheels store off-peak energy as kinetic energy. They have been used extensively to smooth out power pulses from reciprocating engines. They are physically connected to the engine crankshafts and are larger the smaller the number of cylinders per engine. (They, for example, were very large for old single-cylinder steam engines.) They operate by storing some of the energy given by the cylinders and releasing it during periods of no power pulses so that the speed and power delivery of the crankshaft are steady and continuous. More recently interest in flywheel energy storage has been generated by motor vehicle designers. In the so-called hybrid automobile, for example, the flywheel stores some of the energy of the gasoline engine during periods of low vehicle demands and releases it during periods of high demands, such as during acceleration, hill climbing, etc., and thus operates the engine at a more steady and hence more efficient output.*

The use of flywheel energy storage by utilities was tried only a few years ago. In this the flywheel rotor is physically connected to a motor-generator set. In the charging mode, during off-peak periods, the motor adds energy to the flywheel. In the generation mode, during periods of peak demand, the flywheel rotor coasts driving the generator.

The fluctuations in speed caused by torque variations are reduced to a minimum by the use of flywheels. As kinetic energy is proportional to the mass times velocity squared, the changes in velocity from the addition or subtraction of kinetic energy are reduced by the use of a large mass. Conversely the energy stored in a flywheel can be increased by increasing the velocity. The velocity of a flywheel is defined as $2\pi Rn$. The energy stored in a flywheel is equal to the kinetic energy, given by

$$E = \frac{1}{2g_c} m(2\pi Rn)^2 = \frac{2\pi^2}{g_c} mR^2n^2 \tag{16-7}$$

where E = energy, ft · lb_f or J

m = mass of flywheel, lb_m or kg

g_c = conversion factor = 32.2 lb_m · ft/(lb_f · s^2) = 1.0 kg/(N · s^2)

* Other uses for flywheels include: a bus electrogyro, which is recharged at bus stops, regenerative braking of subway cars that provides acceleration upon start; electrically powered earth movers to limit peak-power demands; elevator drives including regenerative breaking; and plasma physics experiments to provide very high power peaks.

R = radius of gyration,* ft or m

n = revolutions per second = (r/min)/60

The energy E absorbed (or released) by a flywheel between speeds of rotation n_1 and n_2 is thus given by

$$\Delta E = \frac{2\pi^2}{g_c} mR^2(n_2^2 - n_1^2) \tag{16-8}$$

The ratio of the variation in rotational speed to the mean speed n is called the *coefficient of speed fluctuation* k_s, given by

$$k_s = \frac{n_2 - n_1}{n} = \frac{2(n_2 - n_1)}{n_1 + n_2} \tag{16-9}$$

where

$$n = \frac{n_1 + n_2}{2} \tag{16-10}$$

Combining Eqs. (16-8) through (16-10) results in

$$\Delta E = \frac{4\pi^2}{g_c} k_s mR^2 n^2 \tag{16-11}$$

The value of the coefficient k_s depends upon the desired closeness of speed regulation. For engines, it may vary from 0.005 for fine to .2 for coarse regulation. Thus for a given energy absorption ΔE, m and/or R^2 must be high for close speed regulation.

Another important consideration in flywheel design is the stress level a flywheel rotating at very high speed is subjected to. The *theoretical maximum specific energy* (energy stored per unit mass) is dependent upon the stress-to-density ratio and is given by [157].

$$\left(\frac{E}{m}\right)_{\max} = 3.77 \times 10^{-7} k_m \frac{\sigma}{\rho} \tag{16-12}$$

where

E/m = specific energy, kWh/ lb_m

k_m = *mass-efficiency factor*, dimensionless

σ = allowable stress, lb_f/ft^2

ρ = density, lb_m/ft^3

*The radius at which the total mass is considered to be concentrated. For a disc of uniform density ρ, uniform thickness t, and outer radius R_o, with r as a variable radius between 0 and R_o:

$$\int_0^{R_o} \frac{1}{2g_c}(2\pi r\, dr\, t\rho)(2\pi rn)^2 = \frac{1}{g_c}(\pi R_o^2 t\rho)(2\pi R_o n)^2$$

from which $R = R_o/\sqrt{2} = 0.707R_o$. Another use of the radius of gyration is in calculating the moment of inertia $I = R^2m$.

k_m expresses how well a particular flywheel design utilizes the material strength, being a maximum if the stress is uniform throughout the flywheel. The maximum values of k_m are 1.0 in optimum designs with isotropic materials, where radial and tangential stresses are uniform and equal, and 0.5 in optimum designs with materials where only one stress direction can be utilized, such as fiber-reinforced composites. These two maximum values are obtained only in very slender designs where the energy absorbed per unit volume is minimal. In realistic designs k_m and the specific energy are reduced in order to reduce space, mass, and the cost of the safety shield and gas or vacuum chamber (below). The *volumetric specific energy*, energy per unit volume, is given by

$$\left(\frac{E}{V}\right)_{max} = 3.77 \times 10^{-7} k_v \sigma \qquad (16\text{-}13)$$

where E/V = volumetric specific energy, kWh/ft^3

k_v = *volume-efficiency ratio*, dimensionless

k_v expresses how well a particular flywheel design utilizes the material strength and fills the cylindrical volume around the flywheel. For a uniform-density material, k_v equals k_m times the fraction of that cylindrical volume occupied by the flywheel.

The principal parameters that determine the suitability of flywheels for energy storage are the two efficiency ratios k_m and k_v as well as the stress and density. The values of k_m and k_v depend upon the type of material (isotropic, uniaxial composite, variable density) as well as flywheel shape (disc, drum, rod). Figure 16-10 shows the relationship between k_m and k_v for high-performance flywheel designs.

The *strength-density ratio* σ/ρ is high for such materials as glass or silica fibers. However, inevitable manufacturing flaws, which also tend to grow because of stress corrosion, cause these high values to be realized only for short periods or at cryogenic temperatures. Cyclic operation expected in energy storage and release also causes fatigue and growth of small flaws and cracks and is expected to be strength-limiting for most materials.

Vibrational frequencies, coupled with high-cycle fatigue, are also expected to be strength-limiting, especially for slender designs such as thin discs or hoops. Thus the suitability of a design for energy storage depends on the design, on the material, and on the extent of manufacturing flaws and the methods for detecting and reinspecting them—in other words, the stringency of the quality control standards.

Materials for energy-storage flywheels must have high strengths, high strength-density ratio, high resistances to cyclic-crack growth, and high strength density-to-cost ratios. Those under consideration include some alloys, such as the so-called maraging steels, and more promising, composites such as fiber-reinforced plastics. One composite that shows particular promise is a 62 volume percent S-glass in epoxy composite. It has a density of 122.7 lb$_m$/ft^3, an estimated working stress of 21×10^6 lb$_f$/ft^2 for 10^4 cycles (16×10^6 for 10^5 cycles), a stress-density ratio of 170,000 (lb$_f$/ft^2)/(lb$_m$/ft^3) for 10^4 cycles (130,000 for 10^5 cycles), and a cost based on volume production of \$0.80/lb$_m$. Other attractive composites are graphite-epoxy and kelvar-epoxy [157]. By contrast maraging steel has a density of 500 lb$_f$/ft^3, a working stress

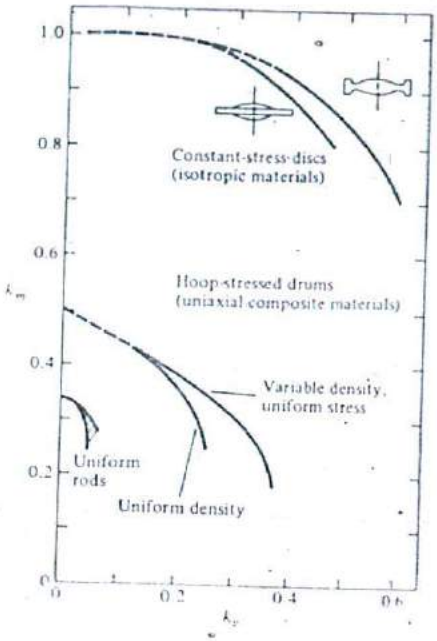


Figure 16-10 Relationship between the mass- and volume-efficiency ratios for high-performance flywheel designs [157].

of $14.5 \times 10^6 lb_f/ft.^2$ and a stress-density ratio of 29,000, all for 10^4 cycles, and a cost of $53/$lb_m$.

Flywheels for energy storage are systems that include, besides the flywheel itself, a number of subsystems. These are a housing; bearings, with ball bearings believed the most suitable; a vacuum pump to minimize windage losses inside the housing; seals to minimize oil and air leakage into the vacuum chamber; and sometimes a containment ring to protect nearby personnel and equipment from flying fragments in case of flywheel rotor fracture.

Losses in a flywheel energy-storage system include windage, bearing and seal friction, vacuum pump input power, and eddy current (hysteresis) and other inefficiencies in the motor generator (or in transmission systems). In early designs these losses were prohibitively large, and much developmental work still needs to be done to arrive at a technically attractive system.

A NASA conceptual design for a flywheel electric-energy storage system that has nearly zero losses is shown in Fig. 16-11. It is designed for a 10,000-kWh substation. The flywheel rotor, made of a filamentary anisotropic composite material to achieve high strength to mass ratio, has inner and outer diameters and height of 14, 20, and 10 ft (4.27, 6.1, and 3.05 m), respectively. It weighs 735,000 lb_m (333.4 metric tons) and rotates at 1250 r/min. To eliminate rotor-bearing friction, the rotor is magnetically levitated by permanent magnets that are incorporated in the stator with sets of teeth

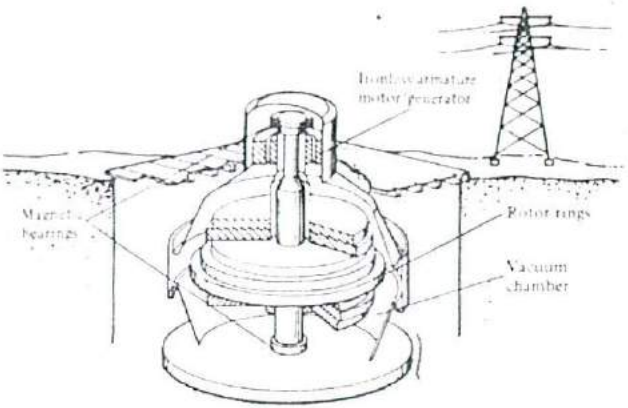


Figure 16-11 A NASA conceptual design of a 10-MWh-capacity flywheel energy storage system.

on both rims facing each other to maintain axial alignment. Alignment in the radial direction is provided by a set of electromagnets in shunt with the permanent magnets. Optical sensors situated along the air gap monitor any radial eccentricity and supply an error signal to the electromagnets to correct the eccentricity.

To eliminate losses from hysteresis and eddy currents, normally present in iron armatures, an ironless motor-generator armature is provided. A contactless electronic commutator is used to control current flow in the motor-generator coils. A permanent magnet in the stator produces a magnetic flux in the gap between rotor and stator. In the motor mode, alternating current is applied to the armature via the electronic commutation that interacts with the flux to produce the necessary force on the rotor. In the generator mode, commutation diodes are connected to the proper phases of the armature coil.

Windage losses are virtually eliminated by operating the flywheel in a sealed evacuated enclosure (vacuum chamber) pumped down to 10^{-3}- to 10^{-5}-torr (1.33×10^{-6} to 1.33×10^{-8} bar) pressure. A safety rotor ring is provided. In addition, the entire system is to be located below ground.

16-6 ELECTRICAL BATTERY STORAGE

The familiar *lead-acid battery* used in motor vehicles is a direct-current battery. It contains a number of voltaic cells (six in a 12-V battery, for example) that are connected in series. Each cell contains several lead plates, connected in parallel, made of grids that are filled with a spongy gray lead, Pb, and which form the anode. Alternating with these are plates of similar design but containing lead oxide, PbO_2, which form

the cathode. All plates are immersed in a water solution of sulfuric acid H_2SO_4, which acts as an electrolyte. The electrolyte of each cell is housed separately in its compartment.

In the discharge mode, direct current is generated. The lead in the anode oxidizes to Pb^{2+} ions that immediately precipitate on the plates as lead sulfate $PbSO_4$. The lead oxide in the cathode reduces to Pb^{2+} that also precipitates as $PbSO_4$. The electrochemical reactions are

Anode: $$Pb(s) + SO_4^{2-}(aq) \rightarrow PbSO_4(s) + 2e^- \qquad (16\text{-}14a)$$

Cathode: $$PbO_2(s) + 4H^+(aq) + SO_4^{2-}(aq) + 2e^- \rightarrow PbSO_4(s) + 2H_2O(aq) \qquad (16\text{-}14b)$$

where (s) and (aq) indicate solid and liquid (aqueous) conditions, respectively.

Thus during discharge all plates are slowly covered by $PbSO_4$, which replaces the lead in the anode and the lead oxide in the cathode, and the concentration of sulfuric acid in the solution slowly decreases. For each molecule of Pb, two molecules of H_2SO_4 ($4H^+$ and $2SO_4^{2-}$) are replaced by two molecules of water ($2H_2O$). This is why the extent of charge of a lead-acid storage battery can be checked by measuring the density of the electrolyte; low density indicates low sulfuric acid concentration and a partially discharged cell.

In the charge mode, the battery can be restored to its original condition by reversing the direction of the current (and electron flow). The reactions represented by Eqs. (16-14) are simply reversed. The charging current must be obtained from a direct-current generator (as in older vehicles) or by an alternator equipped with a rectifier (as in modern vehicles).

The lead-acid battery, then, can be charged and discharged over many cycles and has been widely used to satisfy motor vehicle starter, instruments, lights, and other accessory requirements. Their use as the prime movers of all-electrical vehicles, where they would power drive motors and get charged while idle, as during the night, has run into several main drawbacks. These are unacceptable energy-mass and energy-cost ratios and low cycle life, in which they are almost fully discharged and recharged. These same drawbacks have prevented their use as energy-storage systems for large utility purposes.

The lead-acid battery is therefore limited to the small specialized uses it now enjoys for which the relatively low energy-mass ratio and the high cost of chemicals are not crucial factors.

Research and development has been going on for a number of years to develop advanced storage-battery systems that would have greater energy-mass ratios, lower costs, and greater cycle life. One of these is the *nickel-cadmium battery*, which uses a nickel hydroxide cathode, a cadmium anode, and a potassium-hydroxide-solution electrolyte. This battery is characterized by low mass and is primarily used in portable equipment such as radios and cordless appliances. Another is the *silver-zinc battery* which uses a solution of potassium hydroxide, saturated with zinc hydroxide, as an electrolyte. It has a high energy-mass ratio but also a high cost. It is primarily used

in applications in which low mass is more important than cost. It also suffers from low cycle life, with only 30 to 300 charge-discharge cycles reported for some designs.

Battery systems that are potentially more suitable for utility applications, however, use soluble or liquid reactants and operate at temperatures other than atmospheric. The ones with the most promise at present are:

1. *Sodium-sulfur batteries*. These use molten sodium as one electrode, a sulfur and sodium sulfite mixture as the other, and a solid aluminum oxide electrolyte. They have a high energy-mass ratio and operate at temperatures of about 250°C (480°F). This relatively low temperature allows the use of Teflon seals and aluminum or glass containers. These batteries have a long cycle life because of the lack of solid-solid transformations. The low mass makes the sodium-sulfur battery a contender for the battery of the electrical car of the future.
2. *Lithium-chlorine* and *lithium-telluride batteries*. These are less developed than sodium-sulfur batteries but have similar favorable characteristics.
3. *Zinc-chlorine batteries*. Here a zinc chloride solution is pumped through graphite cells on which the zinc is deposited and the chloride is liberated in gaseous form that is drawn away, cooled in a heat exchanger, and stored in a separate tank. Chlorine, being toxic, is stored as a relatively harmless icy slush. In the generating mode, the chilled chlorine is pumped as a solution back to the cells where it reacts with the zinc to produce electricity. The Gulf and Western Company had originally developed this battery for the purpose of utility-type energy storage but has initially adapted it to a motor vehicle. (In one test, it ran a car for 175 mi at 42 mi/h). This battery has the advantage of constant electric output that does not drop off during discharge as is the case with most other batteries, for as long as there is chlorine in the storage tank, the battery system develops essentially constant power. The system is of course more complex than can be tolerated for personal automobiles because of the need for a complex charger, pumping, and heat-exchanger equipment.

The turnaround (charge-discharge) efficiencies of most batteries are good, about 70 to 80 percent, compared with some 60 percent for pumped hydro. However, it is clear that at this time high-energy, low-mass, long-cycle-life batteries of a type that would meet large utility peak-load demands are still not commercial realities.

16-7 SUPERCONDUCTING MAGNETIC ENERGY STORAGE

In 1911, the dependence of the electrical resistance of metals on temperature was observed by the Dutch physicist Kamerlingh Onnes. In his investigations, he also discovered that the electrical resistance of mercury dropped suddenly to zero when it was cooled to within a few degrees of absolute zero, a phenomenon which Onnes called *superconductivity*.

Other metals exhibit the same phenomenon. The temperature below which they

become superconductive is called the *transition* or the *critical temperature*. All superconducting metals have transition temperatures in the *cryogenic** *range*. The phenomenon arbitrarily has found many applications, and cryogenic engineering has become a specialized science as well as an industry all its own. Besides superconductivity, cryogenic applications can be found in medicine (cryogenic surgery, cryogenic ophthalmology, etc.), food preservation, pollution control, and other areas.

In 1970, the main application was the construction of superconducting electromagnets. These were experimentally used for magnetohydrodynamic power generation; bubble chambers to cool electrical generators, motors and transformers; and electric-power transmission and distribution. The latter application promises no-loss transmission. In the 1970s it was determined that it can best be accomplished by the use of high-purity aluminum cables operating at liquid hydrogen temperatures 20 K (−253°C, −423°F). Commerical success depends upon whether the metal, the gas, and the refrigeration systems can be acquired and operated economically.

Superconducting magnetic energy storage is a concept that initially received attention for pulsed energy storage in which the charge and discharge times have been short. It subsequently became apparent that such a concept is suitable for large-scale energy storage by an electric utility [159]. The concept is based on the principle that energy can be stored in the magnetic field associated with a coil. If the coil is made of a material in a superconducting state, i.e., maintained at a temperature below its critical temperature, then once it is charged, the current will not decay and the magnetic energy can be stored indefinitely. The stored energy can be released back to the network by discharging the coil.

The energy E stored in a coil in which a current I circulates is given by

$$E = \frac{1}{2} LI^2 \tag{16-15}$$

where E = energy, J (joule = watt × second)

L = inductance, H [henry = (volt × second)/ampere]

I = current, A (ampere)

* The term is derived from the Greek *kryo*, which means "icy cold or frost." Cryogenics is said to have been born in 1877 with the liquefaction of small quantities of oxygen at 90 K (−183°C, −298°F). In 1908, helium was first liquified at 4.2 K, though a commercial method for liquifying helium was not developed until 1947. Goddard used liquid oxygen to propel a rocket in 1926. Germany used it on a large scale to propel V-2 rockets during World War II, an application that brought cryogenics to the attention of the world. It is now widely used in the space program. Modern techniques can produce temperatures to within a minute fraction of a degree of absolute zero. The cryogenic range has been arbitrarily defined as extending from absolute zero, or 0 K (−273°C, −460°F), to an upper limit of 123 K (−150°C, −238°F), although most of the research has been done below the boiling point of oxygen, about 90 K. The range is considerably below normal refrigeration temperatures. Besides electrical resistance, other material, physical, and chemical properties such as strength, ductility, and thermal conductivity are also greatly affected when they reach cryogenic temperatures.

The inductance L of a coil is a function of its dimensions, which are characterized, for a coil with conductors of a rectangular cross section (Fig. 16-12) by

$$\xi = \frac{2R}{\sqrt{ab}} \tag{16-16}$$

$$\delta = \frac{a}{b} \tag{16-17}$$

and

$$V = 2\pi Rab = \frac{8\pi R^3}{\xi^2} \tag{16-18}$$

where R = mean radius of coil, m

a and b = width and depth of conductor, m

V = volume of conductor in one coil turn, m^3

and L is given by

$$L = f(\xi, \delta)RN^2 \tag{16-19}$$

where $f(\xi, \delta)$ = form function having the units $(V \cdot s)/(A \cdot m)$

N = number of turns of coil

The energy stored in a coil, Eq. (16-15), can now be written as

$$E = \frac{1}{2} f(\xi, \delta)RN^2I^2 \tag{16-20}$$

Using a current density j given by

$$j = \frac{NI}{ab} \tag{16-21}$$

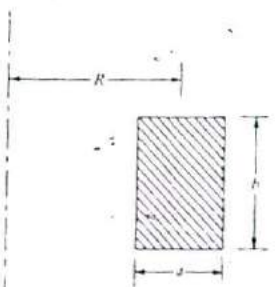


Figure 16-12 Dimensions of a cylindrical coil with rectangular conductors.

gives

$$E = \frac{1}{4}\pi^{-5/3} f(\xi, \delta) \xi^{-2/3} V^{5/3} j^2 \tag{16-22}$$

A coil that gives the maximum value of inductance to volume L/V is called a *Brooks coil* [160]. It has the dimensions

$$a = b \quad \text{and} \quad R = \frac{3}{2} b \tag{16-23}$$

so that for a Brooks coil, $\delta = 1$, $\xi = 3$, and the energy stored in it E_B is given by

$$E_B = 3.028 \times 10^{-8} V^{5/3} j^2 \tag{16-24}$$

For a cylindrical coil, other than Brooks, the energy E is given as a fraction E_B, Eq. (16-24), by a factor F less than 1.0

$$F = \frac{E}{E_B} \tag{16-25}$$

F is a function of ξ and δ of the particular coil and is given in Fig. 16-13.

An important parameter is the volume of material per unit energy stored. This is given by

$$\frac{V}{E} = \frac{V}{FE_B} = \frac{0.33 \times 10^8}{FV^{2/3} j^2} \tag{16-26}$$

where for a Brooks coil $F = 1.0$. Equation (16-26) demonstrates the economy of scale of coils as the cost of the coil is proportional to its volume and thus the cost per

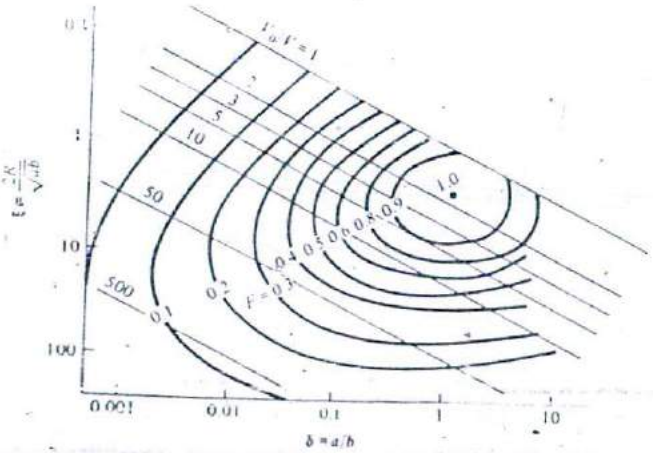


Figure 16-13 Lines of constant factor F relating energy of a cylindrical coil to that of a Brooks coil.

unit energy stored is inversely proportional to its volume to the power 2/3 and to the current density squared. The current density is, however, limited by stability considerations to values between 50×10^6 and 100×10^6 A/m^2.

The main mechanical design problem in magnetic energy storage arises because of the need of a very large structural mass to contain the magnetic field energy. This causes a large radial outward force from the solenoid. The mass is proportional to the material density and the stored energy, and is inversely proportional to the stresses. Such mass, if made of stainless steel, would amount to about 160 kg/kWh and result in unacceptable costs [161]. This consideration led to the selection of bedrock as the structural material with an excavated circular tunnel that would bear the radial outward force and transmit it to the surrounding bedrock.

Figure 16-14 shows an artist's sketch of a section of a proposed 5500-MWh magnetic storage system in which the superconductors are cooled in dewar by superfluid helium (He-II)* at 1 atm pressure and 1.8 K. The total structure is a low-aspect ratio cylinder that has an inner diameter of 1.57 km, a height of 15.7 m, and a thickness of 5 m. The solenoid has 112 turns and carries a 765,000-A current. The conductors are made of aluminum plus NbTi. The struts are made of fiberglass epoxy. The ripples in the conductor and dewar walls are designed to counteract excessive motion on cool down and to reduce magnetic tensile loads. The system has a total radial force of 3.1×10^{10} N, a total axial force of 3.1×10^{11} N, and an average radial pressure of about 4 bar.

The energy transfer between the three-phase ac current from the grid to the dc magnet is accomplished by an ac-dc power converter and inductor using a Graetz thyristor bridge circuitry. The turnaround efficiency (charge-discharge) of this circuitry is said to be greater than 95 percent.

Much of the activity of magnetic energy storage for utility use has taken place in the USA and Japan. A 1-MWh demonstration unit was planned to be built in Japan for the International Science Exposition to be held in Tsukuba Science and Education City in 1985. It would have 12 coils carrying 5000 A, an inductance of 288 H, and major and minor radii of 6.9 and 3.5 m. This plan has now been dropped in favor of a larger 10-MWh unit planned for later construction.

16-8 THERMAL SENSIBLE ENERGY STORAGE

Sensible energy storage is the first of the thermal-energy storage systems to be discussed. In general, thermal-energy storage systems can operate at many desired temperature levels depending upon use and choice of system and material, ranging from refrigeration temperatures to 1250°C. They have found wide use in many industrial applications, such as in the manufacture of cement, iron and steel, glass, aluminum,

* Helium becomes a liquid at 4.2 K and is called helium I. The isotope He^4 (99.99987 percent of all helium) behaves unusually below 2.17 K, the so-called lambda point. It becomes a superfluid, called helium II, that has a thermal conductivity three or four orders of magnitude better than copper at low temperature and surface heat-transfer characteristics about an order of magnitude better than He-I.

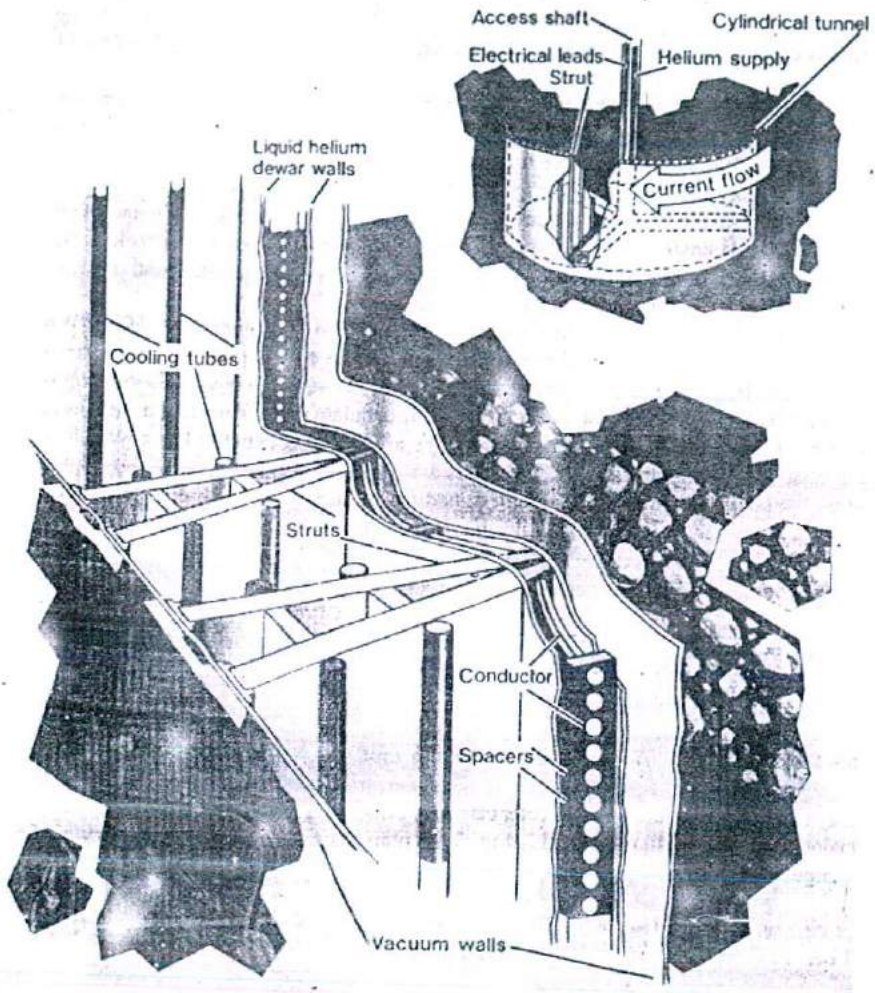


Figure 16-14 Artist's conception of a section of a proposed 5500-MWh magnetic energy storage unit. (*Courtesy of the University of Wisconsin Applied Superconductivity Center.*)

paper, plastics and rubber, and in food processing. Here we will deal with powerplant-related thermal-energy storage, in particular the Rankine-type steam-generator-turbine-condenser cycles.

Sensible energy storage is accomplished by raising the temperature of a material, such as water, an organic liquid, or a solid. The storage density, J/m^3 or Btu/ft^3, is equal to the product of the temperature difference, the specific heat, and the density

of the material chosen. This system is simple in concept but has the disadvantages of variable temperature operation and relatively low storage density. Depending upon the coefficient of thermal expansion of the material, large volume changes may be encountered. Sensible energy storage could employ one of the following devices:

1. Pressurized-water storage
2. Organic liquid storage
3. Packed solid beds
4. Fluidized solid beds

Figure 16-15 shows an example of pressurized-water sensible energy storage [162] system in a powerplant in which the primary heat source is either a nuclear reactor or a fossil-fueled furnace. The base-loaded portion of the plant is capable of supplying more steam than needed during periods of low demand. The excess steam is bled at high pressure via turbine extraction (as in feedwater heating) during these periods of low demand. This extracted steam is fed to steel accumulators and mixed with water, thus producing saturated pressurized water. The accumulators are later discharged

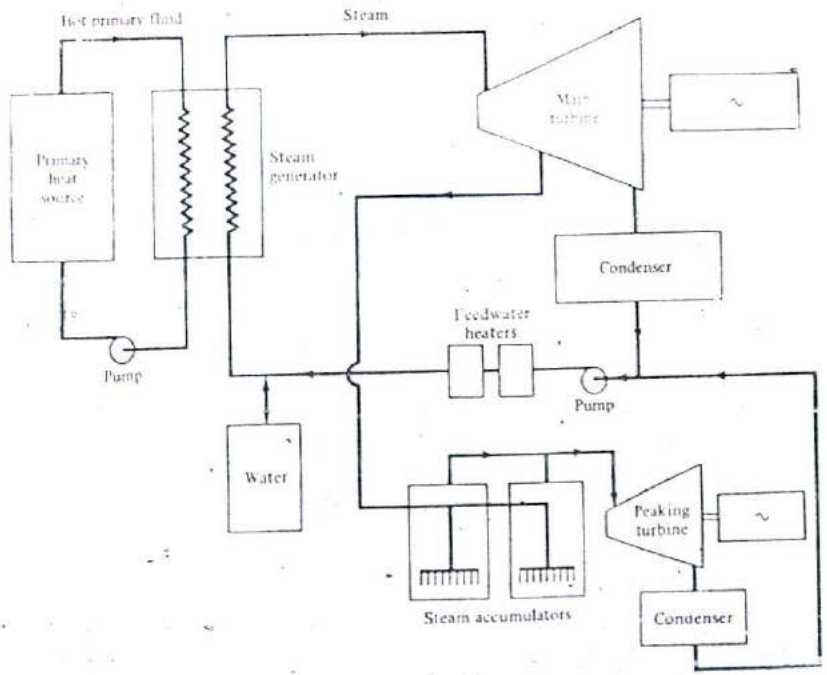


Figure 16-15 Schematic flow diagram of a powerplant with a pressurized-water sensible energy storage system.

through a small peaking turbine during periods of high demand. Discharge continues until a low specified pressure is reached in the accumulators. It has been seen that this results in low and varying steam temperature entering the peaking turbine. Typical values of accumulator high and low pressures are 20 bar, corresponding to a saturation temperature of about 212°C (414°F), and 2 bar, corresponding to a saturation temperature of about 120°C (248°F). Note that while this system involves steam condensing in water during accumulator charge and reevaporating during discharge, the storage medium is the pressurized water in the accumulators and operates over a relatively wide temperature range. Hence it is an example of sensible rather than latent energy storage (Sec. 16-9). The system is sometimes referred to by the misnomer "steam storage."

The storage density of the thermal energy utilized in the peaking turbine per unit volume of the higher-pressure saturated water is given by

$$\text{Storage density} = \frac{1}{v_{f,1}}(h_{f,1} - h_{f,2}) \tag{16-27}$$

where v_f and h_f are the specific volume and enthalpy of saturated water, respectively, and the subscripts 1 and 2 refer to the stored and emptied pressures, respectively. Using the steam tables (SI units), App. A, the storage density for 20 and 2 bars is:

$$\text{Storage density} = \frac{1}{0.0011766}(908.5 - 504.8) = 343{,}107 \text{ kJ/m}^3$$

$$= 95.3 \text{ kWh/m}^3 = 2.7 \text{ kWh/ft}^3$$

Over the range of temperature cited these correspond to about 1kWh/(m³ · °C), 0.016 kWh/(ft³ · °F), and 55.6 Btu/(ft³ · °F). The electric-energy density obtained by the peaking turbine-generator depends upon two efficiencies. The first is *thermal turnaround efficiency* η_{ta}, and the second is the *peaking turbine-generator efficiency* η_p. The former is a complex function of the losses associated with sensible heat transfer to and from the steel walls, structural members of the accumulators, and interconnecting pipework, and the time-dependent convective heat losses to the environment.

The portion representing the ratio of energy stored in the accumulator structure to that stored in the contained water at a given pressure can be shown to be obtained by noting that the thickness t of a cylinder of diameter D is given by $DP/2\sigma$, and hence the ratio for a cylinder height L would be represented by

$$\frac{\pi DLt\rho_s c_s}{(\pi D^2/4)L\rho_f c_f} = 2\left(\frac{P}{\sigma}\right)\frac{\rho_s c_s}{\rho_f c_f} \tag{16-28}$$

where P is the pressure, σ the wall stress, ρ the density, and c the specific heat. The subscripts s and f denote solid and liquid, respectively. The volumetric heat capacities, given by the product ρc, are roughly equal. The ratio P/f is of the order of 0.03 for steel. Thus the contribution of losses by sensible heat transfer to the walls is rather minimal and may be ignored.

The convective heat losses from the water to the environment are therefore the major contributor to the thermal turnaround efficiency. They vary with time and depend

upon the water temperature and the overall heat-transfer coefficient U_s between the water and the outside environment. The time constant τ of the system is given by the product of heat capacity and heat-flow resistance. Thus

$$\tau = \left(\frac{\pi D^2}{4}\rho_f c_f L\right)\left(\frac{1}{\pi DLU}\right)$$

$$= \frac{D\rho_f c_f}{4U} \tag{16-29}$$

If the temperature of the liquid at fully charged conditions is T_1, its time-dependent temperature of $T(\theta)$ decreases with time θ following fully charged conditions at (time zero) due to heat losses alone (no energy withdrawal) (Fig. 16-16). Assuming a lumped capacity system, common in transient heat-transfer calculations where the external heat-flow conductance is low compared with the internal heat-flow conductance (low Biot number), $T(\theta)$ is given by the familiar equation

$$\frac{T(\theta) - T_1}{T_s - T_1} = 1 - e^{-\theta/\tau} \tag{16-30}$$

where T_s is the environmental temperature. Assuming a storage period of θ_t at which the water temperature decreases to T_2,

$$\frac{T_2 - T_1}{T_s - T_1} = 1 - e^{-\theta_t/\tau} \tag{16-31}$$

The thermal turnaround efficiency is given by the energy left in storage at T_2 after heat losses divided by the original energy stored. Thus

$$\eta_{ta} = \frac{h_2 - h_s}{h_1 - h_s} \tag{16-32}$$

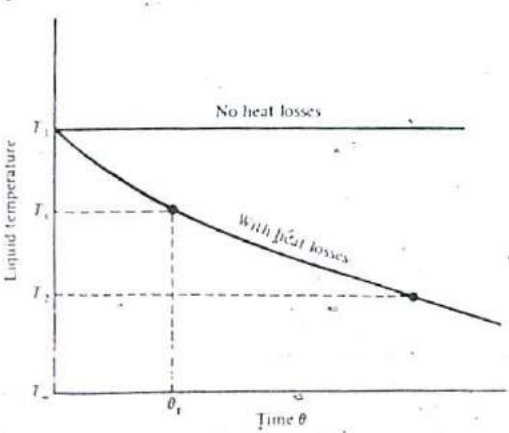


Figure 16-16 Stored liquid temperature-time change in sensible energy storage. T_1 = fully charged; T_2 = end of energy withdrawal; T_s = ambient.

where h_1, h_2, and h_s are the compressed liquid enthalpies at T_1, T_2, and T_s, respectively. Assuming, for simplicity, equal specific heats over the temperature ranges in question

$$\eta_{ta} = \frac{T_s - T_2}{T_1 - T_2} \tag{16-33}$$

Combining Eqs. (16-31) and (16-33)

$$\eta_{ta} = 1 - \frac{T_1 - T_\infty}{T_1 - T_2}(1 - e^{-\theta_s/\tau}) \tag{16-34}$$

It can be seen that this efficiency is a strong function of the ratio θ_s/τ. θ_s is several hours in a daily storage system. The only important variable in τ is U, Eq. (16-29), which depends heavily on accumulator insulations, design, and location. Good insulation and design result in low values of U and therefore high values of τ.

Accumulators may be constructed above ground or underground. Underground accumulators are more costly but have higher insulation and generally higher T_∞ and therefore higher values of η_{ta}. Accumulators in general pose safety problems. A pipe or vessel rupture can release large amounts of energy. The choice of above-ground or underground accumulators, therefore, should be based on the careful evaluation of efficiency, cost, operational problems, and safety. Natural underground caverns may be used if such are available near plant sites or if plants can be located near them, and if they can be properly prepared for high pressure hot water storage. They may result in much lower costs.

The efficiency of the peaking turbogenerator is probably low because of variable inlet conditions and the use of low-temperature saturated steam, small size, insufficiency or absence of feedwater heating, and other factors. An efficiency of 20 to 25 percent is probably reasonable, compared with 33 to 40 percent for the base-load plant.

Example 16-2 A base-loaded 1000-MW powerplant is designed with a sensible thermal-energy storage of the type shown in Fig. 16-15. The thermal energy stored is called upon to produce 4000 MWh daily. The accumulators are 4 m in diameter each and are well insulated so that $U = 5$ kJ/(h · m² · K). The storage time is 15 h. Maximum and minimum storage pressures are 20 and 2 bar. Calculate:

1. The thermal turnaround efficiency.
2. The total accumulator volume.
3. The storage cost in $/kWh if the accumulators cost $300/m³.
4. The minimum released energy if an accumulator vessel or pipe ruptured at 20 bar.

The ambient temperature is 20°C. Take the specific heat of water as 4.35 kJ/(kg · K). Assume a peaking plant efficiency of 25 percent.

SOLUTION Following are the water-saturation conditions from the steam tables (App. A):

At 20 bar: $T_1 = 212.37°C$ $h_{f,1} = 908.5$ kJ/kg $v_{f,1} = 0.0011766$ m³/kg

At 2 bar: $T_2 = 120.23°C$ $h_{f,2} = 504.8$ kJ/kg $v_{f,2} = 0.0010605$ m³/kg

At ambient conditions: $T_a = 20°C$ $h_{f,a} = 293$ kJ/kg

Take an average density of the water as

$$\frac{1}{2}\left(\frac{1}{v_{f,1}} + \frac{1}{v_{f,2}}\right) = 896.43 \text{ m}^3/\text{kg}$$

then

$$\tau = \frac{D\rho_f c_f}{4U} = \frac{4 \times 896.43 \times 4.38}{4 \times 5} = 785.3 \text{ h}$$

1. Therefore

$$\eta_{ta} = 1 - \frac{212.37 - 20}{212.37 - 120.23}(1 - e^{-15/785.3})$$

$$= 1 - 2.0878(1 - 0.981) = 0.96$$

For a peaking plant efficiency of 25 percent, the thermal storage needed is given by

$$\frac{4000}{0.25 \times 0.96} = 16{,}667 \text{ MWh}$$

$$16{,}667 \times 3.6 \times 10^6 = 6 \times 10^{10} \text{ kJ}$$

The mass of water needed to be flashed to steam is given by

$$\frac{6 \times 10^{10}}{h_{f,1} - h_{f,2}} = \frac{6 \times 10^{10}}{908.5 - 504.8} = 1.486 \times 10^8 \text{ kg}$$

2. The water volume at 20 bar is

$$1.486 \times 10^8 \times v_{f,1} = 1.486 \times 10^8 \times 0.0011766$$

$$= 174{,}840 \text{ m}^3$$

The volume of the accumulator will be larger to accommodate a steam blanket on top and the water left at end of discharge.

3. The minimum cost of accumulators would therefore be

$$\$300 \times 174{,}840{,}000 = \$52.5 \times 10^6$$

4. The energy contained that would be released if a rupture occurred is equal to the mass of the flashed water times the difference between the enthalpy of water at 20 bar at ambient conditions (20°C). The minimum corresponds to the above mass and equals

$$1.486 \times 10^8 \times 908.5 - 293 = 9.146 \times 10^{10} \text{ kJ}$$

16-9 LATENT HEAT ENERGY STORAGE

In this system energy is stored in the form of the latent heat caused by phase change, either by melting a solid or vaporizing a liquid. Energy release is accomplished by reversing the process, i.e., solidifying the liquid or condensing the vapor. The storage density here is equal to the product of the latent heat of fusion (or vaporization) times the density of the storage material. It is greater than that in sensible heat storage because the latent heats are much larger than the specific heats of the single phases of the materials. The system has the additional advantage of operating at essentially constant temperature with low volume changes during phase changes. It also has the advantage of a wide choice of materials with different fusion and evaporation temperatures, which allows a choice of operating temperatures and the ability to generate high-temperature steam for the peaking unit. Some sensible heat storage may be added to latent heat storage by further raising the temperature of the resulting molten solid or vapor.

Latent heat energy storage is not, at this writing, considered a simple, operationally reliable solution to the problem of energy storage in electric-generating powerplants. It is, however, included here as a potential solution along with the problems that must be overcome if such a solution is to become a viable one. Although little work has been done on the application of latent heat energy storage to large powerplants, much work has been done on its use for residential and solar heating applications using fused salts that are available for high- and low-temperature operating ranges [163].

Storage materials must possess, in addition to proper transition temperatures and high latent heat, many other necessary physical and chemical properties. Some of these are good thermal conductivity, containability, stability (considering cyclic operation), nontoxicity, and low cost. No material meets all these requirements but some fluoride salts meet some of them. One of the salts considered most suitable for latent heat storage is the 70% NaF–30% FeF_2 eutectic salt, which has a fusion temperature of about 680°C (2256°F) and potentially possesses the highest storage energy density of any thermal-energy storage material, about 1500 MJ/m^3 (~40,000 Btu/ft^3). $ZnCl_2$ is another with a fusion temperature of about 370°C (~700°F) and a potential storage energy density of about 400 MJ/m^3 (~11,000 Btu/ft^3).

Other materials being suggested are silicon, germanium, and sulfides of germanium. These have high heats of fusion, and like water, they expand upon freezing, so that they tend to float upon solidification, which has advantages in heat transfer. Silicon and germanium, however, have fusion temperatures that are too high for powerplant operation and are very reactive. Germanium sulfides have usable fusion temperatures but tend to solidify to a glassy consistency rather than crystallizing, thus posing an undesirable heat-transfer barrier.

In addition to finding a suitable medium, studies have to evaluate the extents of corrosion, erosion, plant start-up and shutdown, etc. Corrosion problems require that the system be free of oxygen and water vapor, which enter the system because of salt volume changes during heat addition and withdrawal, thus posing interesting engineering problems. It can be seen that there are many design and developmental problems

to be overcome before a reliable, economical latent heat energy storage system can be incorporated into an electric-generating powerplant.

A latent heat energy storage conceptual design using the 70% NaF–30% FeF_2 eutectic salt as the storage medium has been proposed by Bundy [164]. The study had the purpose of identifying the technical difficulties and obtaining preliminary cost estimates. It envisaged a high-temperature gas-cooled reactor (HTGR, Sec. 10-12) as the heat source (Fig. 16-17). The helium coolant operates at 48 bar (700 psia), and the various temperatures are indicated on the figure. The storage-system capacity is 7200 MWh, whereas the charge-discharge rates are 600 MW. The peak electric-generating capacity of the plant is 200 MW for 12 h.

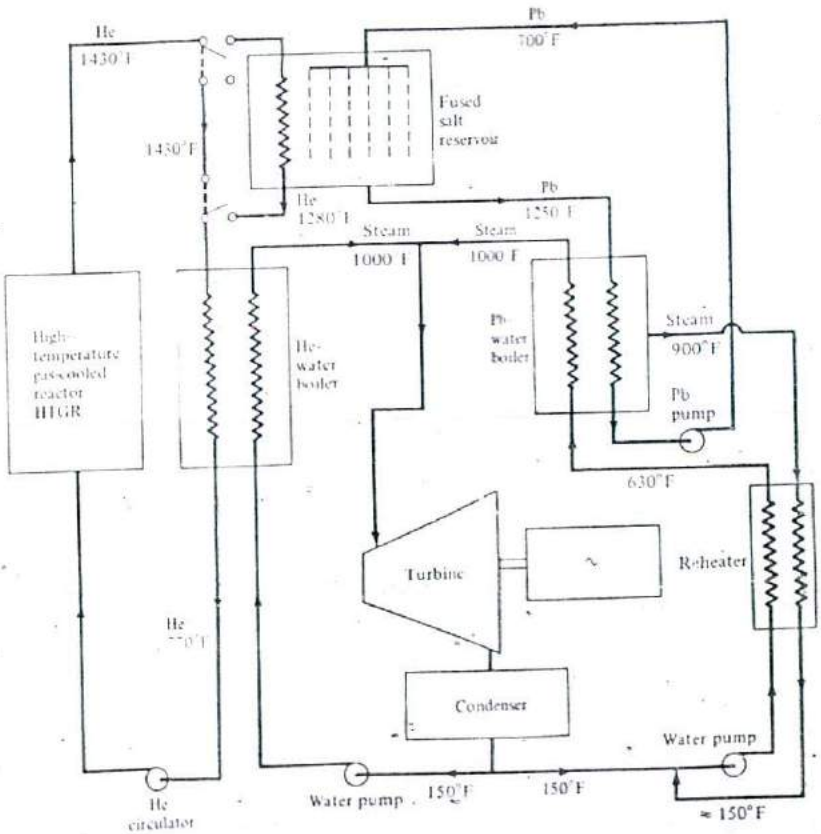


Figure 16-17 A schematic flow diagram of a high-temperature gas-cooled reactor (HTGR) powerplant using a latent heat energy storage system [164].

For the storage capacity of 7200 MWh, 42,000 tons of the eutectic are to be used. In order to give the necessary heat-absorption and heat-release rates, the eutectic is not allowed to freeze completely but instead operates as a slurry. (Recall the undesirability of glassy freezing as with the germanium sulfides.) The total latent heat of fusion is not utilized, and a salt mass of about 80,000 tons is needed. This requires a huge containment vessel about 36 m (120 ft) in diameter and 30 m (100 ft) high.

Another feature of the design is the addition of a secondary heat-transfer loop using molten lead as a heat carrier. Shell-and-tube heat exchangers between helium and the salt slurry, and steam and the salt slurry, have been considered. However, the build-up of solids on the tubes during heat withdrawal would seriously impede the heat-transfer rate and, therefore, the effectiveness of the heat exchanger. This necessitated the addition of the above-mentioned molten-lead loop. During heat withdrawal, therefore, lead is heated from 380°C (700°F) to 675°C (1250°F) in the slurry tank and used in a lead-steam boiler to produce steam for peak-load operation. Lead heating is accomplished by having globules of lead "rain" on top of the slurry, thus sufficiently stirring the reservoir. The globules distort as they fall and thus are expected to "shed" any thin skins of solidified salt. The design lead flow is 2 m^3/s (70 ft^3/s). After passing through the lead-steam boiler, the lead is pumped back to the top of the reservoir against more than 500 psi static pressure via an 800-kW pump.

In addition it is important that the temperature of feedwater entering the lead boiler not be lower than the melting point of lead (325°C, 620°F). This necessitated the addition of a feedwater preheater that uses wet steam from the same boiler. The plant operation, therefore, has the following modes:

1. During base-load operation, helium from the reactor at 775°C (1430°F) is short-circuited directly to the helium-water boiler.
2. During periods of low demand, helium is shunted to the fused salt reservoir, thus storing heat in the slurry at the fusion temperature of 680°C (1260°F) and leaving at 690°C (1280°F) to the helium-water boiler.
3. During periods of peak demand lead is circulated to the reservoir, leaving at 675°C (1250°F) to the lead-water boiler. In all cases steam with the proper flow rate is generated at 540°C (1000°F) and admitted to the same turbine-condenser system. Condensate at 65°C (150°F) is fed back to the helium-water boiler and, during peak demand, also to the lead-water boiler via the preheater.

A good turnaround efficiency for the storage system, more than 90 percent, is expected because the percentage heat losses per cycle are expected to be quite small once the reservoir and other components reach thermal equilibrium.

An economic evaluation, based on 1974 dollars, shows salt costing \$2.15/lb_m in large lots, with the price down to \$0.1 to \$0.5/lb_m if large scale production is attained. This is said to result in a unit energy storage cost of \$3 to \$13/kWh, a unit molten-lead loop cost of \$33/kW, and a unit peak powerplant equipment cost of \$90 to \$110/kW.

16-10 CHEMICAL-REACTION STORAGE

In this mode of energy storage the heat of reaction of reversible chemical reactions is used to store thermal energy during endothermic reactions and to release it during exothermic reactions. Like latent energy storage, this form also offers large energy storage densities and thus has been considered an attractive alternative for some time. (Besides reversible chemical reactions, this category also includes the solution and dissolution of a solid in a liquid and a gas in a solid.) Initial interest focused on low-temperature energy storage for residential heating and cooling. More recent interest contemplates its use to store high-temperature thermal energy suitable for power-generation cycles. In pioneering work by Schulten et al. [165], the following reaction was suggested for long-distance transmission of gas-cooled nuclear-reactor thermal energy

$$CO + 3H_2 \rightleftarrows CH_4 + H_2O \tag{16-35}$$

This and other reversible reactions are listed in Table 16-1 with their operating ranges and heats of reaction.

Chemical-energy storage is now explained with the help of Eq. (16-35). Heat is stored by absorbing it in the endothermic direction of the reaction, from right to left. The enthalpy of formation [167] of $CH_4 + H_2O$ (liquid) at 25°C is given by $(-74.9) + (-286) = 360.9$ kJ (g · mol). The enthalpy of formation of $CO + 3H_2$ at 25°C is $(-110.6) + 0 = -110.6$ kJ (g · mol). Thus, moving from right to left with both reactants and products maintained at 25°C results in a net energy transfer of $(-110.6) - (-360.9) = +250.3$ kJ (g · mol). The positive sign indicates energy added to the reaction, i.e., energy is absorbed and the reaction is endothermic. The reverse reaction, from left to right, results in -250.3 kJ/(g · mol), i.e., energy is

Table 16-1 Reversible chemical reactions under consideration for energy storage*

Reaction	Temperature range, K	Heat of reaction at 298 K	
		Btu/(lb · mol)	kJ/(g · mol)
$CO + 3H_2 \rightleftarrows CH_4 + H_2O$	700–1200	107,640 +	250.3†
$2CO + 2H_2 \rightleftarrows CH_4 + CO_2$	700–1200	106,380	247.4‡
$C_6H_6 + 3H_2 \rightleftarrows C_6H_{12}$	500–750	89,100	207.2
$C_7H_8 + 3H_2 \rightleftarrows C_7H_{14}$	450–700	91,800	213.5
$C_{10}H_8 + 5H_2 \rightleftarrows C_{10}H_{18}$	450–700	135,000	314.0
$C_2H_4 + HCl \rightleftarrows C_2H_5Cl$	420–770	24,120	56.1
$CO + Cl_2 \rightleftarrows COCl_2$		48,420	112.6

* From Ref. [166]

† Higher heating value, including heat of condensation of H_2O.

‡ Heat of reaction per g · mol of CH_4.

released and the reaction is exothermic. The signs have been ignored in Table 16-1. Although the exothermic reaction is common, it will not occur at low temperatures or in the absence of a catalyst or an "igniter," which leads to potentially long storage times. The endothermic reaction is called *reformation** and the exothermic reaction is called *methanation*.†

A schematic of a powerplant with a chemical storage system using the reaction in Eq. (16-35) is shown in Fig. 16-18. During periods of low demand, some heat from the primary heat source is diverted to the reformer (endothermic reactor) to convert the products $CH_4 + H_2O$ to the reactants $CO + 3H_2$, which are stored in a vessel at high pressure, probably 70 bar, but at ambient temperature. During periods of high demand, these reactants are fed to the methanator (exothermic reactor) where heat is generated to run a peak turbine (or generate more steam for the main turbine). In the methanator the reactants are converted to the products $CH_4 + H_2O$, which are stored in a separate vessel for later use in the reformer during periods of low demand.

A thermal turnaround efficiency of this system is estimated (but yet unproven) at 85 to 90 percent [168]. The losses are mainly heat losses to storage vessels and piping and pumping losses of the gases.

The two storage vessels and the two reactors will all have to operate at different pressures. Storage pressures need to be high to minimize vessel size and cost, and the reformer has to operate at low pressures to maximize the rate of the endothermic reaction $CH_4 + H_2O \rightarrow CO + H_2$. There will, therefore, be a large pressure differential between the tube side, which carries the primary heat source fluid (e.g. helium at about 40 bar from a high-temperature gas-cooled reactor), and the gases on the shell side. A similar pressure differential occurs between the steam loop and the gases in the methanator. Such pressure differences require careful design. A complicated scheme to minimize these difficulties envisages the use of compressor-expander sets with a compressor between the reformer and the reactants storage tank and an expander (turbine) between the latter and the methanator. A similar compressor-expander set would be put between the methanator, the products storage vessel, and the reformer, with equal complication. The products expander may supply some of the work required by the reformer compressor because it operates at about the same off-peak time during the cycle. Similarly the reactants expander may supply some of the work required by the methanator compressor during peak hours. Noting the various compressor-expander inefficiencies and the fact that the number of moles of reactants and products are not the same, there will be a net work available during peak operation that may be reabsorbed during off-peak operation. This imbalance in net work of the compressor-expander sets may be remedied by electrical or mechanical storage, and thus we end up with two (or three) forms of energy storage in the same plant.

Some of the problems to be solved before such a storage system can become a

* In general, *reformation* is a process in which low-grade or low-molecular-weight hydrocarbon is catalytically reformed to a higher-grade or higher-molecular-weight hydrocarbon. The term also applies to the endothermic reforming of methane (the process under consideration above) for the production of hydrogen by the reaction of methane and steam in the presence of nickel catalysts.

† *Methanation* is the production of methane from a mixture of carbon monoxide and hydrogen.

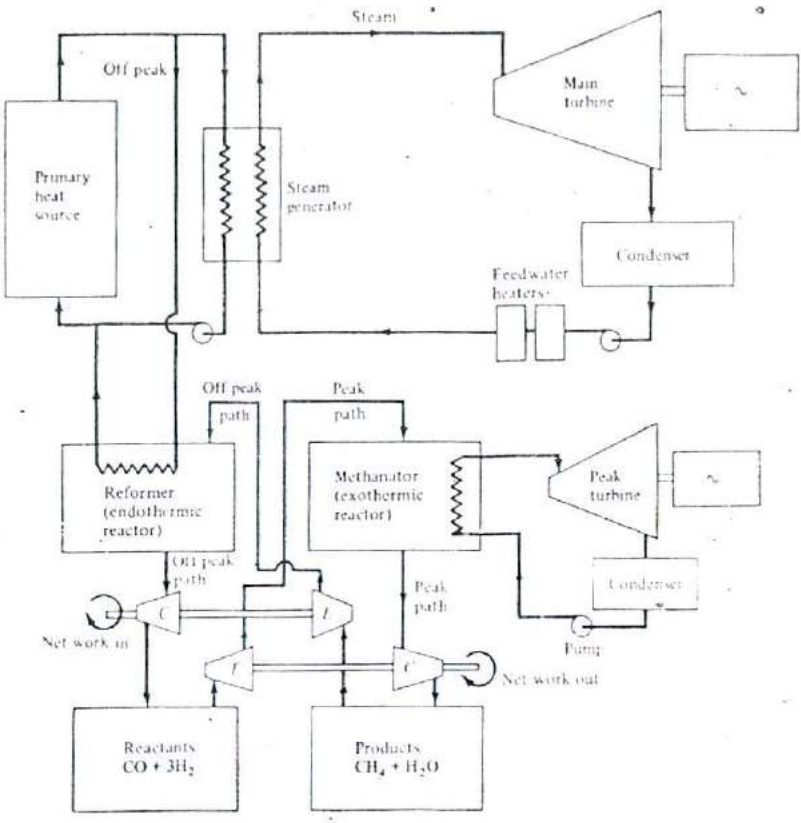


Figure 16-18 Schematic flow diagram of a powerplant with a chemical storage system using the reaction $CO + 3H_2 \rightleftharpoons CH_4 + H_2O$.

serious contender in powerplant use are safety and developmental problems. The major safety problems are those associated with the storage of large volumes of high-pressure flammable and poisonous gases. Developmental problems include the operation of methanators, which in the past were limited to relatively low temperatures to generate steam at high enough temperatures for efficient turbine operation. This entails the availability and use of a suitable catalyst that can operate at high temperatures with a reasonably long lifetime. Other significant problems involve the optimization of the entire cycle to reduce irreversibilities and increase overall efficiency and proper heat-exchanger design in the reformer and methanator. One idea that has been proposed involves the extraction of electrical work from the chemical reaction directly by electrochemical means.

The size of the storage vessels, even with operation near a pressure of 70 bar,

which is compatible with current technology for gas storage, is still very large, of the order of hundreds of thousands of cubic meters. The vessels may either be steel tanks or, to reduce costs, underground caverns if suitable sites are available. Caverns, however, would pose problems of contamination of the gases by impurity gases from underground rocks. Such impurities may cause corrosion in the system and result in poisoning of the catalysts used in the reactors. Careful consideration must also be given to the problem of the diffusion of light gases, such as H_2, through rocks and fissures.

A preliminary, and possibly overoptimistic, economic estimate of the above system, based on cavern storage at \$0.5 to \$2/ft^3, a turnaround efficiency of 85 to 90 percent, and 70 percent conversion of original methane shows storage plant costs of \$35 to \$60/kW and a unit peak powerplant equipment cost of \$90 to \$110/kW, all based on 1975 dollars [168].

PROBLEMS

16-1 A power grid has a hypothetical daily load demand curve that may be represented by half a cosine wave with maximum P_m at time 0 and zero at 24 hours. A 1000-MW powerplant is available for baseload operation with a storage system that has a turnaround efficiency of 0.65. Find the peak load P_m, in megawatts, that can be accommodated by the system and the time at which the system switches from generation to storage.

16-2 A power grid has a load pattern during one 24-h period that averages 600 MW during 18 h and 1200 MW during 6 h. A pumped-hydro energy storage system with an elevation of 100 ft is considered. Calculate (*a*) the power output of a powerplant, in megawatts, that would meet the load demand with and without storage, and (*b*) the volume, in cubic feet, of water that must be pumped to meet storage demand. The electric generator efficiency is 0.8. Water density is 62.4 lb$_m$/ft^3.

16-3 An adiabatic compressed-air storage system is required to generate 230 MW during 5 peak hours, from storage during 10 h of operation of the main powerplant. No compressor intercooling or turbine reheat are used. The compressor and turbine have polytropic exponents of 1.5 and 1.3 and pressure ratios of 100 and 80, respectively; and mechanical efficiencies of 0.92 each. The motor-generator set has a combined mechanical-electrical efficiency of 0.97. Atmospheric air is at 1 bar and 20°C. Air enters the heat storage packed bed at 90 bar and 100°C. The packed bed has heat losses of 8 percent and air leakage losses of 1 percent. Calculate (*a*) the turbine air mass flow rate during peak operation, in kilograms per second, (*b*) the minimum volume of the air storage cavern, in cubic meters, (*c*) the energy storage capacity, in megawatt hours, (*d*) the compressor power input, in megawatts, and (*e*) the turnaround efficiency of the system. Assume a constant air specific heat at constant pressure of 1.05 kJ/kg · K.

16-4 A hybrid air-storage energy system is composed of an air compressor with two stages of intercooling, an aftercooler, a storage reservoir, and a gas turbine with one stage of reheat and regeneration. During 10 h of storage, 100 MW are fed to the motor generator, and air enters the compressor at 1 atm and 50°F. The compressor and turbine overall pressure ratios are 64. The compressor sections have polytropic and mechanical efficiencies of 0.7 and 0.8, respectively. Intercooling and aftercooling reduce the temperature back to ambient. During 4 h of peak generation, air leaves storage and enters a 0.85-effective regenerator after which it is heated in the first combustion chamber to 2000°F. The turbine sections have polytropic and mechanical efficiencies of 0.75 and 0.8, respectively. Reheat in the second combustion chamber is back to 2000°F. The motor-generator set has an efficiency of 0.90. Draw a flow diagram for the system and calculate (*a*) the air mass, in pounds mass, and volume, in cubic feet, stored during off peak, and (*b*) the turnaround efficiency of the system taking into account the equivalent electrical energy of the heat added in the turbine if the main plant thermal efficiency is 0.38. Assume that 1 percent of the air in storage is

lost by leakage. For simplicity take $c_p = 0.24$ and 0.26 Btu/lb$_m$ · °R, and $k = 1.40$ and 1.358 in compressor and turbine, respectively.

16-5 A flywheel in the form of a disc 25 ft in diameter and 10 ft thick runs normally at 3600 r/min. It is made of an anisotropic filament composite material of a uniform density 160 lb$_m$/ft^3. Calculate (*a*) the energy of the flywheel, in kilowatt hours, (*b*) the change in rotational speed and corresponding maximum energy that may be extracted from the flywheel if the coefficient of speed fluctuation may not exceed 0.01.

16-6 A disc-shaped flywheel is made of an isotropic material with a density of 500 lb$_m$/ft^3 and maximum allowable stress of 15×10^6 lb$_f$/ft^2. It has a diameter of 15 ft and a thickness of 6 ft. The mass efficiency factor is 0.9. Calculate (*a*) the maximum energy that can be stored in the wheel, based on stress considerations, (*b*) the maximum rotational speed, in revolutions per minute, and (*c*) the coefficient of speed fluctuation if 2 percent of the energy is withdrawn from it.

16-7 A magnetic energy-storage coil is constructed of a conductor of square cross section 40 × 40 cm, and a mean diameter of 32 m. Calculate the number of turns necessary for a stored energy of 5 MWh if the current is 160,000 A.

16-8 Compressed-water thermal energy storage is used in a steam powerplant as shown in Fig. 16-15. Twelve accumulators are used, each 20 m in diameter and 40 m high. They have an overall coefficient of heat transfer of 0.003 kJ/s · m^2 · K. The daily storage time is 16 h. The maximum and minimum storage pressures are 18 and 3 bar. 80 percent of the total accumulator water volume is used to store and release energy to accommodate a steam blanket on top and water residue at bottom during the charge-discharge cycle. The main and peaking steam plant efficiencies are 38 and 23 percent, respectively. The ambient temperature is 10°C. Calculate (*a*) the thermal energy stored that is available for peaking service, in megawatt hours per day, (*b*) the thermal energy input, in megawatt hours per day, (*c*) the peaking plant electrical energy output, in megawatt hours per day, and (*d*) the ratio of peaking electrical energy to the electrical energy that would have been produced by the main plant.

16-9 A latent heat energy storage system is used in conjunction with a high-temperature gas cooled reactor (HTGR) gas turbine powerplant. The storage material is germanium which has a fusion temperature of 1756°F, a latent heat of fusion of 300 Btu/lb$_m$, and a liquid density of 335 lb$_m$/ft^3. The HTGR operates as a heat source for a regenerative helium Brayton cycle. 10^6 lb$_m$/h of helium enter the compressor at 160°F, a 0.85-effective regenerator, and leave the HTGR at 1850°F. During a charge period of 12 h, 50 percent of the helium enters the main turbine and 50 percent is diverted to the latent heat storage heat exchanger. From there, it leaves at 1790°F to enter the main gas turbine at a lower pressure stage. During 4 h of peak operation, the full HTGR flow enters the main turbine and a peaking Brayton cycle operates on the stored heat. Helium enters the peaking compressor at 140°F, then a 0.85-effective regenerator, a heat exchanger in the storage tank where it gets heated to 1720°F, then the peaking gas turbine. Assume for simplicity that all compressors and turbines are ideal with a pressure ratio of 3, and that there are no heat losses from the storage tank. Draw a flow diagram for the powerplant and *T-s* diagrams for the main and peaking cycles, labeling all points correspondingly. Calculate (*a*) the power produced during off peak operation, in megawatts, (*b*) the energy stored, in megawatt hours, (*c*) the minimum germanium mass, in pounds mass, and storage volume, in cubic feet, and (*d*) the power produced during peak operation, in megawatts. (For helium, $c_p = 1.25$ Btu/lb$_m$ · °R and $k = 1.250$.)

16-10 A chemical reaction energy storage system of the methanation-reforming type is considered for storing 2550 MWh of electrical energy. The system turnaround efficiency is estimated at 0.85. The main powerplant thermal efficiency is 0.38. Calculate (*a*) the individual masses, in kilograms, of reactant and product gases, (*b*) the necessary storage volumes, in cubic meters, assuming storage is at 70 bar and 500°C, (*c*) the maximum mechanical energy to be stored, in kilojoules, assuming for simplicity that pressure, temperature, and pressure drops are the same in all reactors and tanks, and that all expanders and compressors have an efficiency of 0.60.

CHAPTER

SEVENTEEN

ENVIRONMENTAL ASPECTS OF POWER GENERATION

17-1 INTRODUCTION

It should be recognized at the outset that there is virtually nothing people can do to improve their life standards, or even to maintain these standards in the face of growing populations, not to mention bringing up the standards of the billions of people living in substandard conditions around the world, that does not have adverse side effects, particularly on the environment. We can no longer expect the return of the pristine environment that existed in the early history of humankind. This is true whether people are producing increasing quantities of food and clothing, which have become energy-intensive; building dams and other irrigation schemes; or building powerplants to produce the electricity so necessary for industry and domestic uses and the maintenance of that life standard. The important question is whether or not the benefits of these necessary systems outweigh their adverse effects. Some sentiments have been expressed to the effect that the adverse effects of power generation can be arrested solely by conservation. Conservation means more efficient use of our resources and more efficient electric-energy production and use and is commendable. However, conservation alone can only reduce the rate of increase of environmental degradation. It is thus at least of equal importance to study the causes and effects of the adverse effects on the environment and to minimize them as much as possible.

Another factor to recognize is that nature itself contributes large quantities of contaminants to the environment, mainly due to the natural processes of plant and animal decay and natural background radioactivity.

At this point one needs to distinguish between the often used terms contaminant and pollutant. *Contaminants* are those materials, radiations, or thermal effects that are

added to environment beyond what nature itself puts into it. In the 1960s it was estimated that, globally, nature puts into the environment some 10 times the amount of contaminants that people put into it. The contribution of nature is, however, diffuse and thus largely harmless, whereas the contribution by human beings is more localized and concentrated. It follows that *pollutants* are contaminants in concentrations high enough to adversely affect something that people value, such as their environment and health.

Table 17-1 presents a summary of chemical air pollutants from all sources in the United States in 1966. It is to be noted that motor vehicles are the largest contributors, followed by industry and powerplants, and then by small contributions from space heating and refuse. Not included in Table 17-1 is thermal pollution, the warming up of bodies of water and the atmosphere from the above sources as well as nuclear powerplants.

The case of radioactive pollution from nuclear powerplants is even less troublesome than the above sources when compared with the contributions of nature. Table 17-2 presents a summary of average annual exposures per person from all sources. Note that nature is the largest contributor, followed by medical irradiation, whereas releases attributed to the nuclear industry as a whole are relatively miniscule.

Even in abnormal occurrences the picture presented in Table 17-2 holds true. This can be illustrated by two such occurrences, one artificially made, the March 1979 accident at Three Mile Island (TMI-2) powerplant, the other naturally occurring, the May 1980 volcanic eruption of Mount St. Helens in the state of Washington, USA.

The radioactive release from Mount St. Helens was far more significant than that from TMI-2 (Sec. 17-15). It is reasonable to assume that volcanic eruptions and other such natural occurrences have released and will continue to release large amounts of radioactivity into the atmosphere.

Powerplants are, therefore, not the sole or largest contributors to environmental problems. They are, however, a growing concern, as their numbers and sizes will continue to increase in the decades ahead. The powerplant pollutants of most concern are:

Table 17-1 Total United States chemical air pollution (1966)*

Source	Pollutants	
	tons/year	%
Motor vehicles	60	60.6
Industry	23	16.8
Fossil powerplants	20	14.1
Space heating	8	5.6
Refuse disposal	5	3.5

* From Ref. 169.

Table 17-2 Average radioactive exposures per person*

Source	Exposure	
	mrem/yr	%
Natural background	100.0	67.60
Medical irradiation	45.0	30.70
Fallout	0.9	0.60
Miscellaneous	0.7	0.50
Occupational	0.7	0.45
Nuclear industry	0.2	0.15

* From Ref. 170.

1. From fossil powerplants:
   a. sulfur oxide
   b. nitrogen oxides
   c. carbon oxides
   d. particulate matter
   e. thermal pollution
2. From nuclear powerplants:
   a. radioactivity release
   b. radioactive wastes
   c. thermal pollution

In addition, pollutants such as lead and hydrocarbons are contributed primarily by motor vehicles and will not be covered here.

This chapter is devoted to the discussion of these various aspects of electric-power generation and methods to minimize or alleviate their effects. The first part of the chapter deals with the effects of fossil-fuel powerplants, the latter part with those of nuclear powerplants.

17-2 CONSTITUENTS OF THE ATMOSPHERE

The effects of powerplant pollutants on the environment are primarily to the air and water and, to a lesser extent, the land.

The total mass of the earth's atmosphere is estimated at 5.7×10^{15} tons of various major and trace constituents. Table 17-3 shows approximate masses in tons of the major constituents, N_2 and O_2, as well as other constituents that are of main concern in the earth's atmosphere. The table lists the global (total atmosphere) tonnage as well as the tonnage in a portion of the atmosphere roughly lying between 30 to 60°N latitude and below 20,000 ft altitude. This portion of the atmosphere is less than 20 percent of the total, but it corresponds to the area of much of the world's industry and is therefore the receptacle for much of humankind's additions of contaminants to the

Table 17-3 Major and selected constituents of the atmosphere, tons*

Component	Tonnage		Lifetime
	Global	Between 30–60° N latitude	
N_2	4.25×10^{15}	0.55×10^{15}	Indefinite
O_2	1.30×10^{15}	0.17×10^{15}	Indefinite
CO_2	2.80×10^{12}	—	Years
CH_4	5.00×10^{9}	—	Years
CO	6.00×10^{8}	—	Years
NO_x	9.00×10^{6}	2.00×10^{6}	Days
SO_2	2.50×10^{9}	5.00×10^{7}	Days
Particulate matter	1.55×10^{8}	3.00×10^{7}	Days to years

* Data from Ref. 169.

global atmosphere. In addition, the rate of atmospheric mixing between the northern and southern hemisphere is slow, so that the region mentioned above may be considered isolated except for extended periods of time.

The atmosphere is recognized as a self-cleansing environment in which contaminants are continually added and removed. Thus, the amount of any one contaminant at any given time is affected by the mass rates of addition and removal of that contaminant. The concentration of that pollutant is affected by these rates as well as the size of the atmosphere itself. The addition of contaminants is due to both natural causes and artificial causes that are of fairly recent origin. The last column in Table 17-3 represents the average lifetime of each constituent. This is the average residence time of the constituent between addition and removal. The figures in this and the tables to follow in this chapter are only ball park figures because of the doubtful accuracy of measurements, so they should be viewed with caution. They are also bound to vary with time. The relative magnitudes are; however, informative.

We will now discuss the most important contaminants, their effects, and methods of coping with them.

17-3 OXIDES OF SULFUR

Sulfur in the atmosphere exists essentially in three forms: sulfur dioxide, SO_2; hydrogen sulfide, H_2S; and various sulfates. H_2S comes primarily from natural sources. The sulfates come from sea spray and from the oxidation of SO_2.

Sulfur dioxide, SO_2, which primarily comes from artificial causes, is therefore our primary concern, even though it is believed to be responsible for something less than 25 percent of all sulfur in the atmosphere. It is produced in the combustion of coal and oil, mainly in powerplants, but also in steel mills, smelters, and similar

Table 17-4 SO_2 flowchart in the 30° to 60°N latitude*

Additions	Natural (volcanoes)	Powerplants	Industry	Space heating	Solid waste	Motor vehicles
tons/year	Negligible	5×10^7	1×10^7	0.6×10^7	0.3×10^7	0.2×10^7
↓		↓	↓		↓	
Steady state	5×10^5 tons 0.2 ppb, average					
↓		↓	↓		↓	
Removal	Precipitation Gravitation					

* Data from Ref. 169

industries, and space heaters (all also produce some H_2S), with coal responsible for about 70 percent of the total.

Although the mass of SO_2 in the 30 to 60°N latitude region of the atmosphere, which is about 5×10^5 tons (Table 17-3), represents an average of about 0.2 ppb (parts per billion) in that region, the yearly mass added, and removed, is much higher, being of the order of 10^8 tons (Table 17-4). Local SO_2 concentrations vary widely and are usually measured in ppm (parts per million). Urban industrial areas often reach 3.2 ppm, and peaks of 11 ppm have been recorded. SO_2 concentrations below 0.6 ppm produce no ill effects in human beings. Most people, however, become cognizant of sulfur at about 5 ppm and become irritated at about 10 ppm. A 1-h exposure to 10 ppm can cause breathing problems and mucus removal. The effects are further complicated at high air temperatures and humidities, in the presence of aerosols, etc., and they become much more serious when SO_2 is combined with particulates and enters the digestive system.

The effects of SO_2 on bodies of water and on land are discussed in Sec. 17-8.

17-4 OXIDES OF NITROGEN

The oxides of nitrogen come in different forms: nitric oxide, NO; nitrous oxide, N_2O; nitrogen dioxide, NO_2; nitrogen trioxide, NO_3; nitric anhydride, N_2O_5; and nitrous anhydride, N_2O_3. Of these only NO and NO_2 are the significant artificially made oxides; they are commonly referred to as NO_x, pronounced "nox."

Nitric oxide, NO, is formed in the combustion of all fossil fuels. The rate of formation is strongly dependent upon the combustion temperature, being significant only at high temperature. Formation is also dependent upon the oxygen concentration present during combustion and the time allowed for the combustion process. The primary contributors to NO are the motor vehicles, in which combustion does occur at high temperatures, with lesser contributions from the combustion of coal and oil in powerplants, which occurs at lower temperatures. Concentrations of NO in the exhaust

of gasoline automobiles depends upon the fuel-air ratio used and vary between about 3000 ppm near stoichiometric conditions to about 6000 ppm for 80 percent lean mixtures.

In the atmosphere NO rapidly oxidizes to NO_2, a process greatly accelerated by photochemical effects (the presence of sunlight) and by the presence of organic material in the air. NO_2 has a more adverse health effect on human beings than NO. It has an affinity for hemoglobin, which carries oxygen to body tissues. It thus deprives them of oxygen. It also forms acid in the lungs and hence is much more toxic than CO (below) for the same concentrations. It also reduces atmospheric visibility. People begin to recognize the existence of NO_2 by its odor when it reaches concentrations of 0.4 ppm and higher. A continuous exposure to 0.06 to 0.1 ppm of NO_2, however, can cause respiratory illness. A few minutes exposure to 150 to 200 ppm causes obliterations of the bronchiols (the smallest divisions of a bronchial tube), and a few minutes exposure to 500 ppm causes acute edema (swelling from the effusion of a watery liquid into cellular tissue).

The atmosphere in the 30 to 60°N latitude region contains 2×10^6 tons of NO_x (Table 17-3), which coresponds to an average of 1 ppb. The additions, and removals, per year are 2×10^8 tons from natural causes, mainly biological, and 5×10^7 tons from artificial causes (Table 17-5). It should be noted here that the two NO_x compounds represent only a small fraction of the total nitrogen compounds entering and leaving the atmosphere. For example ammonia, NH_3, enters and leaves the atmosphere at a rate some 10 times that of NO_x.

While the average in the 30 to 60°N latitude region is about 1 ppb, local urban concentrations of NO_x can be much higher, ranging between 0.02 and 0.9 ppm. Temporary but severely high concentrations up to 3.9 ppm have been recorded in Los Angeles, which has a rate of addition 100 times the world average. (It is instructive to note that tobacco smoke can contain about 250 ppm.)

Although contributions of NO, by artificial causes on a global scale are far less than those by natural events, local human contributions could be far larger and could

Table 17-5 NO_x flowchart in the 30 to 60°N latitude*

Additions	Natural biological reactions	Motor vehicles	Industry	Powerplants	Space heating	Solid waste
tons/year	20×10^7	2×10^7	2×10^7	0.8×10^7	0.2×10^7	0.2×10^7
↓		↓		↓		
Steady state	2×10^8 tons, 1.0 ppb, average					
↓		↓		↓		
Removal	As nitrates by precipitation, vegetation					

* Data from Ref. 169.

thus give rise to severe health and environmental problems. The effects of NO_x on bodies of water and land will also be covered in Sec. 17-8.

17-5 OXIDES OF CARBON

Carbon monoxide, CO, methane, CH_4 and carbon dioxide, CO_2, are the most widely produced of all contaminants, with CO_2 being the largest of all (Table 17-3).

Carbon monoxide is caused in part by natural causes such as marsh gas, coal mines, vegetation, lightning, and forest fires. However, their contribution to production of CO is small compared with that from human-generated causes, of which more than 90 percent is produced by motor vehicles (Table 17-6). Powerplants produce less than 1 percent. The removal of CO is almost entirely due to natural events whose exact nature is not known with certainty.

The CO additions to the entire earth's atmosphere total about 230 million tons. Local additions are often serious. For example, in the Los Angeles basin alone, some 4 million tons are added annually. The basin average CO concentration increased from about 7 ppm to about 11 ppm between 1957 and 1963 compared with the global 0.1 ppm. Emission-control devices are causing a slow decrease in these concentrations. People who smoke voluntarily expose themselves momentarily to concentrations said to reach 42,000 ppm.

The health hazard of CO, like NO, stems from its depriving body tissues of oxygen because of its affinity for hemoglobin, which carries oxygen to body tissues. A CO concentration of 100 ppm causes headache, 500 ppm causes collapse, and 1000 ppm is fatal.

Carbon dioxide, CO_2, is more abundant and, unlike CO, is largely contributed by powerplants and hence of more concern to us here. Natural causes, such as the decay of organic matter, however, contribute much greater amounts of CO_2 than artificial causes (Table 17-7). Although the CO_2 added to the atmosphere by these

Table 17-6 Carbon monoxide flow chart, entire atmosphere*

Additions	Natural events	Motor vehicles	Industry	Space heating	Powerplants	Solid waste
tons/year	0.2×10^8	2.0×10^8	0.04×10^8	0.04×10^8	0.02×10^8	0.02×10^8
↓			↓	↓	↓	
Steady state	6×10^8 tons, 0.1 ppm, average					
↓			↓	↓	↓	
Removal	Oxidation to CO_2 in atmosphere, dissolution in water, consumption by vegetation, other unknowns					

* Data from Ref. 169.

Table 17-7 Carbon dioxide flowchart, entire atmosphere*

	Natural causes			Artificial causes	
Additions	Organic decay	Volcanoes	Respiration	Combustion	Industry
tons/year	2×10^{11}	1×10^{10}	1×10^{9}	2×10^{10}	2×10^{8}
	↓		↓	↓	
Steady state	3×10^{12} tons, 325 ppm average				
	↓		↓	↓	
Removal	Photosynthesis (2×10^{11} tons/year), ocean absorption, rock weathering				

* From Ref. 169.

causes is considered a contaminant, it is not normally considered a pollutant because it is essential to plant and, therefore, human life. The main removal mechanism of CO_2 is *photosynthesis*. This is the process that occurs in green plants in the presence of light by which water, CO_2, and minerals are converted back to oxygen and various organic compounds.

Despite the necessity mentioned above of CO_2 in the atmosphere, there is increasing concern that the growing combustion of fossil fuels for all types of energy will cause the CO_2 concentration in the entire atmosphere to continue to increase with serious effects on the earth's climate as a result of the greenhouse effect.

17-6 THE GREENHOUSE EFFECT

The concentrations of CO_2 in the atmosphere have slowly but continually increased since 1880 with the evergrowing worldwide combustion of fossil fuels. Since the 1950s, the concentrations have risen at an increasing rate (Fig. 17-1). The addition of CO_2 in the latter part of the decade of the 1970s is believed by some to have reached a level that is beyond the capacity of plant life and the oceans to completely remove it, and about half of the CO_2 added is retained in the atmosphere.

The existence of CO_2 in the atmosphere causes a *greenhouse effect*. The atmosphere, analogous to the glass panes of a greenhouse, transmits the radiation from the sun. Because the surface of the sun is at about 6000 K, most of that radiation is in the shortwave and visible portion of the spectrum, and only a small portion of this radiation is absorbed or scattered back to space by the atmosphere. The transmitted radiation is largely absorbed by the surface of the earth, which is warmed by it.

Part of the resulting heat of the earth is transmitted by various modes of heat transfer (conduction, convection, evaporation, and condensation, which has a negative contribution) to the atmosphere and is ultimately reradiated away from the surface. Because the surface temperatures are low, this reradiation is mostly in the infrared portion of the spectrum. CO_2 has no emission and absorption bands in the short and

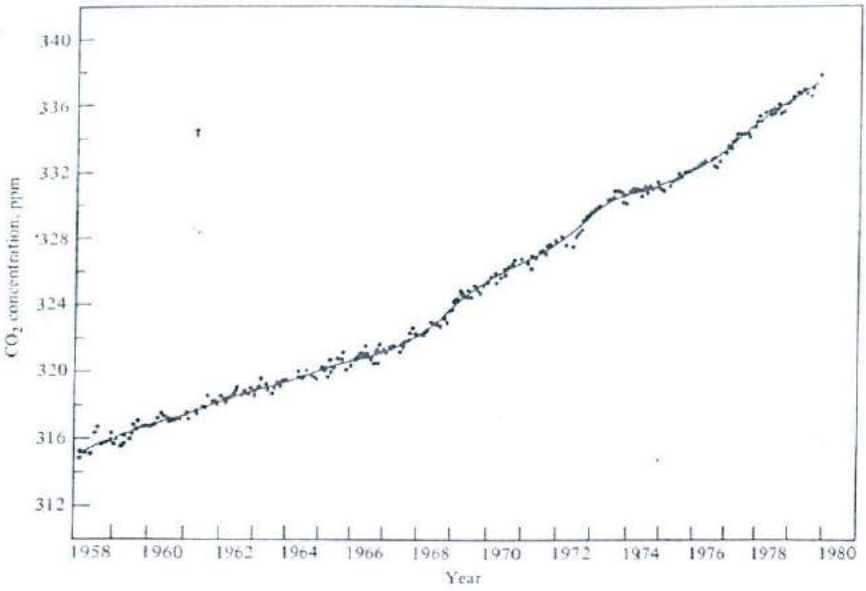


Figure 17-1 Average CO_2 concentrations in the atmosphere up to 1980 with seasonal effects removed. Seasonal fluctuations about average: slightly lower in spring due to absorption by new plants; slightly higher in fall due to release from decaying plants. *(Based on work by C. D. Keeling et al., from Ref. 171.)*

visible wavelengths of the spectrum but does have several infrared bands between the wavelengths 2.36 to 3.02 μm, 4.01 to 4.08 μm, and 12.5 to 16.5 μm. Water vapor, likewise, has only infrared emission and absorption bands in the wavelengths 2.24 to 3.27 μm, 4.8 to 8.5 μm, and 12 to 25 μm. When both CO_2 and H_2O are present, the absorptions are, to a good approximation, additive.

The presence of CO_2 and H_2O in the atmosphere results in absorption of a large portion of the longwave infrared radiations from the surface of the earth and partial radiation of them back to it. In essence, therefore, the atmosphere is not completely transparent to the reradiated energy and, like the panes of a greenhouse, traps much of the energy of the sun. Whereas an equilibrium of sorts existed over the centuries, the growing levels of concentration of CO_2 are expected to cause the earth and its lower atmosphere to warm up to higher temperatures than would otherwise be the case. Indeed, measurements have shown a small warming up already (Fig. 17-2).

It is estimated that if all the fossil-fuel reserves are burned, the current CO_2 concentration in the atmosphere would increase 5- to 10-fold. It is feared, however, that long before this ultimate situation happens, climatic changes might occur that would result in disasterous consequences, such as melting of the polar ice caps, which would result in the raising of sea level and flooding of many coastal areas of the world. Some evidence that this process has already started has been cited.

Somewhat counterbalancing the increasing effect of CO_2 on the atmosphere is the

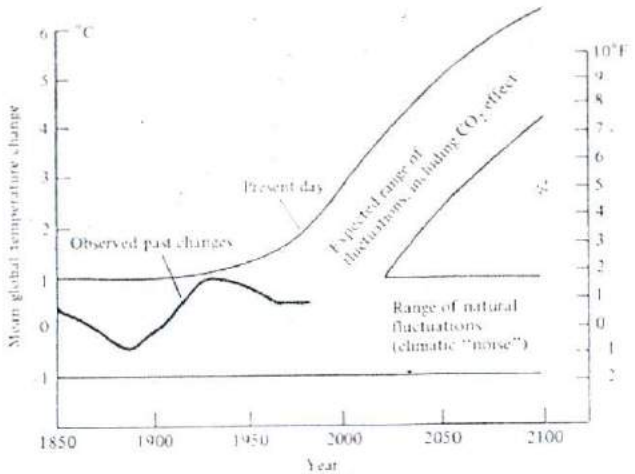


Figure 17-2 Changes in mean global temperature with and without projected CO_2 effects. *(Based on work by J. M. Mitchell, from Ref. 17.)*

increasing content of particulate matter. Particulate matter helps reflect some of the incident radiation from the sun back to space and thus prevents it from reaching the surface of the earth.

17-7 ACID PRECIPITATION

Acid precipitation is the return to earth of the oxides of sulfur and nitrogen in acid form. They take several forms: acid rain and acid snow, dry deposition, and acid fog.

Acid Rain and Acid Snow

Acid fallout in the form of *acid rain* or *acid snow* is one of the more serious environmental hazards of increased concentrations of sulfur and nitrogen oxides in the atmosphere. Pure water has a neutral pH value of 7.0.* The average pH of normal rainfall is a slightly acidic 5.6 because of the formation of mild carbonic acid H_2CO_3 when pure rainwater combines with natural and human-generated carbon dioxide in the atmosphere; it is considered harmless. However, biologists usually consider rainfall with pH values lower than 5.6 to be potentially harmful to plant, animal, and human life. In many parts of the world, however, rainfall has grown increasingly more acidic in recent years. pH values as low as 2.4, about the same acidity as vinegar, have been recorded in England and in widely separated regions of the world.

* *Acidity* and *alkalinity* are measured on a pH scale of 0 to 14. pH = 7.0 denotes neutrality. $0 \leq pH < 7$ represents acidity. $7 < pH \leq 14$ represents alkalinity. The strongest acids have pH values below 1.0.

Acid rain and acid snow are caused by sulfur dioxide, SO_2, hydrogen sulfide, H_2S, and the oxides of nitrogen, NO_x, in the atmosphere. Over a period of time after these gases are emitted, usually hours or days, they are carried along by wind currents and combine with water molecules in the water vapor of the atmosphere to form tiny drops, mainly of nitric acid, HNO_3, and sulfuric acid, H_2SO_4. These aerosollike acids are then returned to the surface of the earth when they encounter rain- or snow-producing clouds at various distances from their place of origin, often as far as hundreds or thousands of kilometers away.

In general SO_2 contributes about 60 percent of the acidity of such precipitation, whereas NO_x contributes about 35 percent. More is known about the relatively simple mechanism of formation of acid rain and snow from SO_2 than the more complex mechanism due to NO_x.

Acid precipitation was first observed in Scandinavia in the 1950s. Excessive acidity is a more recent phenomenon. It has been observed on the North American continent in such places as the northeastern parts of the United States and eastern Canada (Fig. 17-3), where the toxic fumes have crossed the international border in both directions, although their source is often blamed on powerplants in the Ohio valley that export them on prevailing winds. Other affected areas in the United States are the northwestern region, the southern Appalacians, and portions of Florida. In Europe, industrialized countries such as Britain, Germany, and France produce millions of tons of these gases that affect many other countries, some as far away as Scandinavia. Acid rain has also been found in parts of Asia and other world spots.

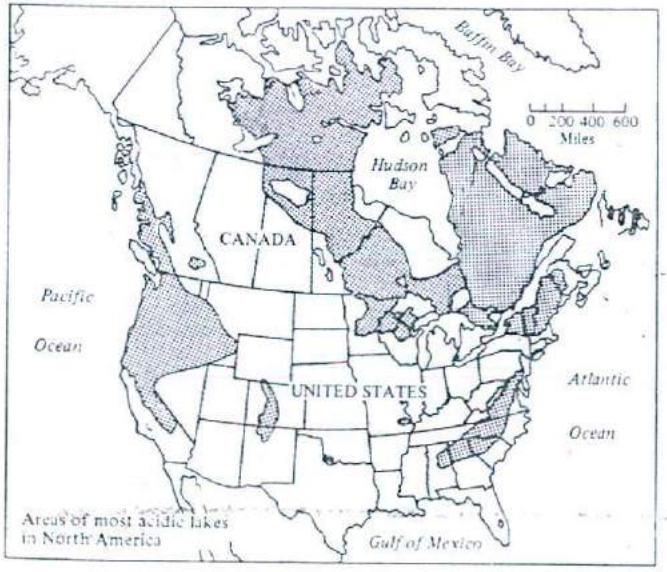


Figure 17-3 Areas of most acidic lakes in North America [172].

This unwelcome traffic across national and international boundaries has prompted multigovernmental conferences to discuss the causes, sources, and extent of acid rain, the outlook for the future, and if possible, to find corrective measures. Treaties between nations defining responsibilities and outlining joint actions may have to be drawn. Expressions of concern were voiced at a 1979 international conference in Toronto by Canadian officials who stated that acid rain is their "most serious environmental problem"; by U.S. officials who announced that "too much damage has already been done by acid rain—too many trout lakes and salmon streams have already been rendered lethal to fish, and valuable wilderness areas are beginning to show signs of acidification"; and by others.

The effect of acid on streams and lakes has resulted in the lowering of pH values of some of them to values betwen 2.8 and 5.0. This acidification causes the decimation or malformation of fish, particularly trout and salmon. It has been estimated that 50,000 lakes in the Adirondack Mountains and Ontario, Canada, have become acidified to the extent that fish population has declined or ceased to exist. High levels of acidity are also said to cause the dissolving of toxic metals such as cadmium, lead, and aluminum out of minerals in the bottom sediments. These toxic metals, like the acids, can destroy fish and also contaminate drinking water.

The effect of acid rain on soil can cause the leaching of essential plant nutrients from the soil and reduce nitrogen fixation by microorganisms, which would make the soil less fertile. It can also dissolve aluminum and cadmium out of soil minerals, as mentioned above, and thus allow them to enter roots and kill trees. A recent (1982) study on the effects of acidity on forests at the University of Vermont showed that on Camel's Hump, a 4100-ft peak in the Green Mountains, half the red spruce trees have died. In West Germany, acid rain is blamed for the death of about 3700 acres of evergreen trees in Bavaria.

Dry Deposition

A particularly lethal form of acidity is called *dry deposition*. This occurs when sulfate particles fall on tree leaves before mixing with water. This dry fallout is said to account for about half the total acid fallout. When these particles mix with surface or rain water, they become concentrated sulfuric acid.

Attempts to alleviate the problem so far (1982) have met with little success. The most serious of these attempts involves dispersal and detoxification of the emissions that cause the acid rain in the first place. Other plans involve the breeding of new plant or animal species that would be acid-resistant. Probably the most effective method is the use of smokestack scrubbers (Sec. 17-9) that remove much of the sulfur from powerplants and industrial furnaces, though they have no effect on nitrogen oxides. They, however, are used only in a few large installations and are expensive to install and operate. Ironically, the dispersal of the emissions by the use of tall smokestacks, thought to be the answer at one time (the solution of pollution is dilution), is effective only in removing particulates and exhaust locally. It has actually encouraged the formation of acid rain by more efficiently sending the emissions to those air currents that transport them to rain clouds, often far away from their point of origin.

Detoxification of lakes by the addition of lime has proven counterproductive because lime has been found to combine with heavy metals in the bottom sediment and to free them, actually increasing the toxicity of water.

The idea of breeding of acid-resistant fish is a proposition that is not taken very seriously by most zoologists.

Acid Fog

A recently noted major acid pollutant is *acid fog*. Its origin is the same as acid rain or snow, i.e., sulfuric and nitric oxides from powerplants and, to a lesser extent, motor vehicles. It forms by the mixing of these pollutants with water vapor near the ground. The acid vapors then begin to condense around very tiny particles of fog or smog, pick up more water vapor from the humid air, and turn into acid fog. When the water in the fog burns off (evaporates) due to the sun or other causes, drops of nearly pure sulfuric acid are left behind. It is these drops that make acid fog so acidic. In Los Angeles and Bakersfield in southern California, the mists have a pH of 3.0 compared with 4 or 4.5 for acid rain. Acid fog 100 times as acidic as acid rain has been detected. Cases have been reported where people had trouble breathing when it was foggy. The problems of fog are now believed by some to be more serious than those of smog in these areas.

Many researchers consider the effects of acid precipitation, especially the changing of soil chemistry, to be irreversible and fear its long-range effects. Monitoring programs of air, soil, and water are being instituted to ascertain these long-range effects. However, the uncertainty about the real extent of the problem adds to the prevailing disquiet regarding it.

17-8 PARTICULATE MATTER

Particulate matter in the atmosphere is composed of smoke, dust, and other solids made of a wide variety of organics and metals. Samples taken in urban areas of the United States between 1960 and 1965 showed average and maximum particulate concentrations in the atmosphere of about 100 and 1250 $\mu g/m^3$, respectively. The Los Angeles basin, by now shown to be a particularly bad case, is estimated to put into the atmosphere some 170,000 tons/year of particulate matter, including that due to SO_2, about 30 times the mass of the atmosphere over that basin. During the London atmospheric pollution crisis of 1962 the particulate concentration rose to 2000 $\mu g/m^3$. There is evidence that air-circulation patterns over industrialized areas cause self-contained dust domes that aggrevate matters over these areas (Fig. 17-4). Nonurban areas in the United States averaged 28 $\mu g/m^3$.

The total particulate matter in the 30 to 60°N latitude region of the atmosphere is about 3×10^7 tons, averaging about 30 $\mu g/m^3$ (Table 17-8). Both natural and human activities seem equally to blame for the presence of particulate matter in the atmosphere. Natural causes include natural dust caused by wind, storms, volcanoes and natural fires, metoritic dust, and fog. Fog, although not strictly a pollutant, con-

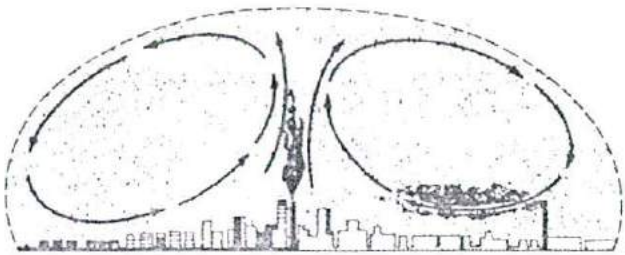


Figure 17-4 Air-circulation pattern over a large industrial urban area, creating a self-contained dust dome.

tributes to undesirable climatic conditions, especially when combined with smoke (smog). Of the human causes, dust and ash that emanate from industrial processes, fossil powerplants, and other combustion processes are the largest contributors, of which powerplants contribute about one-third. Sulfur compounds are larger contributors to particulate matter. This comes about by the SO_2 in the atmosphere (Sec. 17-3) oxidizing to sulfur trioxide, SO_3, which forms H_2SO_4 (sulfuric acid) mist, which in turn reacts with other materials in the air to form, among other things, ammonium and calcium sulfates.

The effects of particulate matter in the atmosphere are many and varied. Besides the obvious effects of decreasing visibility and increasing soiling and corrosion, and the already mentioned effects on climatic conditions, there is a health hazard that is a complex function of concentration and particle size. The size distribution is given by the usual log mean normal distribution curve (below). Numerically, most particles have a diameter below 2 μm, with a numerical average about 1.27 μm. The larger particles, however, although fewer in number, represent a greater mass fraction of the

Table 17-8 Flowchart of particulates in the 30 to 60°N latitude*

	Natural causes			Artificial causes				
Additions	Natural	Meteors	Fog	Industrial	Space heating	Motor vehicles	Solid waste	Sulphates
Tons/year	6×10^7	1×10^7	3×10^7	3×10^7	2×10^6	2×10^6	2×10^6	6×10^7
↓				↓		↓		
Steady state	3×10^7 tons, 30 $\mu g/m^3$ average							
↓				↓		↓		
Removal	Gravitation, impaction, drop nucleation, washing							

* From Ref. 169.

total. It is estimated that an individual breathes about 1 mg of particulate matter per day during times of heavy pollution, with the larger particles depositing in the mucous lining and the smaller ones in the deeper parts of the lungs. Particulate matter in the atmosphere is intrinsically toxic; it absorbs toxic substances and obstructs respiratory passages. An annual mean 100 to 200 $\mu g/m^3$ results in respiratory illnesses, whereas 300 to 600 $\mu g/m^3$ causes a large increase in the number of bronchitic patients.

Particulate-Matter Distribution

A *Gaussian* or *normal distribution* of a statistical quantity, such as the diameter of particles in a large sample, is one in which the numbers of particles of given diameters fall on a bell-shaped curve, symmetrical about a mean diameter, when plotted against the diameter on a linear scale. It is given by

$$N(d) = \frac{1}{\sqrt{2\pi}S} e^{-\frac{1}{2}\left(\frac{d - d_n}{S}\right)^2} \tag{17-1}$$

where

$N(d)$ = number of particles with diameters between d and $d + dd$

d = particle diameter

d_n = mean particle diameter

S = standard deviation of d, having the same dimensions as d and given by

$$S = \left[\frac{\Sigma\left(d_i - \frac{\Sigma d_i}{N}\right)^2}{N - 1}\right]^{0.5} \tag{17-2}$$

where

N = total number of particles

Most particle samples from emissions, however, have size distributions that follow a *log normal distribution*. This has the same symmetrical bell-shaped curve as the Gaussian distribution except that the variable is the *logarithm* of the diameter rather than the diameter itself. It is thus given by

$$N(\omega) = \frac{1}{\sqrt{2\pi}S_\omega} e^{-\frac{1}{2}\left(\frac{\omega - \omega_n}{S}\right)^2} \tag{17-3}$$

where

$\omega = \ln d$

ω_n = mean value of ω or $\ln d$

$N(\omega)$ = number of particles per unit interval betweeen $\ln d$ and $[\ln d + d(\ln d)]$

S_ω = standard deviation of ω

Figure 17-5*a* is a plot of the fraction $N(\omega)/N$ showing the usual Gaussian curve but with a logarithmic abscissa scale for d. Figure 17-5*b* shows a log normal plot of the fraction $N(\omega)/N$ with a linear abscissa scale for d.

The notations on Fig. 17-5*b* have the following meanings.

Count modal diameter The diameter at which the greatest number of particles occurs, represented by the maximum point on the distribution curve

Count or number median diameter The diameter for which 50 percent of all particles or $N/2$ are larger and 50 percent or $N/2$ are smaller by count

Count mean diameter The arithmetic mean diameter of all particles present, e.g., the sum of diameters of all particles present divided by the total numbers of particles N

Area median diameter The diameter for which the surface area of all particles larger than it constitutes 50 percent of the total surface area

Area mean diameter The diameter of a particle that has a surface area equal to the arithmetic mean of the surface areas of all particles

Mass median diameter The diameter for which the mass of all particles with diameters larger than it constitutes 50 percent of the total mass

Mass mean diameter The diameter of a particle that has a mass equal to the arithmetic mean of the masses of all particles

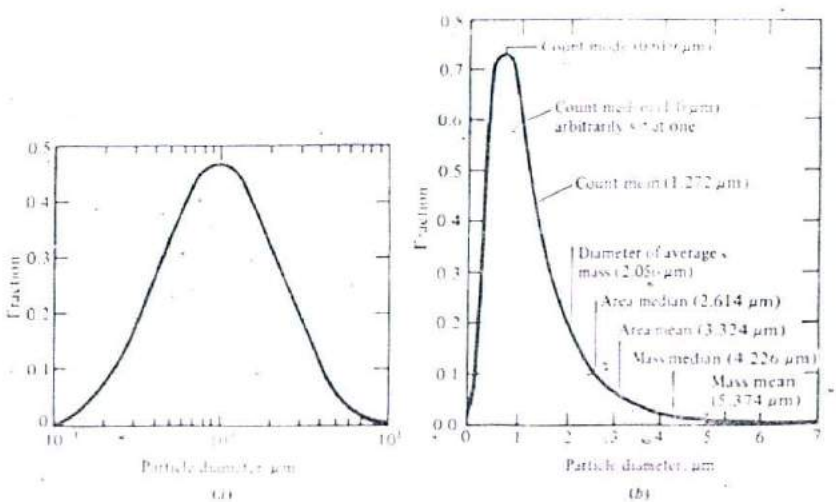


Figure 17-5 Log normal distribution of particle diameters plotted (*a*) on a semilog scale and (*b*) on a linear scale.

Devices that are used to clean up gas streams from the particulate matter they carry usually do better with larger particle diameters. They are characterized by (1) a fractional, or grade, efficiency and (2) an overall collection efficiency.

The *fractional, or grade, efficiency* is a collection efficiency, fraction, or percent of mass removed, for a given particle diameter. It is rather poor for the smallest sizes, increases rapidly with size, and becomes nearly 100 percent for the largest sizes. Figure 17-6 shows typical fractional efficiency curves for collection equipment. The *overall collection efficiency*, on the other hand, is the fraction or percent of mass removed of all particles or above a specified minimum diameter. It is to be noted that although liquid drops in suspension are usually spherical, solid particles are not. Thus the exact curve depends on what type of "diameter" representations are selected, e.g., the diameter of a spherical particle having the same surface area as the nonspherical particle, or the same volume, the Stoke's diameter, and others [173].

One must then be careful in evaluating the effectiveness of collection devices, which are usually characterized by the overall collection efficiency often above a given minimum diameter. Because efficiency is a mass ratio, and given the nature of the size distribution, a good collection efficiency might well mean a good mass removal but a poor numeric removal, as a very large number of small particles escape the collection device.

The majority of particulate matter in the atmosphere usually ranges in size (diameter) from 0.1 to 10 μm, although some are as small as 0.001 μm and as large as 500 μm. Below 0.1 μm, the particles behave like molecules and attain random motions characteristic of collisions with gas molecules. Between 1 and 20 μm the particles tend to be carried along with the air in which they are borne. Above 20 μm the particles

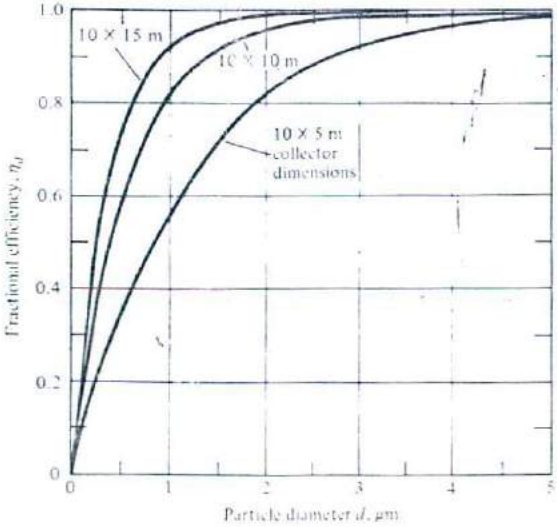


Figure 17-6 Typical fractional efficiency curve for collection equipment. Data plotted using the Deutsch equation for the data of Example 17-1.

attain settling rates that rapidly increase with size (0.3 cm/s for 10 μm, 30 cm/s for 100 μm), and they are, therefore, airborne for relatively short periods of time. The following sizes are of interest:

Particulate matter	*Size, μm*	*Particulate matter*	*Size, μm*
Natural dust	Above 1	Tobacco smoke	0.01–1
Liquid mist	Below 10	Oil smoke	0.03–1
Liquid sprays	Above 10	Coal dust	1–100
Smog	Below 2	Fly ash	1–200
Natural rain	500–10,000	Pulverized coal	3–500

Systems that help solve air quality-control problems associated with fossil-fuel steam-generator exhausts primarily deal with particulate collection and SO_2 emission cleanup. There are four basic types of systems:

1. Flue-gas desulfurization (FGD) (Sec. 17-9):
   a. Wet-type scrubbers
   b. Dry-type scrubbers
2. Particulate collection:
   a. Electrostatic precipitators (Sec. 17-10)
   b. Fabric filters (Sec. 17-11)

17-9 FLUE-GAS DESULFURIZATION (FGD) SYSTEMS

Gas desulfurization can be accomplished by wet, dry, or alkali scrubbing. These methods are covered in this section.

The Wet Flue-Gas Desulfurization System

The wet FGD system, also called a *wet scrubber*, is commonly based on low-cost lime-limestone* in the form of an aqueous slurry. This slurry, brought into intimate contact with the flue gas by various technique, absorbs the SO_2 in it.

The wet scrubbing process was originally developed in the 1930s by Imperial Chemical Industries (ICI) in England. In the modern version of the process, the flue gas is scrubbed with a slurry that contains lime (CaO) and limestone ($CaCO_3$) as well as the salts calcium sulfite ($CaSO_3 \cdot 2H_2O$) and calcium sulfate (in hydrate form, or natural gypsum, $CaSO_4 \cdot 2H_2O$). The SO_2 in the flue gas reacts with the slurry to form additional sulfite and sulfate salts, which are recycled with the addition of fresh lime or limestone. The chemical reactions are not known with certainty but are thought to be

* Lime is calcium oxide, CaO, a white caustic solid, also known as burnt lime, quicklime, and caustic lime. Limestone is a rock composed almost entirely of calcium carbonate, $CaCO_3$, from which building stones and lime are made. When crystallized by heat and pressure, it becomes marble.

$$\left.\begin{aligned} CaO + H_2O &\rightarrow Ca(OH)_2 \\ Ca(OH)_2 + CO_2 &\rightarrow CaCO_3 + H_2O \\ CaCO_3 + CO_2 + H_2O &\rightarrow Ca(HCO_3)_2 \\ Ca(HCO_3)_2 + SO_2 + H_2O &\rightarrow CaSO_3 \cdot 2H_2O \downarrow + 2CO_2 \\ CaSO_3 \cdot 2H_2O + \frac{1}{2}O_2 &\rightarrow CaSO_4 \cdot 2H_2O \downarrow \end{aligned}\right\} \quad (17\text{-}4)$$

One technique employs a *spray tower* downstream of the particulate-removal system (electrostatic precipitator or fabric filter) (Fig. 17-7). The flue gas is drawn into the spray tower by the main steam-generator induced-draft fan where it flows in countercurrent fashion to the limestone-slurry spray. A mist eliminator at the upper exit of the tower removes any spray droplets entrained by the gas. The gas may have to be slightly reheated before it enters the stack to improve atmospheric dispersion.

The sprayed limestone slurry collects in the bottom of the tower and is recirculated back to the spray nozzles by a pump. A system of feed and bleed charges a fresh slurry, under pH control, and discharges an equivalent amount from the circulating slurry. The fresh slurry is prepared by mixing the lime-limestone with water in a "slaker-grinder" and stirred in a slurry tank. The bled slurry is sent to a dewatering system, which is in the form of thickeners and filters or centrifuges, where water is removed from the calcium-sulfur salts. The reclaimed water is used to help make fresh slurry.

The wet scrubber has the advantages of high SO_2 removal efficiencies, good reliability, and low flue-gas energy requirements. In addition, it is capable of removing from the flue gases residual particulates that might have escaped the particulate-removal system.

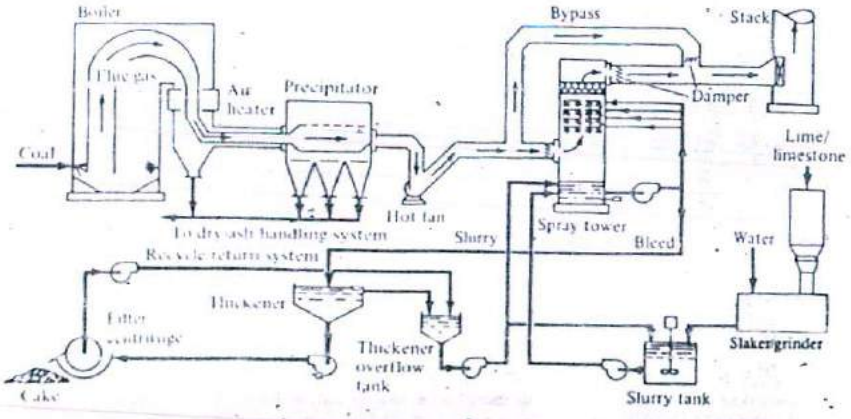


Figure 17-7 Schematic of a wet flue-gas desulfurization (FGD) system with a spray tower (*Electric Forum.*)

A main disadvantage is the buildup of scale in the spray tower and the possibility of plugging. The prevention of such scale is essential to the reliable operation of the tower. Scaling occurs because both calcium sulfite and calcium sulfate have low water solubility, normally around 30 percent, and can therefore form supersaturated water solutions. A minimum liquid-to-gas ratio must therefore be used, its value depending upon the SO_2 content of the flue gas and the expected extent of sulfite oxidation. Precipitation occurs at a finite rate, which necessitates holding the SO_2–absorbing liquor in a delay tank after each pass. An insufficient delay time increases supersaturation and promotes scaling. Another technique for controlling scale is the use of *seed crystals*. These are calcium sulfite and sulfate precipitate crystals, in a supersaturated solution, that are maintained in the SO_2–absorbing liquor. They provide sites around which preferential precipitation takes place and enhance the precipitation rate.

Other disadvantages of the wet scrubber are the reheating of the flue gas, a larger gas pressure drop requiring higher fan power requirements than the dry FGD system (below), and typically higher capital and operating costs.

The waste material from wet scrubbers is a water-logged sludge that poses difficult and costly disposal problems.

The Dry Flue-Gas Desulfurization System

Like the wet scrubber, above, the dry FGD system, also called a *dry scrubber*, utilizes an aqueous slurry of lime, CaO, to capture flue gas SO_2 by forming calcium sulfites and sulfates in spray absorbers (Fig. 17-8). The slurry in this case, however, is atomized, usually by a centrifugal atomizer, into a fine spray that promotes the chemical absorption of SO_2 and, because of the small spray particle size, is quickly dried by the hot flue gases themselves to a particulate suspension that is carried along with the desulfurized gas stream. The reaction particulates as well as those carried by the flue gases (fly ash) are then removed, mainly by a fabric filter (Sec. 17-11), before the gas is drawn by the induced-draft fan to the stack.

A major component of this system is the slurry-generating system. A "slaker" meters lime and water into an agitated tank to prepare a slaked lime slurry which, in turn, is diluted by additional water and processed to remove inert impurities called grits, which are disposed of. The lime slurry is pumped to the spray absorber with the flow controlled by the amount of SO_2 in the flue gas.

Particulates both coming in with the flue gas and generated in the FGD are collected from the absorber and fabric-filter hoppers and sent to a recycling silo for disposal or for recycling of a portion of it with the slurry (depending upon the extent of original utilization of the reactant in the absorber). The recycled slurry is enriched by an alkaline material, such as CaO, MgO, K_2O, or Na_2O.

The main advantages of the dry system are the dry, powdery nature of the waste material, which poses fewer and less costly disposal problems than the wet waste from the wet FGD system (thought these problems are still large), and the mechanical simplicity of the system.

The main disadvantage is that the efficiency of SO_2 removal is lower than that of the wet scrubber. 1979 NSPS (New Source Performance Standards) regulations, which

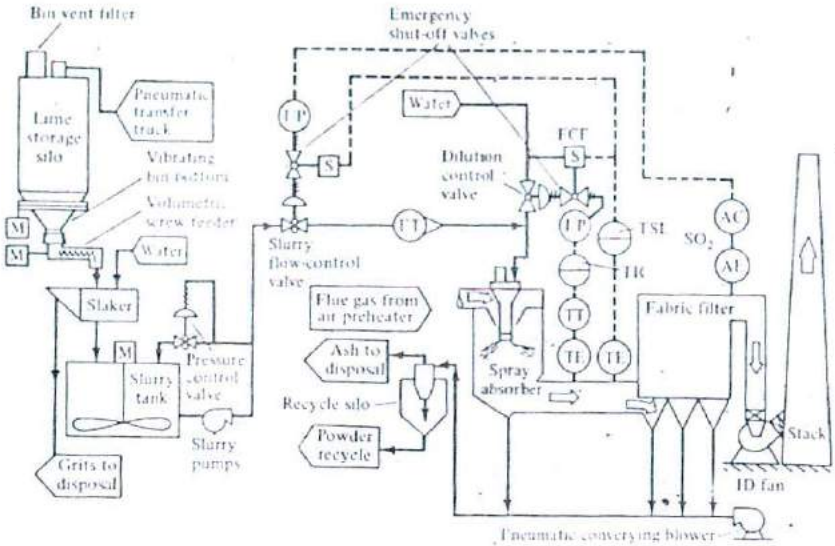


Figure 17-8 Schematic of a dry flue-gas desulfurization (FGD) system (*Electric Forum.*)

specify only 70 percent SO_2 removal in new plants, have encouraged the development of the dry system, however. Other disadvantages are the need for careful design optimization of the spray absorber and the slaker, and the strong dependence of collection efficiency on absorber outlet temperature, which necessitates operating as close as is safe to the saturation temperature that corresponds to the partial pressure of the water vapor in the gas in order to avoid condensation (below the corresponding dew point). This poses problems with filter-bag performance.

Single Alkali Scrubbing

Clear water solutions of either sodium (usually in the form of sodium hydroxide, NaOH, or sodium sulfite, Na_2SO_3) or ammonia (NH_3) are excellent absorbers of SO_2. The advantage of alkali scrubbing is that it avoids the scaling and plugging problems of slurry scrubbing by using alkaline earth. Ammonia scrubbing has the advantage that the scrubber product, ammonium sulfate, can be sold as a fertilizer, but the disadvantage that the process produces troublesome fumes.

A well-developed sodium scrubber is the *Wellman-Lord SO_2 recovery process*, which has found use in powerplants, refineries, sulfuric acid plants, and other industrial installations in the USA and Japan. The process utilizes a water solution of sodium sulfite (Na_2SO_3) for scrubbing and generates a concentrated SO_2 (about 90%), in effect removing the SO_2 gas from other flue gases.

The flue gas from fossil powerplants (or nonferrous smelters) is first pretreated

by cooling and removal of particulate matter, such as by electrostatic precipitators (Sec. 17-10), prior to being sent to the absorber (Fig. 17-9). In the absorber the water solution of sodium sulfite absorbs the SO_2 in the pretreated flue gas to produce sodium bisulfite $NaHSO_3$ according to

$$SO_2 + Na_2SO_3 + H_2O \rightarrow 2NaHSO_3 \qquad (17\text{-}5)$$

The desulfurized gas is reheated before going to the stack in order to improve atmospheric dispersion.

The sodium bisulfite is sent to a forced-circulation evaporator-crystallizer via a surge tank. The evaporator-crystallizer is the heart of the system. The surge tank allows steady flow rates into it despite gas flow and concentration fluctuations. Through the application of low-pressure steam, such as from a turbine exhaust, the sulfite is regenerated in the form of a slurry according to

$$2NaHSO_3 \rightarrow Na_2SO_3 \downarrow + SO_2 \uparrow + H_2O \qquad (17\text{-}6)$$

The H_2O is separated from the SO_2 in a condenser and recycled to a dissolving tank where the sulfite slurry is redissolved and sent back to the absorber via a solution surge tank that has the same function as the one mentioned above.

A small amount of the circulating solution oxidizes to nonregenerable sodium sulfate crystals that must be disposed of. This necessitates purging a small stream of solution and adding fresh sulfate.

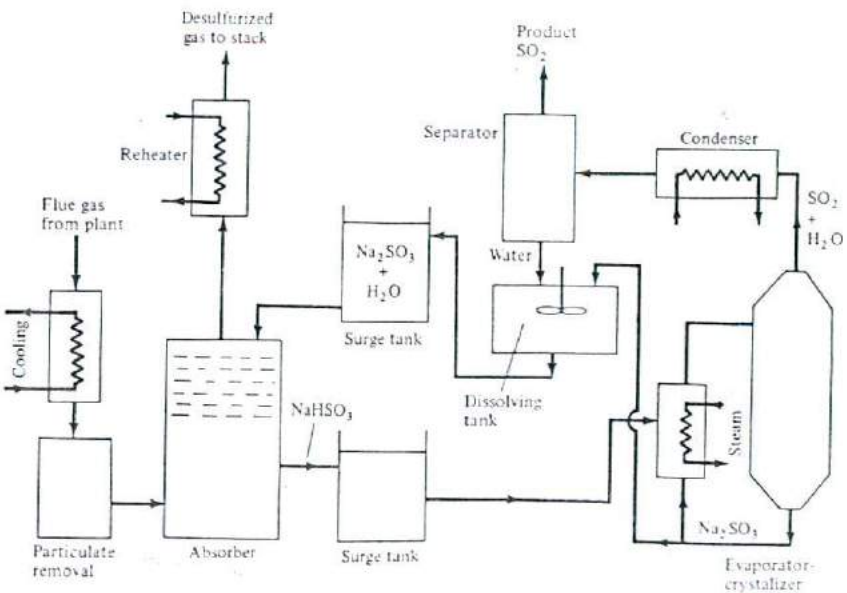


Figure 17-9 Schematic of the Wellman-Lord SO_2 recovery process.

The product SO_2 may be utilized to produce liquid SO_2 or sulfuric acid, on site or in a satellite plant, or to produce elemental sulfur. A well-known process for doing this is called the *Claus process*, which is based on the addition of H_2S according to

$$SO_2 + 2H_2S \rightarrow 3S + 2H_2O \qquad (17\text{-}7)$$

NO Removal

A process for the removal of NO, also by the addition of H_2S, is proposed. It is given by

$$NO + H_2S \rightarrow S + \frac{1}{2}N_2 + H_2O \qquad (17\text{-}8)$$

The combined removal of SO_2 and NO is under study. In both reactions, the H_2S must be completely consumed as it is a pollutant itself.

In 1977 the system was estimated to add an additional $120/kW, or some 12 to 15 percent to the base capital cost of a powerplant. It was said operating costs would increase by about $60/MBtu.

Most scrubbers in use by 1981 have been of the wet type. There is not sufficient experience with the dry type to establish which of the two may be selected by utilities in the future. Presently all scrubber systems are large and occupy a sizable area of a powerplant, have capital costs that run in the tens of millions of dollars for 500- to 1000-MW plants, and consume a sizable fraction of the gross electrical output of these plants. They also require a lot of maintenance, which results in the doubling of operation and maintenance personnel and causes, consequently, larger operation and maintenance costs. In addition, they generate huge amounts of waste that has to be disposed of. There are two types of disposal of FGD wastes: *wet disposal*, called *ponding*, and *dry disposal* in landfills, which are getting scarce. In general utilities are not always eager to build these disposal systems. Nevertheless, some 19,000 MW of FGD and sludge disposal systems were in operation, and 26,000 MW were under construction or planned, in 1981. The Electric Power Research Institute (EPRI) has published the *FGD Sludge Disposal Manual* (CS-1515 under RP1685-1), which incorporates the latest waste-disposal technology and regulations and describes how to design an environmentally acceptable waste-disposal system and the options available for processing and disposal of the wastes.

17-10 ELECTROSTATIC PRECIPITATORS

The principal components of electrostatic precipitators are *two sets of electrodes*. The first is composed of rows of electrically grounded vertical parallel plates, called the *collection electrodes*, between which the gas to be cleaned flows. The second set of electrodes are wires, called the *discharge electrodes*, that are centrally located between each pair of parallel plates (Fig. 17-10). The wires carry a unidirectional, negatively charged, high-voltage (between 20 and 100 kV, but typically 40 to 50 kV) current

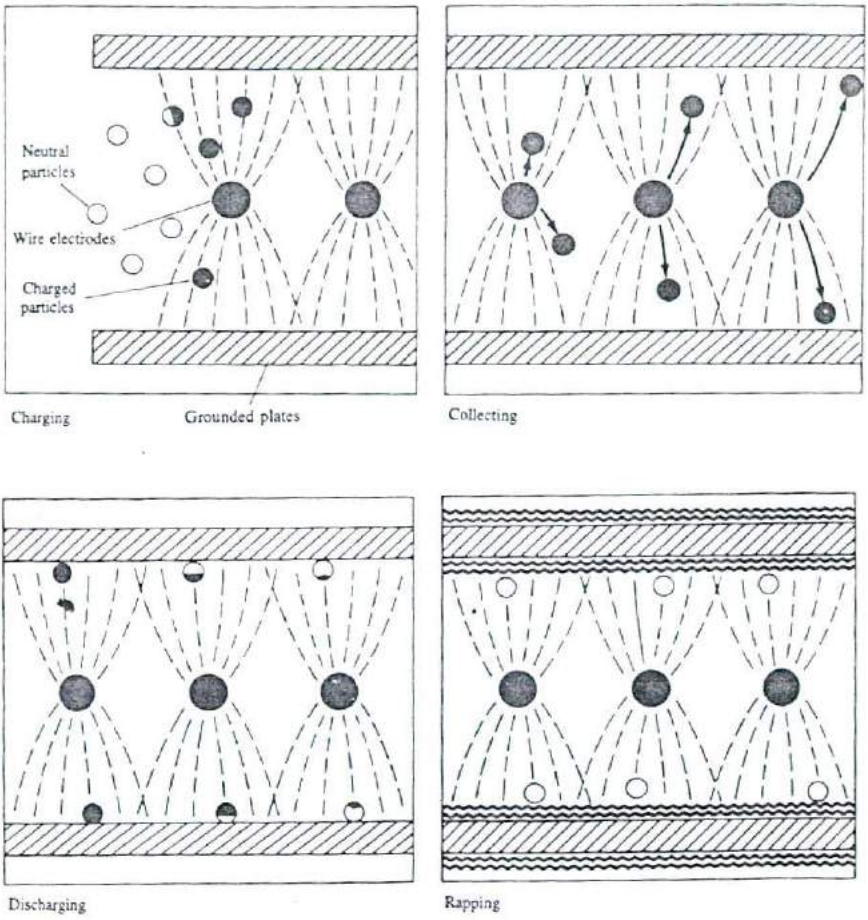


Figure 17-10 Vertical electrodes and grounded plates in an electrostatic precipitator showing four basic operations.

from an external source. The applied high voltage generates a unidirectional, nonuniform electric field whose magnitude is greatest near the discharge electrodes. When that voltage is high enough, a blue luminous glow, called a *corona*, is produced around them. The corona is an indication of the generation of negatively charged gas ions that travel from the wires to the grounded collection electrodes as a result of the strong electric field between them. This process occurs because the electrical forces in the corona accelerate the free electrons present in the gas so that they in turn ionize the gas molecules, thus forming additional electrons and positive gas ions. The new

electrons themselves create more free electrons and ions, which results in a chain reaction or avalanche of free electrons and ions.

The positive ions migrate to the negatively charged wire electrodes. The electrons follow the electric field toward the grounded electrodes, but their velocity decreases as they move away from the corona region around the wire electrodes toward the grounded plates. (A sparkover may occur if the applied voltage and the electric-field strength are high enough so that the avalanche formation of positive ions extends across the entire interelectrode space.)

The negative ions that migrate along the electric-field lines collide with the particulate matter in the gas and charge them with a negative potential. (Random thermal motion creates additional collisions that result in what is called diffusion charging.) This continues until the particles have acquired sufficient charge and migrate to the grounded electrodes due to a force that is proportional to the product of the charge and the electric-field strength. The migration velocity is dependent upon these, as well as on the particle dielectric constant, and on size, being higher the larger the particles.

A theoretical model, based on the assumption of particle Stokes' flow, which is applicable for a Reynolds number below 1, and on the absence of turbulent diffusion and other restrictions, results in the following relationship for the migration velocity of a particle of diameter d

$$V_m = \frac{2.95 \times 10^{-12} p(E/s)^2 d}{\mu_g} \tag{17-9}$$

where V_m = migration velocity m/s

p = a function of the particle dielectric constant that varies between 1.50 and 2.40 for many types of dust, with an average of 2.0

E = applied voltage, V

s = distance between charging and collecting electrodes, m

d = particle diameter, m

μ_g = gas viscosity, kg/(m · s)

Equation (17-9) shows that the migration velocity is directly proportional to the particle diameter and the square of the field strength and inversely proportional to the gas viscosity and, hence, is sensitive to changes in gas temperature because the viscosity of gases increases with temperature. Actual migration velocities may deviate considerably from those predicted by Eq. (17-9), and design values are usually based on empirical observations.

When the particles collect on the grounded plates, they are supposed to lose their charge to ground. The electrical resistivity of the particles, however, causes only partial discharging, and the retained charge contributes to forces holding the particles to the plates. Resistivities that are too high or too low pose problems. High restivity

causes retention of most of the charge, which increases the forces holding the particles to the plates and makes removal more difficult.* The maximum particle resistivity is known to occur around 300°F. This can then be corrected by operating at high gas temperatures, for instance by installing a "hot side" precipitator, upstream of the steam-generator air preheater where the gas temperature is usually in excess of 600°F. Low resistivity, found in particles with high carbon content such as fly ash from spreader stokers, causes them to lose their charge quickly to ground, and thus the forces that hold them to the plates, and to become reentrained by the flue gas. This can be corrected by increasing the holding forces by greater power input and decreasing reentrainment by designing low gas velocities, low electrode heights, and aspect ratios.

Particle Removal

When dust builds up on the plates, it deposits in a layer of increasing thickness with possible reentry into the gas stream unless it is periodically removed. This removal is done by *rapping* the plates to cause shock vibrations that shake the dust into hoppers at the bottom of the precipitator. Properly controlled and timed removal is critical for precipitator performance. The intensity and frequency of rapping of individual collection plates varies from the inlet to the outlet of the precipitator to suit the changing characteristics and collection rates of the dust. It is also customary to rap sequentially so that only a fraction of the accumulated dust is disturbed at any one time. A rapper device is used. It contains a vertical plunger that strikes the collection electrode support system to deliver the necessary shock wave and then returns back to its top position to prepare for the next strike. In one design the downward impact motion is effected by an electromagnetic coil and the return by a spring. In another the plunger is heavier, the impact is by gravity, and the return is by an electromagnet.

The length of the precipitator passage in the direction of gas flow that is necessary to remove a given particle size is obtained by seeing to it that the time required for the particle to migrate to the collection electrode has to be less than the time it takes it to pass through the precipitator at the same velocity as the gas. Neglecting the charging time, the required length would be given by

$$\frac{s}{V_m} \leq \frac{L}{V_g}$$

or

$$L \geq s \frac{V_g}{V_m} \tag{17-10}$$

where

L = length of passage, m or ft

V_g = gas velocity, m/s or ft/s

* High resistivity may also cause the electric field in the dust layer to accelerate electrons sufficiently to produce positive ions, thus reducing the voltage at which sparkover occurs. It may also generate enough positive ions even when voltage is not high enough for sparkover, the result being a *back corona* that neutralizes the unidirectional field. These effects reduce or completely disrupt precipitator performance.

Collection Efficiencies

An electrostatic precipitator, and all other particle-collection devices, has an *efficiency*, already mentioned in Sec. 17-8. The *overall collection efficiency* η_o is given by

$$\eta_o = \frac{\text{mass or concentration of all particles retained by collector}}{\text{mass or concentration of all particles entering collector}} \quad (17\text{-}11)$$

Although the relationships in Eqs. (17-9) and (17-10) are based on highly idealized models, the trends they predict are applicable to the real case. Thus, because the migration velocity V_m is greater for large particles, the length of passage necessary to remove them is smaller. In other words, it is easier to collect larger particles than smaller particles. There is, therefore, a *fractional collection efficiency* η_d (also called the *grade efficiency*) that is given by

$$\eta_d = \frac{\text{mass or concentration of particles of a given size retained by collector}}{\text{mass or concentration of particles of a same size entering collector}} \quad (17\text{-}12)$$

From Eq. (17-12) it can be expected that η_d increases with size of diameter d. η_d is also expected to increase with electrode area and decrease with the flue-gas volume flow rate. Several relationships have been proposed for η_d. A well known one is the *Deutsch expression*, which is derived from physical or probability considerations [174,175]

$$\eta_d = 1 - e^{-(AV_m/Q)} \quad (17\text{-}13)$$

where A = area of collector electrodes, m^2 or ft^2

V_m = migration velocity, m/s or ft/s

Q = flue-gas volume flow rate for each plate, m^3/s or ft^3/s

Example 17-1 Plot the Deutsch fractional efficiency for an electrostatic precipitator that has plates with height × width of 10 × 10 m, and a spacing of 25 cm. The applied voltage is 50,000 V. The mean flue-gas temperature and velocity between plates are 300°C and 1.5 m/s, respectively. Repeat for plate dimensions of 10 × 15 m and 10 × 5 m.

SOLUTION Refer to Eq. (17-9) and use $p = 2.0$, $s = 0.25/2 = 0.125$ m, and $\mu_g = 2.93 \times 10^{-5}$ kg/(m · s)

$$V_m = \frac{2.95 \times 10^{-12} \times 2 \times (50{,}000/0.125)^2 d}{2.93 \times 10^{-5}} = 3.225 \times 10^4 d$$

Refer to Eq. (17-13) and use

$$Q = V_g \times \text{cross-sectional area of flow per plate side}$$

$$= 1.5 \times 10 \times 0.25 \times \frac{1}{2} = 1.875 \text{ m}^3/\text{s}$$

$$A = 10 \times 10 = 100 \text{ m}^2$$

Therefore

$$\eta_d = 1 - e^{-\left(\frac{100 \times 3.255 \times 10^5}{1875}\right)d} = 1 - e^{-1.72 \times 10^5 d}$$

Similarly, for 10 × 15 m and 10 × 5 m plates

$$\eta_d = 1 - e^{-2.58 \times 10^5 d} \quad \text{and} \quad 1 - e^{-0.86 \times 10^5 d}$$

respectively.

η_d is plotted in Fig. 17-6 as a function of d in micrometers (μm). It can be seen that the plates with the larger path length are more efficient, that η_d is essentially 100 percent for particle sizes beyond 3 μm, and that the efficiency drops drastically for small particles. This is not in accordance with practical experience, from which measurements in many precipitators show a turnaround in fractional efficiency for very fine particles in the submicron range, with minimum efficiencies occurring in the 0.1 to 0.5 μm range and efficiencies going back to 90 to 95 percent below 0.1 μm.

The Deutsch equation is now recommended for use in estimating the operation of a precipitator at off-design conditions. In this case a value V_{m_o} is obtained from experimental studies under different operating conditions and used in lieu of V_m, resulting in an overall collection efficiency η_o. V_{m_o} is known as the *effective migration velocity*. Thus

$$\eta_o = 1 - e^{-(AV_{m_o}/Q)} \tag{17-14}$$

Equation (17-14) may now be used to estimate the effect of *changes* in volume flow rate Q (representing changes in plant load) on η_o, or, for the same V_{m_o}, the effect of changes in precipitator design A.

Attempts to arrive at equations more representative of modern high-efficiency precipitator designs [176] are being attempted. Two current ones are

$$\eta_o = 1 - e^{-(AV_{m_o}/Q)^x} \tag{17-15}$$

where x is a variable, fitting most data at a value of about 0.5, and

$$\eta_o = 1 - \left(1 + \frac{AV_{m_o}}{nQ}\right)^{-n} \tag{17-16}$$

where n is a variable, fitting most data in a range between 3 and 5 (but can vary between 2 to 8). Putting $n = \infty$ reverts Eq. (17-16) back to the Deutsch equation. In both equations above, V_{m_o} is the effective migration or drift velocity. For utility fly ash its value can vary between 4 and 20 cm/s.

Figure 17-11 shows an electrostatic precipitator used to clean flue gases from an electric-generating powerplant.

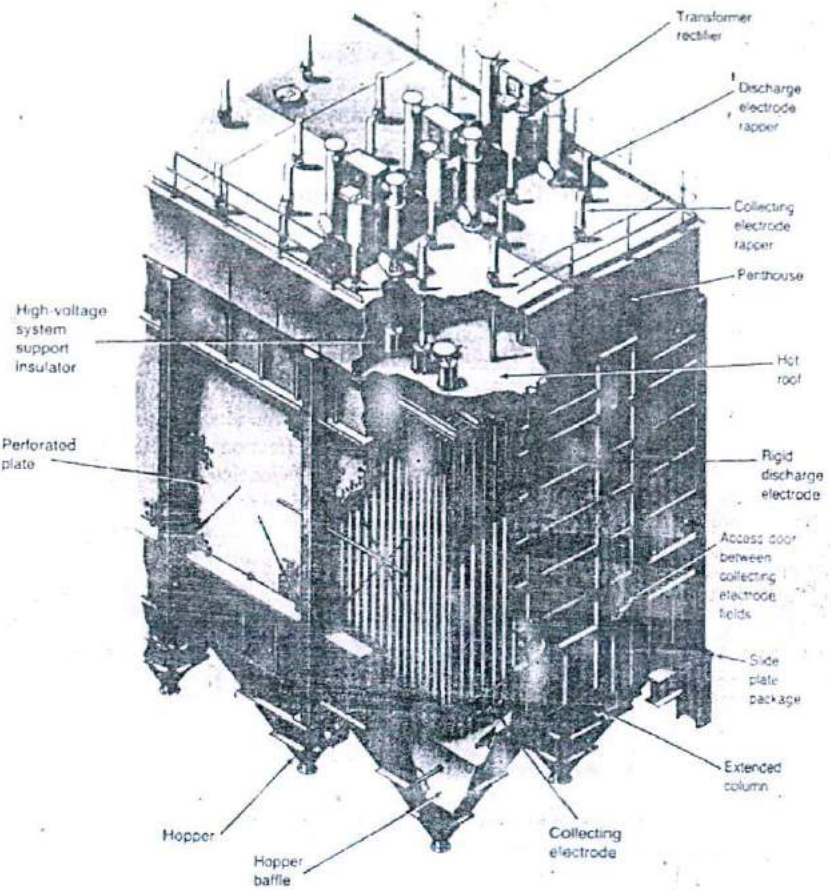


Figure 17-11 An electrostatic precipitator. *(Courtesy Research-Cottrell, Somerville, New Jersey.)*

17-11 FABRIC FILTERS AND BAGHOUSES

Fabric filters are used in powerplants to remove dust particles from a gas stream on a principle similar to that of a household vacuum cleaner except, of course, that the size of fabric filters is far greater. They are made of porous material that retains particulate matter as the carrier gas passes through the voids.

A fabric-filter element is usually made in the form of a long, hollow cylindrical tube that provides a large surface per unit of gas volumetric flow rate. The inverse of this parameter, called the *air-to-cloth*, or *filtering, ratio*, is equal to the superficial gas

velocity; i.e., it is based on the surface area rather than the void flow area within the fabric. It ranges typically between 0.5 to 4.0 cm/s.

A fabric-filter system usually contains a large number of vertical cylindrical fabric-filter elements arranged in parallel rows. Such a system is called a *baghouse* (Fig. 17-12). A powerplant baghouse might contain several thousand such cylinders, each ranging in diameter from 5 to 14 in and in height up to 40 ft. The exact number is determined by their size, the required total capacity, plus an additional number to allow for shutdown of portions of the baghouse for cleaning with the plant on load. This points to one disadvantage of baghouses: their size is large in comparison with other types of particulate-removal systems.

In general, the elements have an open bottom and closed top. They rest on a tube sheet above a dirty-air plenum. The sheet distributes the gas evenly to the bags, allowing it to enter the elements at bottom, deposit its particulate matter on the inside of the

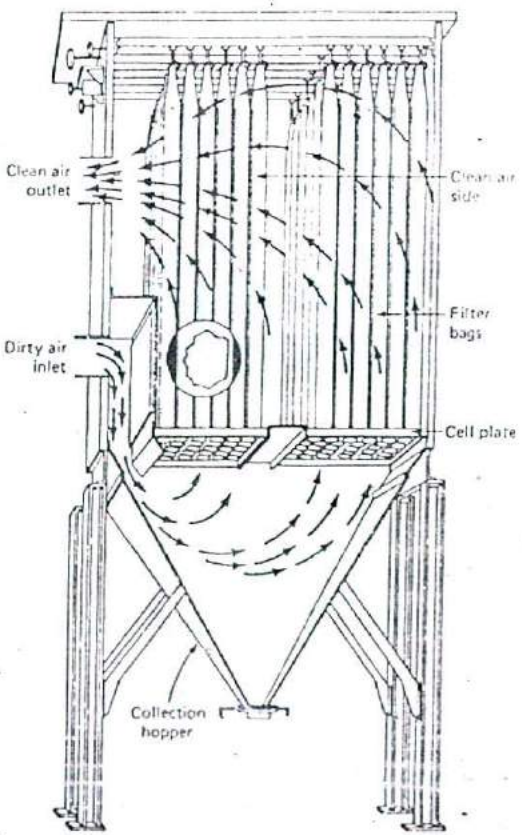


Figure 17-12 Typical baghouse with mechanical shakers. (*Courtesy Wheelabrator Frye, Inc., Mishawaka, Ind.*)

tubes, and pass laterally through the fabric and exit to an outlet manifold where it is drawn out by the plant induced-draft fan.

Collection hoppers, below the tube sheets, are receptacles for collecting the removed particulate matter. This matter usually collects on the inside of the elements in the form of a dust cake that must be made to fall down to the hopper by some means. Such means include mechanical shaking, pulse jets, or reverse airflow.

Mechanical shaking is accomplished by oscillating or vibrating rods attached to the top of the filter elements (Fig. 17-13). The oscillations ripple the bag surfaces, breaking the dust cake and causing it to discharge into the hopper below.

In *pulse-jet* cleaning, the bags are hung from the top, normal flue-gas flow is from the outside in, and dust collects on the outside of the tubes. For cleaning, short pulses of compressed clean air are forced down into the bags through venturis at the top. The pulse fractures and dislodges the dust, which falls to the hopper. The bags in this system are usually shorter than other types (less than 15 ft) to allow for proper cleaning of the tube bottoms.

Most coal-fired powerplant baghouses utilize the *reverse-air method* of cleaning. In reverse-air baghouses, an auxiliary fan forces clean air through a flapper valve into the clean-air plenum of the portion of the baghouse that is shut off for cleaning. This air passes through the filter elements in a reverse direction, from the outside in, resulting in a "backwash" action that collapses the bag and fractures the dust cake. When the bag is brought back on line, it reinflates and dislodges the fractured dust cake, which falls into the hopper. Some designs do away with the auxiliary fan and rely upon the natural collapse and reinflation of the bags due to the loss of vacuum when the clean-air plenum is shut off from the induced-draft fan, and then by returning back on line.

Cleaning may be periodic, which requires shutdown of portions of the baghouse, as explained for the reverse-air system, or continuous, i.e., done on load. Continuous

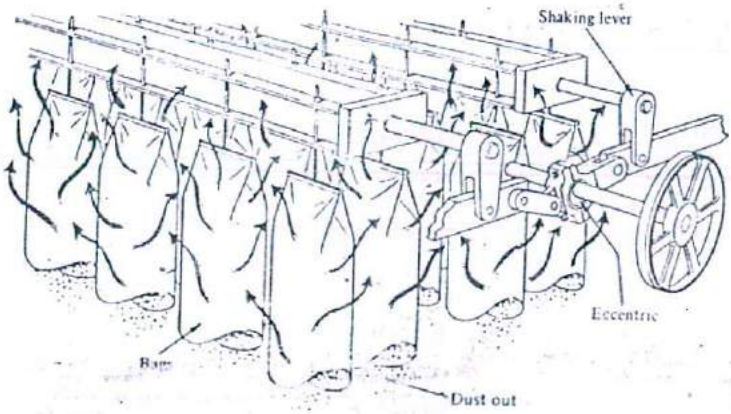


Figure 17-13 Shaker mechanism for the tubular filters of a baghouse. *(Courtesy Western Precipitation Division, Joy Manufacturing Company, Los Angeles, Calif.)*

cleaning is possible with the pulse-jet system because the duration of the pulse is very short.

The bag filter material can fail as a result of high temperature, burning, caking, erosion, chemical attack, and aging. A variety of fabrics have been used, depending upon the type of particulates and flue-gas composition, humidity, and temperature. They include wool, cotton, nylon, glass fiber, polyesters (such as dacron), and aromatic polyamides [177]. Wool and cotton, on one end of the scale, can operate only with low gas temperatures, up to about 175 or 200°F. Glass fibers, at the other end, tolerate high gas temperatures, up to 500 to 550°F. Research is continuing to find fibers that can withstand temperatures beyond 550°F to avoid precooling of the flue gases before they enter the baghouse. A baghouse is usually placed after the air preheater, which has a flue-gas outlet temperature of 300°F or more. High gas temperatures also mean high volume flow rates through the elements. Gas cooling below its dew point, which depends upon the water vapor mole fraction, results in condensation, which is not permissible with fabric filters.

Chemical attack of the fabric is particularly severe with high-sulfur coals. With the shift by many utilities to low-sulfur, high-ash coals, fabric filters have become increasingly attractive in comparison with other particulate-removal systems, such as electrostatic precipitators. Their performance is also less dependent on fuel and flue-gas characteristics, and they have fewer critical design parameters.

Figure 17-14 shows a baghouse of the type used to clean flue gases from fossil-fuel powerplants.

17-12 THERMAL POLLUTION

All thermal powerplants (fossil, nuclear, solar) reject low-availability or low-temperature heat to the environment. A comparison of the amounts of heat rejected by powerplants of different efficiencies should be based on their output, not the heat added. Thus

$$\eta = \frac{W}{Q_A} = \frac{W}{W + Q_R} = \frac{1}{1 + (Q_R/W)} \tag{17-17a}$$

or

$$\frac{Q_R}{W} = \frac{1}{\eta} - 1 \tag{17-17b}$$

where η = plant net thermal efficiency

W = plant net output

Q_A = heat added

Q_R = heat rejected

For plants of 1000-MW output, the heat added, and the heat rejected, in MW, are given as a function of efficiency in Table 17-9. Thus an increase in thermal efficiency of 10 percent, from 30 to 40, results in a reduction in heat rejected of 35.7 percent,

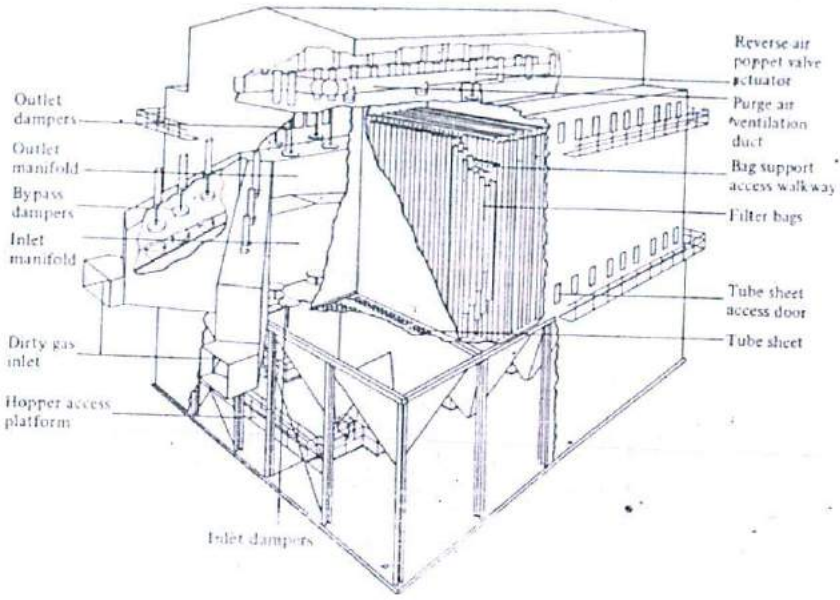


Figure 17-14 A baghouse. *(Courtesy Western Precipitation Division, Joy Manufacturing Company, Los Angeles, Calif.)*

from 2333 to 1500 MW. It can be seen that efficiency has a pronounced effect on heat rejected, greater than the change in its own value.

Because most modern thermal powerplants have efficiencies below 50 percent, actually in the 30 to 40 percent efficiency range, the amount of heat rejected is greater than the plant output. These very large amounts of heat are added to and affect the environment, and because they are mostly added to bodies of water they affect the aquatic ecological system.

The heat rejected in Rankine-cycle type powerplants is usually done via the cooling water of the condenser. The condenser is part of a once-through circulating-water system (the most common) or a closed system (Chap. 7). In the once-through system

Table 17-9 Heat added and rejected, MW, by plants producing 1000 MW, as a function of plant thermal efficiency

Thermal efficiency, %	10	20	25	30	33.3	40	50	60
Plant output W, MW	1,000	1000	1000	1000	1000	1000	1000	1000
Heat added Q_A, MW	10,000	5000	4000	3333	3000	2500	2000	1667
Heat rejected Q_R, MW	9,000	4000	3000	2333	2000	1500	1000	667

large amounts of relatively cool water are taken from the environment, passed through the condenser, and discharged at a higher temperature back to the environment. In the closed system only enough water is drawn from the environment to replace the condenser cooling water that is lost, usually by evaporation in a cooling tower or a cooling pond.

Once-Through Systems

In the case of the once-through system, two effects are of concern. The first is the effect of heat on the large volumes of water as it goes through the condenser cooling system. The second is the effect of discharging the same but now warm water on the lake or stream it originated from. A 1000-MW powerplant, depending upon its thermal efficiency, needs between 250×10^6 to 400×10^6 lb_m/h of condenser cooling water. This corresponds to about 65,000 to 100,000 ft^3/min, or about 30 to 50 m^3/s.

Water in a lake or a stream is a habitat for numerous species of animal and plant life. A good intake system must therefore be designed to screen out these organisms. Nevertheless, simple screens still let through small organisms such as fish eggs, larvae, and plankton. And some larger fish, unable to escape because of the speed and volume of intake water flow, impinge and accumulate on the screens along with other debris from the lake or stream, thus requiring frequent cleaning of the intake screens. A method conceived to minimize impingement and entrainment is the use of a *porous dike* upstream of the intake screen. Built of suitably sized rocks, it slows the speed of water at intake so that small fish are not easily drawn toward the intake screen.

The organisms that do filter through the screens pass through pumps, pipes, hot condenser tubes, and other cooling-water system components before being discharged back to the lake or stream. In this path, they are subjected to buffeting, pressure, and heat, resulting in a high mortality rate. The ecosystem is said to be "stressed." Some ecological studies, however, indicate that ecosystems, like populations, have a natural resilience to compensate for adverse impacts on small parts of the whole.

From an engineering point of view, these organisms, dead or alive, clog filters, pipes, and pumps. Furthermore, bacterial slime and algae grow rapidly on the inside surfaces of the tubes, a condition known as *bifouling*. This is usually accompanied by *scaling*, which is caused by corrosion and the deposition of suspended solids in the water on the same surfaces. Bifouling and scaling reduce the bore of the condenser tubes, reduce heat transfer, and thus reduce condenser effectiveness, which in turn raises the back pressure on the turbine and thus reduces plant efficiency. In addition, these conditions increase pressure drops and pumping power in the circulating-water system, further reducing plant net output.

Bifouling and scaling can be combatted by frequent applications of chemicals such as chlorine. But chlorine and its compounds are discharged with the cooling water and are potentially harmful to the ecosystem.* In severe cases, condenser tubes are cleaned by mechanical means that require costly plant shutdowns.

* The Ocean Water Act of 1977, which mandates that electric utilities change their cooling systems to the "best available technology," requires them to limit the use of chlorine.

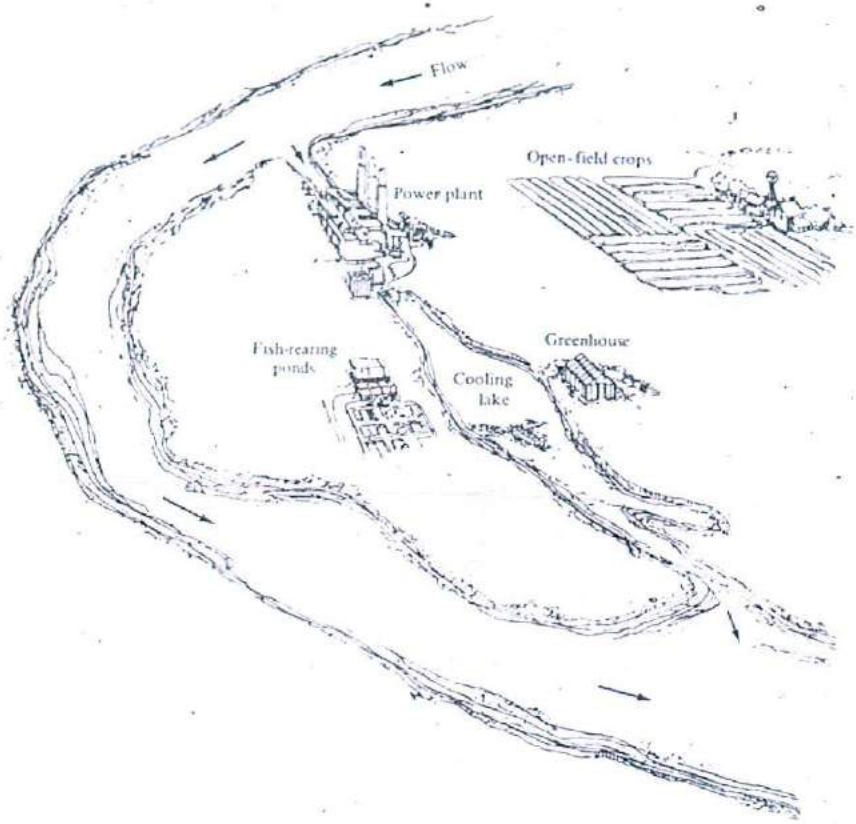


Figure 17-15 Warm cooling water from a powerplant used in fish hatcheries, greenhouses, and open agricultural fields before passing through a cooling lake on its way back to the main river. (*Reprinted from the EPRI Journal.*)

The warm water discharged in a once-through cooling system is some 20 to 25°F (11 to 14°C) above intake. The effect of this on the ecosystem depends upon the plant site, whether the plant is situated on a river, lake, estuary, or ocean, as well as on the workings of the aquatic world it is having an impact upon. Studies of flora and fauna,* necessary to understand the problem completely, are not simple and are time-consuming. Examples are fish spawning and migration patterns, especially in estuaries and sheltered coastal areas where environmental disturbances can cause great damage, the effect of small concentrations of chlorine on various species of aquatic life, etc.

* Plants and animals. In classic mythology: Flora is the goddess of flowers; Fauna is a Roman goddess, the sister of Faunus, the god of nature and patron of farming and animals.

Warm-water discharges in large volumes were once suspected of causing major ecological damage. It has, however, been recently demonstated that with good planning and management, warm water can be beneficial. It can for example be used to boost fish production in hatcheries (Fig. 17-15). (Commercial operations are already under way; an example is the Long Island Oyster Farm, operated in conjunction with the Long Island Lighting Company plant in Northport, New York.) It can also be used in agriculture, where it has been found to increase materially the production in greenhouses and open fields in cold climates. (An example is an agricultural facility operated in conjunction with the Northern States Power Company plant in Sherburne County, Minnesota.) Long-range economic questions, however, arise as to the relative gains from increased agricultural production versus costs of constructing the facilities, pumping the water, etc.

Closed Systems

Closed systems take in only sufficient water to make up for losses by evaporation from cooling towers, ponds, etc. They use corrosion-inhibiting additives with the cooling water. The systems are periodically flushed out, which releases these additives to the body of water on which the plant is situated, thus resulting in water pollution.

In general it is believed that fish mortality caused by powerplants is insignificant when compared with their natural mortality rate. It is also a fact that aquatic life is resilient and compensates naturally for the decrease in its population by producing more young or by increasing the survival rate of the normal number of young population, although this compensation is not always automatic and requires further study. Finally, an assessment should take into consideration the relative benefits of supplying the electric energy needed for the welfare of humankind and the loss, regrettable as it is, of an insignificant quantity of aquatic life, especially when the plant sites are chosen with care.

17-13 NATURAL AND ARTIFICIAL RADIOACTIVITY

Just like gaseous and particulate matter, which are caused by both natural and artificial events, radioactivity or radiation* in the environment is also caused by both natural and human-generated events. Of all environmental radioactivity, the portion contributed by nuclear powerplants in normal operation is miniscule. The history of nuclear-powerplant operation strongly suggests that even with abnormal operation (accidents), that portion is still insignificant. This suggests that the crisis atmosphere periodically generated by opposition to nuclear powerplants on this issue is largely unjustified.

Natural radioactivity has *always* been present. It comes from the sun and outer-

* The term *radiation* is a broad term that includes light (electromagnetic) and radio waves. However, it is often used to mean *radioactive* or *ionizing radiation*, which can present a health hazard. It will be used in the latter sense in this section.

space; it exists in numerous earth materials and in food, water, and air. It is generated by natural eruptions and volcanoes. It even exists within our own bodies; the human body contains about 0.35 percent (by mass) potassium, of which 0.0118 percent is radioactive potassium 40. The total of these is often called *natural background radiation*. Its level varies widely from location to location around the earth but averages about two-thirds of all radiation present.

It is instructive here to compare a natural occurrence with a human-made abnormal one. These are the eruptions from Mount St. Helens in the state of Washington, USA, that first erupted in May 1980, and the March 1979 accident at Three Mile Island nuclear powerplant unit No. 2 (TMI-2). The President's commission to investigate TMI-2, the Kemeny Commission, estimated in its report [178] that a total of about 2.5 million curies (Ci) of noble gases, mostly xenon, were released over the course of the accident. On the other hand, an extensive study by Battelle Pacific Northwest Laboratories of the ash from Mount St. Helens estimates that up to 3 million Ci of radon gas were released in the eruption of one day, May 18, alone.

Both xenon and radon are noble gases that are chemically and biologically inert. The difference, however, is that radon decays to a series of radioactive daughter elements that are chemically and biologically active. Thus the radioactive release from Mount St. Helens due to the gases alone is much more significant than that from TMI-2. In addition, the ash from the eruption at Mount St. Helens that spread over vast areas of the state of Washington and beyond was found to contain significant radioactivity from isotopes such as radium 226, potassium 40, thorium 232, polonium 210, and lead 214. Newly fallen ash was also found to contain rather high concentrations of the short-lived radon daughters lead 214, bismuth 214, and polonium 214. Note also that Mount St. Helens has erupted with varying intensity several times since May 1980.

Of the artificial sources of radioactivity we are subjected to, medical irradiations (x-rays, etc.) account for the largest portion, about 30 percent of the total. Occupational exposures, fallout from nuclear weapons tests, and miscellaneous sources (such as high-altitude flying) account for less than 1 percent each. Releases from the nuclear-power industry, including fuel manufacturing and reprocessing and powerplant emissions, account for some 0.15 percent of the total (Table 17-2).

Both natural and artificially generated radiations may be classified as particles and electromagnetic radiation. The particles include beta (β) or ${}_{-1}e^{0}$ (electrons in a free state); alpha (α) or ${}_{2}He^{4}$ (helium nuclei); as well as positrons ${}_{+1}e^{0}$ (positively charged β); neutrons, n; protons, p or ${}_{1}H^{1}$; tritons, ${}_{1}H^{3}$; and fission products. The electromagnetic radiation includes gamma (γ) rays, x-rays, and Bremsstrahlung. Examples of radioactive reactions (or disintegrations) that cause these radiations are:

Beta:
$$ {}_{19}K^{40} \xrightarrow{1.28 \times 10^{9}\ \text{years}} {}_{20}C^{40} + {}_{-1}e^{0} \qquad (17\text{-}18) $$

$$ {}_{6}C^{14} \xrightarrow{5730\ \text{years}} {}_{7}N^{14} + {}_{-1}e^{0} \qquad (17\text{-}19) $$

Alpha:
$$ {}_{94}Pu^{239} \xrightarrow{24{,}000\ \text{years}} {}_{92}U^{235} + {}_{2}He^{4} \qquad (17\text{-}20) $$

$$_{88}Ra^{226} \xrightarrow{1600\ \text{years}} {}_{86}Rn^{222} + {}_{2}He^{4} \qquad (17\text{-}21)$$

$$\text{Positron: } {}_{15}P^{30} \xrightarrow{2.5\ \text{min}} {}_{14}Si^{30} + {}_{+1}e^{0} \qquad (17\text{-}22)$$

$$\text{Neutron: } {}_{54}Xe^{137} \xrightarrow{3.9\ \text{min}} {}_{54}Xe^{136} + {}_{0}n^{1} \qquad (17\text{-}23)$$

The original isotope is often called the *parent*. The first isotope on the right-hand side is called the *daughter*. The emitted particle is the radiation. (Gamma decay by itself does not alter the isotope, only its energy level, however γ rays often accompany other radiations.) The daughter may be stable or radioactive; if radioactive, it in turn decays, resulting in a radioactive chain, sometimes of considerable length. The half-life of each parent, shown above the arrows, is defined as the time during which one-half of the original parent nuclei decays and one-half is left. One-quarter is left after two half lives, one-eighth after three, etc. (Sec. 9-8).

The Curie

A radiation dose means that a person has been exposed to and has absorbed some radiaton energy. Radiation has both quality and quantity. The quantitative physical unit of radioactivity is the *curie*, Ci (and its fractions millicurie, mCi; picocurie, pCi, 10^{-12} Ci, etc.). 1 Ci = 3.70×10^{10} disintegrations per second. The number of curies emitted by a radioisotope depends upon both its mass and its half-life.

Example 17-2 Compute the activity in disintegrations per second of 1 g of radium 226. Ra^{226} has an atomic mass of 225.0245. It decays into radon gas with the emission of α particles, with a half life $\theta_{\frac{1}{2}}$ = 1600 year = 5.049×10^{10} s.

SOLUTION Initial number of atoms of Ra^{226} in 1 g is

$$N_o = \frac{\text{Avogardro's number}}{\text{atomic mass}}$$

$$= \frac{6.0225 \times 10^{23}}{226.0245} = 2.6645 \times 10^{21}$$

$$\text{Decay constant } \lambda = \frac{0.6931}{\theta_{\frac{1}{2}}} = \frac{0.6931}{5.049 \times 10^{10}} = 1.3727 \times 10^{-11}\ \text{s}^{-1}$$

$$\text{Activity} = \lambda N_o = \lambda \frac{0.6931}{\theta_{\frac{1}{2}}} = 1.3727 \times 10^{-11}$$

$$\times\ 2.6645 \times 10^{21} = 3.6576 \times 10^{10}\ \text{dis/s}$$

This activity is small compared with the initial number of atoms. The activity of radium may thus be considered constant, a true phenomenon for any radioactive species with a long half-life. Early measurements of radioactivity indicated that 1 g of radium

had an activity of 3.70×10^{10} dis/s instead of the more accurate value given above. 3.7×10^{10} was, and still is, adopted as the numerical value for the curie. A curie is also used to indicate the quantity of any isotope having 1 Ci of radioactivity.

The Rad and the Gray

While the curie is a physical quantitative unit that indicates the number of radioactive events or disintegrations, it must be recognized that different radioisotopes emit different radiations with different energies. A more significant unit from the point of view of biological effect is the *rad*. The rad is a unit of radiation *energy* absorbed. 1 rad = 0.01 J/kg (4.3×10^{-6} Btu/lb_m), 1 millirad = mrad = 0.00001 J/kg. Some higher-than-average natural background levels, measured in mrad/year, emanate from monazite sand in Egypt (220 to 475), some beaches in Rio de Janeiro, Brazil (550 to 1250), the city of Kerala, India (800 to 8000), granite areas in Sri Lanka (3000 to 7000), and others. The rad is now being replaced by another unit in the SI system of units, called the *gray* (symbol Gy). 1 Gy = 1 J/kg = 100 rad.

The Rem and the Sievert

The biological effect of radiation on human beings must further take into account not only the total energy absorbed but also the relative biological effects of different types of ionizing radiation on people, such as the number of cells damaged by this radiation. Thus the rad is multiplied by a factor called the *relative biological effectiveness* (RBE), also called the *quality factor Q*, to obtain a more meaningful unit called the *rem*, for *roentgen equivalent man* (a millirem, *mrem*, is one-thousandth of a rem). Thus

$$1 \text{ rem} = 1 \text{ rad} \times \text{RBE} \tag{17-24}$$

some RBE values are 0.6 for 4-MeV gamma rays, 1.4 for 1-MeV electrons, 4 to 5 for thermal neutrons, and 2 to 10 for 1-MeV neutrons. These values are relative, based on an RBE for 200 kVp x-rays equal to 1. In the SI system of units, Gy replaces the rad, and therefore a new unit called the *sievert* (symbol Sv) replaces the rem. 1 Sv = 100 rem.

In addition, the rate at which the radiation is received is important. An analogy here may be made with drinking liquids. Some drinks are more harmful to health than others. A small quantity of a potentially harmful drink may not be harmful. A large quantity, say taken in the course of one evening, is. However, that same quantity would not be harmful if taken over a long period of time, say weeks. Thus the rate, mrem/h or mrem/year, is also important. Table 17-10 lists some examples of doses and dose rates we are exposed to in our normal lives.

Radiation effects are a complex subject. A complete treatment is beyond the scope of this text. They are, however, covered in the next sections where appropriate. For a fuller treatment, the reader is referred to specialized books on radiation and on health physics [179–184].

Table 17-10 Some common doses and dose rates of radioactivity

Source	Dose, mrem	Dose rate, mrem/year
1 diagnostic x-ray	20	
1 transatlantic flight	2	
Cosmic rays		45
Soil		15
Food, water, and air		25
Brick house		50–100
Concrete house		70–100
Wooden house		30–50
TV set		1–10
Living in the vicinity of a nuclear powerplant		1
Average background:		
New York		100
London		100
Paris		120
Denver		125
Kerala, India		400

17-14 NUCLEAR POWER AND THE ENVIRONMENT

In the United States, and doubtless in almost all countries constructing nuclear powerplants, federal licensing proceedings for each plant require the inclusion of detailed environmental statements to be issued as public documents. In the United States, these should be in accordance with the National Environmental Policy Act of 1969 (NEPA). Such statements must assess not only the impact upon the environment that is associated with the construction and the operation of the powerplant, but also the effect of the transportation of radioactive materials to and from that plant.

Besides thermal pollution (Sec. 17-12) which it shares with almost all types of powerplants, nuclear power's effects on the environment stem mainly from (1) the nuclear fuel cycle, (2) low-level dose radiations from nuclear-powerplant effluents, and (3) low- and high-level dose radiations from wastes.

The Fuel Cycle

Most nuclear powerplants in operation or under construction in the world today are using, and will continue to use for the near future, ordinary (light) water cooled and moderated reactors: the pressurized-water reactor (PWR) (Sec. 10-2) and the boiling-water reactor (BWR) (Sec. 10-7). A small number use the heavy water cooled and moderated reactor (PHWR) (Sec. 10-14). The expectations are that the fast-breeder reactor powerplant (Chap. 11) and perhaps an improved version of the gas-cooled

reactor powerplant (Sec. 8-11) will come on line in increasing numbers in the twenty-first century. Almost all current water reactors use slightly enriched uranium dioxide, UO_2, fuel. The fuel has to go through a cycle that includes prereactor preparation, called the *front end*, in-reactor use, and postreactor management, called the *back end*. A typical fuel cycle may or may not incorporate fuel reprocessing in the back end (Fig. 17-16). The different processes are briefly explained below.

1. *Mining* of the uranium ore.
2. *Milling* and *refining* of the ore to produce uranium concentrates, U_3O_8.
3. *Processing* to produce of uranium hexafluoride, UF_6, from the uranium concentrates. This provides feed for isotopic (U^{235}) enrichment.
4. Isotopic *enrichment* of uranium hexafluoride to reach reactor enrichment requirements. This is done invariably now by the gaseous diffusion process.
5. *Fabrication* of the reactor fuel elements. This includes conversion of uranium hexafluoride to uranium dioxide UO_2, pelletizing, encapsulating in rods, and assembling the fuel rods into subassemblies.
6. *Power generation* in the reactor, resulting in *irradiated* or *spent* fuel.
7. *Short-term storage* of the spent fuel.
8. *Reprocessing* of the irradiated fuel and *conversion* of the residual uranium to uranium hexafluoride, UF_6 (for recycling through the gaseous diffusion plant for reenrichment) and/or extraction of Pu^{239} (converted from U^{238}) for recycling to the fuel-fabrication plant. Reprocessing can reuse up to 96 percent of the original material in the irradiated fuel with 4 percent actually becoming waste.
9. *Waste management*, which includes long-term storage of high-level wastes.

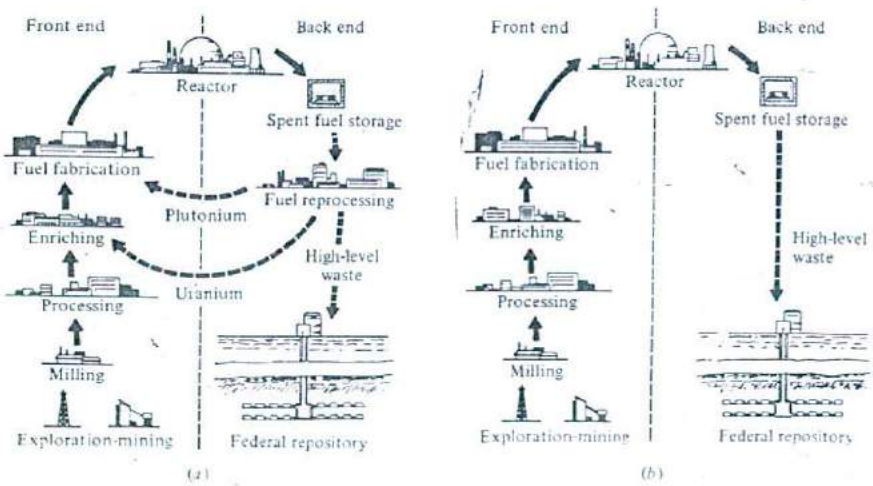


Figure 17-16 A typical nuclear fuel cycle (*a*) with reprocessing and (*b*) without reprocessing [186].

Step 8, reprocessing, may be bypassed, which results in disposal of both reusable fuel and wastes. This is the current (1982) U.S. Department of Energy process for dealing with irradiated fuel. The fuel assemblies are stored for at least 10 years and then buried. This is the so-called *throw-away* fuel cycle (Fig. 17-16*b*).

Wastes

The wastes associated with nuclear power can be summarized as:

1. *Gaseous effluents.* Under normal operation, these are released slowly from the powerplants into the biosphere and become diluted and dispersed harmlessly.
2. *Uranium mine and mill tailings. Tailings* are residues from uranium mining and milling operations. They contain low concentrations of naturally occurring radioactive materials. They are generated in large volumes and are stored at the mine or mill sites.
3. *Low-level wastes (LLW).* These are classified as wastes that contain less than 10 nCi (nanocuries) per gram of transuranium contaminants and that have low but potentially hazardous concentrations of radioactive materials. They are generated in almost all activities (power generation, medical, industrial, etc.) that involve radioactive materials, require little or no shielding, and are usually disposed of in liquid form by shallow land burial (Fig. 17-17).
4. *High-level wastes (HLW).* These are generated in the reprocessing of spent fuel. They contain essentially all the fission products and most of the transuranium elements not separated during reprocessing. Such wastes are to be disposed of carefully (Sec. 17-16).
5. *Spent fuel.* This is unreprocessed spent fuel that is removed from the reactor core after reaching its end-of-life core service. It is usually removed intact in its fuel-element structural form and then stored for 3 to 4 months under water on the plant

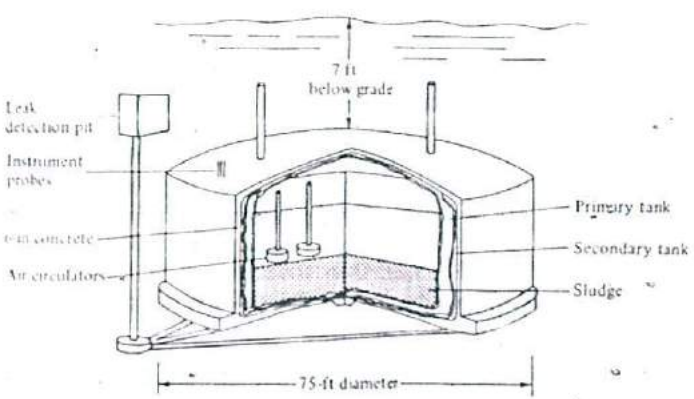


Figure 17-17 A typical low-level liquid-waste storage tank with double-walled containment.

site to give time for the most intense radioactive isotopes (which are the ones with shortest half-lives) to decay before shipment for reprocessing or disposal. Lack of a reprocessing capacity or a disposal policy has resulted in longer on-site storage, however. If the spent fuel is to be disposed of in a throw-away system (without reprocessing), it is treated as high-level waste.

17-15 RADIATIONS FROM NUCLEAR-POWERPLANT EFFLUENTS

Radiations from nuclear-powerplant effluents are low-dose-level types of radiations. The effluents are mainly gases and liquids. Environmental concerns about nuclear powerplants are prompted mainly by the effects of these radiations on the populations living near the plants. Sources of effluents vary with the type of reactor.

In both pressurized-water reactors (PWR) and boiling-water reactors (BWR), two important sources of effluents are (1) the condenser steam-jet air ejectors and (2) the turbine gland-seal system. The ejector uses high-pressure steam in a series of nozzles to create a vacuum, higher than that in the condenser, and thus draws air and other noncondensable gases from it. The mixture of steam and gases is collected, the steam portion condenses, and the gases are vented to the atmosphere (Sec. 6-3). In the gland seal, high-pressure steam is used to seal the turbine bearings by passing through a labyrinth from the outside in so that no turbine steam leaks out and, in the case of low-pressure turbines, no air leaks in. The escaping gland-seal steam is also collected and removed. In the BWR, the effluents come directly from the primary system. In the PWR, they come from the secondary system, so there is less likelihood of radioactive material being exhausted from a PWR than a BWR from these sources.

The primary-coolant radioactivity comes about mainly from fuel fission products that find their way into the coolant through the few small cracks that inevitably develop in the very thin cladding of some fuel elements. Such activity is readily detectable. However, to avoid frequent costly shutdowns and repairs, the system is designed to operate as long as the number of affected fuel elements does not exceed a tolerable limit, usually 0.25 to 1 percent of the total. Also, some particulate matter finds its way into the coolant as a result of corrosion and wear (erosion) of the materials of the primary system components. These become radioactive in the rich neutron environment of the reactor core. Corrosion occurs because the radiolytic decomposition of the water passing through the core results in free O_2 and free H and OH radicals as well as some H_2O_2. These lower the pH of the coolant and promote corrosion. Finally, radioactivity in the primary coolant may be caused by so-called *tramp uranium*. This is uranium or uranium dioxide dust that clings to the outside of the fuel elements and is insufficiently cleaned off during fabrication. It will, of course, undergo fission, and its fission products readily enter the coolant. The problem of tramp uranium is being minimized by improved processing and quality control.

The primary coolant is cycled through a *demineralizer system* (Sec. 6-8) that removes the contaminants by an ion-exchange process. Corrosion is inhibited by the slow addition of small amounts of lithium hydroxide, LiOH, to control acidity, and

by the addition of hydrazine, NH_2NH_2, during shutdown to remove the radiolytic oxygen.

Of the above sources, the neutron activiation of the corrosion and wear products represents the major activity in the primary coolant. The materials irradiated include Zircaloy, Inconol, stainless steel, carbon steel, and other steel and copper alloys that may be rich in nickel, chromium, and cobalt. The principal "crud" activity in PWRs is due to Co^{58}, which results from the neutron irradiation of Ni^{58} with the release of a proton (hydrogen nucleus). In BWRs it is due to Co^{60}, which results from the irradiation of Co^{59}. Other activities in both reactor types are due to Fe^{59}, Cr^{51}, Mn^{54}, Zr^{95}. Zircaloy 4, used as cladding in most water reactors, contributes very little to the crud because the oxide film adheres well to the zircaloy.

Another form of activation in the primary coolant in water reactors is the result of the irradiation of the primary coolant itself. The main radioactivity is due to the neutron capture of oxygen in the water. (Neutrons captured by hydrogen convert it to nonradioactive deuterium.) The most important of the oxygen reactions, because of the high energy γ emitted, is the $O^{16}(n,p)N^{16}$ reaction. It has a microscopic cross section of 1.4×10^{-5} barn and is given by

$$_8O^{16} + {}_0n^1 \rightarrow {}_7N^{16} + {}_1H^1 \qquad (17\text{-}25)$$

N^{16} is a radioactive β and γ emitter, reverting to O^{16}, with a half-life of 7.2 s. The β rays are mainly of 3.8, 4.3, and 0.5-MeV energy. Gamma rays are mainly of 6.13- and 7.10-MeV energy. Another reaction of somewhat less importance is caused by the neutron capture by O^{18}, which is present to the extent of 0.024 percent of all oxygen. The reaction is $O^{18}(n,\gamma)O^{19}$. O^{19} is also a β and γ emitter of 29-s half-life that converts to stable F^{19}. A third reaction of some importance is due to O^{17}, present to the extent of 0.037 percent of all oxygen. The reaction, $O^{17}(n,p)N^{17}$, results in N^{17}, also a β and γ emitter of 4.16-s half-life, which reverts back to O^{17}. Although the cross section for this reaction is greater than the first one by a factor of about 10^3, its effect is reduced by the small concentration of O^{17} in water. These and other resultant isotopes that yield only a few weak radiations are shown in Table 17-11.

Impurities other than corrosion and erosion products also exist in the primary water. The main one is argon 40, which enters into solution in water from the atmosphere, where it exists to the extent of 1 percent by volume. It undergoes the

Table 17-11 Principal activation of water in reactors

Isotope	Half-life	Concentrations	BWR release, μCi/s
N^{16}	7.20 s	1.0×10^{-2}	1.7×10^{4}
O^{19}	26.80 s	8.0×10^{-4}	1.4×10^{3}
N^{17}	4.16 s	1.6×10^{-3}	2.6×10^{3}
N^{13}	9.9 min	6.5×10^{-3}	1.2×10^{4}
F^{18}	109.8 min	4.0×10^{-3}	7.2×10^{3}

$Ar^{40}(n,\gamma)Ar^{41}$ reaction. Ar^{41} is a β and γ emitter with a 1.83-h half-life that decays to stable potassium 41. With limited water exposure to the atmosphere and hold decay tanks used for effluents, the effect of this reaction is minimal.

Although all these activities can be released with effluents from water-reactor powerplants, the BWR is unique in that the primary coolant is also the working fluid and hence the gaseous isotopes, in particular, are more likely to be released to the atmosphere. The fourth column in Table 17-11 indicates the possible release rates in a 1000-MW BWR.

A problem that is more characteristic of PWRs than BWRs, on the other hand, is that of *tritium*. Tritium, a gaseous emitter of 12.25-year half-life, is primarily the result of using chemical shim with boric acid in the primary water in PWRs (Sec. 10-5). A little less than 20 percent of all boron is B^{10}. Upon neutron capture it undergoes the reaction $B^{10}(n,T)2\alpha$ given by

$$_5B^{10} + {}_0n^1 \rightarrow {}_1H^3 + 2{}_2He^4. \tag{17-26}$$

by which a tritium atom, $_1H^3$ or T, and two α particles (helium nuclei) are released. This reaction has a neutron-energy threshold of about 1.5 MeV, below which it will not take place. The tritium, like ordinary hydrogen, becomes a diatomic gas, $_1H_2^3$ or T_2, or combines with hydrogen to become HT.

Other tritium-producing reactions are due to lithium and deuterium. Lithium enters the primary coolant through the use of LiOH in the demineralizer or ion exchanger, which is used to help maintain the pH value of the primary water at an alkalinic 9.5. Lithium 6 constitutes about 7.4 percent of all lithium. Upon neutron capture, it undergoes the reaction $Li(n,\alpha)T$, given by

$$_3Li^6 + {}_0n^1 \rightarrow {}_1H^3 + {}_2He^4 \tag{17-27}$$

This reaction occurs at all neutron energies. Again the tritium becomes T_2 or HT gas. Tritium production from this source can be eliminated by substituting KOH or NH_4OH for LiOH in the demineralizer. It may be noted here that BWRs use no chemical shim and no lithium compounds, and, hence, the tritium in their liquid effluents is less than 10 percent of that in PWRs.

Deuterium dioxide or heavy water, H_2^2O or D_2O, is present to the extent of 0.015 percent of all water. Upon neutron capture one or both deuterium atoms in the heavy-water molecule undergoes the reaction $D(n,\gamma)T$, given by

$$_1H^2 + {}_0n^1 \rightarrow {}_1H^3 + \gamma \tag{17-28}$$

resulting in DTO or T_2O. This reaction contributes insignificantly to the production of tritium when compared with the preceding two. Tritium is also generated as a result of the use of boron-bearing control rods, which usually contain boron in the form of B_4C. (Reactors using Ag-In-Cd control material produce less tritium.) Tritium is also generated in *ternary fission*, i.e., fission that results in three, instead of two, fission fragments, one of which is tritium. A small fraction of this tritium, estimated at 1

percent, escapes the fuel through the Zircaloy cladding and enters the coolant. (Stainless steel cladding allows a much higher percentage of tritium to pass through.) Most of this tritium, therefore, is released in fuel-reprocessing plants rather than at the reactor site.

When tritium, generated as T_2 or HT gas, enters ordinary water H_2O, one T atom replaces one H atom in the water resulting in HTO and releasing hydrogen gas H_2 according to

$$\left.\begin{aligned} T_2 + H_2O &\rightarrow HTO + HT \\ \text{and } HT + H_2O &\rightarrow HTO + H_2 \end{aligned}\right\} \quad \text{(17-29)}$$

HTO is physically and chemically similar to H_2O and becomes an integral part of it. Some of this "tritiated water" eventually finds its way into the environment.

In *heavy-water reactors*, as it is to be expected, the nearly 100 percent D_2O coolant accounts for particularly large tritium production, according to Eq. (17-28). As with light-water reactors, heavy-water reactors also suffer from N^{16} production, Eq. (17-25).

In *high-temperature gas-cooled reactors* that are helium-cooled (the HTGR, Sec. 10-12), tritium is generated by the neutron activation of He^3, which is present to the extent of 0.00013 percent of all helium. It is also generated by ternary fission to a greater degree than in water reactors. Tritium, however, can be removed from helium by absorption on a titanium sponge, which requires regeneration, normally every few months.

In *liquid-metal-cooled fast reactors*, the primary coolant, sodium, becomes intensely radioactive during plant operation. All naturally occuring sodium is made up of the isotope Na^{23}. When subjected to neutrons, it undergoes the reaction $Na^{23}(n,\gamma)Na^{24}$. Na^{24} is a radioisotope of about 15-h half-life that decays into stable Mg^{24} while emitting γ radiations, mainly of 2.76 and 1.38 MeV. The primary system, however, is separated from the steam cycle by a sodium intermediate system (Sec. 11-3) that does not become radioactive. The primary system operates at low pressures, below those of the intermediate and steam systems, so there is a very low likelihood of the radioactive sodium's leaking into the atmosphere and none of its leaking into the intermediate and steam systems.

One advantage of sodium is its ability to combine with or retain other elements. Some fast-reactor fuel elements are designed so that their gaseous fission products, such as iodine, xenon, and krypton, are vented into the coolant. Others may release fission products upon cladding failure. Sodium tends to retain some of these products, forming sodium iodide or holding cesium in solution, so that they do not escape to the gas blanket (usually argon) that separates sodium from air. Xe and Kr, on the other hand, are not retained by Na and would escape into the gas blanket.

A discussion of the biological effects of low-level radiation on human beings is a large subject and is beyond the scope of this text. It is, however, believed to be slight when compared with other hazards, such as toxic wastes [185].

17-16 HIGH-LEVEL WASTES

We will be concerned here with the high-level wastes that result from the spent fuel. High-level wastes, because of the intense exothermic activity (Sec. 9-7), generate too much heat for early passive burial and have to be cooled, usually by air circulation or other means, possibly for decades, before they can be permanently stored.

The level of activity is not as long as generally perceived. Although some fission products have extremely long half-lives, it should be recalled that the intensity of radiation is not a sole function of the half-life but is also a function of the energy generated in the reaction. Figure 17-18 [186,187] shows the relative energy generated by some of the more important fission products versus time. The level of activity is so high the first 10 years that storage can probably be best accomplished if the wastes

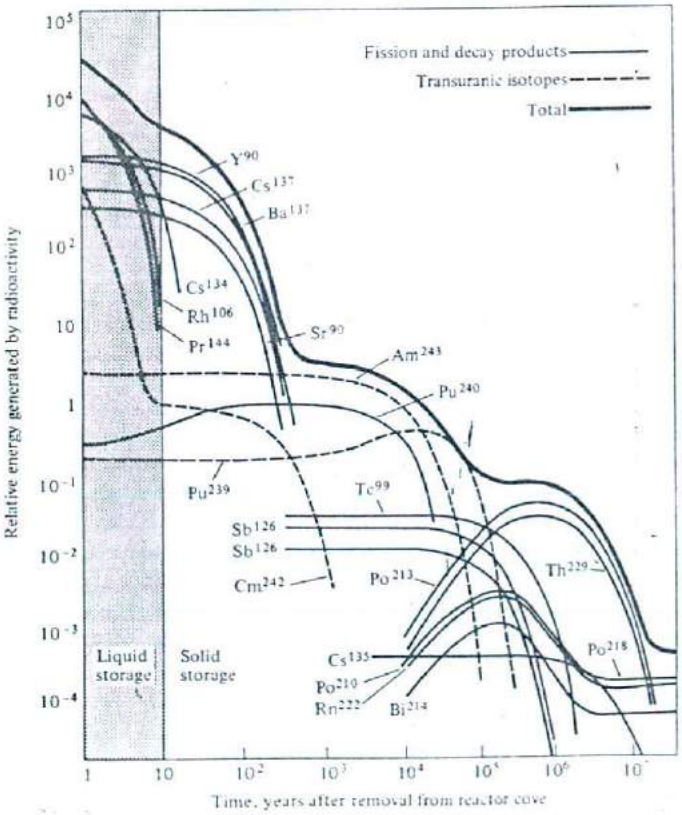


Figure 17-18 Relative energy generated by the more important fission products in high-level waste from spent nuclear fuel [186].

were in liquid form. After 10 years, the level drops by nearly an order of magnitude, thus permitting storage in solid form. It is interesting to note another and sharper drop in energy generated between 100 and 1000 years.

Figure 17-19 shows the relative "hazard" generated by the high-level waste and that generated by the original uranium ore as extracted from the ground. It shows that the high-level waste hazard drops below that of the ore it originally came from after about 800 years. The argument, based only on the half-lives of the isotopes, that stored nuclear waste would be a hazard to humanity for tens of thousands of years is, therefore, an inaccurate one.

Biological Effects of High-Level Wastes

Although all possible efforts are made to isolate high-level wastes from the biological system, it is instructive to study their effects. The principal effect is the destruction of body cells in the vicinity of the irradiated region. The effects are classified as somatic or genetic.

Somatic effects are limited to the exposed individuals. They are a direct result of the doses received by cells and manifest themselves in some form of malignancy. There is much information on high-dose irradiation effects on small animals that suggests that the frequency of effects within their population is proportional to the dose. There is, on the other hand, very little information on human beings. The only groups that have received high doses are the survivors of the atomic bombing of Hiroshima and Nagasaki, those receiving therapeutic radiation cancer treatment, and some occupationally exposed workers, such as those who work in underground uranium mines.

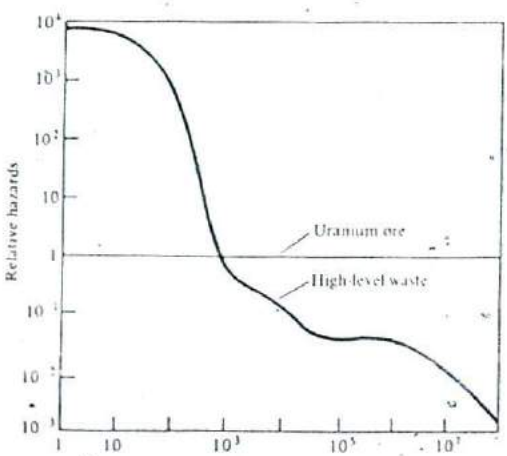


Figure 17-19 Ratio of hazards of high-level waste to those of original uranium ore versus time. *(From Ref. 188.)*

High-dose levels of radiation can result in leukemia, which occurs most frequently within a few years after doses of 50 to 500 rad. By 25 years, its frequency drops to levels that are normally encountered in the absence of radiation. Lung cancers have been observed in Hiroshima survivors who received 30 to 100 rad of gamma radiation. Estimates were that 10 cancer cases at 250 rad to 40 cases at 30 rad develop per rad for each million people during the first 25 years after exposure. Other information is available for the incidence of breast cancer (6 to 20 cases), thyroid cancer (40 cases), and other types of cancer (40 cases), all per rad for each million in the first 25 years after exposure to levels between 60 and 400 rad. Uranium miners exposed to at least a few hundred rads of alpha radiation from radon gas and its radioactive daughters show a high incidence of lung cancers. On the other hand, current evidence indicates few, if any, somatic effects can be detected at doses below 10 rad.

Genetic effects can be transmitted to the descendants of exposed individuals and thus affect unexposed generations. They are radiation-induced changes in the genetic materials of sex cells. They manifest themselves in different ways: (1) gene* mutations (changes) that result in changes in the functions of individual genes, (2) chromosome† aberrations due to breakage and reorganization of chromosomes, and (3) changes in the number of chromosomes. Such changes can result in offspring abnormalities, ranging from mild to lethal. Unfortunately (or rather fortunately), useful and adequate human data on the effect of high doses of radiation are not available and estimates of high doses to human reproductive cells are based on research on mice and other species. Such estimates yield ranges as wide as 30 to 1500 mutations per million babies per rad of acute exposures to males, and about half of that to females. Based on the response of mouse ovaries, it is expected that the effect on females may approach nil if conception occurs a sufficient time after exposure. Further, it is believed that dominant gene mutations are induced in the first-generation offspring of an irradiated population but that gene mutations appear at a higher frequency and last many more generations than chromosome mutations. Of the known human cases, however, about 75,000 children born to parents irradiated at Hiroshima and Nagasaki, and examined periodically since 1945, show no increased frequency of congenital malformations, stillbirths, or growth and development abnormalities.

* A *gene* is the carrier of information in the nucleus of a living cell that determines the physical characteristics of living things, such as the shape of the eyes in a human or the color of a flower or a plant. Genes are inherited, which is the reason why offspring resemble their parents. Genes were once thought to possess a physical structure. They are now thought of as the function or operational unit by which heredity is transmitted from parent to offspring.

† A chromosome is a threadlike microscopic part which exists in the nucleus of the cell and which carries hereditary information in the form of genes. The chromosome contains deoxyribonucleic acid, DNA, and ribonucleic acid, RNA, attached to a protein core. The arrangement of the components of the DNA molecules determines the genetic information. Each body or somatic cell contains a certain number of chromosomes, called diploid. Reproductive cells contain exactly half that number, called haploid. Fertilization occurs when two such reproductive cells combine to reproduce what is called a zygote with a diploid set of chromosomes.

Fuel Reprocessing

As indicated previously, spent fuel can either be stored directly or reprocessed. There are advantages and disadvantages to both schemes. The throw-away system (the former) avoids the costs and hazards associated with a reprocessing plant. The latter utilizes the unused uranium, converted plutonium, and other radioisotopes for use in a wide variety of services, such as isotopic generators, medicine, agriculture, and industry. There are also indications that the energy generated by the high-level waste produced after reprocessing is lower than that generated by the intact spent fuel by ratios of about 0.83 after 10 years, 0.38 after 100 years, and 0.06 after 1000 years [186].

Reprocessing of spent fuel is done by dissolving it, usually in nitric acid, then removing the converted plutonium and unspent uranium by solvent extraction. The remaining solution contains more than 99.9 percent of the nonvolatile fission products, plus some constituents of the cladding of the fuel elements, traces of plutonium, uranium, and others, and most of the resulting transuranium elements.

This remaining solution constitutes the high-level wastes. It is usually concentrated by evaporation and then stored as an aqueous nitric acid solution, usually in high-integrity stainless steel tanks. Permanent storage in liquid form, however, requires continual supervision and tank replacement over an indefinite period of time.

The experience with short-term tank storage has generally been good, though some leakage has been encountered, particularly in tanks used for storage of military wastes. It is now generally believed that, for the long term, a storage system based on solidification of the wastes would be more acceptable.

The conversion of the liquid wastes to a solid form has been studied since the 1960s, including large-scale pilot operations. Advanced processes are currently being developed. The aim is to convert the wastes to a solid product that is not liable to leakage, requires less supervision, and is more suited to final disposal. This solid product should maintain its mechanical strength. It should have good thermal conductivity, as it will continue to generate heat from radioactive decay for a long time, though at a decreasing rate. Ideally it should have a low leach rate.

Glasses and ceramics are now considered to be the most suitable forms for this final disposal. About 30 different processes have been developed over the past 20 years. The basic processes are shown in Fig. 17-20. The simplest one involves evaporation and denitration (or calcination) to form a granular or solid calcine. This is considered an interim product, since it does not meet all the above requirements; it is treated further by being mixed with additives and is then melted to form glasses or ceramics.

A second process involves mixing the additives with the original waste solution, then evaporating, denitrating, and melting this mixture to form the glasses or ceramics.

A third process uses an adsorption process and treatment at high temperature to produce the ceramics.

In recent years, attempts at improving the properties of the above glass or ceramic final products have been made. These essentially involve the further formation of either the calcine or glass into metal matrixes or coated particles to improve their leach resistance.

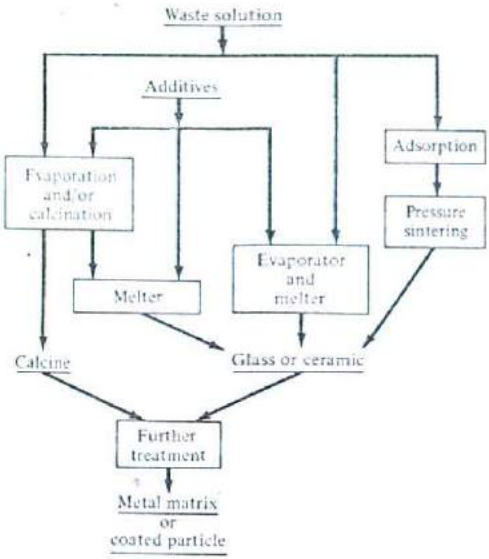


Figure 17-20 Basic high-level waste solidification processes.

Historically, the first attempt at converting wastes into glass was made at Chalk River, Canada, in 1960. This was closely followed by another developed at Harwell, England, and later by several attempts in the United States. In the United States a new plant was under construction in 1980. It is based on a 1963 process, used in a processing plant in Idaho, by which the waste is solidified by spraying it into a fluidized bed and then calcined at 400 to 500°C, thus producing a granular product that is then stored in air-cooled bins in underground vaults. Other promising plants are to be found in several countries, such as France, India, Germany, and the USSR.

Most solidification plants produce off-gases of steam and oxides of nitrogen that usually contain some fine particulate carryover and volatile radionuclides. These gases must be treated. All processes involve high temperatures and, of course, high levels of radioactivity. This combination imposes severe demands on plant design and operation. It is expected, however, that workable, commercially attractive solutions will emerge in the late 1980s. This is not late, as the problem of high-level waste is not expected to be of major effect for a few decades.

Disposal

The final disposition of the wastes, with or without the above treatments, is also of major concern. Many countries are undertaking activities involving underground disposal in deep geological formations. These activities include the investigation of suitable sites and suitable methods of storage in these sites. The main objectives, of course, are the protection of present and future populations from potential hazards. The suitable

sites must be free of flowing groundwater, but the storage vessels must demonstrate reliability even in flowing-water conditions.

The disposal of low- and intermediate-level wastes (such as those used in research and medicine) has been done at relatively shallow depths in many countries. For example, since 1967 such wastes in solid form have been packaged in concrete or steel drums and buried in the old Asse Salt Mine in Germany.

If the spent fuel is to be disposed of in a throw-away process, it is buried intact.

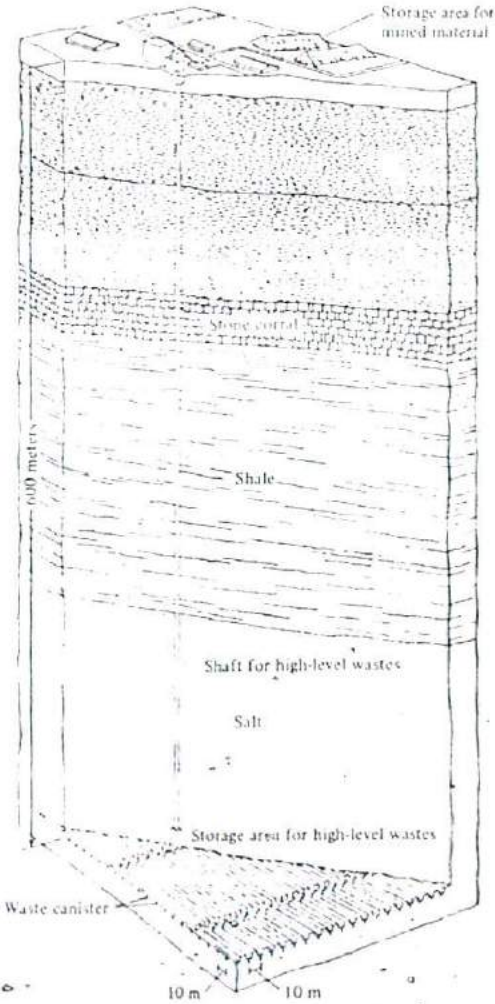


Figure 17-21 A conceptual depository of high-level waste in rock salt formations [186].

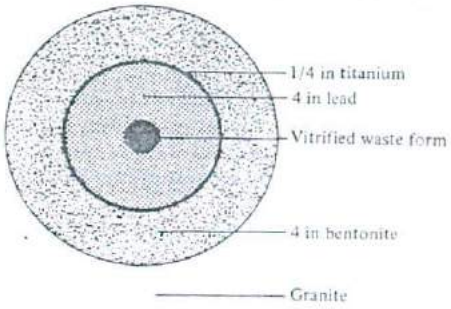


Figure 17-22 Cross section of a proposed canister for vitrified high-level waste.

If it is reprocessed, then it is buried either as a liquid or in solid form. There are several strategies for burial, most of them in deep salt or granite formations below ground or below the sea bed. In the United States, as of this writing, no final decision on high-level waste disposal has been made by the government.

A National Waste Terminal Storage Program was initiated in 1976. It includes the identification of suitable rock formations, in situ tests, and plans aimed at the establishment of up to six federal repositories. A Waste Isolation Pilot Plant (WIPP) in New Mexico is now being studied for the receipt of military wastes by the mid-1980s. Other federal repositories are planned for commercial-powerplant wastes. This also includes the disposal of spent reactor core fuel elements, should a decision be made not to treat them but to operate on a throw-away fuel cycle basis. The search includes sites in salt formations, shale, crystalline rock (volcanic basalt), the injection of liquid waste into isolated porous strata, and the injection into fractures induced in impermeable formations. Repositories are to be licensed and regulated by the U.S. Nuclear Regulatory Commission (NRC).

In France, which has the largest per capita nuclear program, plans are being drawn for long-range storage under the Alps. Other European countries have other diverse and innovative plans. The problem, although technically soluable, is laden with political, emotional, physical, and economic problems. Figure 17-21 shows a conceptual depository for the storage of high-level waste in rock salt formations for thousands of years. In the figure, the solidified waste is placed in canisters that are stored in holes drilled in rock salt with a spacing of about 10 m to allow for the efficient dissipation of energy without exceeding permissible temperature limits of either the canisters or the salt. It is estimated that each canister (producing about 10 kW at the time of storage) will require about 100 m^2 of salt for cooling. This means that about 0.5 km^2 would be needed to store all the high-level waste produced annually in the United States in 1980, if all electrical production were from nuclear powerplants. Figure 17-22 shows the cross section of a canister of Swedish design for disposal in granite. It shows vitrified waste surrounded by 4 in of lead, 0.25 in of titanium, 4 in of bentonite (an absorptive and colloidal clay mineral), and finally, granite.

PROBLEMS

17-1 A sample of particulate matter in the atmosphere has the following statistical count distribution. The particulate matter is assumed to have uniform density and the particles are approximated as spheres. d_i is the mean diameter, in micrometers, within each group i.

i	d_i	Count	i	d_i	Count
1	0.2	174	8	1.5	1602
2	0.3	347	9	2.0	1174
3	0.4	578	10	3.0	694
4	0.5	730	11	4.0	403
5	0.6	936	12	5.0	236
6	0.8	1271	13	6.0	150
7	1.0	1622	14	8.0	82

(*a*) Calculate the count, area, and mass mean diameters, and the standard deviation, in micrometers. (*b*) Plot on a semilogarithmic graph the count, area, and mass distributions, in percent, versus diameter. (*c*) Calculate the percent count and mass of particles that can be ingested with diameters of 1 μm and less, and (*d*) estimate the count modal diameter, in micrometers.

17-2 The particulate matter sample of Prob. 17-1 is acted upon by a collection device. Assuming that the device preferentially collects the larger particles, calculate the fraction of all the particles that escape collection, and the maximum diameter that escapes collection, in micrometers, if the device has an overall collection efficiency of (*a*) 95.16 percent or (*b*) 78.2 percent.

17-3 Flue gases from a powerplant contain 1 mass percent SO_2. 1.2×10^5 kg/s of these gases are to be desulfurized by the Wellman-Lord process. In addition, elemental sulfur is to be generated by the Claus process. Estimate the various mass flow rates of the chemicals, in kilograms per second, and the amount of elemental sulfur produced, in tons per day.

17-4 A plate-type electrostatic precipitator is composed of 8-ft-high plates that are 9 in apart. The applied voltage is 50,000 V. The average flue gas velocity between the plates is 4.5 ft/s. Estimate (*a*) the minimum length of the precipitator, in feet, if the particles in the gas vary in size between 1 and 5 μm, and (*b*) the minimum and maximum fractional collection efficiencies using the Deutsch equation. Take gas viscosity as 2.95×10^{-5} kg/ms.

17-5 A plate-type electrostatic precipitator is composed of plates that are 8 ft high, 13.44 ft long, and 9 in apart. The average flue gas velocity at a given load is 4.5 ft/s. At these conditions the overall collection efficiency is 95 percent. Estimate (*a*) the change in that efficiency if the flue gas volume flow rate is increased by 15 percent, and (*b*) the change in the particulate matter mass removed, in percent. Assume that the flue gas temperature and particulate matter concentration and distribution in it remain unchanged.

17-6 A powerplant using a once-through cooling system is considered for construction on a river that has a water mass flow rate of 10^9 lb$_m$/h. The river water temperature at a given time of the year is 60°F. The plant is designed to have a net efficiency of 38 percent with a condenser cooling water temperature rise of 22°F. At the plant site, the river has a more-or-less uniform width of 1 mi. Environmental regulations do not permit plant operation to result in a mixed river water temperature rise of more than 2°F, 3 mi downstream of the plant. Assuming a water surface overall heat transfer coefficient of 10 Btu/h · ft^2 · °F (Sec. 7-10), calculate (*a*) the fraction of river water used for cooling, and (*b*) the maximum net power of the plant that can meet the above regulations.

17-7 Calculate the mass of carbon 14 and xenon 137, in kilograms, that would produce an activity of 1 Ci if their atomic masses are 14.00323 and 136.9080, respectively.

17-8 Calculate (*a*) the radioactivity of 1 g each of potassium 40 and plutonium 239 in curies if their atomic masses are 39.9740 and 239.0522, respectively, and (*b*) the activity of each after 1000 years.

17-9 Chlorine 36 has an atomic mass of 35.96852 and a half life of 3.1×10^5 years. It is a β emitter. The most probable energy of the emitted β particles is 0.25 MeV. For 1 kg of Cl^{36}, calculate (*a*) the activity, in curies and (*b*) the biological dose rate, in sieverts per second and millirems per second, assuming a quality factor (relative biological effectiveness) of 1.2, and that all radiation falls on a 75-kg body.

17-10 When an isotope A with a concentration N_A nuclei/m^3 is irradiated in a neutron flux ϕ with a microscopic absorption cross section σ_A and forms a daughter radioisotope B that decays with a half-life $\theta_{1/2}$, the concentration of the daughter N_B at any given time θ is equal to the neutron absorption reaction rate $N_A\sigma_A\phi$ (Sec. 9-12) times the quantity $(1-e^{-\lambda\theta})/\lambda$, where λ is the decay constant of B. Consider a water-cooled reactor and the reaction $O^{16}(n,p)N^{16}$. Water has a density of 800 kg/m^3. The average neutron flux is 10^{18} neutrons/s · m^2. Calculate the concentration of N^{16} and its activity, Ci/m^3, after 1 h of irradiation.

17-11 Repeat Prob. 17-10 but for a sodium-cooled reactor, considering the $Na^{23}(n,\gamma)N^{24}$ reaction for irradiations of 1 h, 30 d, and 300 d. Sodium is at a density of 760 kg/m^3. Na^{23} has a neutron microscopic absorption cross section of 2 barn and an atomic mass of 22.98977. The neutron flux is 10^{19} neutrons/s · m^2.

17-12 A pressurized-water reactor is chemically shimmed with boric acid (Sec. 10-5). The natural boron concentration is 1950 ppm. The water density is 800 kg/m^3. Consider the reaction $B^{10}(n,T)\alpha$. B^{10} constitutes 19.78 percent of all boron, has a molecular mass of 10.01294 and a thermal neutron microscopic cross section of 3,837 barn. The average neutron flux is 10^{18} neutrons/s · m^2. Calculate the tritium activities after 1 h, 30 d, and 300 d of irradiation.